## *Geochemistry and petrogenesis of forearc peridotites, ODP Leg 125*

Parkinson, Ian J.

# Geochemistry and Petrogenesis of Forearc Peridotites, ODP Leg 125

by

**Ian J. Parkinson BSc. (Hons) (Notts)**

A Thesis submitted in partial fulfilment of the

requirements for the degree of

Doctor of Philosophy

Department of Geological Sciences

University of Durham

April 1993

**To my parents**

# Abstract


**Geochemistry and Petrogenesis of Forearc Peridotites, ODP Leg 125**

ODP Leg 125 recovered peridotites from Conical Seamount in the Mariana forearc and Torishima Forearc Seamount in the Izu-Bonin forearc. The peridotites recovered comprise about 95% harzburgites and about 5% dunites, which are variably serpentinised (mostly 60-100%). The Leg 125 peridotites represent some of the first extant peridotites recovered from a forearc setting. A detailed petrographic, mineral and bulk-rock chemical study of the peridotites has been undertaken in order to elucidate information about melting and fluid processes in the forearc mantle wedge.

The harzburgites are highly refractory in terms of their mineralogy and geochemistry. They have low modal clinopyroxene, highly magnesian olivine (Mg# = 91.1-93.6) and orthopyroxene (Mg# = 91.6-93.2) and chrome-rich spinels (Cr# = 60-80) and very low incompatible element contents (Ti <80 ppm). Furthermore they are more refractory than the most depleted abyssal peridotite, which suggests that the harzburgites can be interpreted as residues to extensive partial melting (>20%). The Ti concentrations in the clinopyroxene indicate that the harzburgites are residues to ~25% fractional melting.

However, petrographic and other geochemical information show that the Leg 125 harzburgites have had a complicated melting and enrichment history. Many samples have olivine fabrics which are interpreted as having formed beneath a spreading ridge. Orthopyroxenes have lobate grain boundaries often associated with fresh olivine neoblasts. This texture is interpreted as showing the incongruent melting of orthopyroxene, a process which happens at low pressures (~3 kb) and high water pressures. These two types of textures indicate that the peridotites have had a two stage melting history. Moreover, the V concentrations in the clinopyroxenes can be explained by ~15% partial melting at low oxygen fugacities (FMQ-1), followed by 5-10% melting at high oxygen fugacities (FMQ+1). Oxygen thermobarometry calculations are in accordance with the peridotites last equilibrating under oxygen fugacities of greater than FMQ+1.

The bulk-rocks have chondrite-normalised REE patterns showing extreme U-shapes with $[La/Sm]_N$ ratios in the range 5.03-250.0 and $[Sm/Yb]_N$ ratios in the range 0.05 to 0.25; several samples have possible small positive Eu anomalies. On extended chondrite-normalised plots the bulk-rocks also show enrichments in Sr and Zr relative to their neighbouring REEs and are enriched in LREE, Rb, Cs, Ba, Sm, and Eu relative to abyssal peridotites. Covariation diagrams based on clinopyroxene data show that Sr, Ce, Nd, Sm, Eu and Zr are enriched in the clinopyroxenes and that the enrichment took place during or after melting. The enrichment component is most likely a melt derived from the underlying subduction zone. A multistage melting and enrichment model is proposed for the peridotites where they first melt 10-15% beneath a spreading ridge. The resulting depleted spinel lherzolite is enriched and then melted again 10-15% above the subduction zone to produce the spatially associated boninites. A final enrichment event takes place during and after this melting event to produce the characteristic trace element enrichments in the Leg 125 peridotites.

# Declaration

I declare that this thesis, which I submit for the degree of Doctor of Philosophy at the University of Durham, is my own work and is not substantially the same as any which has previously been submitted for a degree at this or another university.

Ian J. Parkinson

University of Durham

April 1993

The sweeter the sin the bitterer the taste in my mouth
I see seven towers, I only see one way out
You got to cry without weeping, talk without speaking and scream without raising your voice
You know i took the poison from the poison stream then i floated out again
*(Running to a Stand Still)*

The third line sums up getting things done in Durham sometimes.

**Acknowledgements**
Firstly I would like to thank my supervisor Julian Pearce for advice and guidance over the past three and a half years and for giving me the chance to get my foot in the publishing door so early on in my thesis.

To the many Durham postgrads who have made my time in Durham lots of fun. The class of '92, Mikey 'Boyo' Curtis, Mark 'Victorian Father' Wharton, Steve 'Knuckles' Moss, Doug 'E' Fresh, Gary 'Sploob' Ingram. The originals Geraldo, Huntyboy, Jon, Ken, Chris, Alick and the other Chris. The rest of the rabble in no particular order- Jane, Ivan, Boo, Sarah A, Michele M, Michele H, Zöe, Mr and Mrs Bole, Sue, Paul, Trish, Pete, Danny, Miles and anyone else that slips my mind (remember when you read this that I have n't been to bed for two days!).

Mark and Mike are thanked for putting aside their theses to help this one get a lot closer to completion. Also Charlotte and Sarah for helping too.

Dimitri Kostopoulos is thanked for his continuing enthusiasm for all things mantle and for always being there to give advice on a variety of geochemical and philosophical topics.

The other post-docs from upstairs especially 'Big Sal' Gibson and Dave 'Alien' Peate for their advice and friendship

The boys in the boat, Pete, Danny and Mark for an enjoyable two years and the famous victory at Durham. Also, Tricky for coaching and our numerous coxes, Wendy, Julie, Kate, Trish, Jane and especially Swebby.

Everyone at the radiogenic isotope lab at RHBNC for putting up with my three visits down there and for helping me extract REE analyses out of the powders with seemingly nothing in them and for the unsuccessful attempt at extracting a Nd isotope out of the said same powders. Matthew Thirlwall and Gerry Ingram (Cheer up Gerry) are thanked for running the samples and Elaine, Chopper, Sharky and Ceri for keeping me company (?) and Ceri for much beer during the Christmas '91 visit. N.B. never try and sleep on the floor of a mass. spec. lab.

Thanks to the various inhabitants of Room 202 for putting up with my general untidyness and for providing stationary for me and Markyboy. The originals Chris Bedford, Chezza and Markyboy. Mehmet and Iannie. Kate 'calling radio Moscow' Lawson and the recent additions Vicky Bole and 'Johnnie' Wilson.

To the inhabitants of the Allergate residence past and present. Gerald and John. Hunty, Tim, Paula and Zöe. To Mrs Williams for being very patient with some of my rent (non-) payments.

Tony Gibbons for being the cheapest mechanic in the world.

To the technical staff especially Dave Asberry for being patient with my outstanding department debt (it will soon be gone I promise Dave). Jerry Dresser for preparing slides especially the set for VSG which appeared in the space of a day. George Randall for producing lots of high quality thin sections. All the other technical staff for help over the last three years- Ron L, Carol, Lynn, Karen, Alan, Dave S, George and Dick for making the column stand.

The keeper of the XRF, Ron Hardy is thanked for being patient with my persistent attempts to get low level data out of the XRF, for putting up with my untidyness and and keeping the machine on the go during some trying times over the last three and half years.

The 'Australians' Tony Crawford and Dick Arculus for their ubiquitous appearence at conferences and for always being supportive to myself and Marky. Also Dick for our deeply thought out Royal Society proposal.

The man who payed for myself and Mark's unfeasibly expensive Thai meal after the Western Pacific meeting, April 1990 when we only has a tenner to rub together between us.

During the last three years I've had recourse to get data from various sources, far and wide:

Frank McDermott (Open University.....not that far really) for some torium and uranium figures.

Gwendy Hall (Geological Survey of Canada, Ottawa) is thanked for taking interest in my work on precious metal mobility and giving me the chance to analyse some of the Leg 125 fluids in Ottawa. J. C. Pelchet and Judie Varve are thanked for their patience and skill in obtaining high quality precious metal analyses at such low levels. The Hall family (Gwendy, Graham, Gemma and Grandad) are thanked for their great hospitality in Ottawa (better than the gaol!) and for a great weekend at their cottage in the lakes.

To Kevin Johnson (Bishop Museum, Hawaii) for some timely ion microprobe data during the summer of 1992 and for useful e-mail discussions on partial melting processes in the mantle.

To Jeff Ryan (University of South Florida) for (too late in the day for this thesis) Li and B analyses on some of the peridotites.

To Teru Ishii (Oceanographic Institute, Tokyo) for the large amount of electron microprobe data.

To Julie Morris (ex-DTM ) for her interest in getting some Be isotopes and her untimely marriage before the analyses were done!?

Everyone at the Gulf Coast Repository, Texas A&M for making my fortnight of core logging a lot more fun than it should have been. John Miller for his liberal interpretation of the sampling rules albeit under considerable pressure from me and his less than liberal politics?! Mimi, Chris and Peggy for introducing me to Jello and peanut butter. The student slaves Pat and Dave for a great last nites booze-up at A&M.

Elaine is thanked for picking me up at my lowest ebb and helping me to survive the last twelve months.

This thesis is dedicated to my parents for there continued support both finacial and moral during the last three and half years (i.e. Baltimore street corner with six dollars in my pocket). I not sure I would finished without them....

## Geochemistry and Petrogenesis of Forearc Peridotites, ODP Leg 125


| **Chapter 1: Introduction** | **Page** |
|---|---|
| 1.1 Mantle Melting Processes Above Subduction Zones | 1 |
| 1.2 Ocean Drilling Program Leg 125 | 2 |
| 1.3 Thesis Description | 3 |
| **Chapter 2: Background to ODP Leg 125 and Tectonics of the Western Pacific** | |
| 2.1 Introduction | 5 |
| 2.2 Present Day Western Pacific | 5 |
| 2.2.1 Izu-Bonin Region | 5 |
| 2.2.1.1 Serpentinite Seamounts | 7 |
| 2.2.2 Mariana Region | 9 |
| 2.2.2.2 Serpentinite Seamounts | 9 |
| 2.3 Summary of the Tectonic and Magmatic History of the Western Pacific | 12 |
| 2.4 Objectives of ODP Leg 125 | 14 |
| 2.4.1 Core Descriptions | 15 |
| 2.4.1.1 Site 778 | 15 |
| 2.4.1.2 Site 779 | 16 |
| 2.4.1.3 Site 780 | 16 |
| 2.4.1.4 Site 783 | 17 |
| 2.4.1.5 Site 784 | 18 |
| 2.4.2 Principal Scientific Results of Leg 125 | 19 |
| 2.4.2.1 Forearc Basement Rocks: Hole 786B | 19 |
| 2.4.2.2 Fluid Geochemistry | 22 |
| 2.4.2.3 Mafic Clasts from Conical and Torishima Forearc Seamount | 24 |
| 2.5 Summary | 26 |
| **Chapter 3: Mantle Processes and Modelling** | |
| 3.1 Introduction | 27 |
| 3.2 Mantle Melting | 27 |
| 3.2.1 Introduction | 27 |
| 3.2.2 Melting Beneath Spreading Ridges | 28 |

3.2.3 Melting Above Subduction Zones 32
3.3 Extensive Parameters for Melt Modelling 35
3.3.1 Introduction 35
3.3.2 Composition of the Mantle 35
3.3.3 Melting Coefficients 38
3.3.3.1 Mineral Facies in the Mantle 38
3.3.3.2 Anhydrous Mantle 38
3.3.3.3 Garnet-Spinel Transition 39
3.3.3.4 Spinel-Plagioclase Transition 40
3.3.3.5 Melting Coefficients During Anhydrous Melting 42
3.3.3.6 Hydrous Mantle 44
3.3.3.7 Melting Coefficients for Hydrous Mantle Melting 47
3.4 Distribution Coefficients 48
3.4.1 Mineral-Melt Partition Coefficients 48
3.4.2 Mineral-Aqueous Fluid Partition Coefficients 49
3.4.2.1 Fluids in the Upper Mantle 51
3.4.2.2 Partition Coefficients 52
3.5 Diffusion Coefficients 52
3.6 Modelling of Mantle Melting and Melt/Mantle Interaction 55
3.6.1 Trace Element Approaches 55
3.6.2 Equilibrium Batch Melting 56
3.6.3 Fractional Melting 56
3.6.4 Incremental Melting 56
3.6.5 Disequilibria Melting 60
3.6.6 Dynamic Melting 60
3.6.7 Partial Disequilibrium Melting 63
3.6.8 Open System Melting Models 64
3.6.9 Mantle/Melt Interaction Models 64
3.6.10 Geochemical Effects of Melt Percolation 66
3.6.11 Kelemen Melt/Mantle Interaction Models 67
3.7 Realistic Physical Models For Mantle Melting 69
3.8 Summary 72

**Chapter 4: Petrology and Mineral Chemistry**
4.1 Introduction 73
4.2 Modal Mineralogy 73
4.3 Primary Minerals 74
4.3.1 Olivine 74

4.3.2 Orthopyroxene 76
4.3.3 Clinopyroxene 78
4.3.4 Spinel 81
4.4 Alteration Minerals 81
4.4.1 Amphibole 81
4.5 Serpentinisation 84
4.6 Integrated Deformation and Alteration History of Leg125 Peridotites 87
4.7 Mineral Chemistry 88
4.7.1 Olivine 89
4.7.1.1 Comparison with Other Peridotites 91
4.7.1.2 Dunites 92
4.7.2 Orthopyroxene 93
4.7.2.1 Comparison with Other Peridotites 96
4.7.3 Clinopyroxene 98
4.7.3.1 Comparison with Other Peridotites 100
4.7.4 Spinel 100
4.7.4.1 Comparison with Other Peridotites 104
4.7.4.2 Dunites 106
4.7.5 Amphibole 107
4.8 Conclusions on Mineral Chemistry 110
4.9 Petrogenetic Applications of the Mineral Chemistry 112
4.9.1 Geothermometry and Geobarometry 112
4.9.1.1 Introduction 112
4.9.1.2 Spinel-Olivine Geothermometry 113
4.9.1.2.1 Results 114
4.9.1.3 Pyroxene Geothermometry 115
4.9.1.3.1 Results 118
4.9.1.4. Orthopyroxene-Spinel Geothermometers 121
4.9.1.4.1 Results 121
4.9.2 Geobarometry 123
4.9.3 Thermal History of Leg 125 Peridotites 124
4.9.4 Oxygen Thermobarometry 125
4.9.4.1 Results 128
4.9.4.2 Discussion 129
4.10 Calculating Equilibrium Melt Compositions 129
4.11 Trace Element Analysis of Leg 125 Minerals 134
4.11.1 REE Geochemistry of Clinopyroxene 135
4.11.2 Other Trace Elements 135

4.11.3 Transition Elements 138
4.11.4 Petrogenesis from Trace Element Geochemistry 138
4.11.5 Nature and Timing of Trace Element Enrichments 138
4.11.6 Extent of LREE, Zr, and Sr Enrichment 139
4.11.7 Mechanisms of LREE, Zr, and Sr Enrichments 142
4.11.8 Interaction Models 142
4.11.8.1 Keleman Reactions 142
4.11.8.2 Open System Melting Models 143
4.11.8.3 Melt Percolation Models 143
4.12 Nature of the Enrichment 145
4.13 Transition Element Data - Evidence For Hydrous Melting? 146
4.14 Conclusions For The Chapter 150

**Chapter 5: Geochemistry**

5.1 Introduction 152
5.2 Notes on Analytical Techniques 152
5.3 Effects of Alteration on Bulk-Rock Chemistry 152
5.3.1 Serpentinisation 152
5.3.1.1 Major Elements 153
5.3.1.2 Trace Elements 153
5.3.2 High Temperature Alteration 160
5.3.3 Further Evidence 160
5.4 Primary Geochemical Variations in the Leg 125 Peridotites 160
5.4.1 Introduction 160
5.4.2 Major Elements 161
5.4.3 Compatible Transistion Elements 162
5.4.4 Incompatible Transition Elements 165
5.4.5 High Field Strength Elements 168
5.4.6 Large Ion Lithophile Elements 169
5.4.7 Rare Earth Elements 170
5.5 Petrogenesis 172
5.5.1 Introduction 172
5.5.2 Estimates of Degree of Partial Melting in the Leg 125 Peridotites 173
5.5.2.1 Major Elements 173
5.5.2.2 Transition Elements 176
5.6 Petrogenesis of Bulk-Rock Peridotites from Trace Element Data 178
5.6.1 Trace Element Enrichment Patterns 178
5.6.2 Adjusted Extended Chondrite-Normalised Patterns 178

5.6.3 Nature and Timing of Trace Element Enrichments 182
5.6.4 Extent of Trace Element Enrichment 183
5.7 Causes of LREE, Zr and LILE Enrichment 186
5.8 Relationship Between Peridotites and Spatially Related Boninites 187
5.9 Comparison Between Forearc Peridotites and Supra-Subduction Zone Ophiolitic Mantle Sequences 190
5.10 Chapter Summary 191

**Chapter 6: Discussion and Conclusions**
6.1 Discussion 193
6.1.1 Melting and Fluid Processes Above Subduction Zones: Evidence from the Leg 125 Peridotites 193
6.1.2 Mantle Melting in the Western Pacific in the Eocene 196
6.2 Further Work
6.3 Principal Conclusions of the Thesis 198

**References** 201

**Appendices**
**Appendix A: Analytical Techniques** 229
**Appendix B: Values** 234
**Appendix C: Calculations** 237
**Appendix D: Major and Trace Element Data** 250
**Appendix E: Ion Microprobe Data** 269

**In the pocket at the back of the thesis copies of 3 published abstracts and 3 published papers**

**Presentations**
April 1991. Talk at EUG, Strasbourg.
May 1991. Poster at the Britain in the ODP meeting, Royal Society, London.
November 1991. Department seminar, Durham.
December 1991. Talk at AGU Fall meeting, San Fransisco.
January 1992. Poster at VSG meeting, Lancaster University.
May 1992. Poster at VSG/MSG meeting, Cambridge.
January 1993. Keynote talk (for JAP) at VSG meeting, Open University.

**Publications**

Parkinson, I. J., Pearce, J. A., Ingram, G., and Thirlwall, M., 1991. Rare earth element geochemistry of Leg 125 peridotites. *Terra Abstracts*, **3,** 48.

Parkinson, I., Pearce, J., Thirwall, M., Ingram, G., and Johnson, K., 1991. Trace element geochemistry of peridotites from the Izu-Bonin-Mariana forearc, ODP Leg 125. *EOS*, **72,** 239.

Pearce, J., Peate, D., Parkinson, I., Arculus, R., van der Laan, S., Murton, B., and Thirlwall, M., 1991. Boninite genesis at the initiation of subduction: evidence from ODP Leg 125. *EOS*, **72,** 540.

Parkinson, I. J., Pearce, J. A., Thirlwall, M. F., Johnson, K. T. M., and Ingram, G., 1992a. Trace element geochemistry of peridotites from the Izu-Bonin-Mariana forearc, Leg 125. *In* Fryer, P., Pearce, J. A., Stokking, L. B., *et al.*, *Proc. ODP, Sci. Results*, **125,** College Station, TX (Ocean Drilling program), 487-506.

Parkinson, I. J., Hall, G. E. M., and Pearce, J. A., 1992b. Palladium, platinum, and gold distribution in serpentinite seamounts in the Mariana and Izu-Bonin forearcs: evidence from Leg125 fluids and serpentinites. *In* Fryer, P., Pearce, J. A., Stokking, L. B., *et al.*, *Proc. ODP, Sci. Results*, **125,** College Station, TX (Ocean Drilling program), 507-518.

Pearce, J. A., van der Laan, S. R., Arculus, R. J., Murton, B. J., Ishii, T., Peate, D. W., and Parkinson, I. J., 1992. Boninite and harzburgite from Leg 125 (Bonin-Mariana forearc): a case study of magma genesis during the initial stages of subduction. *In* Fryer, P., Pearce, J. A., Stokking, L. B., *et al.*, *Proc. ODP, Sci. Results*, **125,** College Station, TX (Ocean Drilling Program), 623-674.

Pearce, J. A., and Parkinson, I. J., in press 1993. Trace element models for mantle melting: applications to volcanic arc petrogenesis *Ian Gass Memorial Volume.*

# Chapter 1
# Introduction

## 1.1 Mantle Melting Processes Above Subduction Zones

Recent advances in our understanding of melting processes in the mantle have concentrated on mid-ocean ridge and intraoceanic settings. Here the volume and composition of melts have been successfully modelled by adiabatic decompression melting of the mantle and pooling of instantaneous melt fractions (Klein and Langmuir, 1987; McKenzie and Bickle, 1988; Niu and Batiza, 1991). The success of these models is a reflection of a good understanding of the temperature régimes in these settings, a reasonable idea about mantle flow and melt segregation processes below spreading centres and a number of good melting experiments of anhydrous peridotite on which to base the predictions of melt composition. Our understanding of the melting processes has also been aided by a large number of sub-oceanic mantle samples, known as abyssal peridotites, being available for detailed geochemical analyses.

When melting above subduction zones is considered, many of the physical parametres which are well known at mid-ocean ridge and inter-oceanic settings are poorly understood. The temperature distribution both in the mantle wedge and subducting slab is poorly known and very model-dependent, although more realistic thermal models have been developed in recent years (Peacock, 1991; Davies and Stevenson, 1992). Both mantle and melt flow within subduction systems is thought to be complicated with the potential for mantle and melts to be constantly recycled. Melt extraction models for subduction zones are still at a relatively simple level (Spiegelman and McKenzie, 1987). "Wet" peridotite melting experiments are difficult to undertake because of quenching problems and iron loss to the platinum capsules during the experiments. Experiments which have circumvented these problems can be counted on one hand. Our understanding of the melting processes is further hampered by the limited number of "true" oceanic sub-arc residual peridotite samples which may contain a great deal of information about mantle melting processes above subduction zones. Peridotite samples from destructive plate margins which have been reported in the literature include those from the Puerto Rico Trench (Bowin et al., 1966), the Cayman Trough in the Caribbean Sea (Eggler, et al., 1973), the Mariana Trench (Bloomer,

1983; Bloomer and Hawkins, 1983), the Ogasawara Palaeoland (Ishii, 1985), the Tonga Trench (Shcherbakov and Savelyeva, 1984; Bloomer and Fisher, 1987) and the Luxon arc (Philippines) (Maury et al., 1992). These studies include bulk-rock major element analyses and mineral chemistry analyses but none have concentrated on the trace element geochemistry. Some ultrabasic tectonites from the basal sections of ophiolites may be good analogues for sub-arc mantle although they may represent fragments from pre-arc lithosphere rather than "fully blown" sub-arc mantle (Pearce et al., 1984). This thesis looks at the geochemistry of a suite of oceanic sub-arc mantle samples recovered by drilling from two forearc regions from the Western Pacific.

### 1.2 Ocean Drilling Program Leg 125

During the late 1980's the *Joides Resolution* was based in the Pacific Ocean for the purpose of drilling a large number of holes in the Pacific seafloor in order to understand a variety of geological processes. Ocean Drilling Program (ODP) Leg 125 took place between February and April of 1989 with the aim of drilling a series of holes into the lithosphere of both the Mariana and the Izu-Bonin forearcs. The Leg had two principal aims. This was to drill a deep hole into the early Eocene forearc basement located on the outer arc high of the Izu-Bonin forearc in order to address the question of lithosphere formation during the initial stages of subduction of the Pacific plate. This aim was met when over 700 m of Eocene basement was recovered from Hole 786B. This Hole contained a variety of boninitic and andesitic volcanic rocks associated with the initial stages of magmatism in the forearc.

The second aim of the Leg was to drill into two serpentinite seamounts, one from each of the forearcs, in order to investigate the genesis of these poorly understood features. A series of such seamounts are found between the inner trench wall and outer forearc high, spanning the length of the two forearc systems. Earlier dredging of one of the these seamounts had yielded peridotites and basaltic material entrained in serpentinite muds. This seamount, called Conical Seamount because of its distinctive shape, has aragonite chimneys located on its summit, from which cold fluids are slowly oozing. Initial studies on the composition of these fluids found they had high pH, low chlorinity and elevated light hydrocarbon contents. The distinct compositions of the fluids were thought to relate to two processes. Firstly the high pH is a common feature of serpentinising fluids both from natural samples (Barnes and O'Neil, 1969) and from experimental studies of serpentinisation (Janecky and Seyfreid, 1986) so that active serpentinisation of peridotites within the seamount was thought to be operating. Secondly, the low chlorinity of the fluids was thought to represent the influx of fresh water from beneath the seamounts possibly from dehydration reactions within the

underlying subducting Pacific plate. The rôle of water in controlling both the major and trace element characteristics of subduction zone magmas has been long known (e.g., Green and Ringwood, 1968; Hawkesworth et al., 1877) and so the chance of sampling more pristine "slab-derived" fluid was a major reason to drill sites on Conical Seamount.

During the drilling Leg three sites where drilled on Conical Seamount and a further two sites on Torishima Forearc Seamount in the Izu-Bonin forearc. Torishima Forearc Seamount is different to Conical Seamount, as it is draped with Pliocene sediments and shows no evidence of actively venting fluids and so is thought to be "extinct" as a throughway for deep fluids.

A detailed petrological and geochemical study of peridotite samples recovered from both seamounts is presented in this thesis. Specific questions pertaining to melting and melt/fluid interaction within the sub-arc mantle wedge are addressed. Firstly, petrological and geochemical criteria are put forward which indicate that some of the melting history of the Leg 125 peridotites occured at high water contents above a subduction zone. This counters proposals that the peridotites could have been accreted from the down-going Pacific plate and so represent the top of normal oceanic lithosphere (Bloomer, 1983). Trace element concentrations in clinopyroxene and the bulk-rock peridotite are used to understand the type of melting processes which occur within the mantle wedge and the amount and type of melt/mantle interaction. The geochemistry of the peridotites is assessed in the light of the geochemistry of lavas erupted in the forearcs of both the Mariana's and Izu-Bonin regions and a model is proposed for magma genesis during the initial stages of subduction in the Western Pacific during early Eocene times.

### 1.3 Thesis Description

A brief summary of each of the chapters is presented below;

Chapter 2 discusses the tectonic setting of the past 45 million years of the western Pacific and describes the rationale for drilling at the various sites and the principal scientific results of Leg 125. For the Holes where peridotite samples were studied, a brief description of the stratigraphy of the hole is given as well as any other pertinent information such as the fluid geochemistry.

Chapter 3 considers the details of much of the modelling used in the thesis. Over the last ten years there has been a huge upsurge in the amount of material published on the

physics of melt generation and migration, melting experiments and geochemical data for both bulk-rock and minerals from peridotites. Chapter 3 reviews the published ideas for melt generation below spreading ridges and above subduction zones as well as the different models for producing geochemical changes by melt migration. The principal parameters that control the geochemistry of both melts and melting residues, the initial source composition of the mantle, the initial mineralogy of the mantle, the phase proportions of the phases entering the melt phase during melting, the distribution coefficients of various elements and the diffusivities of various elements are discussed in relation to melt generation both below spreading ridges and above subduction zones. A quantitative description of many of the published melting and melt/mantle interaction models is provided. The mathematics describing these models can be found in Appendix C. Finally, the application of these many models is discussed with respect to realistic models of mantle melting and melt/mantle interaction.

Chapter 4 describes the petrography and mineral chemistry of the Leg 125 peridotites based on descriptions of hand specimens and polished thin sections and on over 3000 published electron microprobe analyses and a smaller number of ion microprobe analyses. Electron microprobe data is used to calculate temperatures, pressures (where possible) and oxygen fugacities. Ion microprobe data was used to constrain partial melting and melt/mantle interaction models. The calculations from these data are used to discuss the petrogenesis of the Leg 125 peridotites and their application to models of melt generation above subduction zones.

Chapter 5 presents the major and trace element bulk-rock geochemistry of the Leg 125 peridotites. These data are used to constrain the petrogenesis of the peridotites. Rationale are described which may help to distinguish peridotite samples involved with the genesis of melts above subduction zones from those formed at spreading ridges and other tectonic settings.

Chapter 6 discusses the conclusions of the thesis and puts forward a model for magma-genesis during the initial stages of subduction in the Western Pacific during early Eocene times. A discussion of further studies of ophiolitic mantle sections is presented in the light of the findings on extant sub-arc mantle samples presented in this thesis.

# Chapter 2
# Background to ODP Leg 125 and Tectonics of the Western Pacific

## 2.1 Introduction

This chapter describes the background and objectives to the drilling which took place on ODP Leg 125. The past and present day tectonic setting of the Western Pacific is described. Details of the locations for the drilling sites and the core recovery and core description are provided. The principal scientific conclusions from ODP Leg 125 are presented so that the geochemistry and petrogenesis of peridotite samples recovered on this Leg, which are described in chapters 4 and 5, are set in context.

## 2.2 Present Day Western Pacific

Figure 2.1 shows the principal tectonic components of the present day Western Pacific Ocean. The Western Pacific represents the largest intraoceanic destructive plate margin in the world and so has been the site of much detailed study over the past twenty five years. The map in Figure 2.1 shows that the Western Pacific Ocean comprises of a complex series of basins, troughs, inactive and active ridges, rifts and active island arcs. The region can be broadly divided into two large terranes, one bounded by the linear Bonin trench in the north and the other by the arcuate Mariana trench in the south.

### 2.2.1 Izu-Bonin Region

The Bonin trench marks the boundary between the Philippine Sea plate in the west and the Pacific plate in the east. It runs for 2000 km, reaches depths of over 9500m and strikes approximately 350° (Honza and Tamaki, 1985). In this region the Pacific plate is being subducted due west, and so there is about 10° in the obliquity of subduction. In the northern part of the trench, the Pacific is subducting at 70 mm $a^{-1}$ and in the southern part at 50 mm $a^{-1}$ (Seno et al., 1987). From east to west the Izu-Bonin system is made up of a forearc terrane, the active Izu-Bonin island arc, the incipient Izu-Bonin back-arc basin and the Shikoku Basin. The forearc terrane comprises an inner trench wall, an outer arc high, a forearc basin and a frontal arc high. The inner trench wall has a 50 km-wide along strike terrace. The forearc terrane has suffered only limited deformation since its

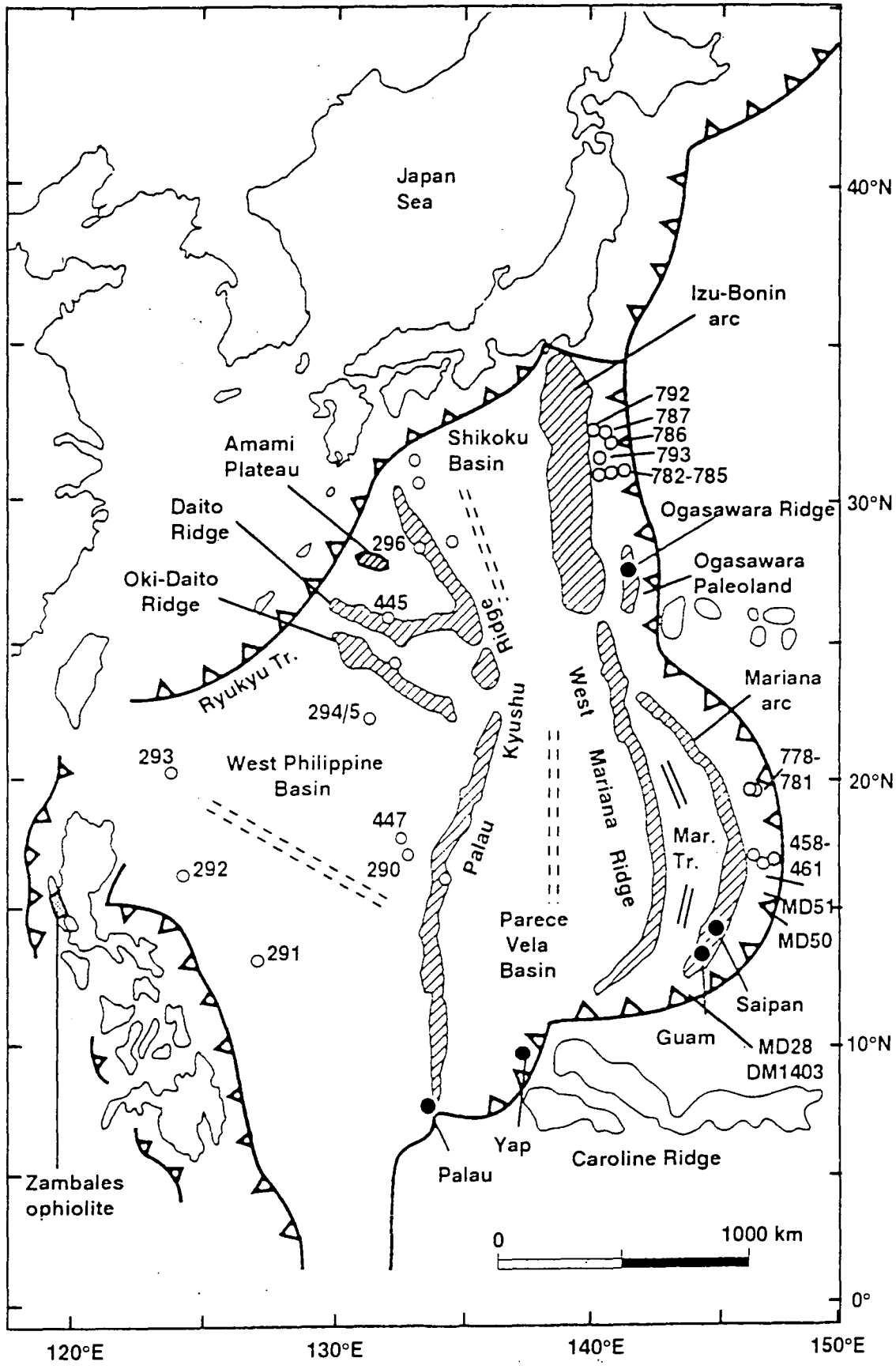


**Figure 2.1.** Map of the Western Pacific showing the location of Eocene-Oligocene and other terranes, drill sites (open circles) and dredge sites discussed in this chapter (from Pearce et al., 1992b).

inception in the Eocene (Honza and Tamaki, 1985). A broad forearc basin filled with volcanoclastic and hemipelagic sediments is bound by the outer-arc high to the west and the frontal-arc high to the east. In the southern part of the Izu-Bonin system the outer-arc high is expressed sub-aerially as the Ogasawara Ridge and includes the Bonin group of which Chichijima is a member. North of 30°N the outer-arc high is sub-aqueous and more subdued. The trench slope has only small amounts of offscraped Pacific material and no accretionary prism has developed (Taira and Pickering, 1991), in contrast to many convergent margins. The lack of an accretionary prism is thought to be related to tectonic erosion and the fact that the trench hinge-line is advancing more rapidly than the Pacific plate is retreating (Carlson and Mortera-Gutiérrez, 1990).

### 2.2.1.1 Serpentinite Seamounts

Between 20 and 50 km landwards of the trench, between the outer-arc high and the trench, are a series of serpentinite seamounts. The seamounts are most common north of 30°N. They range in size from 10 to 20 km in diameter and 200 to 1400 m high and are spaced at intervals of 15 to 60 km (Ishii, 1985). One of these seamounts, Torishima Forearc Seamount, was the location of two drilling sites during ODP Leg 125 (see Figures 2.1 and 2.2b). Torishima Forearc Seamount is located at 30°55'N, 141°47'E, 30 km east of the trench axis and 20 km above the underlying subducting Pacific plate. The seamount is 1400 m high and 20 km in diameter and has been the site of dredging surveys (Ishii, 1985; Kobayashi, 1989) and seismic and gravity surveys (Horine et al., 1990). Bathymetric studies of the seamount show that it has a steep western flank and a more shallow sloping eastern flank (Figure 2.2). Horine et al. (1990) have described the internal structure of both the seamount and inner trench wall from their seismic and gravity studies. The seamount is mantled by a 1 km thick sedimentary sequence which has no internal reflectors and is thought to be composed of serpentinite muds. Below this cap of serpentinite is material with strong internal reflectors, which Horine et al. (1990) believe to be the substrate on which the serpentinite flows are deposited. Gravity models for the Izu-Bonin outer forearc indicate that the seamount must be underlain by low density material (< 2.69 g $cm^{-3}$) down to the décollement and that this material is serpentinised ultramafic rock (Horine et al., 1990). Sediments around the seamounts are uplifted and the terrace on which the seamounts are found is also elevated relative to the rest of the inner trench wall. This uplift has probably formed by fluids from the underlying subduction zone hydrating the mantle wedge. The volume increase and density decrease accompanying this hydration causes the relative uplift of the inner trench wall terrace. The manifestation of the hydrated mantle wedge on the sea floor is the emplacement of serpentinite flows (Horine et al., 1990; Fryer, 1992).

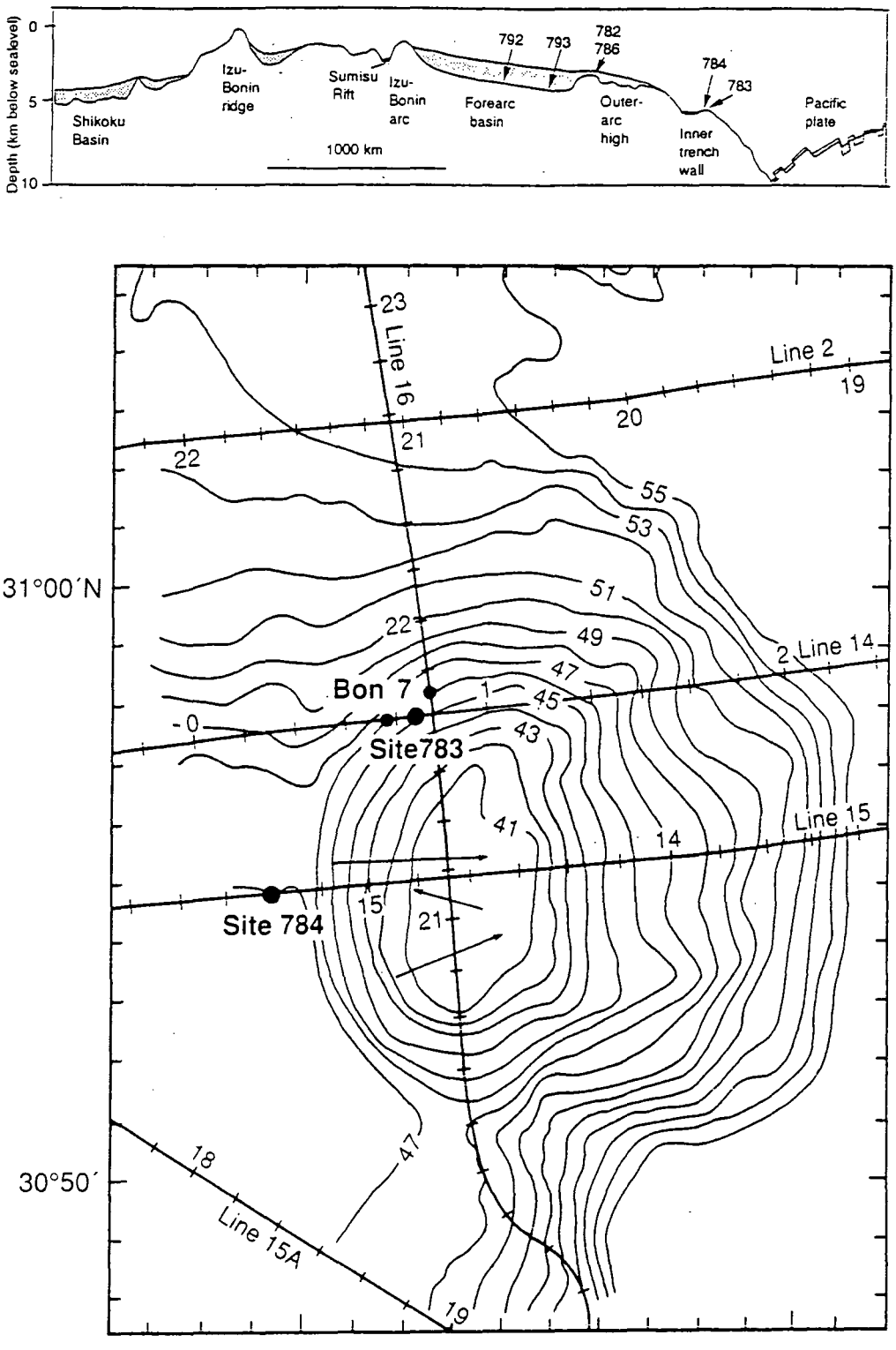


**Figure 2.2. a).** Cross section of the Izu-Bonin forearc showing the position of the Leg 125 drill sites (from Pearce et al., 1992b). **b).** Bathymetric map of Torishima Forearc Seamount with countours at 100-m interval below sea level (from Fryer, 1992).

Dredge surveys of forearc seamounts at 26°N and Torishima Forearc Seamount have been described by Kobayashi (1989) and Ishii (1985) respectively. A variety of sedimentary, igneous and metamorphic rocks have been collected from these seamounts. Serpentinised harzburgite and dunite are the principal rock types with subordinate amounts of gabbro, dolerite, basalt and volcanoclastic rocks. Many of the basic rocks are variably metamorphosed. In contrast to peridotites dredged from Mariana Trench (e.g. Bloomer, 1983), Ishii et al. (1992) have described both lherzolite and harzburgite samples from the inner trench wall of the Ogasawara area of the Izu-Bonin region, with lherzolite being more common deeper in the trench. This observation indicates that a normal mantle cross-section with more fertile peridotite occuring at depth, may be exposed in the inner trench wall of the Izu-Bonin region.

### 2.2.2 Mariana Region

The Mariana trench is an arcuate feature separating the subducting Pacific plate in the east from the Philippine Sea plate in the west. The trench is 2500 km long and is the deepest trench in the world reaching depths of over 10000 m in places. The Pacific plate is being subducted due west at a rate of 8-10 cm $a^{-1}$ and the angle of subduction varies greatly from 12° under the forearc to near vertical under the Mariana Island arc. In contrast to the linear Izu-Bonin system, the Mariana system has a strongly arcuate trench. This is thought to have formed because the Mariana backarc is actively spreading and has spread the greatest in the centre of the backarc basin (see geological history, Section 2.3). From east to west the Mariana region has the Mariana forearc terrane, the active Mariana arc, the actively spreading Mariana backarc basin, the West Mariana Ridge, the Parece Vela marginal basin and the Palau-Kyushu ridge. The forearc terrane is slightly different to that of the Izu-Bonin system. Again, there is an inner trench wall, an outer arc high and a forearc basin. There is no terrace in the inner trench wall and this area has undergone greater deformation. Several re-entrants exist in the trench wall where it is believed seamounts on the descending subducting plate have collided into the trench. There, they have been subducted and have caused extensional deformation in the overlying trench wall. Again, there is no large sedimentary accretionary prism in the Mariana system and the rocks found in the trench are exposed mantle material and some offscraped material from the Pacific plate (Bloomer, 1983). The absense of an accretionary prism is thought to be due to efficient subduction erosion.

#### 2.2.2.2 Serpentinite Seamounts

Bathymetric, seismic, dredging and submersible studies in the Mariana forearc have identified a series of serpentinite seamounts along the whole length of the Mariana

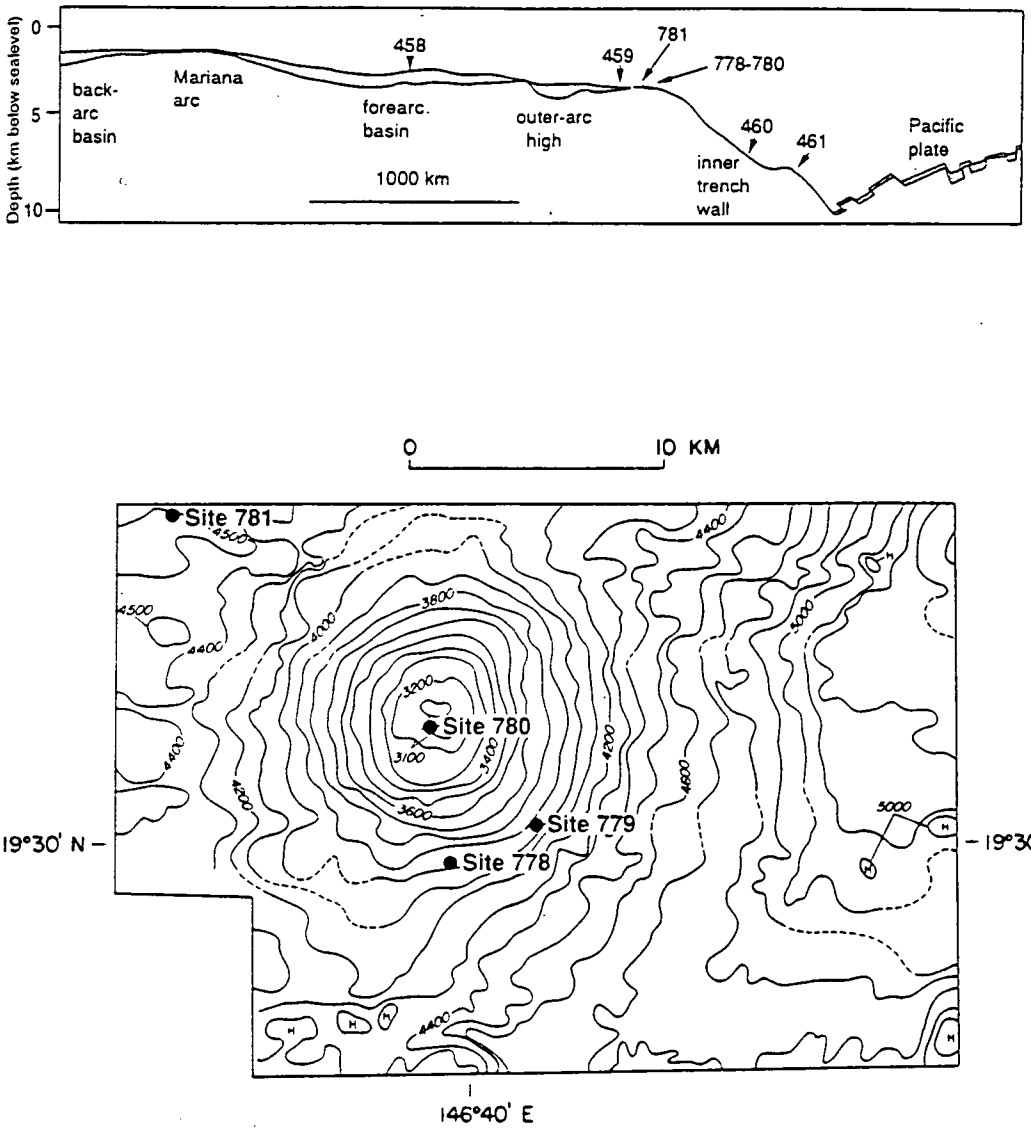


**Figure 2.3. a).** Cross section of the Mariana forearc showing the position of the Leg 125 drill sites (from Pearce et al., 1992b). **b).** Bathymetric map of Conical Seamount with contours in m intervals below sea level (from Fryer, 1992).

region (Fryer and Fryer, 1987). These are 50 to 120 km from the trench axis and are located to the west of the slope break of the inner trench wall and so are located in a different position to the seamounts in the Izu-Bonin region. The seamounts are 500 to 2500 m high and 10 to 30 km in diameter. One of these seamounts, Conical Seamount, has been the centre of much interdisciplinary study and is also the location for three drilling sites on ODP Leg 125 (see Figure 2.3).

Conical Seamount is located at 19°35'N, 146°40'E, 80 km west of the trench axis and 30 km above the underlying subducting Pacific plate. It is 1500 m high and 20 km in diameter and, as its name suggests, has a conical shape. Seismic studies of the seamount and surrounding areas have shown that the seamount is located at the intersection of two fault zones (Fryer et al., 1990). Several small horsts and graben are also located near the seamounts and this indicates that the area is under active extension. Reflection profiles of the seamount show that the seamount is draped with thin flows which, from dredging studies, have been shown to be composed of serpentinite mud.

Dredging and submersible dives on the seamount and surrounding area have resulted in many important observations. Rocks samples from the summit and flanks of the seamount are predominantly serpentinite muds in which clasts of serpentinised ultramafic rock together with subordinate amounts of pelagic sediment, metabasalts and metagabbros are entrained. The serpentinite muds drape the sides of the seamount and are thought to have flowed down from the summit. The summit of the seamount is relatively flat and is covered in a field of aragonite chimneys up to 10 m high. During the *Alvin* submersible dives, dense fluids emanated from the chimneys when their tops were broken by the submersible. The composition of the aragonite is different from deep-sea aragonite sampled from fracture zones and slow spreading ridges, being enriched in Mg, depleted in Sr and having a lighter carbon and heavier oxygen isotope signature. The fluids sampled were slightly lower in temperature than the ambient sea water and had high pH, low chlorinity and high methane contents (Fryer et al., 1987). The importance of the fluid geochemistry in discussed later in this chapter (Section 2.4.2.2).

Rocks have been sampled from a graben near the seamount (Johnson and Fryer, 1988) and from various depths within the trench wall (Bloomer, 1983; Bloomer and Hawkins, 1983). The variety and distribution of rock types is important in our understanding of the origins of the serpentinite seamounts and the evolution of the forearc terrane. Bloomer (1983) and Bloomer and Hawkins (1983) have described the

distribution of igneous rocks dredged from the Mariana trench. Serpentinised harzburgites and dunites have been sampled from all structural levels of the trench and their geochemistry and tectonised fabric indicates a residual rather than cumulate origin. The widespread distribution of peridotites in the trench points toward peridotite being the dominant rock type exposed in the inner trench wall. A host of different volcanic rocks have been sampled in the trench; these have boninitic, island arc, MORB and alkalic affinities. The MORB and alkalic samples are thought to represent accreted material from the Pacific plate. The alkali basalts are specifically thought to represent material from seamounts which are known to have collided with the trench. Limestones associated with alkali basalts contain Mesozoic microfossils, indicating that the seamounts must be part of the old Pacific plate as subduction only began in the Western Pacific in the middle Eocene (Bloomer, 1983). The island arc and boninitic rocks are believed to have a different origin. Boninitic and island arc type magmatism is known to be common in the Mariana forearc during the Eocene (see geological history, Section 2.3) The origin of the boninitic and island arc samples dredged from the trench can be best expalined by tectonic erosion exposing Eocene lithosphere in the trench. The peridotites could have been accreted from the Pacific plate or be related to magmatism above the subduction zone in the Eocene, or both. One of the main aims of this thesis was to discover which of these two origins was applicable to the Leg 125 peridotites on the basis of their geochemistry (see Chapters, 4, 5 and 6).

Johnson and Fryer (1988) have described volcanic rocks from a graben in the forearc 70 km from the trench axis. These rock have a MORB geochemistry and cherts which yielded a radiolarian age (of 130 Ma) are found in close proximity. If this age applies also to the lavas then the only possible source of these rocks is the Pacific plate as they predate magmatism in the forearc. Johnson and Fryer (1988) propose that, even at distances of 70 km from the trench, material from the underlying slab may be faulted and accreted into the forearc terrane. All these studies point to the forearc terrane being formed during a complicated history of magmatism above the subduction zone, uplift of serpentinised material and accretion of material from the underlying old Pacific plate.

### 2.3 Summary of the Tectonic and Magmatic History of the Western Pacific

Numerous reviews of the tectonic and magmatic evolution of what is the most important intraoceanic subduction system in the world have been published (Karig, 1975; Hussong and Uyeda, 1981; Natland and Tarney, 1981; Pearce et al., 1992b; Taylor, 1992). A very brief summary of the tectonomagmatic history of the Western Pacific is presented below as a way of providing a context for the drilling of ODP Leg

125 and the studies presented in this thesis and is not intended as a detailed review of subject.

The Western Pacific has been the focus of much study on destructive plate margin processes. Three main types of study have been undertaken: 1) marine geophysical surveys, 2) geological and geophysical studies of the subaerial exposures of the volcanic basement, 3) drilling and dredging surveys of all parts of the subduction zone system. Radiogenic dating and palaeomagnetic studies have been critical in producing tectonic models for the western Pacific.

The evolution of the Izu-Bonin-Mariana arc-basin system began in the early-middle Eocene at about 45 Ma when the Pacific plate began to subduct westward beneath the Philippine Sea plate (see review in Pearce et al., 1992b). Magmatism along the whole length of the Izu-Bonin-Mariana system occurred during the inception of this subduction zone with boninitic magmatism being especially prevalent (Pearce et al., 1992b; Taylor, 1992). Boninitic rocks with middle Eocene ages have been found in the Ogasawara Islands (on Chichijima), Hole 786B in the northern section of the Izu-Bonin forearc, the Facpi Formations on Guam and the Sankakuyama Formation on Saipan on the Mariana ridge (Pearce et al., 1992b; Reagan and Meijer, 1984; Mejier, 1983). In contrast some tholeiitic magmas have been found on Hahajima in the Bonin Islands and at Hole 782 in the northern Izu-Bonin forearc, indicating there was considerable along-strike variability in the early magmatism.

The arc-basin system evolved through the late Eocene and early Oligocene with the development of an intraoceanic volcanic arc built on the forearc basement (Karig 1975). Magmatism associated with the development of this arc can be found in the boninitic sills found in Hole 786B, the calc-alkaline, boninitic and tholeiitic lavas of the Alutom Formation on Guam, the andesitic Hagman Formation on Saipan, boninitic lavas drilled during DSDP Leg 60 and some of the older lavas from the Northern Palau-Kyushu Ridge (Pearce et al., 1992b).

In the early to middle Oligocene rifting split this arc and active spreading in the Parece Vela backarc basin separated a remnant of the early volcanic arc (the Palau-Kyushu ridge). At this time the structural difference between the Mariana region and Izu-Bonin region began to develop. Spreading started in the central Parece Vala basin at about 31 Ma propagating northwards and southwards and thus giving the basin its distinctive "bowed-out shape". Spreading initiated at about 25 Ma in the Izu-Bonin region forming crust of the early Shikoku Basin. Spreading propagated southwards and the

Mariana and Izu-Bonin systems became linked at about 23 Ma and continued as a single spreading centre until 17 to 15 Ma (Kobayashi and Nakada, 1979). Arc volcanism may have dramatically decreased in intensity from 31 Ma as there is little record of volcanic ash in sedimentary record from 26-17 Ma (Taylor, 1992).

Arc rifting occurred again in the late Miocene when the active Mariana Island arc separated from the remnant Western Mariana Ridge about 6-8 Ma (Hussong and Uyeda, 1981). Rifting in the Mariana backarc basin (the Marianas), which separates the Western Mariana Ridge from the active Mariana Island arc is propagating northwards and unzipping the Mariana arc (Stern et al., 1984). In contrast, rifting of the central active Izu-Bonin arc started only at about 2 Ma and the whole of the arc is thought to be presently in extension (Taylor, 1992).

The repeated rifting of the various island arcs formed in the western Pacific during the last 45 Ma means that oldest rocks associated with the inception of subduction in the Pacific are to be found at the eastern and western margins of the Philippine Sea. Middle Eocene ages for volcanic rocks found in the Izu-Bonin-Mariana forerarcs close to the trench axis mean that ultramafic rocks exposed in the same areas may also have middle Eocene ages and record information about the initial stages of magmatism in the Western Pacific.

### 2.4 Objectives of ODP Leg 125

ODP Leg 125 took place between February and April 1989 in the Mariana and Izu-Bonin forearcs of the Western Pacific. The drilling cruise had two principal objectives: 1) to drill holes into the forearc basement to help understand the evolution of the forearc lithosphere and to try to sample igneous rocks formed during the initial stages of subduction in the Western Pacific. 2) drill holes into two serpentinite seamounts with the aim of both understanding their genesis from structural and geochemical studies and by sampling pore water fluids from these seamounts to try to understand the dewatering processes of the underlying mantle wedge and subducting lithosphere.

The first aim was met in holes 781, 782 and the deep hole of 786B where 780m of volcanic basement was drilled. The second aim was met in holes 778A, 779A, 779B, 780 A,B,C and D in the Mariana forearc and holes 783A and 784A in the Izu-Bonin forearc. The samples analysed in this thesis were taken from Holes 778A, 779A, 779B, 780C and D, 783A and 784A. Some of the samples were collected for the author on the *Joides Resolution* (by J. A. Pearce and B. J. Murton) before the author commenced the Ph.D. studentship. Further samples were collected by the author in 1990 from the

Gulf Coast Repository, Texas A&M University, and the author also undertook detailed core descriptions. Some pore fluid samples were also collected on the boat for geochemical analysis at Durham. It should be noted that the original intention of the Ph.D. project was to study the mobility of platinum group elements (PGE) during serpentinisation. A small study of the precious metal content of some of the pore-fluids was undertaken at the Geological Survey of Canada, Ottawa in the summer of 1990 and published in the ODP Scientific results volume (Parkinson et al., 1992b; a copy of this paper is in the pocket at the back of this thesis). The project then concentrated on other aspects of the geochemistry of the peridotites because of the very low PGE content of the peridotites and the difficulty in determining their concentrations.

A detailed description of the rocks recovered in the holes studied in this thesis is provided below along with the rationale for drilling the holes at each specific site.

### 2.4.1 Core Descriptions

#### 2.4.1.1 Site 778

Site 778 was drilled at 19º29.93'N, 146º39.94'E on the southern flank of Conical Seamount in 3913.7 m of water. The aim of drilling at this site was to try to understand both the internal morphology of the seamount and the underlying basement by trying to drill right through the serpentinite flows to the underlying basement. Seismic studies showed that the serpentinite flows are 500 m thick and the underlying sediment 250 m thick, so that a 750 m hole would be necessary to penetrate basement. One hole (778A) was drilled at this site which penetrated 107.6 m into the seamount and recovered 22.8 m of core (Shipboard Scientific Party, 1990a). Drilling then stopped for technical reasons having only penetrated the upper serpentinite flows. Shipboard scientists divided the core up on lithological grounds into two units (Shipboard Scientific Party, 1990a).

**Unit 1** (**Subunit 1A,** 0-7.2 metres below sea floor (mbsf)) comprises lower/upper Pleistocene-Holocene serpentinite-rich sediment and serpentinite flows. The serpentine is dominantly clay and usually blue-grey to grey-green in colour. Some more coarse-grained silty serpentine units also exist and there is a serpentine marl breccia at the base of the subunit.

**Unit I** (**Subunit IB,** 7.2-29.8 mbsf) comprises lower-middle Pleistocene to lower Pleistocene sandy marls and contains pebbles of serpentinite, vesicular volcanic rocks and a foraminifer-bearing serpentinite sandstone.

**Unit II** (29.8-107.6 mbsf) comprises sheared serpentinite containing clasts of serpentinised tectonised harzburgites with some metabasalts, serpentinised dunite, metagabbro and vein material.

### 2.4.1.2 Site 779

Site 779 is at 19º30.75'N, 146°41.75'E halfway up the southeast flank of Conical Seamount. The site is in 3947.2m of water and is located 3.5 km northeast of Site 778. Two holes were drilled at Site 779; 779A which was a deep hole reaching 317.2m and 779B which was a single spudded 9m core.

Hole 779A was drilled with very similar aims to hole 778A, to drill through the serpentinite flows into the underlying basement. Again only serpentinite flows were recovered from the hole, but they contained a greater amount of solid ultramafic material than those from hole 778A. Core recovery was similar to 778A with about 22.9% recovered. Hole 779B recovered 96.7% of its 9m core and aimed to recover the uppermost sediments without drilling disturbance to study the serpentinite-sea water interface. The shipboard scientists divided the core into three units (Shipboard Scientific Party, 1990b).

**Unit I** (0-10.6 mbsf in Hole 779A and 0-9 mbsf in Hole 779B) comprises Holocene (?) to lower Pleistocene unconsolidated sediments and serpentinite flows.

**Unit II (Subunit IIA,** 10.6-216.2 mbsf) comprises lower Pleistocene to lower Pliocene (?) or upper Miocene (?) sheared serpentinite.

**Unit II (Subunit IIB,** 216.2-303.0 mbsf) is the same as Subunit IIA but with detrital serpentinite sediments.

**Unit III** (303.0-317.2 mbsf) comprises a serpentinite breccia with convolute layering.

### 2.4.1.3 Site 780

Site 780 is located on the west-southwest side of the summit of Conical Seamount where four holes were drilled in 3100 m of sea water. 780A, located at 19°32.51'N, 146°39.27'E was a spudded core and recovered 100% of its 3.5m. 780B is located at 19°32.47'N, 146°39.22'E cored 18.2m and recovered 10.34m. Hole 780C, located at 19°32.53'N, 146°39.21'E, was the deepest hole and cored 163.5m with total recovery of 14.4m. Hole 780D is located 19°32.55'N, 146°39.20'E, where 32.4m was drilled and 9.09 recovered.

Previous *Alvin* submersible dives had suggested that the site was covered with poorly consolidated serpentinite flows and is the site of several of the aragonite chimneys from

which fluids are being vented. The four holes were drilled with three primary objectives (1) to understand the physical properties of the serpentinite flows matrix and entrained clasts; (2) to sample pore water fluids from the holes with a view to understanding the composition and origin of the fluids which were least likely to be contaminated by sea water, and (3) to look for the potential of ore deposits within the seamount (Fryer et al., 1990).

On the basis of lithology and biostratigraphy, the shipboard scientists divided the cores up into two major lithological units (Shipboard Scientific Party, 1990c).
**Unit I** (0-3.5 mbsf in Hole 780A; 0-18.2 mbsf in Hole 780B; 0-14.0 mbsf in Hole 780C; 0-15.4 mbsf in Hole 780D) comprises middle Pleistocene(?) to Holocene(?) multicoloured sand- and silt-sized serpentine. Also, there are intervals of foraminifera rich clays and some filamentous opaque mineral aggregates are found. These are interpreted as remnants of bacterial mats (Shipboard Scientific Party, 1990c). Some sand to pebble size clasts of serpentinite and assorted lithic clasts also occur.
**Unit II** (14.0-163.5 mbsf in Hole 780C; 15.4-32.4 mbsf in Hole 780D) comprises intervals of serpentinised tectonised harzburgites and dunites in a serpentinite matrix.

#### 2.4.1.4 Site 783

Site 783A is located on the middle of the northern flank of Torishima Forearc Seamount at 30°57.86'N, 141°47.27'E. One Hole was drilled in 4648.8 m of water and 46.95 m of the 168.20 m core was recovered.

The drilling at this Site was aimed at understanding the internal morphology and distribution of rocks within the seamount as a variety of sedimentary, igneous and metamorphic rocks had been previously dredged from this seamount (Kobayashi, 1989). Shipboard scientists have divided the core into two lithological units (Shipboard Scientific Party, 1990d).
**Unit I** (0-120.0 mbsf) comprises middle or early Pleistocene to early Pliocene (?) silt-sized detritus. The composition of the detritus varies down the Hole from volcanic derived material at the top of the hole to a mixture of volcanic material and up to 10% serpentinite silt at the base. The volcanic siltstone is made up of glass (7-58%), pyroxene (0-2%), chlorite (0-2%) and epidote (0-7%) with traces of epidote in some samples (Shipboard Scientific Party, 1990d). Thin (1-2 cm) ash layers are also present in this unit, often overlain by some pumice fragments. Some marlstone and claystone fragments are also found in the core. The small biogenic contribution in the unit is made up of spicules, radiolarians, diatoms, silicoflagellates, nannofossils and foraminifers. The foraminifers have been used to date the unit.

**Unit II** (120.0-158.20 mbsf) comprises phacoidal sheared serpentinite with clasts of serpentinised harzburgites of unknown age. The lower 10 m of the core consists of blocks of serpentinised harzburgite. The boundary between units I and II is not clear, although the top of unit II is composed of a mixture of volcanic siltstone and serpentinite and the boundary may be gradational. The phacoidal serpentinite is blue-grey in colour, displays convolute bedding and is composed of fine-grained serpentine and chlorite. Although no fossils were found in the serpentine, unit I is probably a continuation of unit II and so unit II is probably at least early Pliocene in age (Shipboard Scientific Party, 1990d).

### 2.4.1.5 Site 784

Site 784 is located at 30°54.49'N, 141°44.27'E on the western flank of Torishima Forearc Seamount approximately 7 km southwest of Site 783. One hole was drilled in 4900.8 m of water and 218.28 m of the 425.30 m core was recovered.

Seismic studies of Torishima Forearc Seamount (Horine et al., 1990) indicate that the western part of the seamount is underlain by an easterly-dipping fault. Hole 784A is located above the trace of the fault and was drilled to understand the distribution of rock types in the seamount and to see whether the underlying basement could be sampled. Also interstitial water samples were taken in order to undertake geochemical analysis and understand their origin. On the basis of lithology and biostratigraphy the core was divided up into two units (Shipboard Scientific Party, 1990e).

**Unit I (Subunit IA,** 0.0-126.4 mbsf) is composed predominantly of feldspar- and glass-rich silt/claystone. Varying amounts of pumice also occur. Silt-sized detritus is also present and is composed of glass (21-53%), feldspar (8-22%), pyroxene (0-7%), epidote (-03%), amphibole (0-2%) and rare chlorite. Discrete ash layers are distributed through the core and have sharp basal contacts. Diatoms from the upper part of this unit give a late Pleistocene age (Shipboard Scientific Party, 1990e).

**Unit I (Subunit IB,** 126.4 302.7 mbsf). This subunit is dominantly made up dark grey glass-rich silty claystone. The claystone is made up of glass (15-52%), feldspar (0-15%), pyroxene (0-3%) and trace amounts of chlorite, amphibole and zeolite. Diatoms yield an age of early Pliocene (?) to middle Miocene for the subunit . Again ash layers are present with good sharp basal contacts and are composed of volcanic glass, feldspar, pyroxene and opaques. This subunit differs from subunit IA by having abundant sedimentary and structural features. Sedimentary features such as graded beds, parallel laminations, a Bouma sequence and extensive bioturbation are common. Synsedimentary microfaults, water-escape structures and tension gashes are also common.

**Unit I** (**Subunit IC**, 302.7-321.1 mbsf) comprises intercalated grey-brown claystone and dark blue-grey silt-sized serpentine. The claystone is made up of clay (90-100%), serpentine (0-2%), feldspar (1-3%) and glass (1-7%). No sedimentary features are seen in the claystone and it is also devoid of fossils. The lowest part of the subunit is a serpentinite micro-breccia with large 5-6 cm rounded clasts of serpentine and smaller (1-2 mm) angular grains. The intercalation of the claystone and serpentine is thought to represent small flows of serpentine flowing down the side of the seamount and interfingering with the deposition of pelagic sediments.

**Unit II** (321.1-425.3 mbsf). The lowest unit, in this core is a microbreccia containing blocks of serpentinised harzburgite in a sheared phacoidal serpentine matrix. Near the base of the unit the harzburgite becomes quite continuous and blocks are up to 100 cm long and are broken up by layers of phacoidal serpentine and silt-sized serpentine. This unit is thought to correlate with unit II in Hole 783A (Shipboard Scientific Party, 1990).

### 2.4.2 Principal Scientific Results of Leg 125

This section summarises some of the principal scientific results of Leg 125 in order to put some of the studies in this thesis into context. All the results of Leg 125 can be found in the Proceedings of the Ocean Drilling Program, Scientific Results, Leg 125 (Fryer, Pearce, Stokking et al., 1992). However, the three main results discussed here are those for the forearc basement rocks from Hole 786B, the geochemistry of pore-fluids from the two seamounts and the geochemistry of the mafic clasts from the two seamounts.

#### 2.4.2.1 Forearc Basement Rocks: Hole 786B

Detailed studies of the major element (Arculus et al., 1992), trace element (Murton et al., 1992) and isotopic (Pearce et al., 1992a) geochemistry of the boninites cored in Hole 786B have recently been published. Hole 786B was a deep (720 m) hole which recovered a variety of volcanic rocks which represent some of the earliest lithosphere generated after subduction was initiated in the western Pacific. Peridotites recovered from Torishima Forearc Seamount are located along strike to the south from Hole 786B and may be representative of either the residual mantle to the volcanic rocks in 786B or a possible source for forearc volcanic rocks. Clearly therefore, the petrogenesis of the rocks recovered in Hole 786B is important in understanding the genesis of the Leg 125 peridotites.

The forearc basement cored at Hole 786B contains three boninite series. The base of the sequence in 786B comprises Eocene low-Ca boninite and low-Ca bronzite andesite

pillow lavas and dykes. The main part of the sequence is of Eocene intermediate-Ca boninite and its fractionation products. These two series have ages of around 41 Ma. The final series are early Oligocene intermediate-Ca to high-Ca bonintes which occur as sills and dykes and cross cut the main basement edifice. They have ages of 32 Ma (Mitchell et al., 1992).

The principal trace element characteristics of these lavas are shown in Figure 2.4 where chondrite-normalised REE patterns and MORB-normalised trace element patterns are presented for representative lavas from Hole 786B. The boninites have flat to U-shaped REE patterns and have low REE contents relative to lavas from the active Mariana island arc. On the MORB-normalised diagram the 786B boninite exhibit several characteristic features. They exhibit selective enrichment in LILE relative to the HFSE, positive Zr and Hf anomalies relative to Sm, negative Ti anomalies relative to Y and MREE and a negative Nb anomaly relative to La and Th (Pearce et al., 1992b).

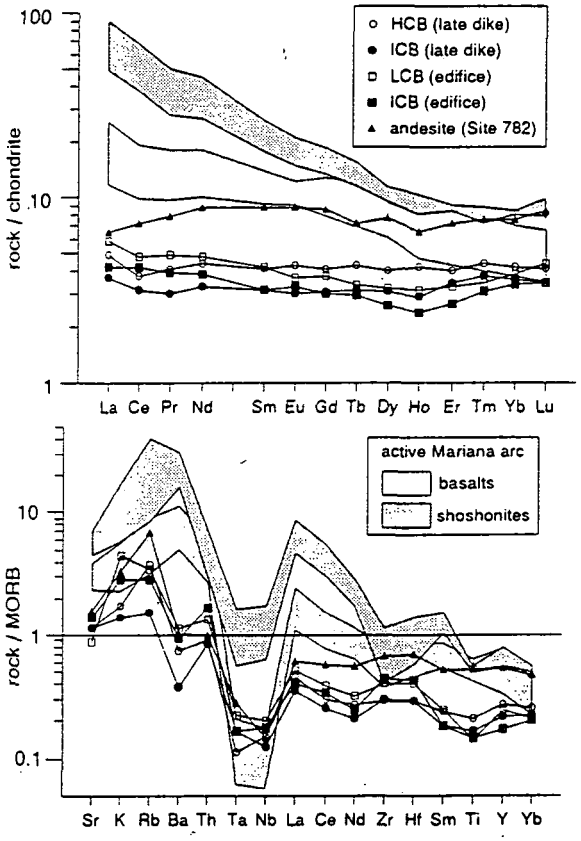


**Figure 2.4. a).** Chondrite-normalised REE patterns and **b).** MORB-normalised trace element patterns of representative low-Ca, intermediate-Ca, high-Ca and tholeiite from Hole 786B. Also shown are the fields for calc-alkaline basalts and shoshinites from the active Mariana and Bonin arcs (from Pearce et al., 1992b).

The LILE enrichments relative to the HFSE are characteristic of some subduction zone lavas. However, the positive Zr and Hf anomaly relative to Sm is a feature charateristic of some boninites (Sun and Nesbitt, 1978; Cameron et al., 1983; Hickey-Vargas, 1989) but is not found in the active Mariana and Izu-Bonin calc-alkaline lavas.

Isotopically the boninites plot on the Northern Hemisphere Reference Line (NHRL) between Pacific MORB mantle (PMM) and Pacific Volcanogenic Sediment (PVS) on a $^{208}Pb/^{204}Pb$ versus $^{206}Pb/^{204}Pb$ plot (Figure 2.5). They do not plot towards pelagic sediments in contrast to many island arc volcanics. On a εNd versus $^{206}Pb/^{204}Pb$ the samples also plot between PMM and PVS. On a εNd vesus εSr they plot parallel to the PMM-PVS trend but at higher εSr values.

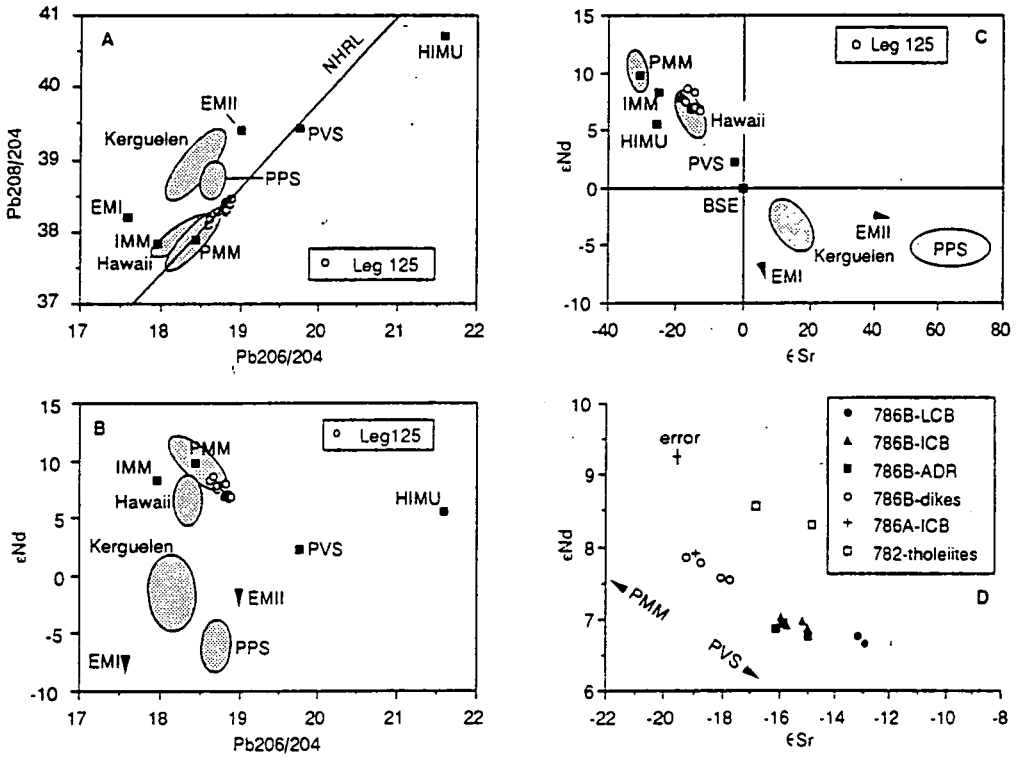


**Figure 2.5**. Main isotopic covariation diagrams showing the distribution of data from Leg 125 boninites in comparison to fields and points for the nearest hot-spots (Hawaii and Kerguelen), Pacific MORB mantle (PMM), Indian MORB mantle (IMM), Pacific Pelagic Sediment (PPS) and Pacific Volcanogenic Sediment (PVS) and the isotope "end-members" EMI, EMII and HIMU (from Pearce et al., 1992b).

Boninites are distinctive volcanic rocks with high MgO and $SiO_2$ contents, high compatible element and low incompatible element contents. Boninites *sensu stricto* are

glassy with a phenocryst assemblage of orthopyroxene and/or clinoenstatite, olivine and Cr-spinel. The consensus opinion of boninite workers is that boninites represent melts from hydrous (but water-undersaturated) melting of a depleted peridotite source at low pressures (<10 kb) (Crawford, 1989 and papers therein). Boninites are most commonly found at convergent margins and most models for their genesis involve the remelting of a previously depleted but variably enriched source above a subduction zone with water from the subducting slab playing a key rôle in many of the models (Crawford et al., 1989; Pearce et al., 1992b and references therein). Boninites with middle Eocene ages are common along the whole length of the Izu-Bonin-Mariana arc-basin system and it is possible that the thermal and tectonic conditions for the production of boninitic melts are met during the initial stages of subduction.

The Leg 125 boninites have LILE enrichments in common with many other boninites but distinctive positive Zr and Hf anomalies. Pearce et al. (1992b) propose that the Leg 125 boninites represent the decompression melting of a metasomatised residual MORB mantle. The distinctive positive Zr and Hf anomalies may have been produced by metasomatism of the boninite source by trondhjemitic melts generated by fusion of the subducting slab in the amphibolite facies. The melting of the downgoing slab and melting of a depleted peridotite source impose strict thermal constraints on petrogenetic models. Thermal modelling by Peacock (1991) and Pearce et al. (1992b) require both the subducting slab and overlying mantle wedge to be young and very hot and subduction beneath or of an active spreading ridge during the intial stages of subduction may provide the thermal and tectonic conditions to generate boninitic melts (Pearce et al., 1992b).

#### 2.4.2.2 Fluid Geochemistry

In addition to the pore-waters collected from the summit of Conical Seamount by *Alvin* submersible dives (Haggerty, 1987; Fryer et al., 1987), interstitial pore-waters were collected from both Conical and Torishima Forearc Seamount during Leg 125. The pore-water samples were usually produced by squeezing a 10 cm section of the core (serpentinite mud or pelagic sediment) and collecting the fluids. Some pore-waters were also sampled *in situ* and fluid temperatures were measured down the holes. Mottl (1992) has intergrated the results of the pore-water geochemistry with previously published results on fluids from the serpentinite seamounts (Haggerty, 1987) and fluids sampled in other convergent margins.

Earlier in this chapter it was shown that serpentinite seamounts are a common feature of intraoceanic forearcs where there is no sedimentary accretionary prism. The close

distance of many of these seamounts to the top of the underlying subducting slab (as little as 20 km in the case of Torishima Forearc Seamount) coupled with the abundance of fault zones in the outer forearc regions means that deep subduction-derived fluids could be readily sampled at the serpentinite seamounts. Furthermore, Tatsumi (1989) has shown that much of water carried down in the subducting oceanic plate may be driven off below forearc regions by dehydration reactions.

Fluids from the two seamounts have distinctive geochemistries. Pore-water fluids from Conical Seamount have approximately half the chloride and bromide content of seawater, pH up to 12.6, high methane, ethane and propane contents and high sulphide and ammonia contents. The fluids are also enriched with respect to seawater in alkalinity (x26), sulphate (x1.7), K (x1.5), Rb (x5.6) and B (x10) and are depleted in Ca, Li, Mg and Sr (Mottl, 1992). There are differences in the chemistry of the fluids sampled at the summit site (Site 780C) and the flank sites (Sites 778A and 779A) with fluids from Site 780C showing the most extreme of the chemical characteristics described above. The fluids from Site 780C are moving upwards at velocities greater than a few mm per year and are most likely to record the signature of deep-seated fluids (Mottl, 1992).

Low chlorinity high methane fluids are characteristic of pore-fluids sampled above subduction zones. Most of these fluids have been collected from sedimentary accretionary prisms. The freshness of these waters with respect to seawater has been explained by water derived from fresh water aquifers within the accretionary prism and the breakdown of gas hydrates to produce the high methane contents. The chlorinity of the Conical Seamount pore-fluids is the lowest reported from the ocean basins. There is little evidence to suggest that a fresh water aquifer or gas hydrates are present below Conical Seamount (Mottl, 1992). This leads to two explanations for the unique fluid chemistry from this seamount, that the serpentinisation process takes chlorine from the fluids or that a deep-seated fresh water component is introduced. Although chlorine may be taken up during serpentinisation (Rucklidge, 1972; Rucklidge and Patterson, 1977; Janecky and Seyfried, 1986) the rapid decrease in the chlorinity with depth at Hole 780C is too great to be maintained by serpentinisation reactions alone especially as the fluids are moving upwards. It is therefore likely according to Mottl, (1992) that a component of the pore-fluids sampled at Hole 780C is from dewatering of the underlying subducting slab 30 km below. Serpentinite seamounts may then act as important conduits for deep-seated fluids in forearc regions.

In contrast fluids sampled in Holes 783A and 784A are consistent with fluids derived purely from low-temperature serpentinisation of peridotites by seawater. These fluids have pH up to 10, low Si, Mn and methane and no ethane and propane. Relative to seawater they are depleted in alkalinity, sulphate, B, K and Mg, have low Li and Rb and similar chloride and bromide. Ca, Sr and Ba are enriched in these fluids (Mottl, 1992). The fluids collected from Holes 778A and 779A are a complex mixture of those from 780C and 783A and 784A.

Torishima Forearc Seamount is not actively venting fluids and so is thought not to be a conduit to deep-seated fluids at the present time. However, Sakai et al. (1990) have studied the stable isotope compositions of serpentinised peridotites from several seamounts (including Torishima Forearc Seamount) in the Izu-Bonin-Mariana forearcs. Sakai et al. (1990) found that peridotites with ductile sheared textures had hydrogen and oxygen isotopic signatures consistent with interaction in the mantle wedge with fluids derived from the subducting slab. Peridotites with mesh-textured serpentinite have higher $\delta D$ and lower $\delta^{18}O$ than the sheared peridotites formed by low-temperature interaction with seawater. Although the pore-waters sampled from Torishima Forearc Seamount do not have have a deep-seated fluid component, some peridotites sampled in the seamount do record the interaction of the mantle wedge with fluids from the subducting slab presumably at depth in the mantle wedge.

### 2.4.2.3 Mafic Clasts from Conical and Torishima Forearc Seamounts

The geochemistry and metamorphism of mafic clasts from the two seamounts has been described by Johnson (1992) and Maekawa et al. (1992) respectively. Metabasic clasts entrained in the serpentinite mud have a wide range of compositions. Volcanic rocks with boninitic compositions are common. A few clasts have shoshonitic compositions, and a number of samples have MORB-like geochemistry. The metamorphic grade of the clasts ranges from low temperature zeolite-facies, through higher tempertaure prehnite-pumpelllyite facies to lower greenschist facies. Some samples contain blue amphibole and lawsonite and Maekawa et al. (1992) have estimated that these clasts may have attained metamorphic conditions of 150-250°C and 5-6 kb.

From these studies it is likely that the serpentinite seamounts have sampled mafic rocks from a variety of depths and sources within the mantle wedge. The appearance of MORB-like rocks in the seamounts may be explained in three different ways; 1) MORB-type rocks being generated in the forearc mantle; 2) accreted slabs of Pacific plate being trapped in the forearc wedge or 3) direct sampling of material from the underlying Pacific plate. Radiogenic dates from these clasts would help constrain their

origin with respect to these three models. Figure 2.6 shows three scenarios for the emplacement of the various mafic clasts into the serpentinite seamounts. It is apparent from these models and from both the fluid geochemistry and metamorphism of the mafic clasts, that serpentinised peridotites from the seamounts may have been sampled from a variety of sources and depths within the mantle wedge. Geochemical studies of these peridotites will hopefully constrain their origin.

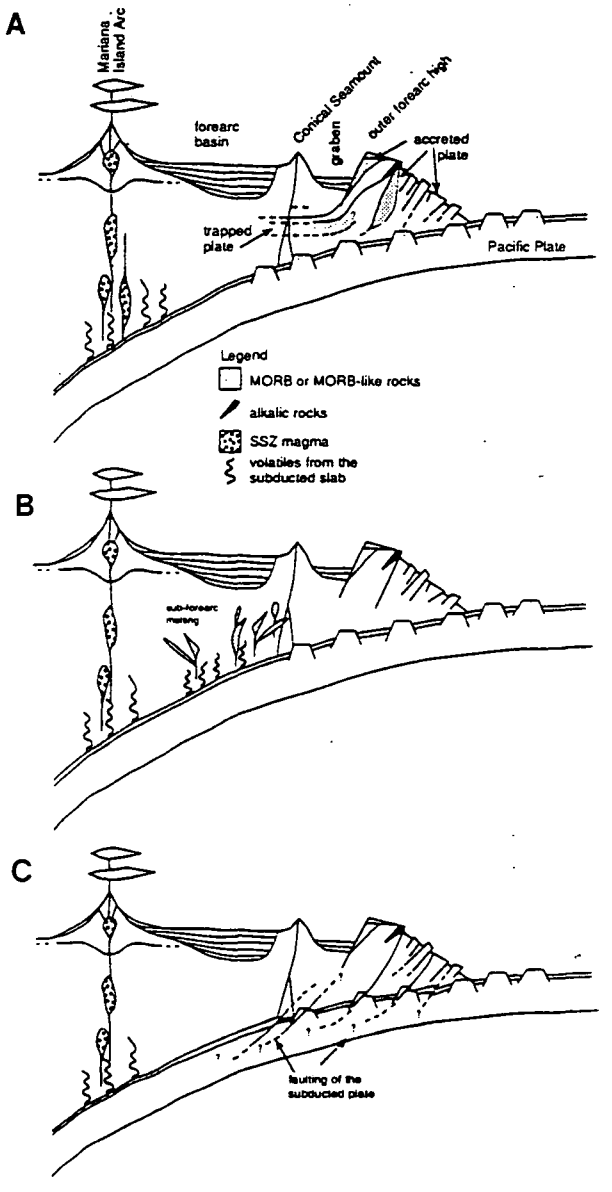


**Figure 2.6**. Three scenarios for sampling mafic clasts in the seamount seamounts. **a**). Derivation of MORB-like melts from a fragment of trapped melt. **b**). Derivation of the MORB-like lavas from deep forearc magmatic sources. **c**). Derivation of the MORB-like melts from fragmented portions of subducted plate within the source region of the serpentinite muds (after Johnson, 1990).

## 2.5 Summary

The Izu-Bonin-Mariana arc-basin system is the largest inter-oceanic convergent margin system in the world. Recent drilling on ODP Legs 125 and 126 has provided important samples from the Izu-Bonin-Mariana forearcs from which information about volcanism, crustal accretion and fluid processes in the mantle wedge can be drawn. Studies of the Eocene basement drilled in Hole 786B in the Izu-Bonin forearc confirm that boninitic magmatism is an important component in lithosphere generation during the initial stages of subduction. Peridotites from Conical Seamount in the Mariana forearc and Torishima Forearc Seamount in the Izu-Bonin forearc are possibly the best examples of arc-related peridotites yet discovered. They may record much information about melting and enrichments processes in the mantle wedge (see chapters 4 and 5). Furthermore, the serpentinite seamounts are likely to be conduits for fluids from the underlying subducting slab and probably play an important role in balancing geochemical budgets in subduction zone systems.

# Chapter 3
# Mantle Processes and Modelling

## 3.1 Introduction

This chapter reviews and discusses melting, melt segregation and melt/mantle interaction processes in the mantle. The chapter is divided into three sections. Firstly a review of the current models for mantle melting in the upper mantle is presented with special reference to melting in the oceanic mantle beneath spreading ridges and above subduction zones. Secondly, as an introduction to the modelling used in this thesis, the extensive parameters used in the melt modelling are discussed. Finally a detailed discussion of the numerous mantle melting and mantle/melt interaction models is provided with worked examples. In the light of the geochemistry of residual peridotites, a model most applicable to melting and mantle/melt interaction in the upper mantle is put forward.

## 3.2 Mantle Melting

### 3.2.1 Introduction

Over the last ten years there have been great advances in our understanding of the melting processes in the mantle. This stems primarily from three different approaches: firstly a deeper understanding of the physics of melting and melt segregation has developed from theoretical studies (e.g., McKenzie, 1984; Navon and Stolper, 1987: Spiegelman and McKenzie, 1987; Scott and Stevenson, 1989), and its applications to the chemistry of melts and melting residues; secondly a series of melting experiments has been undertaken on realistic mantle compositions (e.g., Jaques and Green, 1980; Falloon and Green, 1987, 1988; Kinzler and Grove, 1992a) which allow us to understand the effects of temperature and pressure on the melts produced by partial melting of peridotite; finally, the availability of high quality trace element data in peridotite minerals from mid-ocean ridges (e.g., Johnson et al. 1990; Johnson and Dick, 1992), continental lithospheric mantle (Bodinier et al., 1988; Rampone et al., 1991; Rampone et al., in press) and arc-related peridotites (Parkinson et al., 1992a; Kelemen et al., 1992) have helped constrain models of melting and melt migration.

The following sections look at current models for melting below spreading ridges and in the mantle wedge above subduction zones, both of which may apply to the Leg 125 peridotites.

### 3.2.2 Melting Beneath Spreading Ridges

Melting below the world's spreading ridges generates approximately 20 $km^3$ of magma per year, by far the most important (volumetrically) process for generating magmas on the earth. Although, melting below spreading ridges has long been thought to take place by pressure release (decompression) melting, with material rising adiabatically to the surface (Turner and Verhooegen, 1960; Ahern and Turcotte, 1979), it is only during the last ten years that quantitative models of the volumes and compositions of melts generated by adiabatic decompression melting have been developed (McKenzie, 1984; Klein and Langmuir, 1987; McKenzie and Bickle, 1988; Niu and Batiza, 1991). The principles behind decompression melting are shown in Figure 3.1a and b. The melting mantle is best viewed as a rising column in which fertile mantle enters the column at the base and rises up until it reaches its solidus where it starts to melt. Directly below the axis of the spreading centre, melting will continue until the Moho is reached, although this may not be the case away from the ridge axis (Spiegelman and McKenzie, 1987; Scott and Stevenson, 1989). The amount of melting undergone in the column is directly related to the length of the melting column which is controlled by two critical factors; the temperature of the mantle upwelling into the base of the column which controls the depth at which the mantle crosses its solidus; the final pressure at which the melting stops which controls how far the mantle can decompress above a given solidus. A cursory look at Fig 3.1b shows that hotter mantle has a longer melting column (and hence more total melting) as it crosses the solidus at greater depths. From the above description of decompression melting, it is obvious that one of the important quantities in modelling melting columns is the amount of melt generated per kilobar (kb) (melting per unit of pressure is preferred than per unit length of column for calculation reasons) of decompression. Ahern and Turcotte (1979) suggest a value of 1.2% $kb^{-1}$ whereas as McKenzie (1984) suggest values between 0.8 and 1.5% $kb^{-1}$ with an average of 0.95% $kb^{-1}$. Kostopoulos and James (1992) propose that the value will change with the changing composition of the mantle (and hence pressure) during melting so that fertile mantle just above its solidus will generate 2.5% $kb^{-1}$ whereas depleted mantle at the top of the column will generate only 0.5% $kb^{-1}$. They believe an average of 1.4% $kb^{-1}$ would describe melting in most situations. This point has also been developed by Plank and Langmuir (1992). However, if these differences exist their importance would only be apparent if small degree melts are

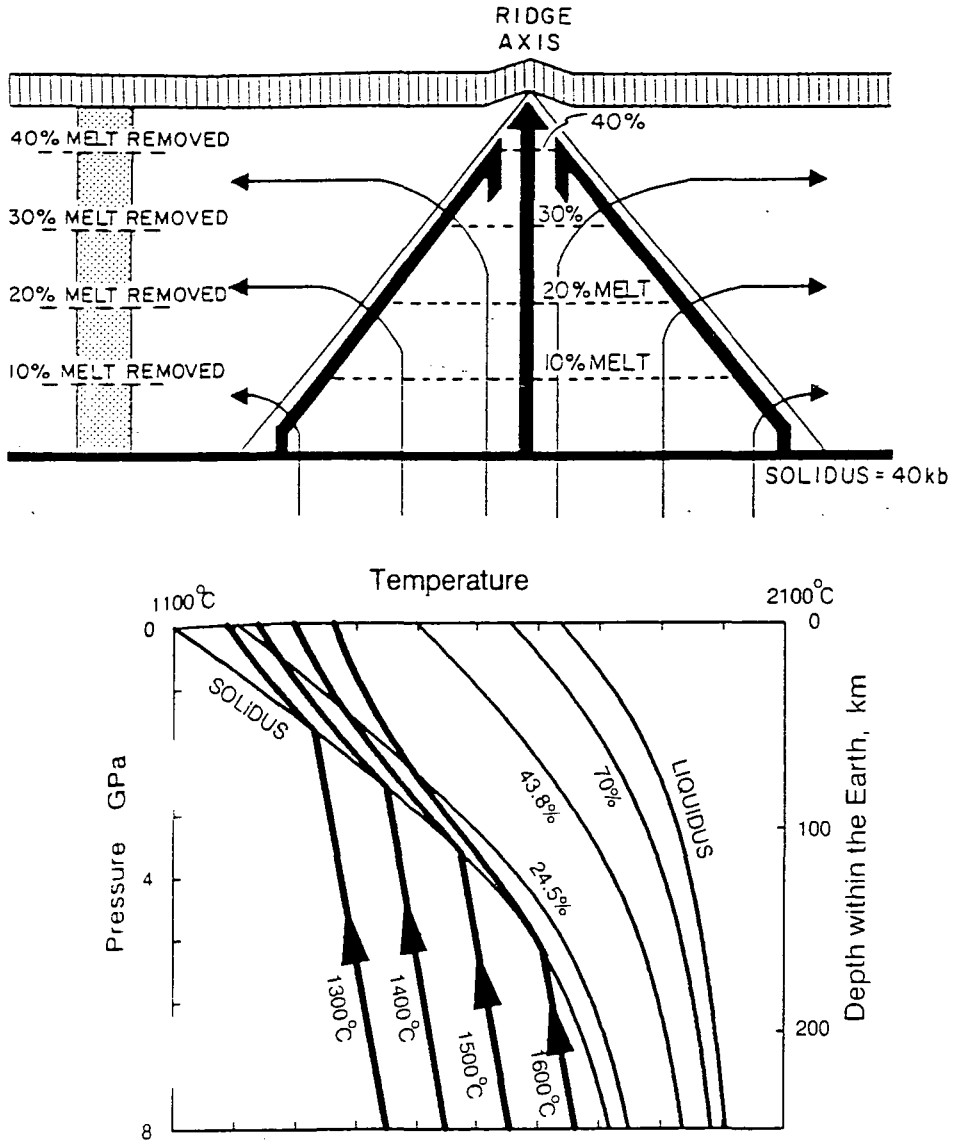


**Figure 3.1 a)**. Schematic model of the melting column beneath a ridge axis. Light solid arrows show mantle flow lines; heavy solid arrows show melt flow field after Spiegelman and McKenzie (1987); dashed lines within melting zone show percent melting above solidus. Oceanic crust is indicated by vertical ruling. Residual melting column resulting from the extraction of melt (stippled) is shown on the left, (from Klein and Langmuir, 1989). **b)**. Isentropic paths for mantle upwelling, calculated using parameterisations given by McKenzie and Bickle (1988) with an entropy of melting of 400 J $Kg^{-1}$ $°C^{-1}$ for four potential temperatures (from McKenzie and O'Nions, 1991).

sampled at the surface. If all the instantaneous melts produced in the column are pooled, then the effect would be to increase the average pressure and temperature of melting.

An important consideration for the compositions of both melts and residual peridotites produced is the type of melting (batch, fractional or some other) beneath the ridge. This will depend upon the amount of melt that has to exist in the matrix before it can form an inter-connected network and separate. Experimental and theoretical studies (Waff and Bulau, 1979; McKenzie, 1984) indicate that the value is very low (~1%) and

may be even lower if the matrix is deforming (Bussod and Christie, 1991; Daines and Kohlstedt, 1993). Experiments by Fujii et al. (1986) on olivine and olivine-orthopyroxene matrices have shown that increasing the amount of pyroxene will increase the amount of melt needed before separation occurs, so that a fertile lherzolite may have a separation porosity of ~2.5% and a depleted harzburgite less than 1%. In contrast, recent work by Daines and Kohlstedt (1993) show that pyroxene has very little effect on the extraction of basaltic melts. Furthermore, experiments on deforming partially molten peridotites by Bussod and Christie (1991) provide evidence that the effects of deforming the peridotite matrix far outweigh the mineralogical effects, and melt can easily separate from the matrix at very low melt fractions. McKenzie's (1984) paper on compaction of partially molten rock centres around the matrix continually deforming and compacting during partial melting to allow the melt to separate, so several lines of evidence point to separation at very small melt fractions. This means that melting of an adiabatically rising mantle is best described by a process close to fractional melting. As will be discussed later in this chapter, the melting residues are more sensitive to the type of melting because of the pooling effect that many of the sampled melts have undergone. Trace element concentrations in clinopyroxenes from abyssal peridotites can only be modelled by near-fractional melting, with some possible melt interaction (Johnson et al., 1990; Johnson and Dick, 1992), which provide direct evidence that melting below ridges is likely to be fractional.

Table 3.1 shows estimated degrees of partial melting for mantles of different potential temperatures using a melt generation rate of 1.2% $kb^{-1}$, and also includes the thickness of crust generated and the temperature and pressure of the solidus intercept. As with Klein and Langmuir (1987) and Kostopoulos and James (1992), the crustal thicknesses are lower than McKenzie and Bickle (1988) because melting only proceeds to the Moho rather than the surface. For high potential temperatures, the latter effect produces some large overestimates in the thickness of crust generated.

| Potential temperature (°C) | 1273.43 | 1316.73 | 1403.08 | 1445.97 |
|---|---|---|---|---|
| Solidus temperature (°C) | 1300 | 1350 | 1450 | 1500 |
| Solidus pressure (kb) | 14.76 | 18.48 | 26.07 | 30.05 |
| Total melting (wt.%) | 21.49 | 24.75 | 29.59 | 31.33 |
| Crustal thickness (km) | 5.62 | 8.212 | 13.96 | 17.11 |

**Table 3.1.** Estimated degree of total melting, crustal thickness and temperature and pressure of solidus intersection for different mantle potential temperatures.

The correlation between crustal thickness generated and total degree of melting in the column should mean that residual peridotites recovered from areas with elevated potential temperatures will be more refractory. Dick et al. (1984) have elegantly shown the relationship between spinel composition and the geoid anomaly in the North Atlantic. The spinels increase their Cr# and decrease their Mg# in the peridotite as the Azores Triple junction is approached. The increase in the depleted nature of the residual peridotites towards a known thermal anomaly led Dick et al. (1984) to propose that the composition of residual peridotites sampled along the world's spreading ridges is directly linked to the thermal structure of the asthenosphere. This observation is in accordance with the models of melt generation below spreading ridges described previously (e.g., Klein and Langmuir, 1987; McKenzie and Bickle, 1988).

The good correlation between the thermal structure of the asthenosphere and the composition of residual peridotites is not surprising. However, if fractional melting is the prevalent melting process in the sub-oceanic mantle then unless there is efficient mixing of the instantaneous melt fractions generated by each increment of melting, it is unlikely that a correlation will exist between the thermal structure of the asthenosphere and the melts generated. Klein and Langmuir (1987) produced a detailed study of basalts from the world's spreading centres and found a strong correlation between the basalt chemistry and the bathymetric depth of the ridge, and thus thickness of crust produced. One of their key observations is the positive correlation of $Na_2O$ with bathymetric depth. As Na is incompatible during mantle melting, the obvious conclusion from this correlation is that the low Na basalts represent higher degree melts. Thus, it is likely that an efficient pooling mechanism does occur below spreading ridges. However, Klein and Langmuir (1989) note that basalts from some ridge systems exhibit local trends which run at at ninety degrees to the global trend on a $Na_8$ versus $Fe_8$ plot and that these may represent instantaneous melts rather than pooled average melts (point and depth average of McKenzie and Bickle, 1988). Furthermore, melt inclusions found in olivines in MORB samples by Sobolev et al. (1991) have incredibly depleted trace element characteristics, consistent with their being instanteous melts from a depleted mantle. Elliot et al. (1991) describe the chemistry of depleted picrites from Iceland in terms of depleted melts from the upper part of the melting column which had lost melt at depth. These last two papers provide strong evidence that fractional melting is an important process in the mantle and that both pooled and instantaneous melts may be samples at the earth's surface.

Two important conclusions can be drawn from the above discussion. Firstly, it is unlikely that many melts we see at the surface can have been in equilibrium with a specific "bit" of the mantle; in fact, Johnson et al. (1990) state that there are no magmas sampled at mid-ocean ridges which are in equilibrium with any abyssal peridotite, based on the trace element content of peridotite clinopyroxenes. The best a magma can relate to in terms of its equilibration history is its average temperature and pressure of melting (see Klein and Langmuir, 1987; Albarède, 1992). Secondly, both instantaneous and aggregated melts must travel through the mantle and may interact with residual mantle higher up the melting column. Some of these points will be developed in the later sections considering the specific melting and melt/mantle interaction models.

### 3.2.3 Melting Above Subduction Zones.

A logical progression from the success of models which predict the volume and composition of melts at mid-ocean ridges and intraoceanic settings, is to apply similar models to melting above subduction zones. As described in Section 1.1 many of the physical parameters required for modelling melting in the mantle wedge are poorly known. However, recently, attempts have been made to model the volume and composition of melts generated above subduction zones (e.g., Plank and Langmuir, 1988; Davies and Bickle, 1991; Pearce and Parkinson, in press). There are considerable differences in these models. Davies and Stevenson (1992) and Plank and Langmuir (1988) can be viewed as end-member models with the models of Pearce and Parkinson (in press) being intermediate to these two.

Davies and Stevenson (1992) present a physical model for the source region of subduction zone lavas (Figure 3.2). Water is generated by a series of dehydration reactions in the subducting slab at various pressures and temperatures. The water generated hydrates the overlying peridotite to form an amphibole peridotite which acts as a mechanical boundary layer between the cold subducting slab and the hot, overlying convecting mantle wedge (Tatsumi, et al., 1983; Davies and Stevenson, 1992). The amphibole peridotite produced is dragged downwards until about 30 kb is reached at which point the amphibole starts to breakdown. Water is released which moves upwards and creates more amphibole which is then dragged down until it dehydrates again. This process continues, and the net effect is to move water across the wedge and into the source region of arc lavas. The effect of introducing water to the source region of subduction zone lavas is to lower the solidus of the peridotite (see Section 3.3.6). The solidus will be defined by the amount of water present (in effect the flux of water per km of arc length) and Davies and Stevenson (1992) predict that a

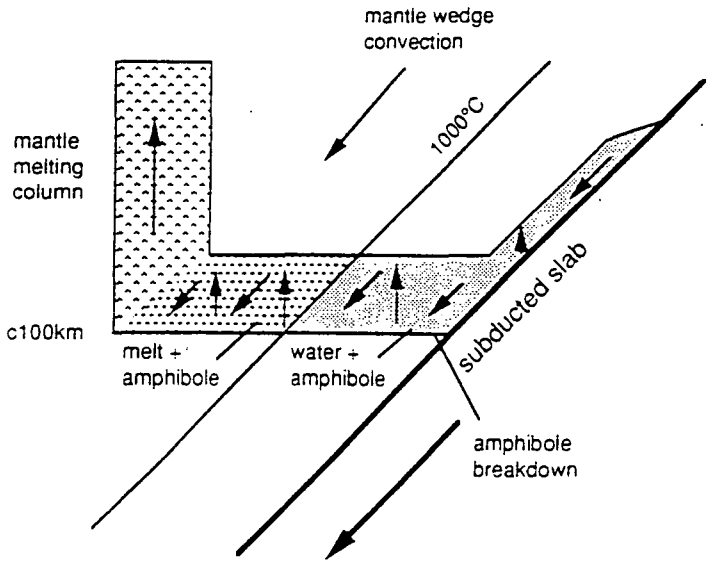


**Figure 3.2**. Mechanism for melting above subduction zones as proposed by Tatsumi et al. (1983) and Davies and Bickle (1991) and Davies and Stevenson (1992). The arrows indicate transport of mantle, aqueous fluid and melt.

water-undersaturated peridotite solidus will be present in the source area. Green (1973, 1976) has undertaken water-undersaturated peridotite melting experiments and Davies and Bickle (1991) have parameterised these experiments so that the amount and composition of melts generated by melting of a water-undersaturated peridotite can be predicted. Davies and Bickle (1991) propose that a maximum of 8-10% melting may generated by this hydrous fluxing mechanism alone, without any recourse for decompression melting.

Plank and Langmuir (1988) using similar arguments to Klein and Langmuir (1987) looked at the relationship between crustal thickness and the chemistry of primitive subduction zone magmas. They believe that the mantle wedge melts by decompression melting and there should exist strong relationships between crustal thickness and lava chemistry. The relationship they find is that island arcs built on thick lithosphere have high $Na_2O$ contents compatible with low degrees of partial melting, whereas arcs built on thin lithosphere have low $Na_6$ ($Na_2O$ content at 6% MgO) values compatible with high degrees of melting. The principal conclusion of Plank and Langmuir (1988) is that the thickness of the lithospheric cap controls the length of the melting column in the mantle wedge and has the greatest influence on the magma chemistry. Furthermore,

they find that the degrees of partial melting in the mantle wedge are similar to those beneath spreading ridges (10-20%).

These two models address different aspects of magmatism above subduction zones but are in many ways contradictory. Davies and Stevenson's (1992) model for the movement of water across the wedge is strongly supported (see Hawkesworth et al., 1993), yet it is difficult to reconcile the small amount of melting that Davies and Bickle (1991) predict to occur within the mantle wedge with the large amount of data available for subduction zone magmas which suggest they are high to very high degree melts, often of a depleted source (Pearce and Parkinson, in press). Plank and Langmuir's (1988) arguments for decompression melting are strong yet there are characteristics of arc magmas which strongly support both the involvement of water (to produce LILE enrichments) and the breakdown of amphibole controlling the characteristic 110 km depth to Benioff Zone feature of so many volcanic arcs. Pearce and Parkinson (in press) consider that these two end member models may both operate. Data for intraoceanic arcs are compatible with high degree melts which in mid-ocean ridges would suggest high potential temperatures. However, there is little evidence to suggest that melting starts in the garnet field (a consequence of high potential temperature) and Pearce and Parkinson (in press) propose that the extra amount of melting is provided by the hydrous fluxing effect that Davies and Bickle (1991) describe. The mantle then decompresss until the dry solidus is crossed and melting then proceeds in a manner similar to that below mid-ocean ridges.

Figure 3.3 shows schematic diagrams for melt generation at a mid-ocean ridge and in the mantle wedge with a thick and thin lithospheric cap. The approximate percentage of melt generated in each situation are also plotted in a manner similar to the diagrams in Eggins (1992). The highest degree of partial melting is generated in a mantle wedge with a thin lithospheric cap. From Figure 3.3 it can be seen that residual peridotites from the top of this melting column would be more refractory than those from the top of a mid-ocean ridge melting column. The composition of melts in intraoceanic subduction zones indicate that their sources are variably depleted with respect to basaltic components, but also variably enriched with respect to LILE and LREE. Recycling of mantle material in the wedge implies that residual peridotites from the sub-arc mantle may be extremely depleted in basaltic components but variable enriched in incompatible trace elements.

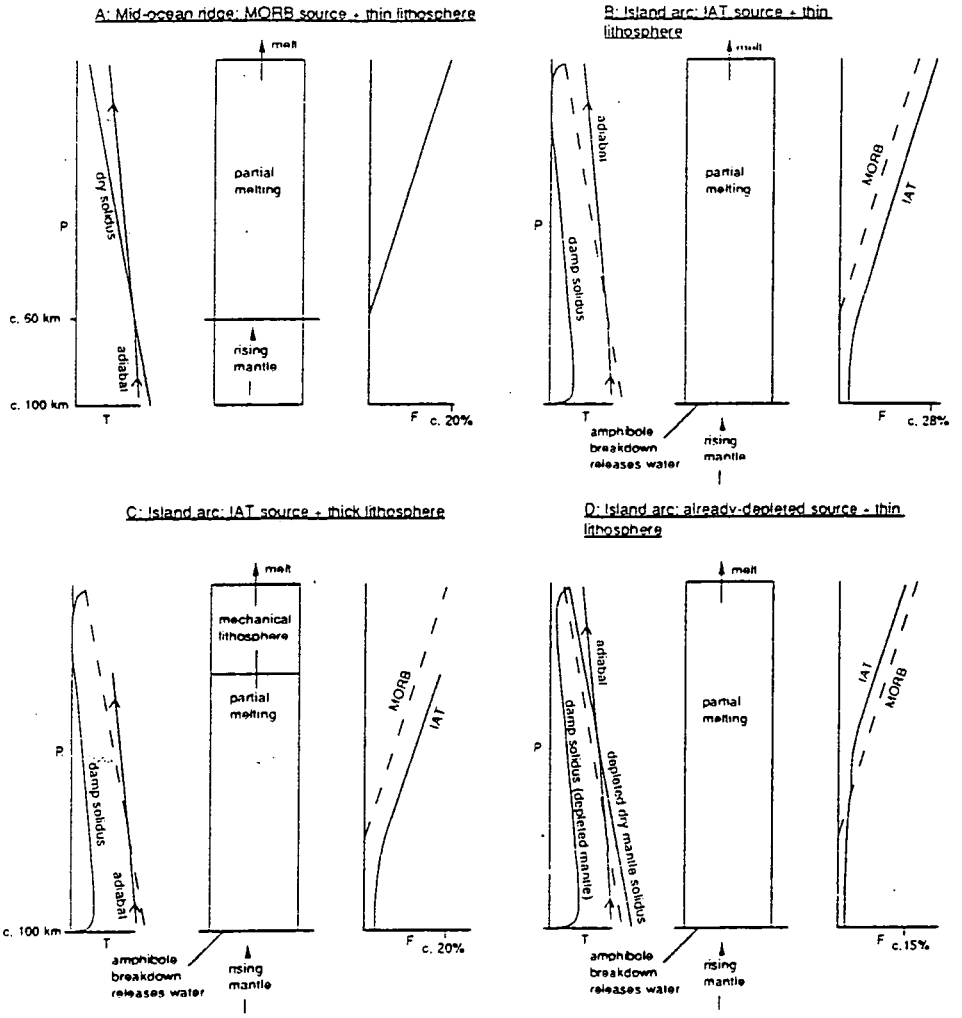


**Figure 3.3**. Melt generation for **a**). a mid-ocean ridge, **b**). an arc volcano built on thin lithosphere, **c**). an arc volcano built on thicker lithosphere and **d**). an arc volcano built on thin lithosphere with a depleted mantle source showing the approximate percentage of melt likely to be generated during the ascent of a mantle column in each case (from Pearce and Parkinson, in press).

## 3.3 Extensive Parameters for Melt Modelling

### 3.3.1 Introduction

This section considers the various parameters which are used in the modelling calculations undertaken in this thesis. These parameters include geochemical and mineralogical composition of the mantle, the melting coefficients most likely for melting in the shallow upper mantle under anhydrous and hydrous conditions, the mineral/melt and mineral/fluid distribution coefficients for mantle minerals and diffusion rates of elements in mantle minerals.

### 3.3.2 Composition of the Mantle

The composition of the upper mantle has been the source of much speculation as it provides one of the most important constraints on the composition of the melts and

residues produced by mantle melting. The composition of the mantle can be defined by two different criteria, its geochemical composition and its modal mineralogy.

Various studies of both the major and trace element composition of the mantle have been published (Loubet et al., 1975; Jagoutz et al., 1979; Hart and Zindler, 1986; Kostopoulos and James, 1992). The results from these studies are used here and are augmented with major and trace element analyses from peridotites from the Ojen Massif, southern Spain which have geochemical characteristics of the fertile upper mantle. Table 3.2 shows the major and trace element compositions the fertile upper mantle used in this thesis.

Isotopic and trace element studies of N-MORB suggest that the source for these melts has been depleted by a previous melting event, which has generated mantle which is incompatible element depleted with respect to bulk-silicate earth (BSE) and occured long enough ago for characteristic isotopic ratios to develop (Zindler and Hart, 1986). This depleted mantle is known in the literature as depleted MORB mantle (DMM). In this thesis it is termed fertile MORB mantle (FMM) as it is still fertile with respect to basaltic components. The reason for changing the terminology is that mantle which has suffered more recent melt extraction events and is strongly depleted in basaltic components is an integral part of melt generation above subduction zones (Pearce and Parkinson, in press) and especially in the generation of boninitic melts (see Crawford, 1989).

Lavas associated with hot-spots may have sources which are enriched in incompatible elements and are more like BSE in composition. These are termed enriched fertile mantle (EFM) here. Also, the sources of some melts generated above subduction zones must be depleted with respect to basaltic components but enriched in incompatible elements (Hickey and Frey, 1982; Pearce and Parkinson, in press). This mantle is termed enriched depleted mantle (EDM) and the trace element composition of this and EMM are also shown in Table 3.2.

The mineralogy of the upper mantle depends on its pressure, temperature and composition. A detailed discussion of the mineral facies found in both the anhydrous and hydrous upper mantle for differing P-T-X conditions is provided in Section 3.3.3. For fertile mantle two different routes can be taken to derive the modal mineralogy. Firstly, point counting of samples which have geochemical characteristics of FMM. Secondly, least squares modelling using the bulk and mineral compositions of the same samples. Kostopoulos (1991) summarises the many different modal compositions

| | BSE | DMM | ERM | EFM | Ojen |
|---|---|---|---|---|---|
| Ni | 2190 | 2020 | 2150 | 2060 | 1972 |
| Cr | 2580 | 2500 | 2500 | 2700 | 2393 |
| Mg | 37.8 | 38.4 | 37.04 | 42.16 | 36.32 |
| Co | 102 | 106 | 105 | 116 | 96.24 |
| Fe | 8.8 | 8.8 | 9.35 | 9.4 | 9.28 |
| Mn | 0.135 | 0.13 | 0.14 | 0.12 | 0.14 |
| Sc | 17.1 | 15.5 | 14.2 | 6.7 | 16.42 |
| V | 82 | 78 | 76 | 40 | 70.63 |
| Ga | 4.5 | 4 | 3.7 | 2.5 | 3.29 |
| Al | 4.45 | 3.75 | 3.3 | 1.89 | 4.01 |
| Ca | 3.6 | 3.25 | 4.35 | 1.2 | 3.57 |
| Y | 4.55 | 3.9 | 8.1 | 2.85 | 3.73 |
| Ti | 0.21 | 0.175 | 0.51 | 0.17 | 0.186 |
| Zr | 11.2 | 9.2 | 95 | 26.8 | 7.85 |
| Nb | 0.71 | 0.2 | 6 | 0.6 | 0.08 |
| Rb | - | 0.177 | - | - | 0.7 |
| Sr | - | 4.32 | - | - | 22.21 |
| Cs | - | - | - | - | 0.17 |
| Ba | - | - | - | - | 13.59 |
| La | 0.62 | 0.31 | - | - | 0.21 |
| Ce | 1.76 | 0.96 | - | - | 0.65 |
| Nd | 1.2 | 0.96 | - | - | 0.72 |
| Sm | 0.39 | 0.39 | - | - | - |
| Eu | 0.147 | 0.147 | - | - | - |
| Gd | 0.518 | 0.518 | - | - | - |
| Dy | 0.644 | 0.644 | - | - | - |
| Er | 0.42 | 0.42 | - | - | - |
| Yb | 0.418 | 0.418 | - | - | - |
| Lu | 0.064 | 0.064 | - | - | - |

not shown above but ERM is

**Table 3.2.** Composition of BSE, DMM, EFM, EDM, and EMM (from Pearce and Parkinson, in press). Also shown is the composition of a fertile peridotite from the Ojen Massif which has a composition similar to DMM.

on what evidence do you make this Zr Nb?

which have been published, of which there is some considerable variation. Kostopoulos and James (1992) and McKenzie and O'Nions (1991) have published modal mineralogies based on modal analyses and least squares modelling respectively for peridotites in different mineral facies. In the light of these studies and some least squares modelling undertaken at Durham the modal mineralogy for a fertile spinel peridotite used is olivine 58%, orthopyroxene 26%, clinopyroxene 14% and spinel 2%. For fertile garnet peridotite the modal mineralogy used is olivine 60.1%, orthopyroxene 18.9%, clinopyroxene 13.7% and garnet 7.3%. The modal mineralogy of an amphibole-bearing peridotite is harder to assess because of the wide compositional range of amphibole. As modelling in this thesis is directed towards melting of hydrous mantle above a subduction zone, pargasitic amphibole is the amphibole most likely to be stable in a fertile amphibole peridotite. The modal mineralogy used is 59.9% olivine, 24.7% orthopyroxene, 3.8% clinopyroxene and 11.6% amphibole (McKenzie and O'Nions, 1991).

### 3.3.3 Melting Coefficients

Melting coefficients are one of the cornerstones of mantle melting models. They represent the proportions of phases entering the melt and so control both the composition of the liquids and the mineral proportions and compositions of the melting residues. Before a detailed study of coefficients is provided it is necessary to consider the possible mineral phases which are stable in the upper mantle under differing P-T-X conditions. The presence of different aluminous phases (plagioclase, spinel, garnet or amphibole) in the mantle is of key importance because of their distinctive mineral/melt distribution patterns.

#### 3.3.3.1 Mineral Facies in the Mantle

The presence of different mineral facies in the mantle has been known for a considerable time. O'Hara (1967) gives a detailed review of the stability fields of various mineral facies in P-T space in the CMAS and CMASH systems. Since that paper there have been a series of experiments on both the position of mineral facies in progressively more complicated (and hence more natural) systems such as the CMASCr and a series of melting experiments using natural peridotites..

#### 3.3.3.2 Anhydrous Mantle

In the absence of water the mineralogy of peridotites thought to exist in the upper mantle is composed of forsteritic olivine, two alumina-saturated pyroxenes and an aluminous phase. This aluminous phase is anorthite at low pressures, spinel at moderate pressures and pyrope garnet at high pressures. Univariant reactions may be

written to describe these facies boundaries (O'Hara, 1967). However, the stability field of these facies as determined in synthetic systems may have limited use when applied to melting in the upper mantle. Furthermore, many of the experiments which generated the position of the stability fields only consider a fertile mantle composition rich in basaltic components such as alumina and calcium, whereas models for generation of basalts by decompression melting have the composition of the mantle varying explicitly with pressure and temperature, with more depleted mantle at lower pressures (e.g. Klein and Langmuir, 1987).

To understand how the positions of the facies boundaries may vary under different P-T-X conditions it is neccessary to look carefully at some of the more recent experimental work as well as the petrology of natural peridotite samples.

#### 3.3.3.3 Garnet-Spinel Transition

**Experimental**

The stabilty of garnet and spinel peridotites has been studied in a number of systems from simple synthetic to natural (MacGregor, 1965, 1970; O'Hara et al., 1971; O'Neill, 1981 and Nickel, 1986). Nickel (1986) summarises much of the earlier work and suggests that the chromium plays a key rôle in increasing the pressure of the transition. In his experiments there is a transition zone where both garnet and spinel are stable. McKenzie and O'Nions (1991) have paramaterised Nickel's data for the transition with respect to temperature and their parameritisation is used here where the spinel-out boundary is defined as

$$T = 666.7P - 400 \tag{3.1}$$

and the garnet-in boundary as

$$T = 666.7P - 533 \tag{3.2}$$

where $T$ is in °C and $P$ is in GPa. For modelling purposes, the transition can be taken as linear across the zone. When modelling decompression paths across the transition, the thickness varies on the potential temperature of the adiabat because each adiabat has a slightly different slope. The pressure at which each transition is crossed needs to be solved by numerical iteration for a given adiabat. The modal mineral change brought about by the reaction garnet peridotite to spinel peridotite has been calculated in the CMAS system by O'Hara et al. (1971) and normalised to spinel as

$$2.2722\ Opx + 0.5936\ Cpx + Sp = 0.9889\ Ol + 2.8769\ Gt \qquad (3.3)$$

**Natural**

Many examples of garnet peridotites exist from peridotite massifs and xenoliths brought up by kimberlite and alkaline magmas. These samples tend to be representative of the continental lithosphere (Menzies et al., 1987). However, garnet has not been reported as a phase within oceanic mantle samples. This is probably because these samples are brought to the surface relatively slowly compared with xenoliths. Furthermore, they also melt as they rise to the surface so that the transition of garnet to spinel is readily accomplished. However, in Johnson et al.'s (1990) detailed ion microprobe study of diopsides from abyssal peridotites, clinopyroxenes in abyssal peridotites associated with hot-spots have REE patterns which are consistent with their having been in equilibrium with garnet at some stage of their melting history. Thus, in areas of elavated potential temperature, where melting is initiated in the garnet stability field, clinopyroxenes that subsequently stabilise in the spinel field can inherit a signature from the breakdown of garnet especially with respect to elements retained in garnet during partial melting such as the HREE, Ti and Sc.

### 3.3.3.4 Spinel-Plagioclase Transition

**Experimental**

The transistion from spinel peridotite to plagioclase peridotite is more difficult to assess from the existing experimental data. Green and Hibberson (1970) and Green and Ringwood (1970) have addressed the question of plagioclase stability in the upper mantle. They define the stability field as being below 8-10 kb in the likely temperature range for the shallow upper mantle. However, the composition of the peridotite used in their experiments was extremely fertile with respect to basaltic components. Recent experimental work by Jaques and Green (1980) is more useful in addressing the question of plagioclase stabilty in a decompressing, melting mantle.

In Jaques and Green's (1980) 1 atm. and 2 kb experiments on both pyrolite -40% olivine and Tinaquilla -40% olivine, melting proceeds rapidly for the first 30 °C above the solidus achieving 5-10% partial melting. The effect on the residual mineralogy is that the initially stable plagioclase dissappears rapidly and MgAl spinel rapidly changes by solid solution to Cr-spinel. The results from these experiments can be incorporated into a melting situation beneath a mid-ocean ridge by considering the composition of the residual peridotite as it melts along a 1280 °C potential temperature adiabat. Melting starts when the solidus is crossed at 15.5 kb and by the time the mantle has reached the likely upper stability of plagioclase (~10 kb) it will have melted at least 7%

if not more. The residual peridotite will be a Cr-spinel bearing lherzolite, depleted in Ca and Al and the formation of anorthite plagioclase from spinel is highly unlikely. The effect of taking more and more depleted peridotites to lower pressures (by melting along higher temperature adiabats), is that the spinel-plagioclase transition is pushed to lower and lower pressures. In reality it is unlikely that Prinzhofer and Allègre (1985) are correct in suggesting that plagioclase is ever stable as a residual melting phase in peridotites in the oceanic upper mantle. It should be noted that recent experimental work by Kinzler and Grove (1992 a,b) has plagioclase as a stable phase in many of their experimental charges at low pressure and a detailed discussion is presented in terms of melt generation in the plagioclase stability field. However, the bulk composition of the peridotite-basalt mixtures in their experiments has CaO and $Al_2O_3$ contents of up to 10%, which allows the stabilisation of plagioclase. The composition of other residual phases in the experiments are also correspondingly too fertile to be representative of the depleted shallow upper mantle.

**Natural**

Plagioclase peridotites have been described extensively from ophiolites (Menzies, 1973; Menzies and Allen, 1974; Dick, 1977; Quick, 1981), the ocean basins (Dick and Fisher, 1984; Girardeau et al., 1988; Johnson and Dick, 1992), and orogenic massifs (Obata, 1980; Zipfel and Wörner, 1992; Rampone et al., in press). Several models have also been put forward for the origins of these plagioclase peridotites, which can be broadly split into two end-members; those which propose that the plagioclase has crystallised from either impregnated or unsegregated basaltic melt; and those in which plagioclase forms from the sub-solidus breakdown of spinel. From the published work on these samples it is apparent that plagioclase peridotites have different origins depending on whether the samples are oceanic or continental.

As noted by Menzies and Allen (1974) and discussed by Dick and Fisher (1984) and Dick (1989) the oceanic plagioclase-peridotites represent (texturally and chemically) the incomplete extraction of basaltic melt from a spinel peridotite and geochemically can be best viewed as the mixing and impregnation of a basaltic melt in a depleted spinel peridotite matrix. In ophiolites, such "plagioclase lherzolites" occur structurally high up in the ultramafic tectonite sections and it is likely that the formation of these impregnated harzburgites is a feature of the interaction of residual mantle with pooled melts below the Moho. Likewise abyssal peridotite samples are from high structural levels, located just below the Moho.

The five phase peridotites described by Girardeau et al. (1988), Zipfel and Wörner (1992) and Rampone et al. (in press) are possibly the only peridotites in which plagioclase may have formed by reaction from spinel as plagioclase. Texturally plagioclase forms coronas around the spinel grains as well as forming granoblastic domains of olivine, plagioclase and pyroxenes. However, the peridotites in both cases have formed by the sub-solidus rise of the mantle during which there was limited melting, so mantle of relatively fertile composition is brought to low pressures. This process seems to be restricted to the initial incipient rifting of continental margins or continental areas which are thinned slowly or where tectonic denudation allows mantle to rise along a sub-solidus path to the surface (Rampone et al., in press). These types of processes do not apply to decompression melting beneath spreading ridges. Finally, the incomplete reaction of spinel to plagioclase in what are often old peridotites suggests that the reaction is somewhat sluggish even in fertile peridotites.

The above discussion suggests that the facies of plagioclase peridotite may never exist in the oceanic upper mantle and that there is no evidence to suggest that plagioclase is either a melting or residual phase during decompression melting of the mantle (cf., Viereck et al., 1989; Kinzler and Grove, 1992b). The presence of true plagioclase lherzolites is resticted to continental tectonic settings. The plagioclase stabilty field found on the top of the inversion diagrams in McKenzie and O'Nions (1991) is somewhat misleading given the melting processes they describe.

### 3.3.3.5 Melting Coefficients During Anhydrous Melting

A detailed study of the many published melting coefficients has been presented by Kostopoulos (1991). There are several methodologies which can constrain the melting coefficients used in melt modelling. Firstly, the most simple method is that the melting coefficients used should produce residual peridotites whose modal mineralogy is consistent with the modal mineralogy trends defined by the abyssal peridotites, as these samples are the only natural examples of residues from anhydrous mantle melting. Secondly, phase petrology provides important constraints on suitable melting coefficients.

#### Olivine and Enstatite

Many published melting coefficients have olivine providing a negative contribution to the melt, that is orthopyroxene melts incongruently to produce olivine plus liquid as discovered by Bowen and Andersen (1914). However, more recent experimental work (see summmary in Morse, 1980) show that, in the absence of water increasing pressure has the effect of making orthopyroxene melt congruently and incongruent melting of

orthopyroxene is restricted to very low pressures (≤3 kb). Furthermore, the addition of iron to orthopyroxenes and olivine further inhibits the incongruent melting of orthopyroxene in the dry system (Morse, 1980). The variation in the composition of mantle olivines in progressively more depleted residues is consistent with their compositional change being related to melting of olivine rather than sub-solidus exchange. Kostopoulos (1991) argues that olivine can contribute no more than 10% of the melting coefficients.

**Diopside**

The modal proportion of diopside in peridotites varies from ~14% in fertile mantle to 0% in depleted harzburgites, decreasing with increasing partial melting. Melting experiments in the spinel-field (Mysen and Kushiro, 1977; Jaques and Green, 1980; Takahashii and Kushiro, 1983) all show that clinopyroxene is the first phase to disappear from the melting residue. Estimates of the degree of melting at which clinopyroxene melts out depend on the pressure of the experiment, but range from 22% to 30%. Such melting experiments simulate equilibrium batch melting and are by definition isobaric. Obviously, these experiments are poor representatives of melting processes in the oceanic mantle which are fractional and polybaric. Kostopoulos (1991) has postulated that the melting of peridotites in the shallow upper mantle can be divided into different domains in which clinopyroxene melts out in different proportions, depending on whether clinopyroxene is "free" or dissolved in orthopyroxene and that clinopyroxene is persistent in melting residues to higher degrees of partial melting than the melting experiments suggest. In truth it is difficult to test these more complicated models of melting until more realistic melting experiments can be developed which simulate polybaric near fractional melting. Furthermore, abyssal peridotites sampled from the ocean basins represent the top of the melting column and thus the total amount of melting for the particular melting column from which they are sampled. Although there is a reasonable range in the modal clinopyroxene composition of these peridotites (commonly 2-10%), there is a paucity in samples which represent very low to moderate degrees of partial melting as these are never sampled by the faulting which exposes the abyssal peridotites. Therefore we do not have a full picture of the melting process from solidus to high degrees of partial melting from natural samples. Finally it should be noted that some Alpine and ophiolite peridotites contain enstatite that is undersaturated with respect to diopside, so that residues from very high degrees of partial melting beyond those found in abyssal peridotites must be present in the oceanic mantle (Dick and Fisher, 1984). The ophiolites from which these orthopyroxenes are found have supra-subducion zone

origins suggesting that such high degrees of melting may be restricted to destructive plate margins (i.e. Bonatti and Michael, 1989; Pearce and Parkinson, in press).

**Spinel**

The modal proportion of spinel varies very little from fertile to residual peridotite (~2%) although its composition varies widely and consistently with other residual minerals (Dick and Bullen, 1984; Bonatti and Michael, 1989). Jaques and Green (1980) demonstrate that MgAl spinel changes by solid solution to Cr-spinel at approximately 30 °C above the peridotite solidus, and that the composition of the spinel becomes more Cr-rich with increasing partial melting.

From the above discussion it is apparent that until clinopyroxene disappears from the melting residues, it dominates the melting coefficients with orthopyroxene, olivine and spinel playing increasingly minor rôles. Although it can be argued that melting in the upper mantle is a far more complicated process, with minerals making up different proportions of the melting mode as melting proceeds, melting coefficients used in modelling in this thesis (until clinopyroxene disappears at 25% partial melting) are olivine 10%, orthopyroxene 32%, clinopyroxene 56% and spinel 2%.

**Garnet**

Melting experiments in the garnet stability field relevent to melting below spreading ridges are more limited but suggest that garnet and clinopyroxene dominate the melting mode (Mysen and Kushiro, 1977). The melting modes used in this thesis are those of Kostopoulos and James (1992), of olivine 1.3%, orthopyroxene 8.7%, clinopyroxene 36% and garnet 54%.

### 3.3.3.6 Hydrous Mantle

The effect of water on the melting conditions and mineral stabilities in peridotites has been difficult to assess for a long time. Even now there is a need for more experimental work on the melting behaviour of peridotites under various hydrous conditions. Experiments involving water have been hampered because of Fe loss to the platinum capsules, the problems of quenching glass and quench overgrowths on phases. The most successful experiments are those of Green (1973; 1976) and Wallace and Green (1991) and much of the following discussion is based on these experiments.

**Experimental**

Figure 3.4 shows the stability of different phases in water under-saturated and water-saturated peridotite melting experiments for mantle of pyrolite composition (Green,

1973). The first diagram shows that the position of the water-saturated peridotite solidus lies at a distinctly lower temperatures than the solidus of anhydrous peridotite. The stable hydrous phase is pargasitic amphibole, which is stable below the solidus and up to 30 °C above the solidus at low pressures. The amphibole breaks down at 28-30 kb at which point the solidus bends round to higher temperatures with increasing pressures. For the water-undersaturated experiments the position of the solidus is distinctly different. Here, the solidus is defined by the stability of pargastic amphibole and the solidus shows a distinct inflection back to lower temperatures at 27 kb when the amphibole begins to break down. In both experiments olivine, orthopyroxene and clinopyroxene are important residual phases above the solidus. Garnet is a persistent residual phase at higher pressures (>20 kb) and at temperatures up to 100 °C above the solidus.

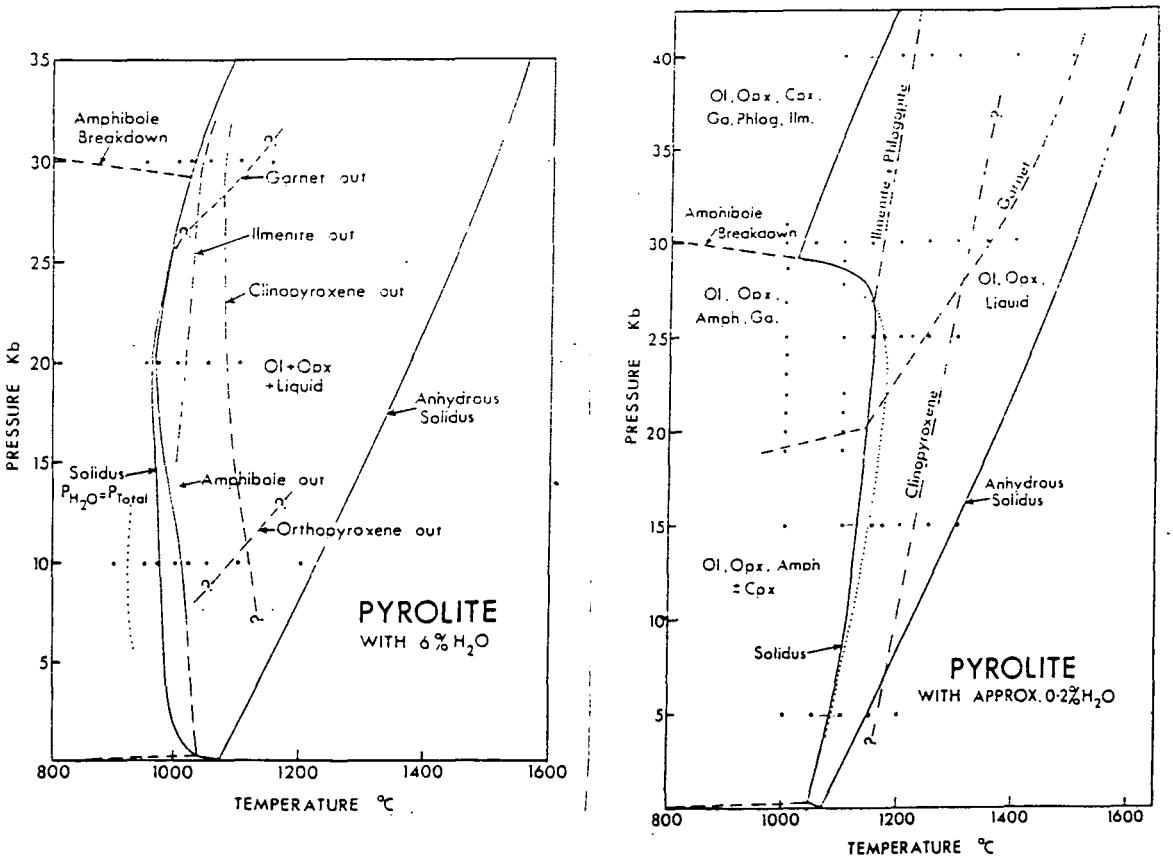


**Figure 3.4.** Experimental determination of **a)**. water-saturated and **b)**. water-undersaturated solidus for pyrolite minus 40% olivine (from Green, 1973). Subsolidus assemblage in **a)**. at 10 kb and 20 kb is olivine + orthopyroxene + amphibole + clinopyroxene, but at 30 kb is olivine + orthopyroxene + garnet + clinopyroxene + phlogopite + titanoclinohumite + ilmenite. In **b)** the subsolidus minerals disappear during melting along the dashed curves marked with the mineral names.

Figure 3.5 shows the results from the experimental work of Wallace and Green (1991). They undertook experiments on the mineral stability and melting behaviour of the more depleted Tinaquilla peridotite under water-saturated and water-undersaturated conditions. The run conditions of these experiments were exactly the same as those in

Green (1973) so direct comparisons of the results can be made. As before, the solidus for the water-saturated peridotite lies at much lower temperatures than the anhydrous solidus. Amphibole breaks down at 26-27 kb, which is at a slightly lower pressure then for water-saturated pyrolite. Again, amphibole is stable for 30 °C above the solidus and clinopyroxene, olivine and orthopyroxene are stable residual phases above the solidus. For water-undersaturated conditions the solidus is again defined by the stability of pargasitic amphibole. The solidus deflects to lower temperatures at the breakdown of amphibole at 26-27 kb. Surprisingly, the melting behaviour of more depleted "wet" peridotite is very different than that of more depleted anhydrous peridotite. With increasingly depleted mantle, the anhydrous solidus is displaced to higher temperatures. With the depleted peridotite under water-undersaturated conditions the lower alkali content of the peridotite restricts the stability of pargasitic amphibole to lower temperatures and pressures and thus forces the solidus to lower temperatures and pressures.

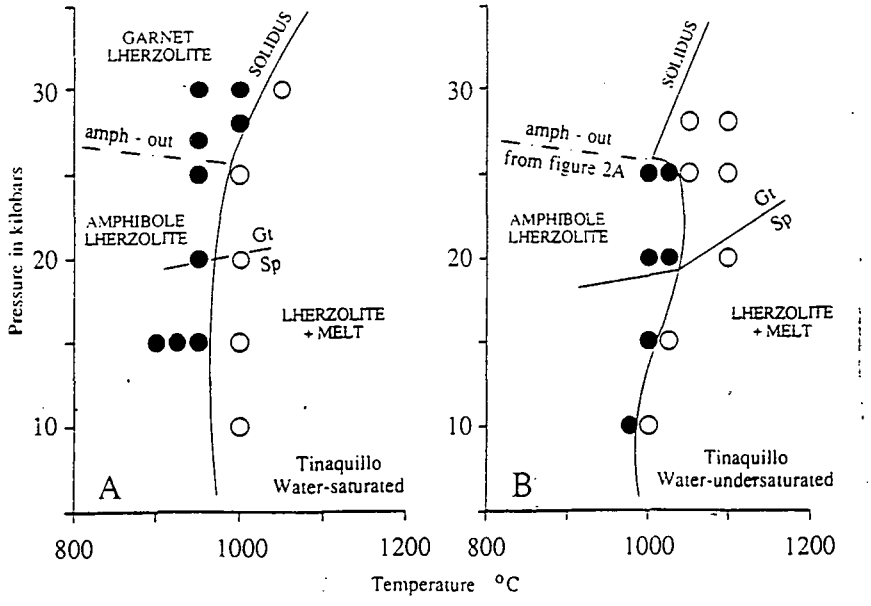


**Figure 3.5.** Phase relationships of Tinaquilla peridotite minus 40% olivine under a). water-saturated and b). water-undersaturated conditions (from Wallace and Green, 1991).

The two papers described above specifically look at the stability of phases in peridotite where the volatile present is water and so hydrous amphiboles are stabilised. Recently, there have been studies on the stability of fluorinated amphiboles (Foley, 1991) and K-rich amphiboles (Sudo and Tatsumi, 1989). These amphiboles are stable to much higher temperatures and pressures than pargasitic amphibole. These phases maybe important in being able to carry water (in amphibole) to great depths (up to 350km), which has major implications for the genesis of back-arc basin lavas and carrying subduction zone signatures into the deep lithospheric mantle (Gibson et al., 1993).

The work of Foley (1991) has the greatest bearing on the potential stability of amphibole in the mantle wedge above subduction zones. The previous discussion on amphiboles argues that hydrous amphiboles are unlikely to be stable in a decompressing, melting mantle wedge. An interesting point from Foley's work is that hydrous amphiboles can change by solid solution to form fluorinated amphiboles and thus facilitate a pressure sensitive dehydration reaction (at 110km?) and yet possibly still stabilise fluoro-amphiboles above the peridotite solidus. An important constraint on this speculation is the amount of fluorine present in the mantle wedge which is likely to be small (J. A. Pearce, pers. comm.). If chlorine has a similar effect to fluorine then the subduction of seawater as inferred from the known elevated chlorine content of arc lavas (Gill, 1981, p. 123) may be important in stabilising these amphiboles.

**Natural**

Amphibole is an important phase in many peridotite samples from oceanic and continental settings. In oceanic samples amphibole has usually formed by influx of hydrothermal fluids and so is secondary in origin (Kimball et al., 1985). Ozawa (1988) has suggested that amphiboles found in ophiolitic peridotites from Japan are formed by the reaction with fluids from dehydration of an underlying subduction zone and are primary in narture. Tatsumi (1989, 1991) has proposed that the formation of amphibole bearing peridotite is a pre-requisite for melt generation in subduction zones. However, the paucity of primary amphibole in arc-related peridotites (this study and many ophiolitic samples) implies that amphibole is an unlikely residual phase during much of the course of melting in the sub-arc mantle. Thus it may only be important during the initial stages of melting above subduction zones as suggested by Pearce and Parkinson (in press).

### 3.3.3.7 Melting Coefficients for Hydrous Mantle Melting

Despite the limited experimental data available, it is clear that hydrous amphibole "melts-out" rapidly once the amphibole stability curve is crossed (Green, 1973;

Wallace and Green, 1991). For melting of an amphibole-bearing peridotite the melting coefficients used are olivine 1.3%, orthopyroxene 8.7%, clinopyroxene 36% and amphibole 54%. Textural studies of the Leg 125 peridotites and phase petrology (Morse, 1980; Fisk, 1986; van der Laan et al., 1989) both provide evidence the the incongruent melting of orthopyroxene is an important process at low pressures and high water content. For this process, the melting coefficients used are 100% orthopyroxene, -70% olivine and 30% liquid based on the reaction stoichiometry of Kelemen (1990).

### 3.4 Distribution Coefficients

#### 3.4.1 Mineral-Melt Partition Coefficients

Among the critical values used in partial melting calculations are the partition coefficients of elements between minerals and melt. For this reason, there have been numerous studies on both the theory and measurement of partition coefficients between different mineral phases and silicate melts. Some studies have concentrated on the distribution of elements between two different phases, which is important in the study of sub-solidus equilibration in peridotites (e.g. Stosch, 1981). Many factors can change the value of a partition coefficient such as temperature, pressure, oxygen fugacity and composition of both the mineral and melt.

The key to using mineral-melt distribution coefficients is that they should be pertinent to the specific problem of interest. For melting in the shallow upper mantle the likely conditions are 1200-1300 °C, 1-30 kb and oxygen fugacities from FMQ-1 to FMQ+1. The variation in oxygen fugacity is based on the likely range within MORB and sub-arc mantle based on the oxygen fugacities calculated from MORB glasses and abyssal peridotites (Christie et al., 1986; Wood et al., 1990) and arc-related peridotites (Wood et al., 1990; Draper, 1991; this study).

Table 3.3 shows the values of the mineral-melt distribution coefficients used in this thesis. Even within the fairly tight bounds of the conditions stipulated above there is a wide range of published values for a given element. One of the major problems with published compilations of partition coefficients is that data is drawn from many different sources. To provide internal consistency for this data set, values have been plotted on Onuma plots (Onuma et al., 1968). These plots also help in interpolating values for elements in minerals where there are no published data. Values in Table 3.3 are based on compilations of McKenzie and O'Nions (1991) and Pearce and Parkinson (in press).

Kostopoulos and James (1992) have critised mantle melting models which utilise single partition coefficient values because of the varying temperature and pressure of the mantle during decompression melting. This critisism is valid as some elements do show strong temperature dependence (e.g. Ni and many of the first series transition elements) and pressure dependence (e.g. Ca and Al). The variation of temperature along a melting adiabat is not too large (approxiamately 100°C along a 1280 °C potential temperature adiabat) so may only affect elements which show very strong temperature dependence. However, pressure does vary substantially along a melting adiabat (13.5 kb for a 1280 °C potential temperature adiabat). Although attempts have been made to produce pressure- and temperature-dependent partition coefficients for elements such as Ca and Al during mantle melting (e.g., Irving, 1978; Hanson and Langmuir, 1978; Mansolis, 1991), there is a large error on some of these coefficients. This is because there is still a need for melting experiments which simulate polybaric fractional melting. Although one of the ultimate aims of igneous petrologists must be to have a set of mineral-melt partition coefficients which are P-T-X-$fO_2$ dependent for melting conditions in the shallow upper mantle, these cannot be calculated at the present time. Accepting that single partition coefficients may not be correct along the whole of a melting adiabat, they do represent a good average for the length of the melting column and, when used in the relevant melting equation, reproduce the compositions found in abyssal peridotites.

Finally, two comments should be made about the partition coefficients. Firstly, vanadium is the only element which shows substantial change in its partitioning behaviour because of the variation in oxygen fugacity, a point noted by Irving (1978) and Shervais (1982). The value for clinopyroxene-melt at an oxygen fugacity of $10^{-12}$ is 0.8 when $V^{3+}$ is dominant whereas at oxygen fugacities of $10^{-10}$ to $10^{-8}$ $V^{4+}$ and $V^{5+}$ are dominant and clinopyroxene-melt coefficient maybe as low as 0.1 (Pearce and Parkinson, in press). Thus, V should be a useful element in discriminating peridotites which have melted under differing oxygen fugacity conditions. Finally, the ratio of some elements behave coherently during melting in the spinel stability field irrespective of pressure, temperature and melt composition. Ti/Zr, Nd/Yb and Dy/Yb are useful ratios as they avoid P-T-X dependence problems (Johnson and Dick, 1992; M. F. Thirlwall, pers. comm.).

### 3.4.2 Mineral-Aqueous Fluid Partition Coefficients

The enrichment of LREE and LILE relative to HFSE in many lavas formed above subduction zones and some metasomatic enrichments in mantle nodules has been ascribed to the interaction of the mantle with fluids selectively enriched in these

| | ol/liq | | opx/liq | | cpx/liq | | gt/liq | | hbl/liq | | Al-sp/liq | |
|---|---|---|---|---|---|---|---|---|---|---|---|---|
| | 1300°C | 1200°C | 1300°C | 1200°C | 1300°C | 1200°C | 1300°C | 1200°C | 1300°C | 1200°C | 1300°C | 1200°C |
| Ni | 9.0 | 15 | 2.5 | 4.5 | 1.5 | 2.5 | 1.3 | 2.5 | 1.5 | 2.0 | 7.5 | 12 |
| Cr | 1.0 | 1.5 | 3.0 | 7.0 | 5.0 | 10 | 5.0 | 10 | 4.0 | 8.0 | 100 | 200 |
| Mg | 3.9 | 4.2 | 2.8 | 3.2 | 1.9 | 2.1 | 2.2 | 2.4 | 1.5 | 1.6 | 3.0 | 3.5 |
| Co | 2.5 | 4.0 | 1.4 | 2.0 | 0.65 | 1.0 | 0.6 | 1.0 | 1.0 | 1.4 | 3.0 | 4.5 |
| Fe | 0.95 | 1.2 | 0.9 | 1.1 | 0.65 | 0.8 | 1.4 | 1.6 | 1.6 | 1.8 | 1.5 | 1.7 |
| Mn | 0.8 | 1.1 | 0.8 | 1.2 | 0.9 | 1.2 | 2.0 | 3.0 | 0.8 | 1.0 | 0.8 | 1.0 |
| Sc | 0.16 | 0.25 | 0.5 | 1.0 | 0.85 | 2.0 | 6.0 | 15.0 | 1.0 | 2.0 | 0.1 | 0.3 |
| V | 0.03 | 0.03 | 0.2 | 0.4 | 0.4 | 0.8 | 0.8 | 1.3 | 1.0 | 2.0 | 0.1 | 0.3 |
| Ga | 0.04 | 0.1 | 0.3 | 0.4 | 0.35 | 0.6 | 0.6 | 1.2 | 1.0 | 1.2 | 4.0 | 4.0 |
| Al | 0.003 | 0.004 | 0.3 | 0.5 | 0.3 | 0.5 | 1.5 | 1.5 | 1.0 | 1.0 | 4.0 | 4.0 |
| Ca | 0.025 | 0.03 | 0.18 | 0.2 | 1.2 | 1.3 | 0.45 | 0.6 | 1.0 | 1.0 | 0.02 | 0.03 |
| Y | 0.005 | 0.015 | 0.08 | 0.15 | 0.5 | 0.7 | 1.0 | 2.0 | 0.6 | 1.0 | 0.001 | 0.01 |
| Ti | 0.01 | 0.04 | 0.11 | 0.25 | 0.35 | 0.4 | 0.3 | 0.4 | 1.2 | 2.0 | 0.1 | 0.15 |
| Zr | 0.005 | 0.008 | 0.04 | 0.06 | 0.15 | 0.18 | 0.2 | 0.3 | 0.25 | 0.4 | 0.01 | 0.02 |
| Nb | 0.001 | 0.001 | 0.01 | 0.01 | 0.06 | 0.08 | 0.1 | 0.01 | 0.3 | 0.6 | 0.01 | 0.02 |
| Rb | - | 0.0001 | - | 0.02 | - | 0.01 | - | 0.0007 | - | - | - | 0.0006 |
| Sr | - | 0.00019 | - | 0.007 | - | 0.067 | - | 0.0011 | - | 0.12 | - | 0.0006 |
| Cs | - | 0.0001 | - | 0.0001 | - | 0.01 | - | 0.0007 | - | - | - | 0.0006 |
| Ba | - | 0.0001 | - | 0.0001 | - | 0.01 | - | 0.0007 | - | - | - | 0.0006 |
| La | - | 0.0004 | - | 0.002 | - | 0.054 | - | 0.01 | - | 0.17 | - | 0.01 |
| Ce | - | 0.0005 | - | 0.003 | - | 0.098 | - | 0.021 | - | 0.26 | - | 0.01 |
| Nd | - | 0.001 | - | 0.0068 | - | 0.21 | - | 0.087 | - | 0.44 | - | 0.01 |
| Sm | - | 0.0013 | - | 0.01 | - | 0.26 | - | 0.217 | - | 0.76 | - | 0.01 |
| Eu | - | 0.0016 | - | 0.013 | - | 0.31 | - | 0.32 | - | 0.88 | - | 0.01 |
| Gd | - | 0.0015 | - | 0.016 | - | 0.3 | - | 0.498 | - | 0.86 | - | 0.01 |
| Dy | - | 0.0017 | - | 0.022 | - | 0.33 | - | 1.06 | - | 0.78 | - | 0.01 |
| Er | - | 0.0015 | - | 0.03 | - | 0.30 | - | 22.00 | - | 0.68 | - | 0.01 |
| Yb | - | 0.0015 | - | 0.049 | - | 0.28 | - | 4.03 | - | 0.59 | - | 0.01 |
| Lu | - | 0.0015 | - | 0.06 | - | 0.28 | - | 5.5 | - | 0.51 | - | 0.01 |

**Table 3.3.** Partition cofficients for olivine-, orthopyroxene-, clinopyroxene-, spinel-, garnet- and amphibole-melt (data sources, McKenzie and O'Nions, 1991 and references therein; Parkinson et al., 1992a and references therein and Pearce and Parkinson, in press and references therein).

elements (Pearce, 1982, 1983; review in Menzies et al., 1987). Compared with our knowledge of mineral-melt partition coefficients, experimental studies of element partitioning between mineral-aqueous fluid and aqueous fluid-melt are very limited. Eggler (1987) provides a review of our current knowledge of the nature of fluids present in the mantle and their properties with respect to dissolving major and trace elements.

### 3.4.2.1 Fluids in the Upper Mantle

Fluids in the upper mantle can be reasonably approximated by the C-O-H system (Eggler, 1987; Wood, 1991). The species of the fluid present in the mantle is controlled by temperature, pressure, oxygen fugacity and mantle mineralogy. At oxygen fugacities between FMQ-1 and FMQ+2, $H_2O$ and $CO_2$ are likely to be the dominant fluid species (Eggler, 1987; Ballhaus et al., 1990; Wood, 1991). The relative stability of hydrous and carbonate phases in the mantle is very important in determining whether free fluids exist. At pressures greater than 16 kb, the stability of carbonate and its strong buffering capacity towards $CO_2$ means that $H_2O$ may exist as a free fluid as long as more $H_2O$ is available than is needed to fully hydrate amphibole or any other stable hydrous phase (Eggler, 1987). At pressures lower than 16 kb, $H_2O$ may again exist as a free phase at $H_2O$ contents greater than 0.3 wt.% because amphibole is a poor buffer of $H_2O$. The low pressure breakdown of carbonates also means that $CO_2$ may also exist in the shallow upper mantle (Eggler, 1987).

The existence of free fluids in the upper mantle is also strongly controlled by their solubility in melts. In the context of melting beneath spreading ridges Michael (1988) has calculated that the mantle source of MORB is essentially anhydrous. Above subduction zones fluids almost certainly exist in the hydrated mantle above the subducting slab, but will be strongly partitioned into the melt phase once melting has been initiated as $H_2O$ behaves as an incompatible element (Michael, 1988). Primitive subduction zone-related melts do have elevated water contents (~2 wt% in boninites; Dobson and O'Neill, 1987; Newman and van der Laan, 1992) but are still water-undersaturated at pressures of melt segregation (Walker and Cameron, 1983). Although Stolper and Newman (in press) assert that there is more than a casual relationship between $H_2O$ and trace element enrichments in subduction zone related magmas, the exact nature of fluid phases in the mantle wedge is still enigmatic.

### 3.4.2.2 Partition Coefficients

Eggler (1987) and Brenan and Watson (1991) have undertaken experiments on the solubilty of major and trace elements in different fluid compositions and their partitioning between mineral and aqueous-fluid. Eggler (1987) has shown that major and trace elements are readily soluble in $H_2O$-rich fluids. However, only the REE are enriched in the fluid relative to a coexisting melt. The solubilty of major and trace elements is very low for $CO_2$-rich fluids and although Eggler (1987) originally suggested that $CO_2$-rich fluids may be efficient carriers of REEs, more recent experimental work has shown that they have extremely low solubilites in such fluids (Meen et al., 1989). Brenan and Watson (1991) have shown that the addition of dissolved salts to $H_2O$ has the effect of reducing the olivine/aqueous-fluid partition coefficient of selected trace elements by up to two orders of magnitude. Furthermore they show that the olivine/liquid partition coefficients behave systematically with the ionic radius of the element under consideration with elements of large ionic radius more strongly partitioned into the fluid (Fig 3.6).

This type of behaviour has been described before (Pearce, 1983; Tatsumi et al., 1986). Hawkesworth et al. (1993) have applied Brennan and Watson's data to fluid processes in the mantle wedge, and have proposed that their mineral-fluid partition values are too high by 2-3 orders of magnitude to develop a trace-element arc signature in the mantle wedge peridotite over a reasonable time scale for acceptable flux rates from the slab. Taken at face value, the interpretation of Hawkesworth et al. (1993) indicates that experiments have yet to be performed with the right fluid composition derived from the slab or that local equilibrium does not occur between the fluid and amphibole peridotite. Until experiments are performed to measure diffusion rates of elements from fluids into mantle minerals under conditions appropriate for the mantle wedge, the exact nature of fluid processes in the mantle wedge is difficult to assess. However, some elements are clearly enriched in the source zone region of subduction zone-related magmas and the correlation between these enrichments and the chemical properties of these elements (i.e. ionic potential) strongly point to fluids playing an important rôle in the genesis of subduction zone lavas (Pearce, 1983; Tatsumi et al., 1986).

## 3.5 Diffusion Coefficients

Knowledge of the rates of diffusion of both cations and anions in mantle minerals at the relevant pressure, temperature and oxygen fugacity conditions of the shallow upper mantle are of great importance in understanding the petrogenesis of peridotites. The information derived from geothermobarometers and many of the more complicated

mantle melting models (e.g. Qin, 1992; Iwamori, 1993) and melt/mantle interaction models (e.g. Navon and Stolper, 1987; Bodinier et al., 1990; Vasseur et al., 1991) require knowledge of diffusion rates.

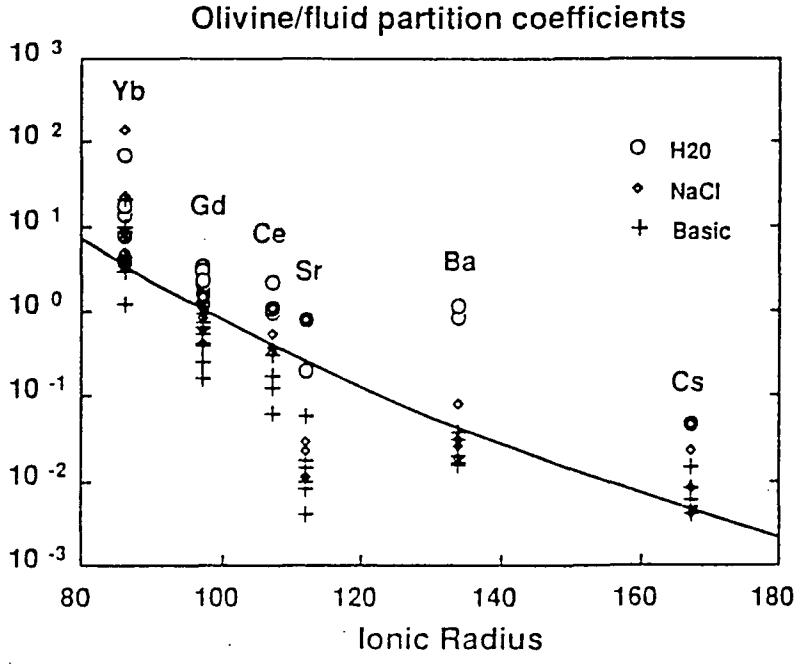


**Figure 3.6.** The olivine/aqueous fluid partition coefficients for Yb, Gd, Ce, Sr, Ba and Cs measured from Brenen and Watson (1991) plotted against ionic radius (R) (from Hawkesworth et al., 1993).

They are a number of publications which address diffusion in silicates during magmatic processes. Hofmann and Hart (1978) have studied how diffusion processes affect the persistence of chemical heterogeneities in the mantle and Hofmann (1980) has reviewed diffusion processes in silicate melts. Freer (1981) provides a useful guide to the terminology of diffusion in silicates and summarises all the relevant diffusion coefficients in silicate minerals and glasses published up to 1981. Chapters by Morioka and Nagasawa (1990), Kramer and Seifert (1990), Chekmir and Epel'baum (1991) and Watson and Baker (1991) in two recently published books are useful guides to the current understanding of diffusion processes in magmatic systems.

Unfortunately there is still a paucity of data on diffusion in mantle minerals. Diffusion of Mg, Co, Ni, Mn and Ca in olivine has been studied by Morioka (1980, 1981, 1983), Ni diffusion in olivine by Clark and Long (1971) and Fe-Mg diffusion in olivine by Buening and Buseck (1973). More data exist for diffusion rates of major elements in pyroxenes (e.g. McCallister et al., 1979; Freer et al., 1982; review by Huebner and Nord, 1981). To date, only two studies exist for trace element diffusion rates in diopsides, those for U and Th by Seitz (1973) and for Sr and Sm by Sneeringer et al.

(1984). A review of cation diffusion in garnets is provided by Chakraborty and Ganguly (1990).

The rate of diffusion in minerals is controlled by a whole host of external conditions such as temperature, pressure, oxygen fugacity, deformation rates and internal conditions such as type and amount of defect density, mineral composition, valency and ionic radius of diffusing element and crystal structure. Detailed discussions of the effect of these different conditions on diffusion rates is beyond the scope of this thesis. However, the results of some of the experiments mentioned above are pertinent to melting and melt/mantle interaction processes in the mantle.

The experiments on Sr and Sm volume diffusion in diopside by Sneeringer et al. (1984) reveal some of the effects that temperature, pressure and defect density have on diffusion rates. The relationship between temperature and diffusion rate can be described by the well-known Arrhenius equation (Freer, 1981; Sneeringer et al., 1984) such that

$$D = D_0 \exp\left[\frac{-Q}{RT}\right] \tag{3.4}$$

where $D$ is the diffusion coefficient, $D_0$ is the pre-exponential term, $Q$ the activation energy, $R$ the gas constant and $T$ the temperature in °K. Data for Sr and Sm diffusion in diopside can be fitted to Arrhenius equations giving diffusion rates in the range $10^{-14}$ to $10^{-16}$ $cm^2$ $s^{-1}$ for temperatures between 1250 and 1100 °C. Sneeringer et al. (1984) also show that increasing pressure of the experiments has the effect of increasing the diffusion rates. Finally, their experiments on natural and synthetic diopsides show that the diffusion rates in natural diopsides are two orders of magnitude faster than those measured in synthetic diopsides. This increase in diffusion rate is thought to occur because of the higher defect density in the natural samples.

The final result discussed above has important implications for volume diffusion rates in minerals during decompression melting in the mantle. Deformation-enhanced diffusion is a well known phenomena in metamorphic geology (Cohen, 1970; Yund et al., 1981; Bell et al., 1986; Kramer and Seifert, 1990). Essentially, the increased strain during deformation sets up dislocation gradients which produce chemical potential gradients which in turn drives the diffusion of cations (Bell et al., 1986). Although only a few experiments exist on deformation of partially molten peridotite, the work of Bussod and Christie (1991) show that local chemical equilibrium between melt and

minerals is achieved in a very short time (<720 hours) in their experiments. Bussod (1991) and Bussod and Christie (1991) show that grain size reduction and recrystallisation occurs readily when molten peridotite is deformed. These processes and the high defect densities in minerals that are likely during decompression melting mean that the diffusion rates that Sneeringer et al., (1984) quote for natural diopside are likely to be minimum values, and may be higher by two orders of magnitude in the light of Kramers and Seifert (1990) work on the effects of strain on the diffusion rates in feldspars.

## 3.6 Modelling of Mantle Melting and Melt/Mantle Interaction

### 3.6.1 Trace Element Approaches

Since the publication of the classic papers by Gast (1968) and Shaw (1970) on the quantitative analysis of the behaviour of trace elements during melting there have been numerous papers using such approaches to understand the petrogenesis of both volcanic and plutonic rocks. There are two approaches in using trace elements to understand melting processes: forward models, where input parametres can be varied to try to reproduce the compositon of liquids and residues during melting; and inverse models, in which the composition of melts are inverted in an attempt to look at source composition or melt fraction with depth. Both methods have their virtues and problems. Forward models tend to be easier to manipulate yet can have so many variable parameters that it can be difficult to assess the effects of these parameters on the petrogenesis of any one sample. Inverse methods tend to be far more complicated mathematically and difficult to use, but try to yield a unique answer for a given set of conditions.

I use forward modelling methods here for ease and because no continuous equations yet exist for more complicated melting models. By writing simpler discontinuous equations and iterating them over very small steps a very good approach to the answers from the continuous expressions may be had. In agreement with Richter (1986) and Williams and Gill (1989), forward modelling with careful use of the input parameters can provide much information about melting processes. To illustrate in detail how different melting models affect the composition of both liquids and residues during melting, worked examples of both some of the more commonly known melting processes such as described in Shaw (1970) and some new and more complicated melting models are provided. Descriptions of the equations used can be found in Appendix C. To facilitate easy comparison with previous work concentrations in the liquids and residues relative to the concentration in the original solid are plotted against the degree of melting. Rather than use a single D value, three elements have been

chosen which have different D values for the four main mantle minerals. These are Ce a highly incompatible element, Yb a moderately incompatible element and Ni a compatible element. The original modal composition is 58% olivine, 26% orthopyroxene, 14% clinopyroxene and 2% spinel. the melting mode is 0.10 olivine, 0.32 orthopyroxene, 0.56 clinopyroxene and 0.02 spinel and proceeds over the range of partial melting thought to exist in the mantle (0-25%).

### 3.6.2 Equilibrium Batch Melting

Equilibrium batch melting is probably the simplest melting model, although not necessarily the simplest physically. The melt generated does not leave the matrix and is in chemical equilbrium with it. Figure 3.7 shows the compositions of liquids and residues for a highly incompatible, moderately incompatible and compatible element. The liquids have high concentrations of the incompatible elements initially but level off to relatively constant compostions at moderate to high degrees of melting. The compatible element increases very slightly with degree of melting. In the residues, the concentration of the highly incompatible and moderately incompatible element drop off steadily, and the concentration of the compatible element increases steadily.

### 3.6.3 Fractional Melting

Fractional melting can be seen as the other extreme from equilibrium batch melting. Every infinitesimal drop of melt produced is in equilibrium with the residue but is then completely extracted. From Figure 3.8 it can be seen that the highly incompatible elements have extremely high concentrations in the first few melt fractions, but their concentrations drop off rapidly at higher degrees of melting. However, the concentrations of the incompatible elements in the aggregated fractional liquids are very similar to those of batch equilibrium melts. In contrast, the concentrations of incompatible elements in the melting residue are depleted very rapidly. Fractional melting can thus produce strong fractionations of incompatible element ratios in residual peridotites.

### 3.6.4 Incremental Melting

Incremental melting can be viewed as an intermediate process between equilibrium batch melting and fractional melting. The melt fraction at which melt is extracted can be varied. As the melt fraction decreases the compositions of instantaneous liquids and melting residues tend towards those of fractional melting. If the melt fraction is increased, the compositions of liquids and residues tend towards those of batch equilibrium melting. Figure 3.9 shows the effect of varying the melt fraction present before extraction.

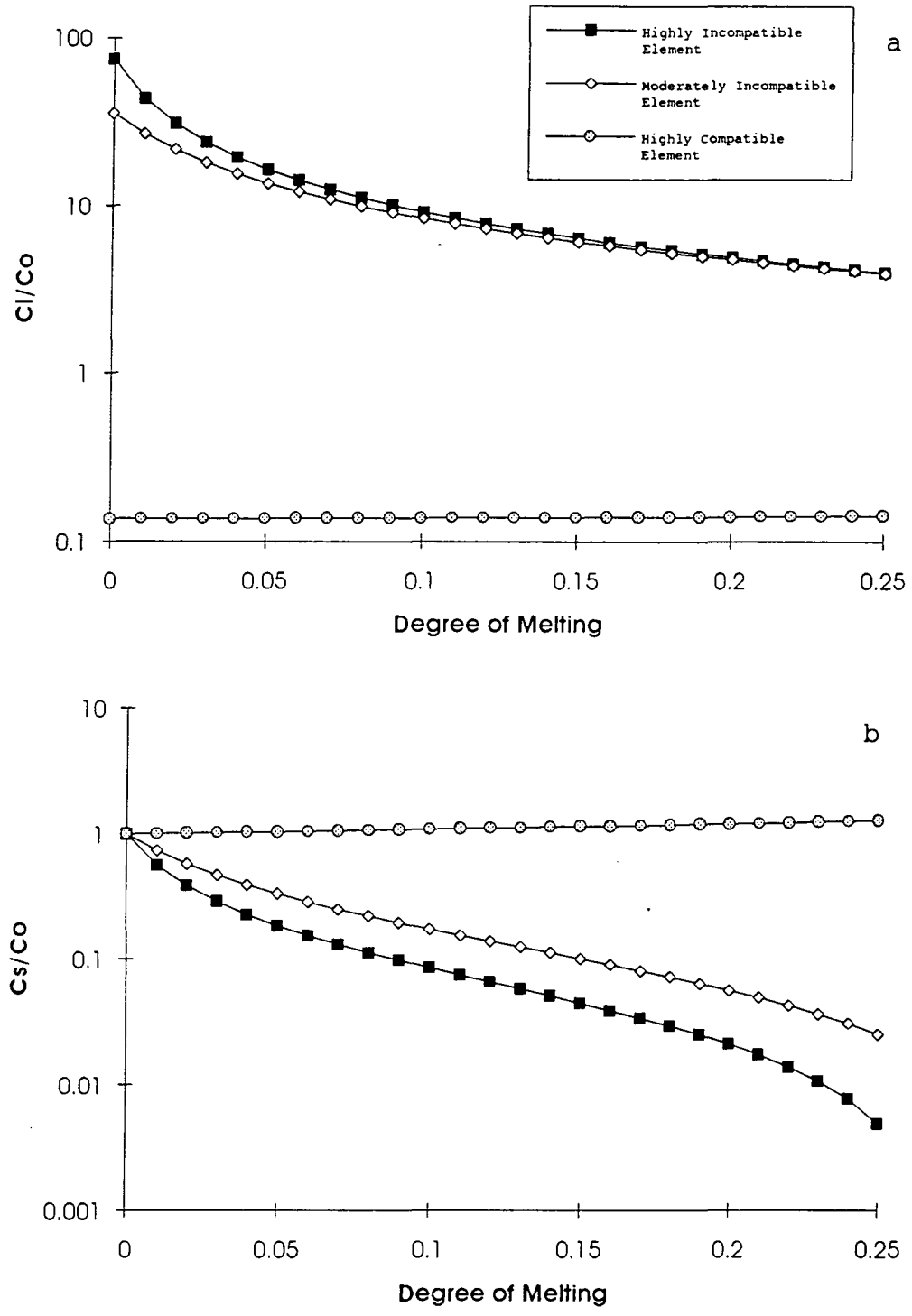


**Figure 3.7** Plot of **a**). liquids and **b**) residues during equilibrium batch melting for a highly incompatible, moderately incompatible and highly compatible element (see text for details).

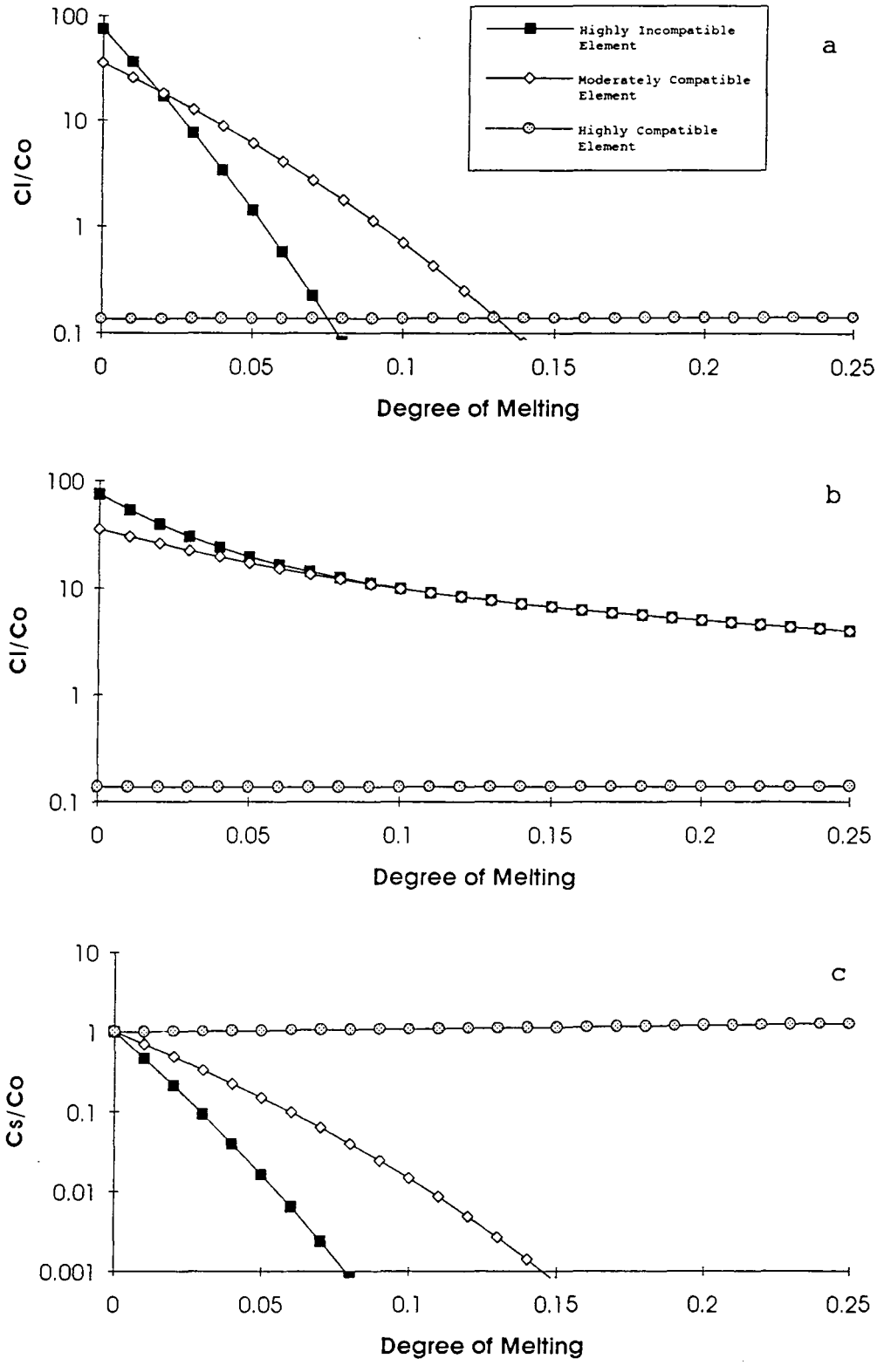


**Figure 3.8** Plot of **a**). instantaneous liquids, **b**). aggregated liquids and **c**). residues for a highly incompatible, moderately incompatible and highly compatible element during fractional melting.

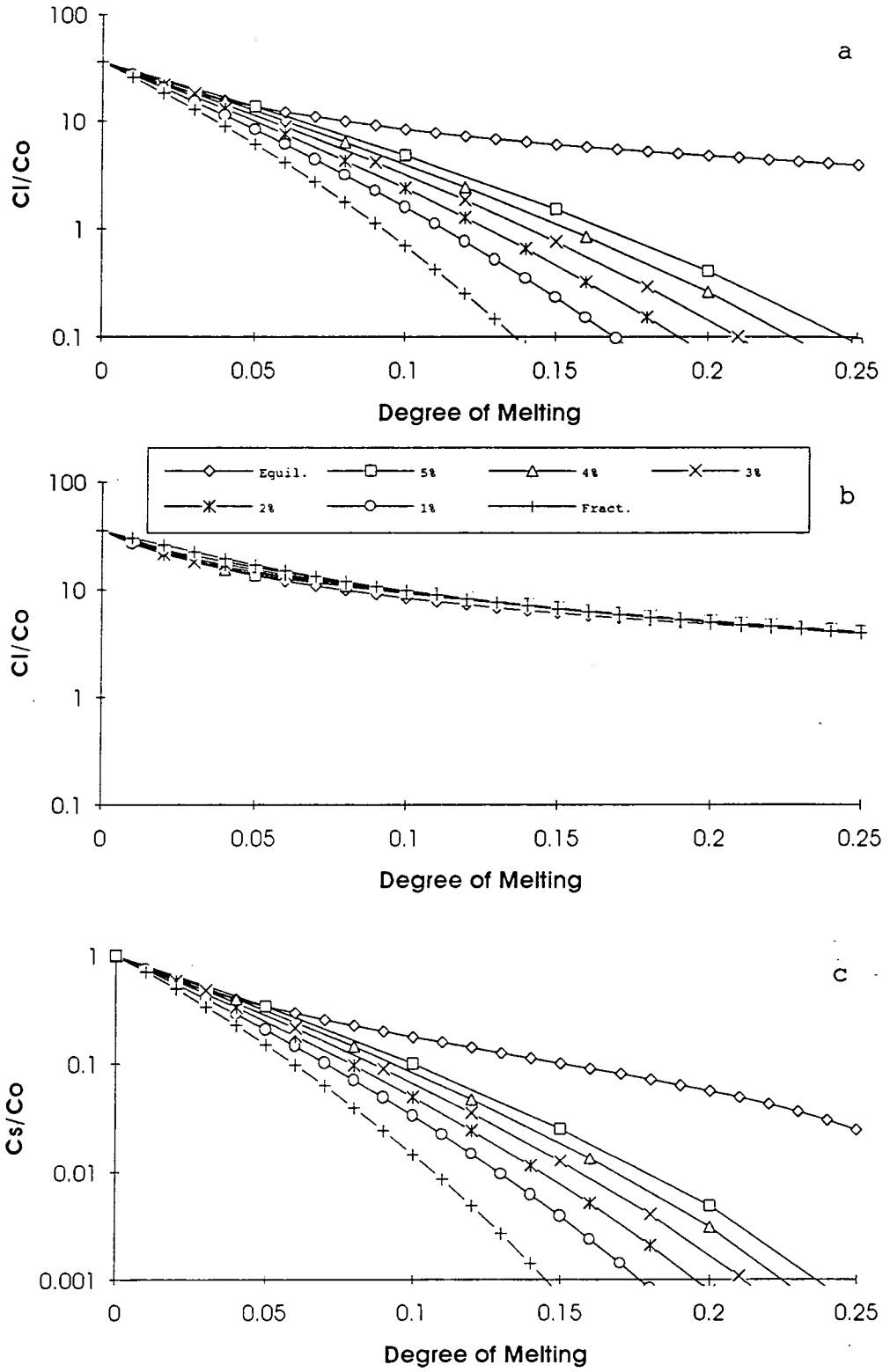


**Figure 3.9** Plot of **a**). instantaneous liquids, **b**). aggregated liquids and **c**). residues incremental melting, The patterns are generated for a moderately incompatible element and 1, 2, 3,4 and 5% melt increments. Fractional and equilibrium batch melting compositions are also shown.

### 3.6.5 Disequilibria Melting

Disequilibrium mantle melting was first proposed by O'Nions and Pankhurst (1974) to explain variations in the Sr isotope composition of mid-Atlantic ridge basalts. Although Allègre and Minster (1978) formulated equations for disequilibrium melting, it was not until Prinzhofer and Allègre (1985) developed melting models to explain the U-shape REE patterns of the New Caledonia ophiolitic peridotites that this type of melting model became popular. Recently Bedard (1989) and Sawyer (1991) have further popularised the model. During disequilibrium melting the mineral phases melt out either modally or non-modally with their own composition. Thus, the composition of the liquids are independent of the degree of melting. During non-modal disequilibrium melting the liquid stays constant throughout the melting and is a function of the melting mode and the initial concentration of the solid. The residues do vary with degree of partial melting but the residual minerals keep their original composition (see Appendix C). Figure 3.10 shows the composition of the liquids and residues generated during non-modal disequilibrium melting. The liquids have very different compositions to those generated by any other type of melting and the compatible element has especially high concentrations. For the residues the concentrations of the incompatible elements drop off at a fairly constant rate and are very much a reflection of the fact that clinopyroxene melts out the fastest and contains the highest proportion of the incompatible elements.

### 3.6.6 Dynamic Melting

McKenzie (1985) describes a melting process which he termed dynamic melting, although Langmuir et al., (1977) and Wood (1979) had previously proposed similar processes. McKenzie envisages that the mantle melts with a continuous porosity (rather than the discontinuous one as in the incremental melting model). The melt in this porosity is continuously filled with melt which has the composition of the instantaneous liquids as melt from the previous increment of melting is extracted. The effect of having a porosity is to increase the incompatible element concentrations in the melting residues and decrease their concentration in the small degree partial melt fractions. Figure 3.11 shows the effect of having various amounts of porosity during melting. These have been modelled slightly differently from the equations of McKenzie (1985) which do not achieve mass balance at low melt fractions (see Appendix C). Here, the porosity is represented by a phase with a distribution coefficient of one so it will be in equilibrium with the instantaneous melts.

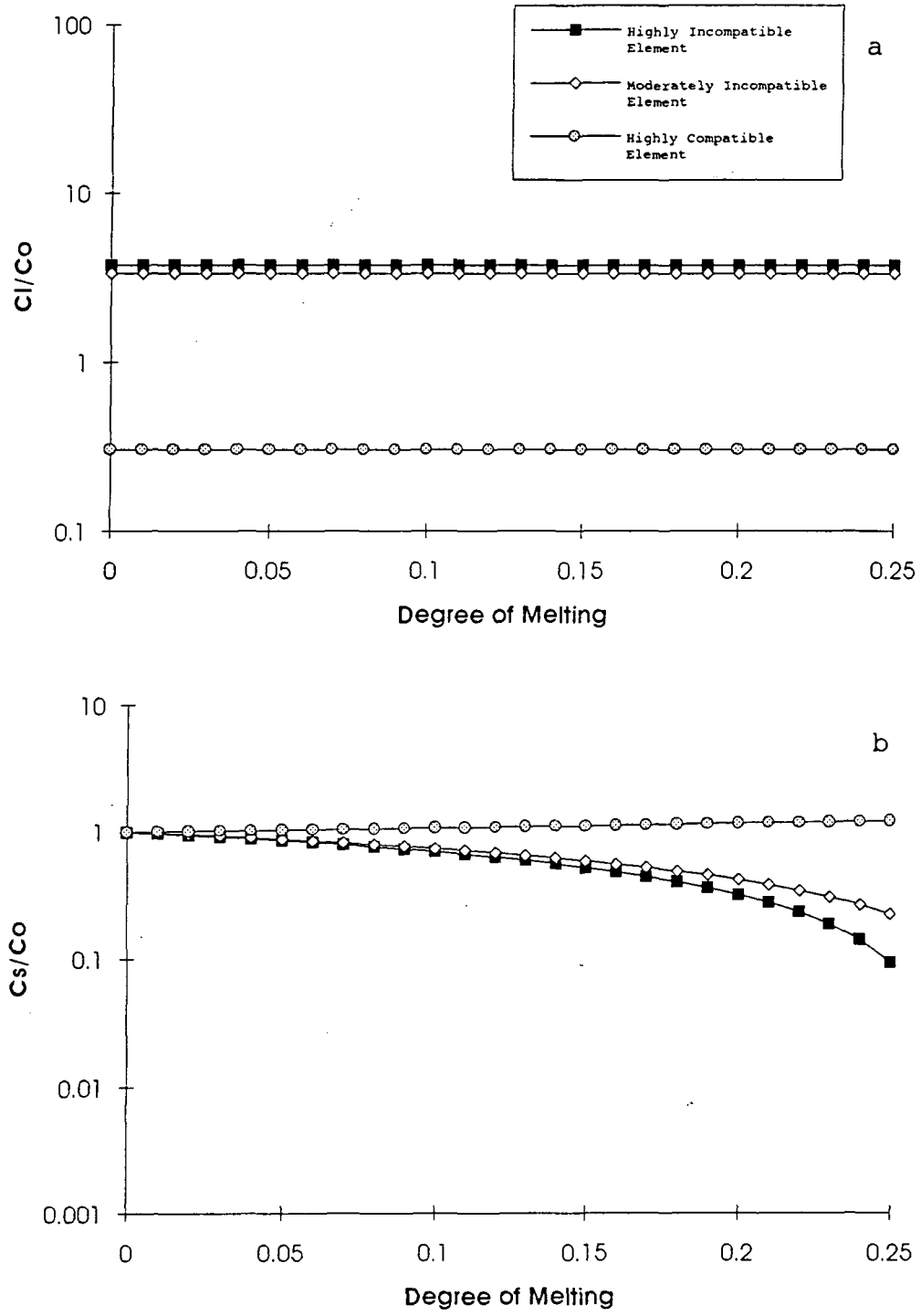


**Figure 3.10** Plot of **a**). liquids and **b**). residues for a highly incompatible, moderately incompatible and highly compatible element during disequilbrium melting.

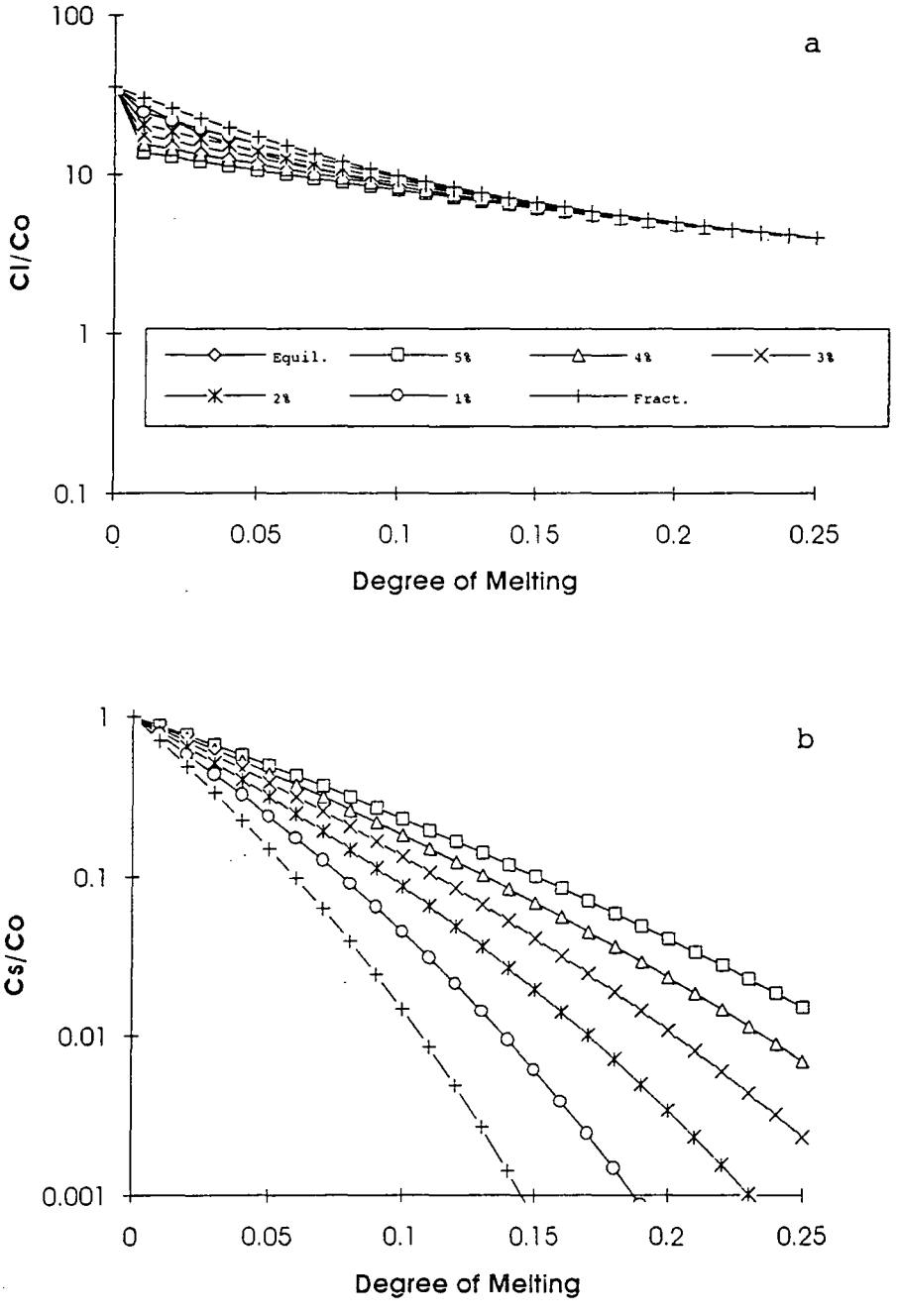


**Figure 3.11** Plot of **a**). aggregated liquids **b**). residues for dynamic melting. The patterns are generated for a moderately incompatible element and 1, 2, 3, 4 and 5% porosity. Fractional and equilibrium batch melting compositions are also shown.

### 3.6.7 Partial Disequilibrium Melting

Recently, Qin (1992) and Iwamori (1993) have studied the effects of disequilibrium partial melting. Their treatment of this type of phenomenon is different from that envisaged by Prinzhofer and Allègre (1985) and Bedard (1989). All the models described earlier in this chapter (except disequilibrium melting) assume instantaneous equilibrium between mineral and melt, even in the case of fractional melting, so the partitioning of elements is described by an equilibrium partition coefficient. Qin (1992) suggests that, for complete equilibration to occur, the rate of melting must be similar to the rate of diffusion of elements through the residual mineral grains. If this is the case then melting is described by equilibrium batch melting or fractional melting if melt segregation is efficient. If the rate of melting is far greater than the rates of solid diffusion then melting is described by the disequilibrium melting models of Bedard (1989). Qin (1992) proposes that during melting in the mantle a case somewhere in between these end members occurs. Qin (1992) provides partial differential equations which need to be solved numerically to describe this intermediate process (see Appendix C). To quantify the effect of disequilibrium, Qin calculates a Non-Equilibrium number (NE) which is shown on a plot of melting rate versus diffusion rate on Figure 3.12. The value of this NE is a function of the melting rate, the diffusion rate and the grain size. Decreasing the grain size has the effect of reducing the likelyhood of disequilibrium (see discussion at end of chapter).

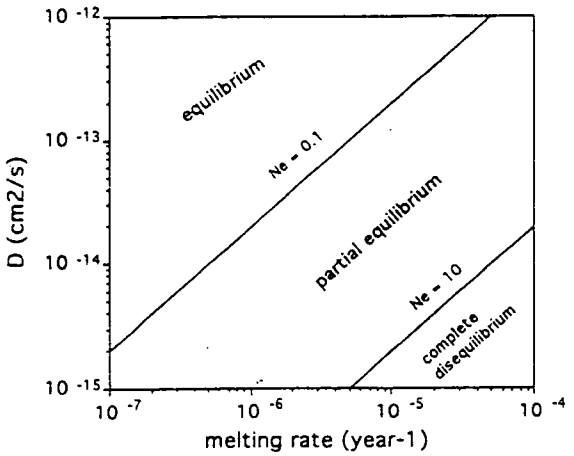


**Figure 3.12**. Mapping of different melting behaviours for highly incompatible elements ($D$ <0.01). on a melting rate versus diffusion rate plot. Parameters chosen are a grain size of 0.5 cm diameter, a residual porosity of 1%. Increasing the grain size and/or decreasing the residual porosity will shift the boundaries upwards (after Qin, 1992).

Iwamori (1993) expands the problem to consider dynamic melting in which melt segregation takes place by porous flow and diffusion-controlled chemical equilibrium has to be considered. The effect of these melting models is that, with increasing disequilbrium lavas are less enriched in the highly incompatible elements and the residues are thus less depleted. The implications for the compositions of melting

residues are difficult to assess quantitively because there are such limited data for diffusion rates of different cations in mantle minerals. However, a qualatitive estimate would be that highly incompatible elements will show the disequilibrium effect the most (i.e., Figure 4, Qin, 1992) and so reduce a ratio such as Ti/Zr in the melting residues.

### 3.6.8 Open System Melting Models

Johnson and Dick (1992) describe a process in which decompressing mantle in a melting column may interact continuously with transient melts generated within the column. From the description of their model provided in Johnson and Dick (1992), the mantle melts fractionally but with a small porosity. At any point above its solidus the mantle may interact with the aggregated melt generated at that point in the column. The aggregated melts are presumably pooled externally before they interact with peridotite. The residual mantle is forced into equilibrium with a specified fraction of the aggregated melt and a new residual composition is calculated for each increment. The effect on the composition of the residual peridotite depends on the both the mass fraction of aggregated melt it equilibrates with and the respective composition of the peridotite and melt.

Johnson and Dick (1992) have used this type of modelling to demonstrate how trace element concentrations and certain trace element ratios such as Ti/Zr and $[Nd/Yb]_N$ in abyssal peridotite clinopyroxenes show very distinct changes at high degrees of melting (see Figure 3.13). At low degrees of melting the trace element concentrations in the peridotite are high and buffered by the melt composition whereas, at high degrees of melting, even equilibrating with small amounts of the aggregated melt has a profound effect on the very depleted peridotite. On Figure 3.13 it can be seen that a peridotite equilibrating continuously with 0.5% melt flattens out the Ti/Zr ratio in the residual clinopyroxene and decreases the $[Nd/Yb]_N$ ratio with increasing degrees of melting. Interacting with larger amounts of melt tends to send clinopyroxene compositions back down the trend defined by lower degrees of melting and reproduces the type of melt/mantle interaction trends that Elthon (1992) has proposed to explain the trace element composition of abyssal peridotite clinopyroxenes. The composition of the aggregated liquids in this model is very similar to those of aggregated fraction melts.

### 3.6.9 Mantle/Melt Interaction Models

Over the last ten years there has been a succession of models which look at the geochemical effects of interacting melts with mantle, from simple models of melt moving through a static mantle (Navon and Stolper, 1987; Bodinier et al., 1990), to

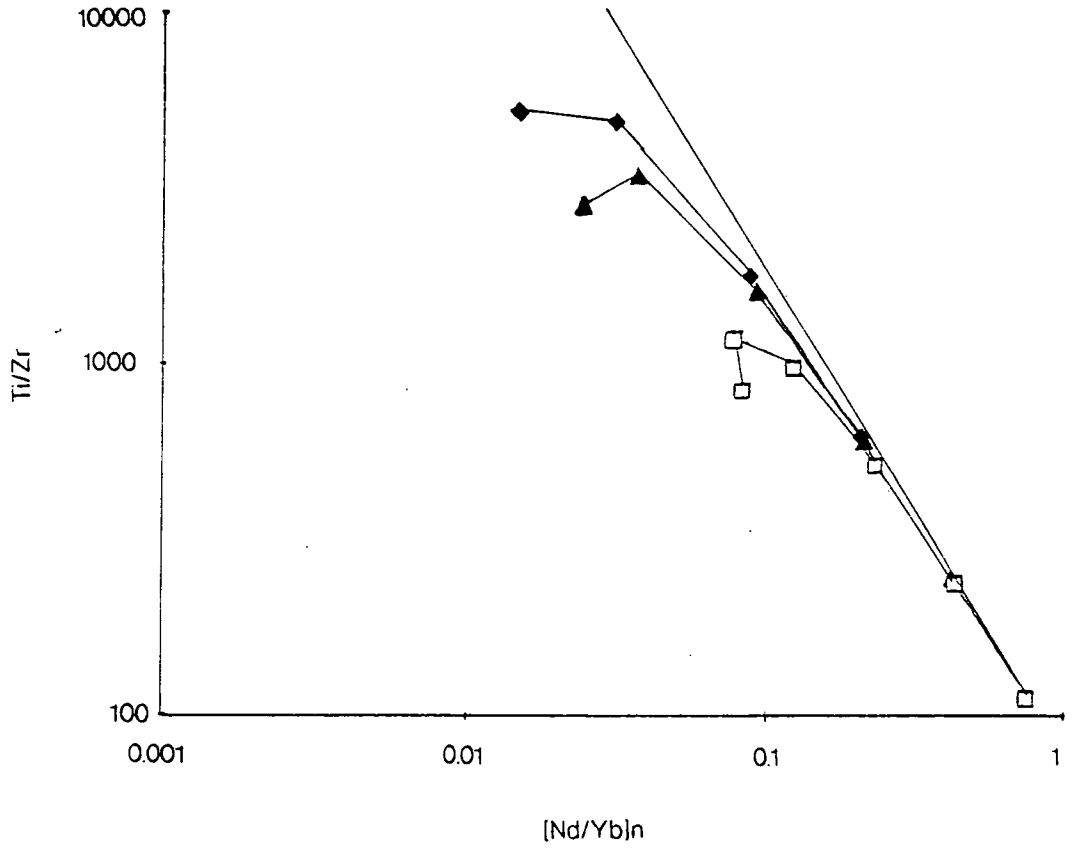


**Figure 3.13.** Plot of Ti/Zr against $[Nd/Yb]_N$ in residual clinopyroxenes showing the effects of open system melting. Solid line is fractional melting, 0.5% trapped melt (solid diamonds), 1% trapped melt (solid triangles) and 5% trapped melt (open squares). Each trend represents 0-25% melting.

complicated models of melting, melt migration and melt interaction (Qin, 1992; Iwamori, 1993). Also, a series of papers by Kelemen and co-workers (Kelemen, 1986; Kelemen, 1990; Kelemen et al., 1990; Kelemen at al., 1992) consider specific mantle/melt interactions and have proposed that such processes may be prevalent within the upper mantle and have major influences on the genesis of calk-alkaline lava series.

The following sections describe the geochemical effects of some of these models. Some of these models are applied and discussed further in chapters four and five to the mineral and whole-rock data. A more general discussion of the validity of these models within the upper mantle is provided in chapter six.

Langmuir et al., (1977) provided the first quantitative model of mantle/melt interaction in their dynamic melting model where they had a small amout of melt trapped after each melting increment. However, they concentrated on the composition of the liquids generated by such melting and simply stated that it seemed physically realistic that not all of the melt generated would separate during melting.

### 3.6.10 Geochemical Effects of Melt Percolation

McKenzie (1984) and Navon and Stolper (1987) have described models whereby the mantle acts as a chromatographic column for the melts percolating through it. As a melt percolates through the mantle elements will move with a velocity related to their incompatibility with respect to the mantle through which it is travelling. The incompatible elements will travel with a faster effective velocity than the more compatible elements. During this percolation process the composition of both the melts and the matrix change. In front of the percolating melt the matrix retains its original composition whereas behind the percolating melt the composition of the matrix is equal to the composition of the original liquid times the bulk distribution coefficient of the matrix.

Vasseur et al. (1991) develop the models of melt percolation further by taking into account diffusion into the solid. Rather than assuming instantaneous equilibration between fluid and matrix, the composition of the solid is controlled by the volume diffusion rate of an element into the solid. The amount of equilibration between the fluid and matrix is then a play-off between the diffusion rate into the solid, the percolation rate of the fluid and the grain size of the matrix. Obviously, a fine-grained matrix will have a better chance of equilibrating with the melt at a given diffusion and percolation rate. Finally, given the low values for diffusion rates of elements in mantle minerals the model calculations are very sensitive to percolation velocity.

Apart from the effects of changing the percolation velocity and grain size of the matrix several other parameters may be varied in the melt percolation models, includ the initial composition of the percolating melt. Finally, the geochemical effects of melt percolation have strong temporal variations. If the matrix through which the melts percolate is viewed as a column with length $T_C$, then the most incompatible elements will reach the end of the column first. With time the compatible elements will also reach the end of the column. Therefore, for strong fractionation of the highly incompatible to compatible elements to be preserved in the matrix it is necessary to switch-off the percolation process before the more compatible elements have reached the end of the column.

### 3.6.11 Kelemen Melt/Mantle Interaction Models

As noted above, Kelemen and co-workers have described the interaction of mantle-derived melts with the peridotite wallrock through which they are travelling (Kelemen, 1986; Kelemen, 1990; Kelemen et al., 1990; Kelemen at al., 1992). The following section describes one of the reactions that Kelemen et al., (1992) have postulated to be important in the continental and sub-arc mantle, that is the reaction of lherzolite with a mantle derived melt to produce harzburgite plus a modified melt. If this reaction is important in generating depleted harzburgites in the sub-arc mantle then the Leg 125 peridotites provide a good test for Kelemen's models.

In this section, the distribution coefficients and melt proportions that are given in Table 1 of Kelemen et al. (1992) are used. The specific reaction that Kelemen studies is the dissolution of clinopyroxene and spinel from the lherzolite and the precipitation of orthopyroxene and olivine. The problem is treated using the assimilation and fractional crystallisation (AFC) models of DePaolo (1981). Under isoenthalpic conditions this reaction involves a mass assimilated ($M_a$) mass crystallised ($M_c$) ratio of 0.97 so that the mass of the liquid decreases with increasing reaction. The composition of the residue, the residual clinopyroxene, the reacting liquid, and the clinopyroxenes that could be precipitated from the reacting liquid, have been calculated for varying input parameters. The composition of the clinopyroxene which would be precipitated from the liquid has been calculated because these are the clinopyroxenes which are plotted in Figure 1 and 2 of Kelemen et al., (1992).

The input parameters which may be varied are the original composition of the mantle, the original composition of the liquid, the $M_a/M_c$ ratio, and the ratio of mass of original liquid ($M_m$) to mass of original peridotite ($M_p$). Varying the last parameter has very strong effects on the composition of the liquid and clinopyroxene which may precipitated from it. If the $M_m/M_p$ ratio is large (>0.1), then to completely react the lherzolite to form harzburgite involves crystallising 2% or less of the liquid for a $M_a/M_c$ ratio of 0.97. The concentration of Nd in the residues and liquids is shown in Figure 3.14. The Nd concentration in the liquid does not increase greatly and the residue drops steadily producing concentrations similar to those from equilibrium batch melting. The Nd of the residual clinopyroxene barely changes in composition during the whole course of the reaction so it would be readily identifiable from those produced by fractional melting in which the concentration is rapidly depleted in incompatible elements.

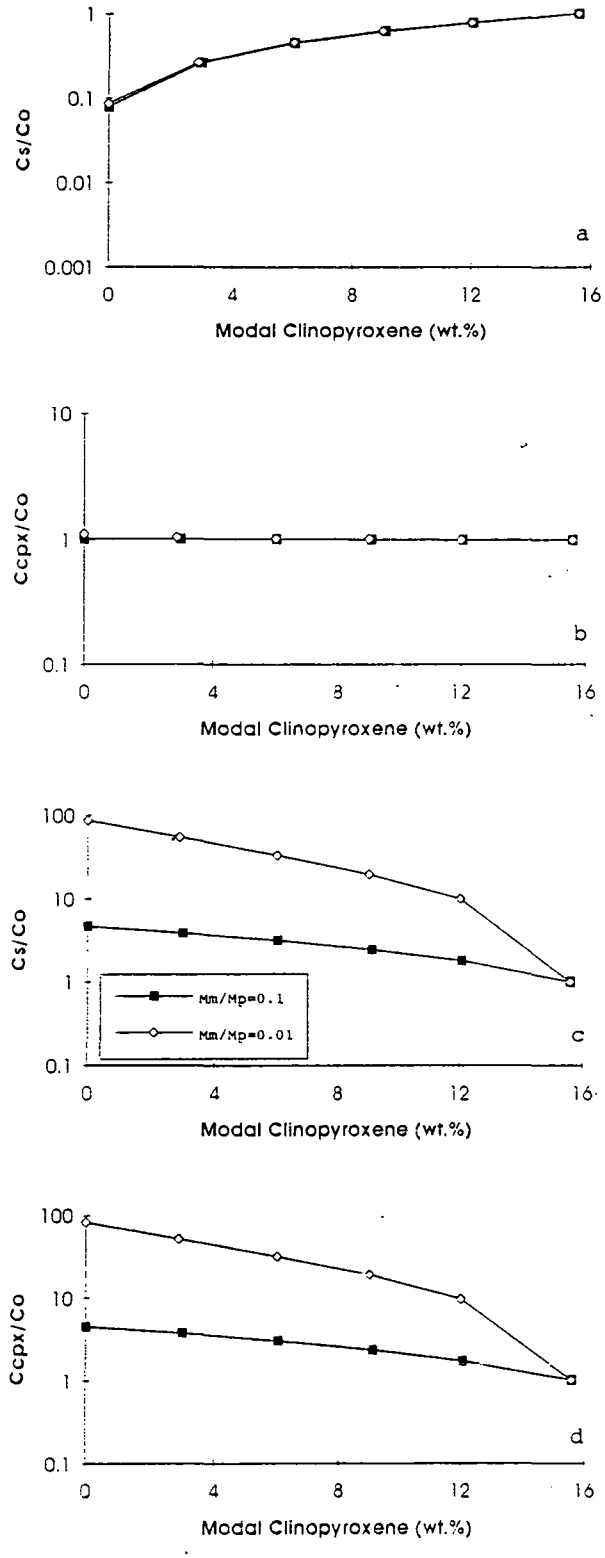


**Figure 3.14**. Concentration of Nd in **a)** residual peridotite, **b)** residual clinopyroxene, **c)** modified liquid and **d)** clinopyroxene which is precipitated from the modified liquid for $M_m/M_p$ ratios of 0.1 and 0.01 against modal clinopyroxene during the formation of harzburgite from lherzolite (see text for details). Reaction progress is from right to left on the diagrams.

If the $M_m/M_p$ ratio is very small (~0.01) then for the reaction to go to completion the magma must crystallise ~60% by mass. This produces very strong enrichment in Nd content of the liquid and clinopyroxene which may be precipitated from this liquid. The concentration of Nd in the residues decreases more rapidly than the previous example, but again the Nd content of the residual clinopyroxene varies very little.

In conclusion the reactions that Kelemen et al. (1992) describe produce distinct trace element patterns in the both liquids and residual minerals. Detailed petrological and geochemical studies of the clinopyroxenes in a peridotite are needed to help in interpreting whether the peridotite has been Kelemenized!

### 3.7 Realistic Physical Models For Mantle Melting

The preceding section reviewed the different types of melting possible during mantle melting and the effects of these on the composition of the liquids and residues. One of the most important features of many of the models is that, at moderate to high degrees of melting, the composition of the pooled liquids becomes insensitive to the type of melting whereas the residues are highly sensitive at virtually all degrees of partial melting. It is pertinent then to look at the composition of melting residues to give us a realistic chance at understanding melting processes.

The data of Johnson et al. (1990), Johnson and Dick (1992) and Parkinson et al. (1992) are some of the best for addressing certain features of the melting. Firstly the question of the melting processes. Two end member processes are easily ruled out. Equilibrium batch melting is difficult to reconcile with any of the clinopyroxene ion microprobe data from the above papers as the neither the extreme depletions of the incompatible elements nor the strong fractionation of ratios such as Ti/Zr can be explained. Disequilibrium melting in the sense of Prinzhofer and Allègre (1985) and Bedard (1989) is also difficult to reconcile as the ion microprobe analyses of residual clinopyroxenes from abyssal peridotites (Johnson et al., 1990) clearly demonstrate a relationship between the proportion of residual clinopyroxene and the clinopyroxene composition. Implicit in this type of desequilibrium melting model is the fact that minerals melt out with their initial composition and their composition does not change with increasing melting.

Models somewhere inbetween the two extremes of equilibrium batch melting and fractional melting, that is incremental models, can be invoked to describe the peridotite geochemistry althouth the increment must be small (<1%) to support the

melting. Finally, the diffusion rates quoted in these models are commonly at the low end of the spectrum. Unfortunately, there is limited data on diffusion rates of cations in mantle minerals at realistic temperatures. However, the experimental work of Sneeringer et al. (1984) is important because they found that diffusion rates in natural diopsides are two to three orders of magnitude faster then that in sythetic diopsides and account for this by an increased dislocation and crystal deffect density allowing quicker diffusion. Again, during melting and deformation the likelihood of increased defect density and thus diffusion rates is strong and may lead to equilibrium distribution coefficients being tended towards. Until, more data on diffusion of elements in mantle materials is available some of the above arguements are tentative although based on realistic interpretations of the available experiments. Detailed, ion microprobe analysis of core to rim traverses in mantle minerals may be a way of seeing whether compositional gradients are retained in these minerals due to diffusion processes.

A question which stems from the above discussion is, "if melting can be described by equilibrium melting coefficients, why cannot minerals constantly re-equilibrate with melts percolating through the melting column?" This question addresses the whole problem of melt segregation processes in the mantle. Certainly, there is ample evidence that melt/mantle interaction does occur between dykes and their surrounding wallrock in orogenic massifs (Bodinier et al., 1989) and some ophiolites (Kelemen et al., 1992). However, these situations seemed to be associated with a dyke being injected into essentially static mantle.

Eggins (1992a and b) has recently studied melt generation beneath Hawaii, from a phase equibrium and theoretical viewpoint. Primitive picrites from Hawaii are in equilibrium with a harzburgitic residue at low pressures yet their trace element geochemistry is consistent with them being generated at high pressures within the garnet stability field. This type of decoupled behaviour between major and trace elements may be explained by the differing diffusion rates of the major and trace elements with mantle minerals. Major elements which have faster diffusion rates in mantle minerals may be re-equilibrating during the ascent of the melt through the mantle whereas the trace elements do not sustantially re-equilibrate during ascent.

From this model the likely melting scenario in the shallow upper mantle is that the mantle is continuously deforming as it decompresses and melts (McKenzie, 1984). This causes grain size reduction, so that the mantle and the melt generated can rapidly equilibrate (Bussod and Christie, 1991). Thus the distribution of elements between

clinopyroxene data. Models such as McKenzies (1985) dynamic melting model are also important although they are similar in nature to incremental melting models except they have a constant porosity rather than a discontinuous one. Again, data from clinopyroxenes argues for the porosity to be no greater than one percent (Figure 3.15).

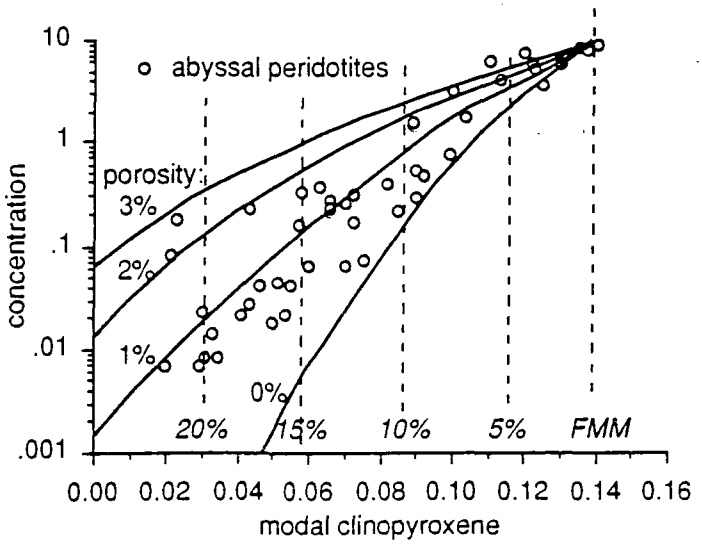


**Figure 3.15.** Plot of modal clinopyroxene against Zr concentration. Fractional melting lines with varying porosity are also shown.

Some of the above processes have the distribution of elements described by equilibrium partition coefficients. The recent papers by Qin (1992) and Iwamori (1993) have considered that disequilibrium may exist between melt and minerals because the diffusion rate of elements in the melting minerals cannot keep up with rate of melting. These models should be taken very seriously as experimental data suggests that diffusion is very slow compared with melting rates. Although this feature in its self is a very powerful argu ment for disequilibrium processes to exist, these more complicated melting models should be put in context of the likely physical processes that exist during decompreesion melting. Firstly these twomodels for mathematical reasons make some simplifications. One of these is that a mineral grain of given radius in the mantle crosses the solidus and melts at a given rate until the mantle either stops melting or the grain melts out. This does not take into account that grain size reduction and recrystallisation must be dominant features for a decompressing deforming mantle (Busseau et al., 1991). Therefore it is unlikely that many grains exist as intact grains through the whole process of melting. Secondly, the non-equilibrium number that Qin (1992) describes to quantitively access desiquilibrium is calculated using a grain radius of 2.5 mm. Although quite small the grain size estimates used in these models are based on grain sizes in peridotites which have undergone considerable sub-solidus textural equilibration and are liable to be overestimates of the true grain size during

minerals and melt is described by an equilibrium distribution coefficient. The melts segregate very efficiently as the mantle compacts and the process is close to fractional melting. The melts segregate into small veinlets (McKenzie, 1985b; McKenzie, 1989; Spiegelman and Kenyon, 1992; Foley, 1992; Spiegelman, 1993) and move upwards. At any point between the solidus and the surface small amounts of the aggregated melt may interact with the mantle. However, the melt ascent is rapid enough so that only the fastest diffusing elements can readily equilibrate with the mantle at that point. As the mantle becomes more depleted, interaction with the melts may produce distinctive trace element signatures (Johnson and Dick, 1992) in the residual peridotite. Below the base of the Moho widespread interaction may occur between melts and the mantle. Melt/mantle interaction similar to that described by Kelemen et al. (1992) is most likely to occur at shallow levels where small dykes can form. Until we have samples which record the melting at depths of 60 to 30 km in the oceanic mantle our understanding of these deeper processes will remain sketchy.

### 3.8 Summary

This chapter has reviewed melting processes beneath spreading ridges and above subduction zones. Melting in both cases is best explained by adiabatic decompression melting. In the mantle wedge above subduction zones some hydrous fluxing melting may increase the amount of melting for a given length of melting column. Therefore residual peridotites from the mantle wedge should be more depleted than those from beneath a spreading ridge. The extensive parameters which are used to model mantle melting have been provided, based on experimental studies and natural samples. These are then used in the many different melting models available to show how these models affect the composition of residues and liquids. These models indicate that the composition of residual peridotites provide the most information about melting processes. Finally a physically realistic model for melting in the oceanic mantle is provided.

# Chapter 4
# Petrology and Mineral Chemistry

## 4.1 Introduction

This chapter gives detailed descriptions of the petrology and mineral chemistry of the Leg 125 peridotites. The first section of the chapter describes the modal mineralogy of the rocks and gives detailed textural descriptions of each of the main minerals. Descriptions of the alteration minerals are also included. The next section presents electron microprobe mineral analyses for the main rock forming minerals and compares these with mineral analyses from peridotites found in other tectonic settings. Petrogenetic applications of the mineral chemistry, such as geothermometry, geobarometry and oxygen fugacity calculations are used to show how these may help us to understand and constrain petrogenetic models for the Leg 125 peridotites. Trace element concentrations analysed by ion microprobe for some of the minerals are described and are used to constrain melting models for the Leg 125 peridotites.

## 4.2 Modal Mineralogy

As described in chapter two most of the peridotites recovered on Leg 125 are variably serpentinised harzburgites with a subordinate number of variably serpentinised dunites. The modal mineralogy of the peridotites was estimated from hand specimens and thin sections. One of the problems of the ODP samples is that some of them tend to be very small with respect to the grain size of the peridotite. The largest sample, I managed to acquire was 10 cm × 3 cm × 2 cm and many of the shipboard samples were smaller. This means that there is a distinct possibility that some of the modal analysis are not representative. Also, many of the samples are strongly tectonised which causes alignment and banding of orthopyroxene porphyroclasts so that some samples have abundant modal orthopyoxene whereas a sample taken 20 cm away in the core may have a much lower orthopyroxene content.

All the peridotites are variably serpentinized, with olivine often being totally altered to lizardite (see serpentinization section). When measuring the modal mineralogy, the original modal contents are estimated from the serpentine pseudomorphs present in the rock. For the harzburgites, the original modal mineralogy is olivine 75-85%, orthopyroxene 15-25%, clinopyroxene 0-1% and spinel 1-2%. Amphibole is present in

some samples but rarely exceeds 1%. When the samples are plotted on a Streckeisen (1976) ultramafic ternary diagram (Fig. 4.1) all the samples plot in the harzburgite field. The effect of the tectonisation is to spread out the peridotites parallel to the olivine-orthopyroxene axis. Bonatti and Michael (1989) used this type of plot to contrast the different modal compositions of peridotites found in different tectonic settings. Fields for the different tectonic settings are also shown in Figure 4.1 and the Leg 125 peridotites plot in the destructive plate margin field compatible with their subduction zone origin.

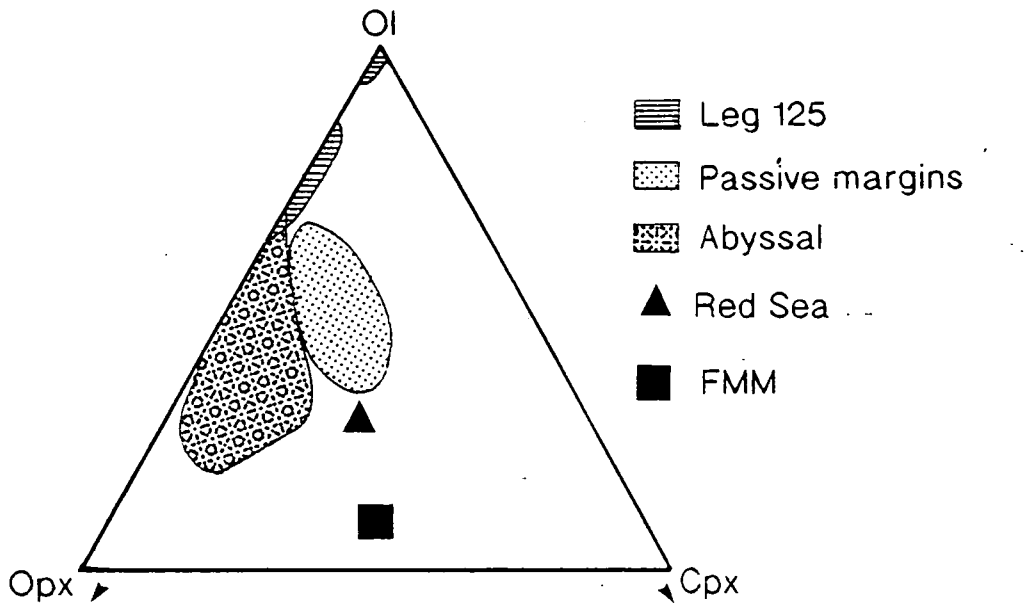


**Figure 4.1.** Ternary plot of modal compositions (after Streckeisen, 1976) showing the position of the Leg 125 peridotites and the fields for peridotites from different tectonic settings (after Bonatti and Michael, 1989).

## 4.3 Primary Minerals

### 4.3.1 Olivine

Olivine is the most common mineral in the Leg 125 peridotites and texturally has several different forms. It is the most serpentinised mineral in the peridotites. In some samples the olivine is completely serpentinised to mesh-textured lizardite and the grain-size and shape of the olivines is difficult to discern. In other samples olivine is remarkedly fresh and petrographic analysis is readily accomplished. Remnants of fresh olivine are found in most thin sections so that some information about the olivine

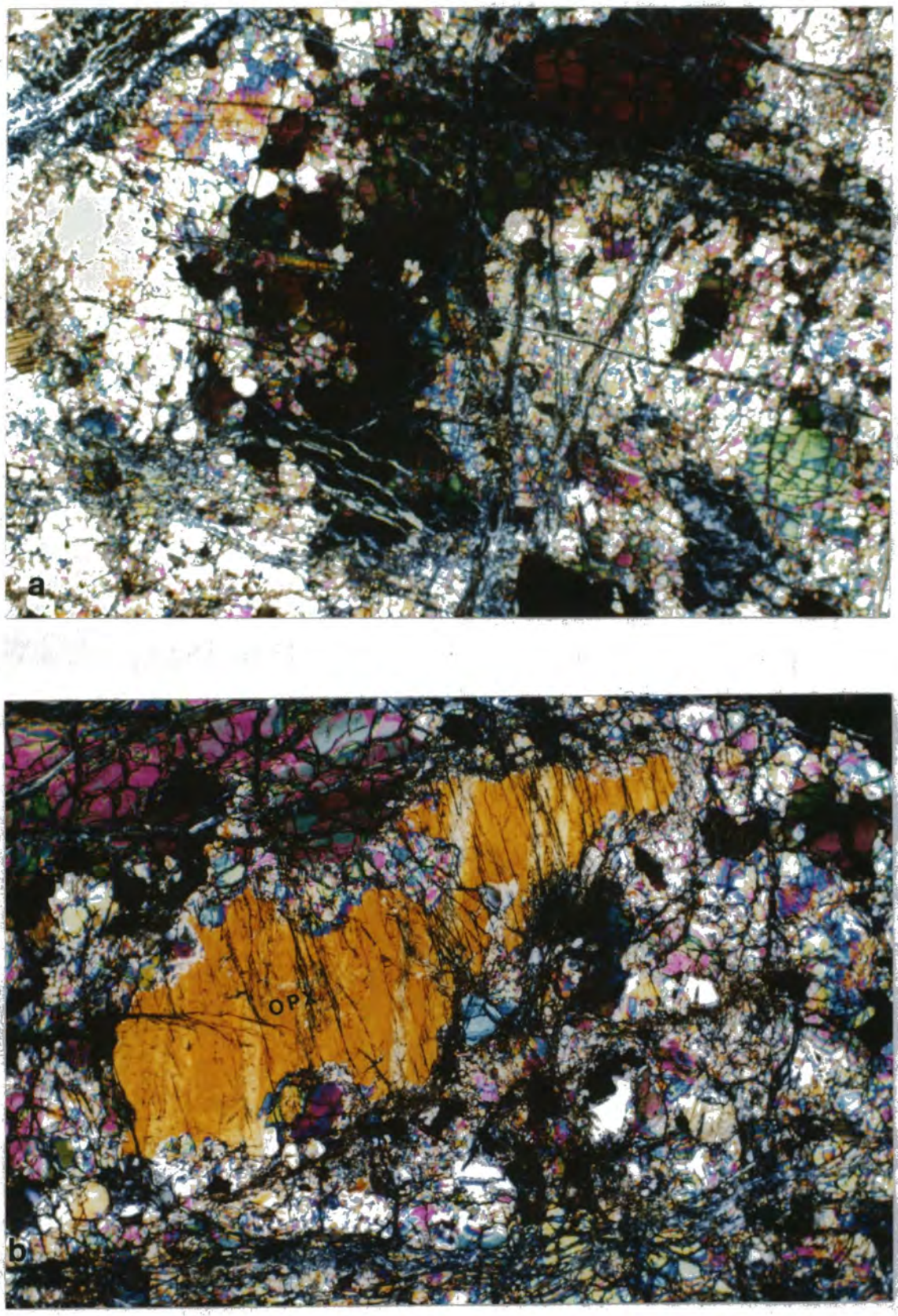


**Figure 4.2.** a). Dunite composed of a matrix of aligned porphyroclastic olivine grains and recrystallised olivine neoblasts. **b)** Strongly recrystallised olivine neoblasts clustering around an orthopyroxene (opx) grain boundary (both photographs in cpl, field of view 6 mm by 3.7 mm). Both photographs from sample 779A 10R-1, 17-21 cm.

extracted from most thin sections. Olivine commonly forms elongated porphyroclasts (terminology from Mercier and Nicolas, 1975 and Harte, 1977) which are aligned and form the principal foliation within the peridotites. This is best seen in thin section, although aligned spinels which also define this foliation are readily seen in hand specimen. These olivine porphyroclasts can be up to 10 mm long and 5 mm wide, although smaller grains are more common. Olivine also occurs as small neoblasts (0.1-0.5 mm) which are principally found at the grain boundaries of orthopyroxenes and have lobate grain boundaries. These are often the freshest olivines within a thin section. Very thin reaction rims are observed between the olivines and orthopyroxenes in some samples. Olivine is commonly included in orthopyroxene grains where it can be fresh or serpentinised depending on the alteration state of the host orthopyroxene. In some samples olivine is found along sub-grain boundaries of the strongly deformed orthopyroxene grains. Clusters of olivines and orthopyroxenes have been observed in some samples. Figure 4.2 illustrates the two common forms of olivine found in the Leg 125 peridotites.

### 4.3.2 Orthopyroxene

Orthopyroxene forms between 30 % and 10% of the mode of the peridotites. It is always found as porphyroclasts of varying size, from 1-2 mm long up to 10 mm long and about 5 mm wide. Unlike olivine and spinel, orthopyroxene is generally not elongated along the direction of the principal foliation although the cleavage planes are generally aligned and grains may optically extinguish together within a thin section. A distinct feature of many of the orthopyroxene crystals are their lobate grain boundaries. In certain samples this lobate feature is extreme (see Fig. 4.3) and fresh olivine neoblasts are commonly found within the lobes of the grains. The lobate grain boundaries are interpreted as resorption features associated with the incongruent melting of orthopyroxene. Exsolution lamallae of clinopyroxene are common within orthopyroxene grains and form very fine lamellae, coarse lamellae or small aligned blebs (see Fig. 4.3). Orthopyroxene grains show obvious signs of both ductile and brittle deformation. Bent orthopyroxene grains with marked undulose extinction are common, with some grains having undergone ductile shearing to form asymmetric grains with good shear sense indicators. Brittle kink-bands have been observed in some thin sections with olivine dynamically recrystallised along the sub-grain boundaries formed. Orthopyroxenes are commonly fresh, except in the most highly serpentinised samples where the orthopyroxene alters to bastite serpentine (lizardite). When orthopyroxenes are cut by chrysotile veins, the orthopyroxene may become serpentinised in the vicinity of the vein.

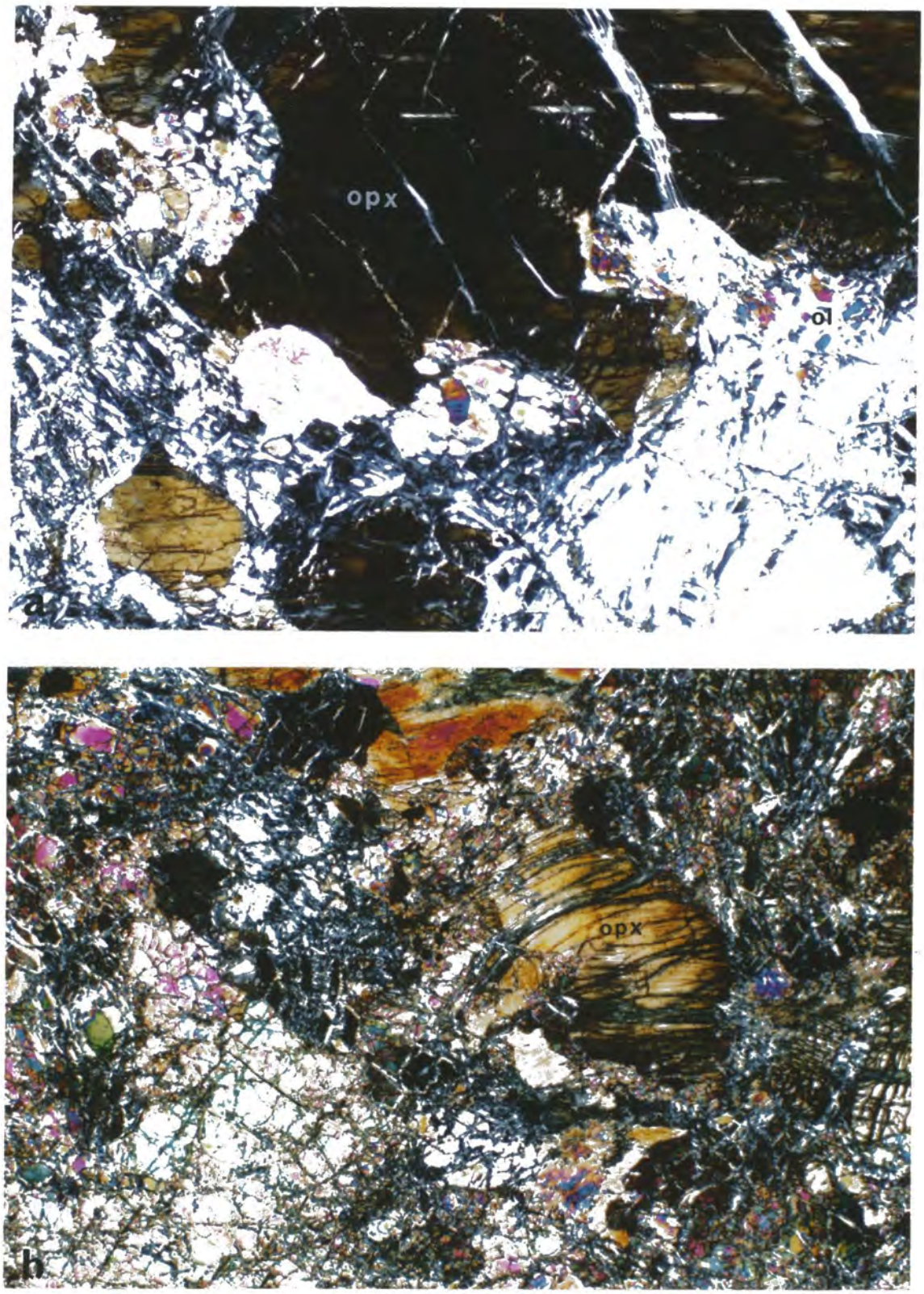


**Fig. 4.3. a**). Photomicrograph showing orthopyroxene (opx) (in extinction) with resorbed lobate grain boundary and fresh olivine neoblasts inside the lobes. **b**). Orthopyroxene (opx) grain with clinopyroxene exsollution lamellae and kink-banding/sub-grain boundaries. Also note serpentine along the cleavage of the grain (both photographs in cpl, field of view 6 mm by 3.7 mm) ( both from sample 779A 14R-1, 40-48 cm).

### 4.3.3 Clinopyroxene

Clinopyroxene makes up a very small part of the mode of the Leg 125 peridotites, usually less than 1%, although reaching 1.5% in one clinopyroxene-"rich" sample. The low clinopyroxene content indicates the very depleted nature of these peridotites. Although volumetrically unimportant, the clinopyroxenes have distinct chemical and textural features which play a key part in understanding the petrogenesis of the Leg 125 peridotites. Clinopyroxenes are found in two distinct forms within the peridotites; those which can be ascribed to having a primary mantle origin and are a residual phase during mantle melting; and those which are secondary and may have crystallised from melt passing through the peridotites. The clinopyroxenes that were analysed by ion microprobe (see trace element geochemistry section) belong to the first category, whereas those discussed in the mineral chemistry section come from both categories. Girardeau and Lagabrielle (1992) have found that the two types of clinopyroxenes have similar but distinct compositions with respect to the residual abyssal peridotites, a point also emphasised by Parkinson et al. (1992).

As already described clinopyroxene is commonly found as exsolution lamellae in orthopyroxene grains. Much of the primary clinopyroxene is found close to orthopyroxene grain boundaries and has distinctive form, with strongly lobate grain boundaries usually interpreted as a partial melting texture (Figure 4.4). Some of these primary mantle clinopyroxenes have been recrystallised to form clinopyroxene-spinel pairs, which Girardeau and Lagabrielle (1992) ascribe to form in the presence of water at low temperatures. These clinopyroxenes are readily recognised in thin section by the distinct rhombic shape of the grains. Clinopyroxene is characterised by very small grains with an average grain size of less than 1 mm.

Secondary clinopyroxenes, possibly associated with percolating magmas, are found in small veinlets which cross the tectonic foliation of the peridotites. These veinlets are most common in peridotites which show evidence for widespread melt/fluid interaction.

These samples usually have amphibole extensively replacing orthopyroxene, chlorite after Cr-spinels and clinopyroxene and patches of plagioclase which is interpreted as unextracted basaltic melt (Menzies and Allen, 1974) and is commonly replaced by fine grained sericite. This last feature has only been discovered in one thin section. Fig. 4.4 shows examples of both forms of clinopyroxene.

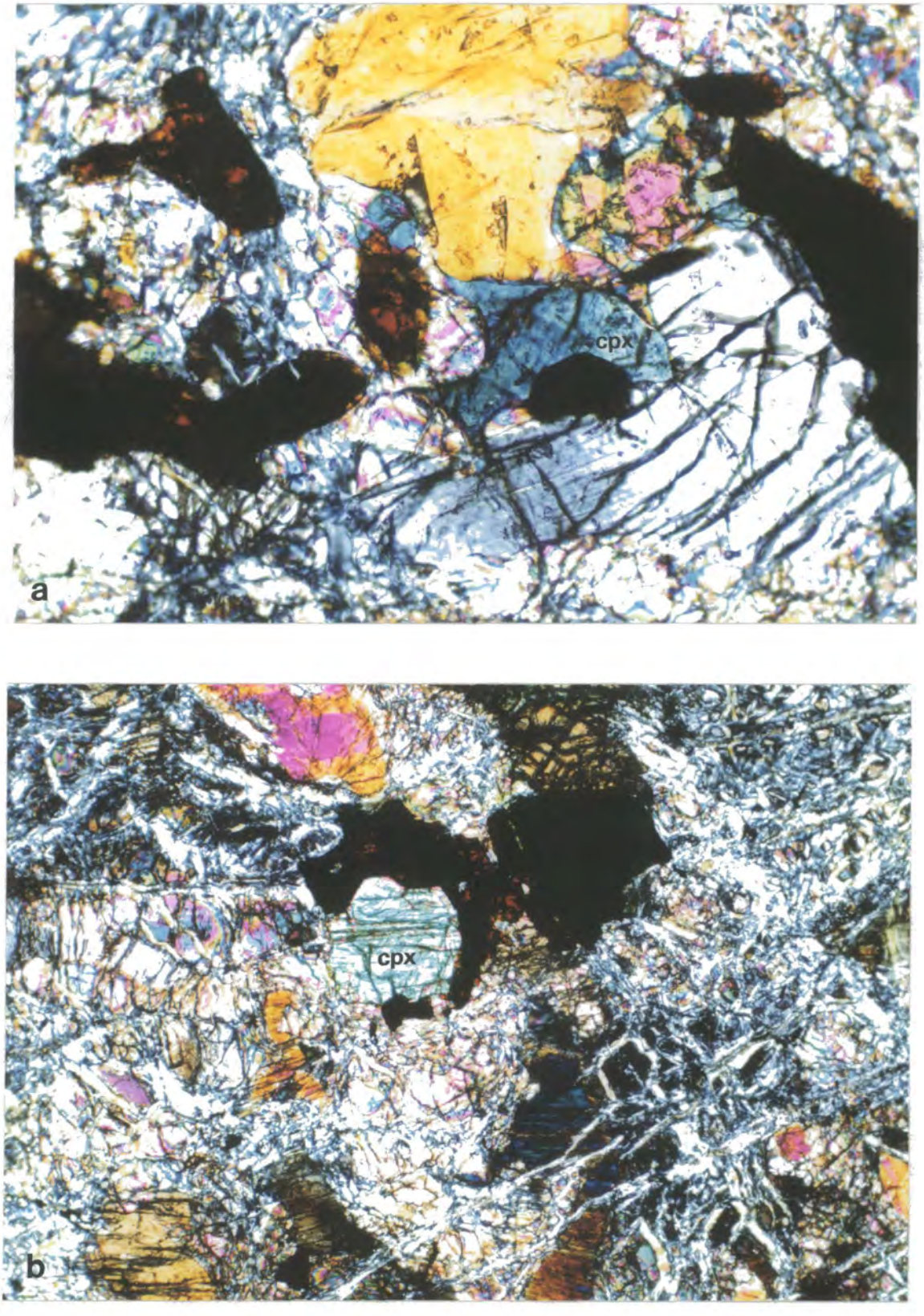


**Fig 4.4. a)** Example of primary clinopyroxene (cpx) associated with orthopyroxene grain boundary, showing excellent lobate grain boundaries (cpl, field of view 1.5mm by 0.9 mm). **b).** Recrystallised clinopyroxene (cpx) surrounded by secondary spinel (cpl, field of view 3 mm by 1.9 mm). Both photo graphs are from sample 779A 14R-1, 40-48 cm.

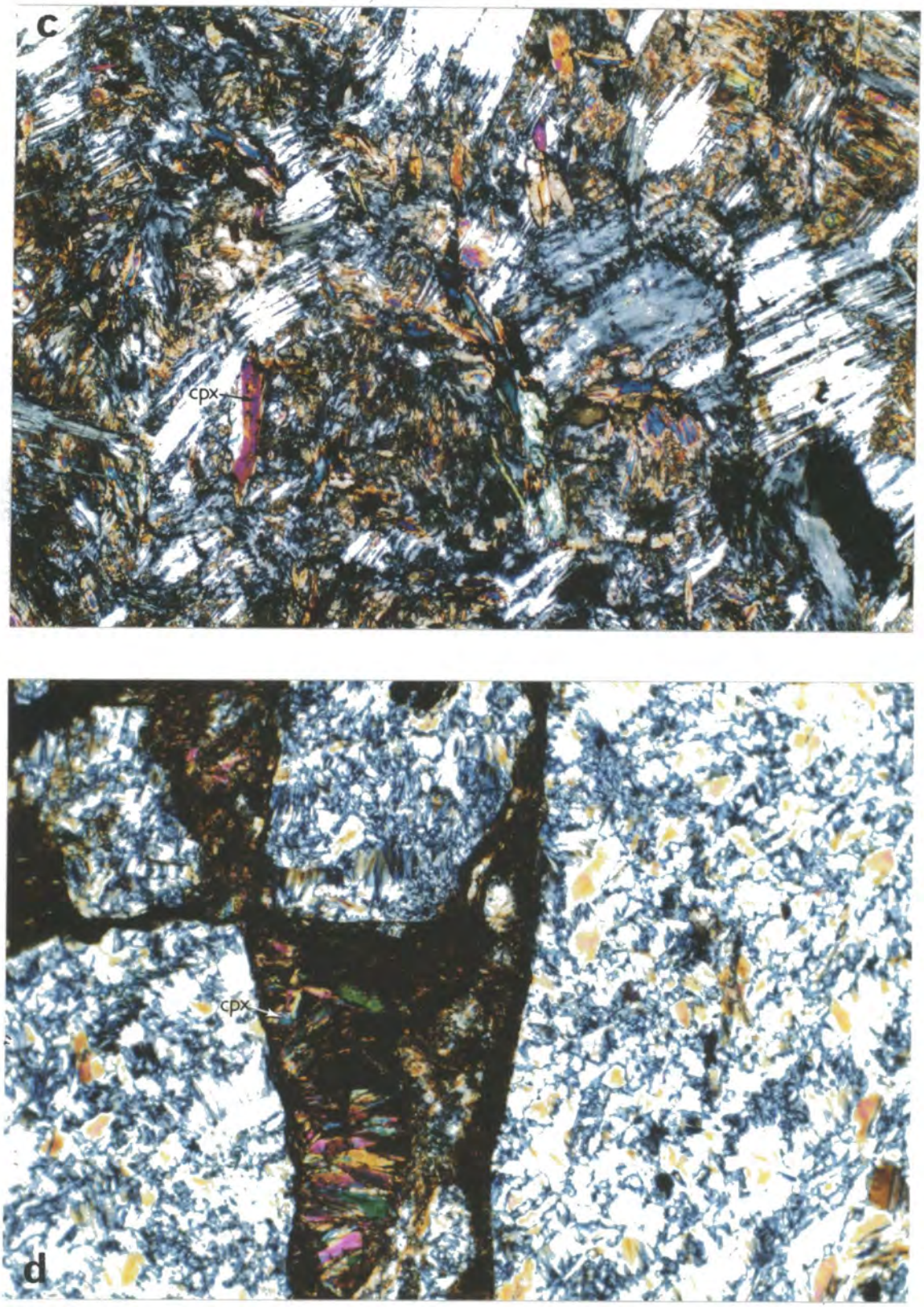


**Figure 4.4** (cont) **c**). Small secondary clinopyroxene (cpx) crystals in a dunite sample. They are interpreted as being crystallised from a melt passing through the peridotite (cpl, field of view 3 mm by 1.9 mm) (sample 779A 8R1, 90-93 cm). **d**). Small veinlet containing clinopyroxene (cpx) crystals which is thought to represent unsegregated melt (cpl,field of view 3 mm by 1.9 mm) (sample 784A 38R-CC, 13-19).

### 4.3.4 Spinel

Spinel is a ubiquitous phase in all the Leg 125 peridotites with a modal abundace of 1-2% in harzburgites and up to 5% in some of the dunite samples. As emphasised in both the olivine and clinopyroxene sections, spinel has several origins in these peridotites. In many of the harzburgites, the spinels are aligned along the principal foliation of the peridotites and are often highly deformed and strung out within the olivine matrix. In hand specimen these deformed spinels are seen as spinel trains. Where the spinels are less deformed, they have anhedral to subhedral rhomb shapes. Relatively undeformed rhomb-shaped spinels are most common in the dunite samples.

Spinels associated with orthopyroxenes have amoeboid shapes and olivines are commonly included in spinel grains and can be either fresh or serpentinised to lizardite depending on whether or not the host spinel is fractured. Spinels, when fresh, have a distinctive red/brown colour, which is indicative of their high Cr contents. Secondary spinels associated with clinopyroxenes have good euhedral form and have generally lower Cr# (Girardeau and Lagabrielle, 1992).

Spinels show various stages of alteration, which are best studied in reflected light. During serpentinisation fluids permeate along grain boundaries and cracks and oxidise the spinels to ferrit-chromit (essentially Cr-rich magnetite). In reflected light this shows up as bright yellow rims around the grey colour of the unaltered Cr-spinel. In highly serpentinised samples, the whole of some spinel grains has been altered to ferrit-chromit. Within the mesh-textured olivine, these spinels may become corroded to much smaller (less than 0.5 mm) rounded grains and blue Cr-rich chlorite is often found distributed in the lizardite around such corroded spinels. Fig. 4.5 shows examples of some of these spinel types.

## 4.4 Alteration Minerals

### 4.4.1 Amphibole

Amphibole is a rare secondary phase found in some of the peridotites. Ishii et al.'s (1992) exhaustive microprobe study of the peridotites only managed to analyse amphiboles from two samples from Hole 784A in the Torishima Forearc Seamount. However, Lagabrielle et al.'s (1992) structural study of the peridotites found amphibole in a number of samples from Conical Seamount. In accordance with these two studies I have found amphibole in a number of samples from both seamounts. Amphibole makes up a varying amount of the mode of the peridotites, from 1% up to 10% in some cases. The amphiboles are tremolites (or chemically Mg hornblendes) and occur principally after orthopyroxene, although some samples are cut by amphibole bearing veinlets.

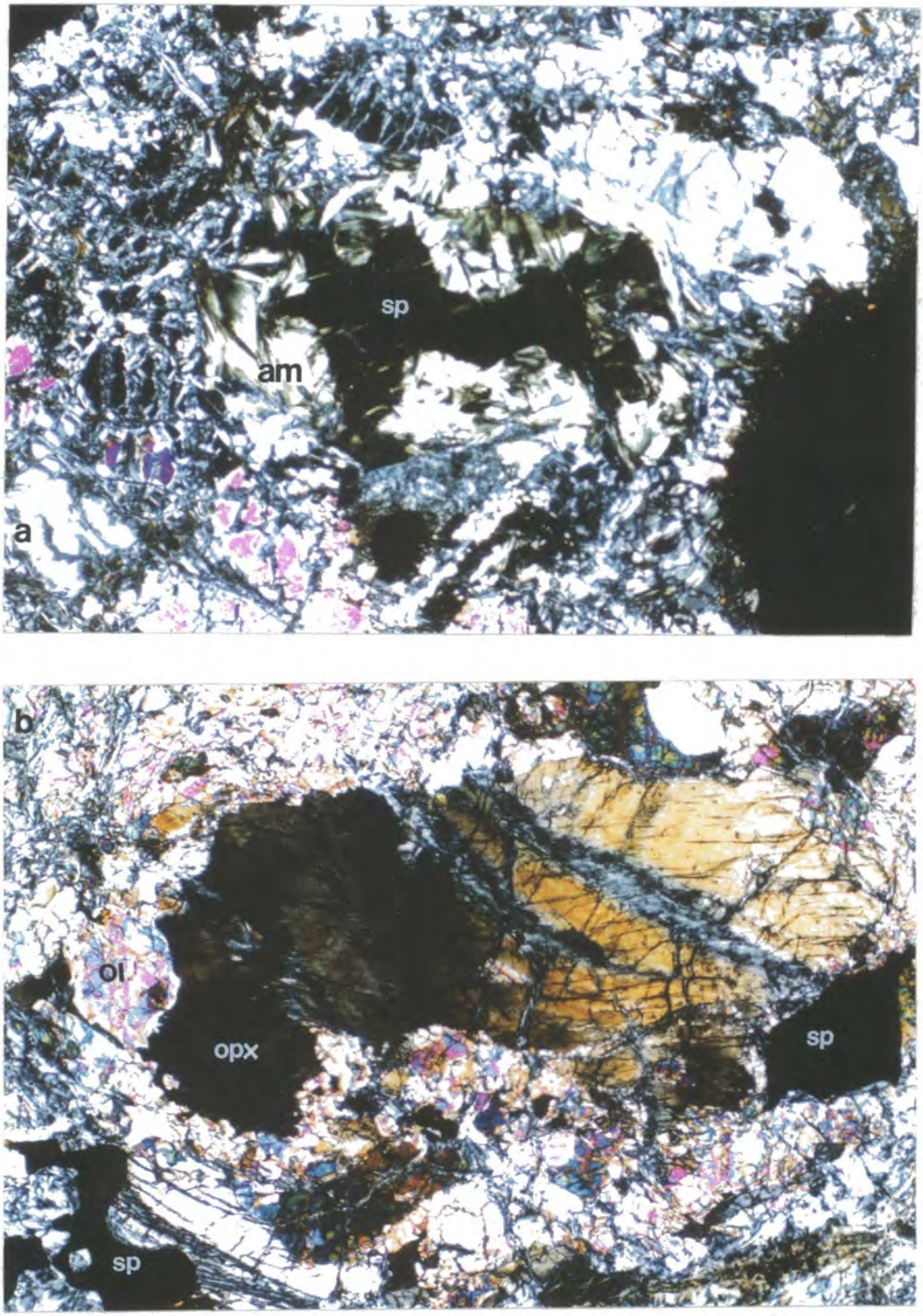


**Fig 4.5. a)** Spinel (sp) with a corona of amphibole (amph) and Cr-rich chlorite. Amphibole is an abundant phase in this peridotite and several of the spinels in this section have reacted to form amphibole (cpl, field of view 3 mm by 1.9 mm) (sample 779A 13R-1, 9-11 cm). **b).** Photomicrograph of a large orthopyroxene (opx) grain surrounded by a matrix of sheared olivine (ol). Spinels are aligned along the fabric defined by the olivine. The spinel (sp) in the left hand corner of the photomicrograph has a distinct amoeboid shape (cpl, field of view 6 mm by 3.9 mm) (sample 779A 14R-1, 40-48 cm)

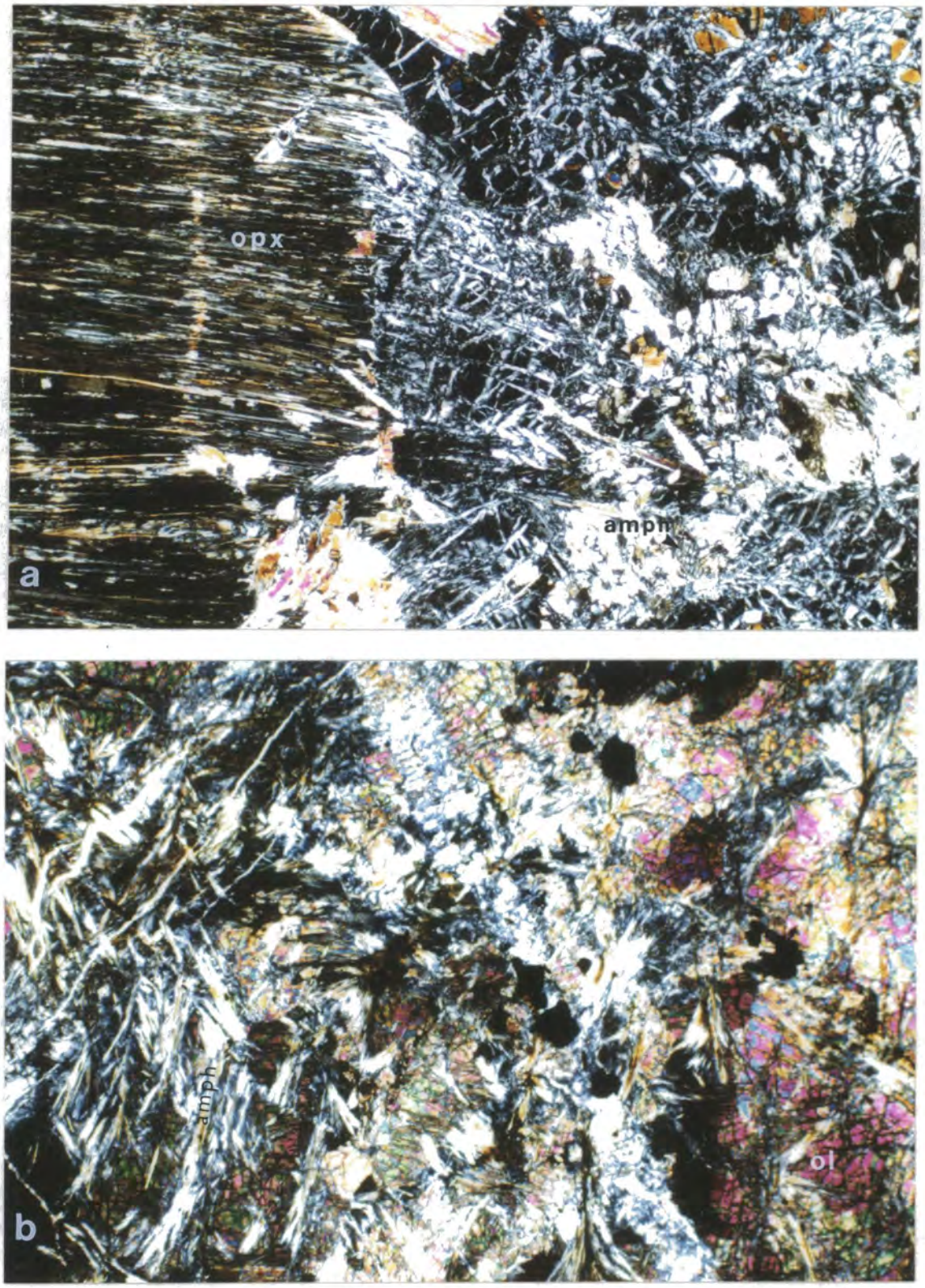


**Fig 4.6 a)** Photomicrograph of a large orthopyroxene (opx) grain. The orthopyroxene is deformed and amphibole (amph) forms in the pressures shadow around the grain. The amphibole is magnesio hornblende (see text) and has two distinct morphologies. Some elongate grains can be seen on the edge of the orthopyroxene. Further away from the pressure shadow more euhedral grains form with good 120° cleavage (cpl, field of view 3mm by 1.9 mm) (sample 779A 13R-1, 9-11). **b).** In this sample small veinlets of fibrous amphibole (amph) cut across fresh olivine (ol). Chlorite is often intergrown with the amphibole and antigorite is also present in the section. (cpl, field of view 3mm by 1.9 mm) (sample 779A 19R-2, 132-140).

Fig 4.6 shows examples of these two principal forms of amphibole. In the samples where amphibole replaces orthopyroxene, the amphibole is intimately intergrown with chlorite and forms fibrous mats of these two minerals which have a distinctive green colour in plane polorised light. In the same thin sections clear acicular tremolites can be found. Orthopyroxene may be completely replaced by the amphibole/chlorite intergrowths or the alteration products may form as pressure shadows around the orthopyroxene grains in ductile shear zones. In a few thin sections amphibole is seen rimming spinel grains, and one sample contains a beautiful corona of euhedral amphibole laths and distinctive blue Cr-rich chlorite (see Figure 4.5). Kimball (1990) has described the formation of hornblende and chlorite from the breakdown of spinel and clinopyroxene in peridotite samples from both fracture zones and ophiolites. The amphiboles surrounding the spinels in these peridotites are thought to have formed by similar reactions to those described in Kimball (1990,) whereby spinel/clinopyroxene pairs break down to form hornblende and chlorite. The exchange of Mg and Cr in this reaction has strong implications for the interpretation of the spinel chemistry and is discussed in greater detail later in this chapter (see olivine-spinel geothermometry). The amphibole formed by the breakdown of orthopyroxene has not been described in the study of Kimball (1990) and may explain why they have distinctly different compositions from the amphiboles described from fracture zones by Kimball et al. (1985).

In some samples amphibole is found in small veinlets (1-2 mm across) cross-cutting dunite samples. Again, the amphiboles are intergrown with chlorite and have lath- to splay-like forms. The few samples in which these veins are found usually show evidence for extensive fluid/melt interaction with impregnated plagioclase, secondary diopside veinlets and the high temperature serpentine mineral antigorite. The olivine in these samples is often exceptionally fresh, except where some lizardite formed around the peripheries of the veinlets. These samples provide ample evidence that the Leg 125 peridotites were associated with the formation and seperation of hydrous melts within the forearc.

### 4.5 Serpentinisation

As noted in previous sections, all the Leg 125 peridotites have been serpentinised to varying degrees. Between the samples and within one thin section there are a whole range of serpentine minerals and textures. The principal serpentine reaction is the formation of lizardite from olivine. This is usually accompanied by the formation of magnetite (Moody, 1976) which is found as small specks in the lizardite and may later oxidise to haematite and produce a distinctive orange/brown staining to the thin

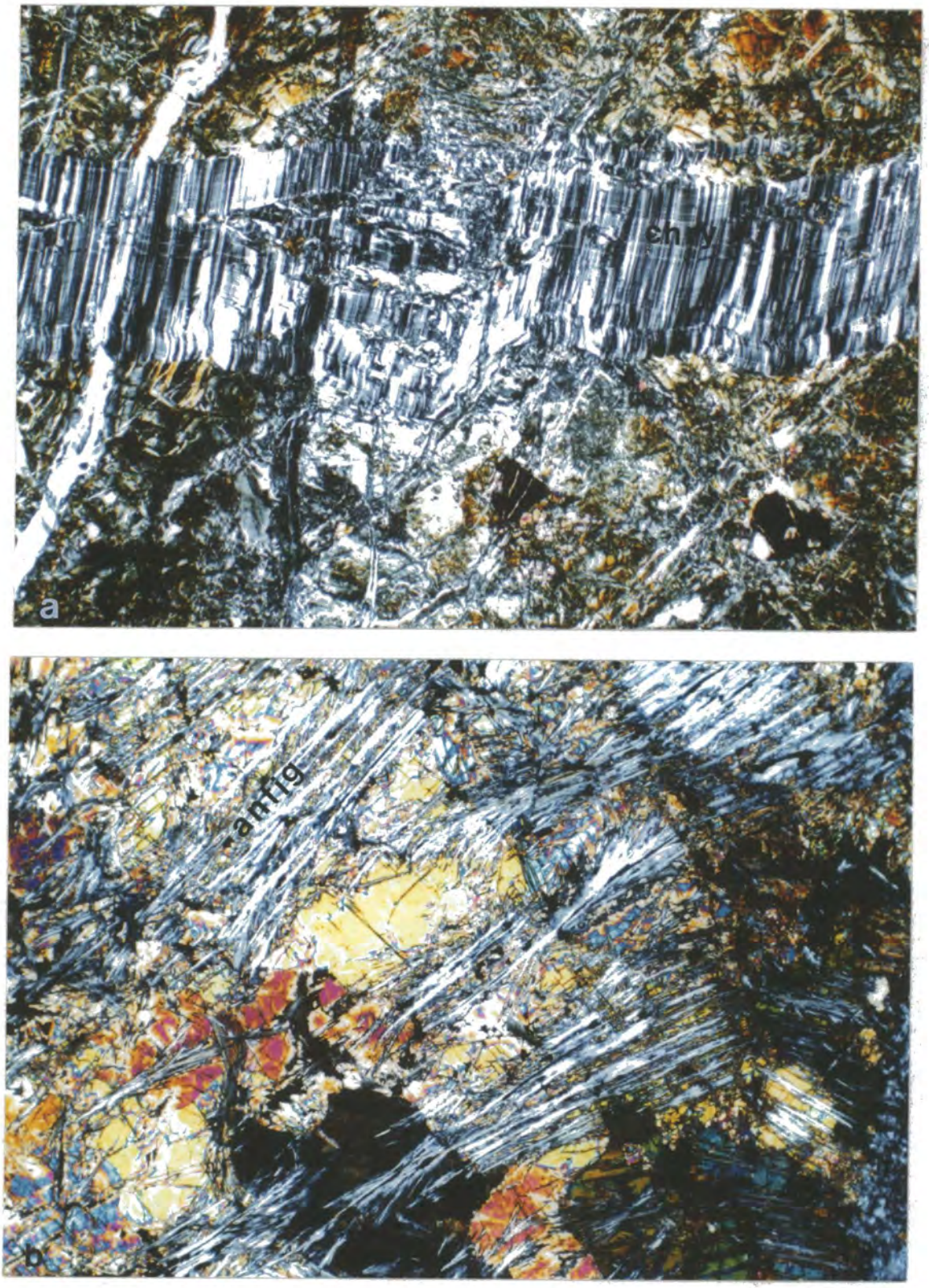


**Fig. 4.7. a).** Photomicrograph of a thick chrysotile (chry) vein cross cutting previously serpentinised olivine. The chrysotile veins are commonly late-stage and cross cut most features in the thin section (sample 779A 9R-2, 11-15 cm). **b)** This photomicrograph shows the distinctive elongate habit of the high temperature serpentine mineral antigorite (antig). Antigorite is commonly found with amphibole in the Leg 125 peridotites. It also seems to be most common in dunitic samples. In this sample the antigorite is replacing large olivine porphyroclasts (cpl, field of view 6 mm by 3.9 mm). Phototgraph from sample 779A 19R-3, 17-21 cm.

sections. The lizardite characteristically forms a mesh-texture when the olivine has been extensively altered, and an hour-glass texture around fresh remnants of olivine when the sample is less extensively altered (e.g., Wicks and Whittaker, 1977). X-ray diffraction (XRD) studies of this serpentine (see Appendix A) show it to be structurally lizardite-6T, a common form of lizardite from magnesian olivine. Orthopyroxene is variably altered to bastite serpentine. Again XRD results suggest that this has the structural form of lizardite-6T. The orthopyroxene is considerably more resistent to serpentinisation and is only completely serpentinised in samples where the all the olivine has reacted to form lizardite. In less serpentinised, samples the alteration of orthopyroxene is restricted to grains that are cut by chrysotile veins which facilitates the influx of fluid to react the orthopyroxene to lizardite.

Many of the samples are cut by an extensive series of cross-cutting serpentine veins. These are very late in the formation of these peridotites as they cross cut all the primary features within the samples including the mesh-textured lizardite. XRD studies show that the veins are chrysotile-2Mc1. In thin section these veins have complicated internal growth structures (see Fig. 4.7) indicative of successive crack-seal formation. Coherent pieces of unserpentinised peridotite are found in some of the larger veins and these veins may displace passive markers such as exsolution lamellae in orthopyroxene grains laterally by several millimetres. Small fluid inclusions have been observed in some of these veins and very fine grained magnetite is very common in these chrysotile veins.

Lizardite and chrysotile are ubiquitous minerals in serpentinised ultramafic rocks. Antigorite is a rare serpentine mineral principally found as a prograde reaction product in metamorphosed ultrabasic rocks (Trommsdorff and Evans, 1974), although it has been described from the Trinity ophiolite as a retrograde reaction mineral by Peacock (1987a). Antigorite has a higher thermal stability than the other two polymorphs of serpentine possibly existing up to temperatures of 500 °C. Antigorite has been observed in several of the Leg 125 peridotites, principally in samples showing evidence for extensive fluid/melt interaction. It is interpretered here as a retrograde reaction mineral. It forms colourless fibrous splays within olivine grains. Some XRD samples were run but no definite antigorite peaks were found, although many of these peaks are difficult to seperate from lizardite peaks. Petrographically though, the antigorite is similar to descriptions of antigorite in peridotites from the Trinity ophiolite (Peacock, 1987a).

Clinopyroxene is never serpentinised in these peridotites and the sequence of increased susceptibility to the effects of serpentinisation of olivine, orthopyroxene, spinel and clinopyroxene is apparent in the Leg 125 peridotites.

### 4.6 Integrated Deformation and Alteration History of the Leg 125 Peridotites

Girardeau and Lagabrielle (1992) undertook a detailed structural study of peridotites from Conical Seamount. Much of the information on the deformation history of the peridotites is obtained from detailed petrofabric studies of olivine which is beyond the scope of this study (and the author). However, detailed studies of many thin sections by the author are intergrated with some of the structural studies of Girardeau and Lagabrielle (1992) to produce a deformation and alteration history of the Leg 125 peridotites. As Girardeau and Lagabrielle (1992) point out, the deformation and alteration processes are intimately linked.

Many of the samples show a strong fabric defined by the alignment of elongate olivine porphyroclasts and deformed trains of spinels. This type of fabric has been interpreted by Nicolas (1986) as indicative of asthenospheric deformation associated with ductile flow of the mantle beneath oceanic spreading ridges. Orthopyroxene grains were also pulled apart to form rectangular-shaped grains during this deformation phase. Petrofabric studies of olivine from relatively coarse-grained peridotites suggest that the olivines had a period of coarsening under high temperature and low stress conditions during which a poikilitic fabric was produced with olivine grains enclosing orthopyroxene and spinel grains. This part of the deformation history of the peridotites is thought to have occurred beneath an oceanic spreading centre (Girardeau and Lagabrielle, 1992).

This primary deformation history is variably affected by a complicated second stage history of annealing and heterogeneous deformation. Many of the peridotites contain olivines which have been strongly recrystallised to form small neoblasts. As described earlier the olivine neoblasts are concentrated around the grain boundaries of orthopyroxene grains which have been strongly resorbed to form lobate grain boundaries. This recrystallisation process occurred at high temperatures. Some of the recystallised neoblasts are suggestive of quasi-hydrostatic conditions at relatively low pressures (Girardeau and Lagabrielle 1992). This is an important observation as it points to the formation of olivine at the expense of orthopyroxene at relatively low (absolute) pressures but at high water pressures. Phase petrology suggests that incongruent dissolution of orthopyroxene only occurs at very low pressures (<3 kb) and is assisted by high water activity (Morse, 1980). van der Laan et al. (1989) have

proposed that low Ca-boninites are a product of peritectic melting (i.e. incongruent orthopyroxene melting).

The formation of olivine neoblasts is associated with development of the more heterogeneous deformation associated with ductile shear zones cutting many of the peridotites. These shear zones represent an intermediate stage between the high temperature deformation of the peridotites and progressively lower temperature deformation and metamorphism of the samples. Shear zones commonly contain orthopyroxene porphyroclasts with amphibole/chlorite pressure shadows. The orthopyroxenes are deformed in the shear zones but are more resistant to strain than the olivine matrix and seem to behave differently. They show both ductile and brittle behaviour, with the development of kink-bands which break up the porphyroclasts. Associated with the lower temperature alteration is the recrystallisation of primary clinopyroxene and the formation of secondary spinel.

At progressively lower temperatures a series of reactions take place associated with fluid/melt interaction with the peridotites. Clinopyroxene is found in veinlets and as discrete crystals which have crystallised from melts passing through the peridotites.

The highest temperature products of fluid interaction are the formation of amphibole around orthopyroxene grains and antigorite after olivine. Kimball et al. (1985) suggest that hornblende in peridotites forms at ~800 °C and Trommsdorff and Evans (1974) indicate that antigorite commonly forms between 250-500 °C. At temperatures <200 °C, mesh-textured lizardite forms from olivine and finally chrysotile veins cut the peridotites initiating the formation of bastite serpentine in some orthopyroxene porphyroclasts. It is apparent from the rather complicated petrography that the peridotites record a history of deformation and alteration, possibly in two discrete stages. Firstly, a high temperature mantle deformation event probably beneath a mid-ocean ridge. Secondly, further high temperature deformation assisted by high water pressures above a subduction zone. This deformation seems to have continued to progressively lower temperatures associated with the continuous interaction with fluids which produce distinctive alteration products.

### 4.7 Mineral Chemistry

During the distribution of the shipboard samples and tasks, Dr Teruaki Ishii chose to undertake the full study of the mineral chemistry of the Leg 125 peridotites. He analysed over 3000 points on a large number of polished thin sections at the

Smithonian Institute, Washington DC. The data from this study are published by Ishii et al., (1992). However his paper does not extend to a thermometric interpretation of the data. After checking the data it was decided that to redo such a large set of mineral analyses would be a waste of time and resources, so the mineral chemistry section presented here uses Ishii et al.'s, (1992) data set but with emphasis on the interpretation of the data and, especially, the petrogenetic implications. The mineral chemistry of each of the four principal rock-forming minerals and amphibole is discussed in turn and comparisons with mineral chemistry data from peridotites from other tectonic settings are illustrated and discussed in terms of the genesis of the Leg 125 peridotites.

### 4.7.1 Olivine

Representative analyses of some olivines are presented in Table 4.1. abstracted from the full data set in the Appendix of Ishii et al. (1992). Olivines in the Leg 125 peridotites are very forsteritic, with Mg# (here defined as Mg×100/(Mg+$Fe^{2+}$)) ranging between 91.10 to 93.60. In detail, olivines from hole 778A range between 92.20 to 93.60, hole 779A from 91.10 to 92.70, hole 780C+D from 91.40 to 92.10, hole 783A from 91.10 to 92.05 and hole 784A from 91.60 to 92.50.

**Table 4.1**. Representative analysis of olivines from harzburgites (from Ishii et al. 1992). *Total Fe as FeO.

| | Conical Seamount | | | | | | | Torishima Forearc Seamount | | | |
|---|---|---|---|---|---|---|---|---|---|---|---|
| Hole | 778A | | 779A | | | 780C | | 783A | | 784A | |
| Core | 2R-1 | 3R-CC | 8R-1 | 22R-3 | 26R-3 | 6R-1 | 18R-1 | 16R-CC | 18R-1 | 37R-1 | 45R-1 |
| Interval | 82-84 | 33701 | 41-45 | 55-57 | 102-105 | 67-69 | 65-67 | 14-17 | 100-103 | 33764 | 95-98 |
| Rock | H810 | H815 | H916 | H952 | H958 | H010 | H035 | H325 | H355 | H410 | H460 |
| Point | 6 | 62 | 32 | 82 | 62 | 33 | 30 | 64 | 55 | 335 | 22 |
| Analysis | 1 | 15 | 12 | 34 | 58 | 2 | 32 | 1 | 1 | 1 | 25 |
| $SiO_2$ | 41.43 | 41.80 | 41.38 | 41.08 | 40.62 | 40.99 | 41.41 | 40.77 | 41.83 | 41.00 | 41.32 |
| $TiO_2$ | 0.01 | 0.02 | 0.01 | 0.01 | 0.01 | 0.02 | 0.00 | 0.01 | 0.02 | 0.01 | 0.01 |
| $Al_2O_3$ | 0.00 | 0.00 | 0.02 | 0.00 | 0.32 | 0.00 | 0.00 | 0.00 | 0.00 | 0.00 | 0.00 |
| FeO* | 6.49 | 7.46 | 7.84 | 8.13 | 7.73 | 8.02 | 8.35 | 8.25 | 7.88 | 7.80 | 7.40 |
| MgO | 51.87 | 50.14 | 50.93 | 49.44 | 49.93 | 51.05 | 49.77 | 49.52 | 49.62 | 49.86 | 50.15 |
| CaO | 0.00 | 0.01 | 0.02 | 0.01 | 0.00 | 0.01 | 0.01 | 0.02 | 0.01 | 0.01 | 0.01 |
| $K_2O$ | 0.00 | 0.02 | 0.02 | 0.01 | 0.02 | 0.02 | 0.00 | 0.01 | 0.01 | 0.00 | 0.01 |
| NiO | 0.40 | 0.26 | 0.33 | 0.34 | 0.33 | 0.41 | 0.37 | 0.33 | 0.38 | 0.36 | 0.36 |
| $Cr_2O_3$ | 0.01 | 0.01 | 0.06 | 0.01 | 0.01 | 0.01 | 0.01 | 0.00 | 0.05 | 0.00 | 0.00 |
| Total | 100.21 | 99.72 | 100.61 | 99.03 | 98.97 | 100.53 | 99.92 | 98.91 | 99.80 | 99.04 | 99.26 |
| O=4.000 | | | | | | | | | | | |
| Si | 0.999 | 1.014 | 0.999 | 1.008 | 0.997 | 0.993 | 1.008 | 1.003 | 1.016 | 1.005 | 1.008 |
| Ti | 0.000 | 0.000 | 0.000 | 0.000 | 0.000 | 0.000 | 0.000 | 0.000 | 0.000 | 0.000 | 0.000 |
| Al | 0.000 | 0.000 | 0.001 | 0.000 | 0.009 | 0.000 | 0.000 | 0.000 | 0.000 | 0.000 | 0.000 |
| $Fe^{2+}$ | 0.131 | 0.151 | 0.158 | 0.167 | 0.159 | 0.162 | 0.170 | 0.170 | 0.160 | 0.160 | 0.151 |
| Mg | 1.864 | 1.813 | 1.833 | 1.809 | 1.826 | 1.843 | 1.806 | 1.816 | 1.797 | 1.822 | 1.824 |
| Ca | 0.000 | 0.000 | 0.001 | 0.000 | 0.000 | 0.000 | 0.000 | 0.001 | 0.000 | 0.000 | 0.000 |
| K | 0.000 | 0.001 | 0.001 | 0.000 | 0.001 | 0.001 | 0.000 | 0.000 | 0.000 | 0.000 | 0.000 |
| Ni | 0.008 | 0.005 | 0.006 | 0.007 | 0.007 | 0.008 | 0.007 | 0.007 | 0.007 | 0.007 | 0.007 |
| Cr | 0.000 | 0.000 | 0.001 | 0.000 | 0.000 | 0.000 | 0.000 | 0.000 | 0.001 | 0.000 | 0.000 |
| Total O | 3.001 | 2.986 | 3.000 | 2.992 | 2.999 | 3.007 | 2.992 | 2.997 | 2.983 | 2.995 | 2.992 |
| Z | 0.999 | 1.015 | 1.001 | 1.009 | 1.006 | 0.993 | 1.008 | 1.003 | 1.018 | 1.005 | 1.009 |
| XY | 2.002 | 1.971 | 1.999 | 1.983 | 1.992 | 2.014 | 1.984 | 1.993 | 1.965 | 1.989 | 1.983 |
| Mg# | 0.934 | 0.923 | 0.920 | 0.916 | 0.920 | 0.919 | 0.914 | 0.915 | 0.918 | 0.919 | 0.924 |

Figure. 4.8 shows plots of Mg# content against FeO and MgO. Although there are obviously strong correlations, these plots illustrate the range of olivine compositions found in the Leg 125 peridotites. In Conical Seamount, olivines from hole 778A are the most refractory whereas those from 779A span a wide range of compositions and those from hole 780C+D plot in the middle of the range defined by hole 779A. On the plot of Mg# versus MgO, data from hole 779A defines a broad positive correlation in which there are trends defined by small groups of data. This feature can also be seen in the spinel data (where the small groups of data are easier to see than in Figure 4.8). Its origins are discussed in the thermal history section where I infer that these trends are related to different sub-solidus reequilibration histories. On the same plot, the data from hole 778A form a distinct trend at lower MgO for a given Mg# which may also be related to sub-solidus reequilibration, although data from hole 778A often plots on distinct trends for other minerals. On both plots a distinct difference in the olivine compositions of samples from hole 783A and hole 784A can clearly be seen. Olivines from Hole 783A are the least forsteritic of any of the holes. The minor elements NiO and $Cr_2O_3$ were also plotted against Mg# but showed no obvious correlation. The lack of a consistant relationship between forsterite content and NiO is surprising considering that Ni is strongly partitioned into olivine. Values from $Cr_2O_3$ shows very little variation with Mg#.

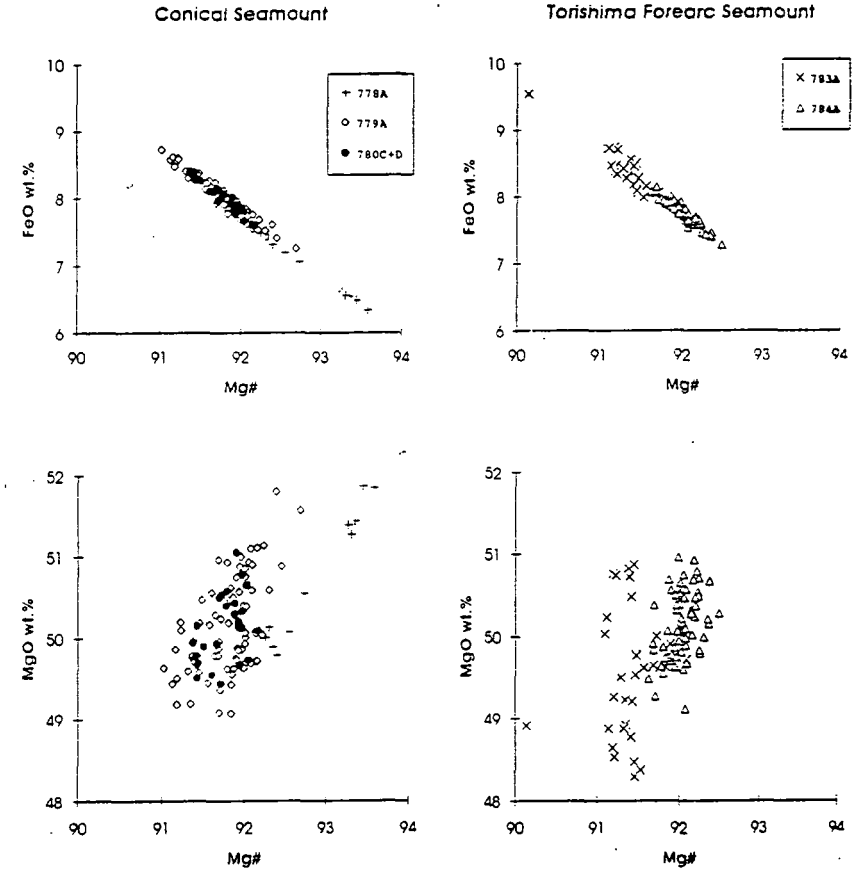


**Fig 4.8.** Plot of Mg# versus FeO and MgO for olivines from peridotites from Conical and Torishima Forearc Seamount.

None of the other elements analysed show any variation with forsterite content, although for $Al_2O_3$, CaO and $K_2O$ this may reflect the fact their concentrations are close to the detection limit of the electron microprobe. Calculations of the liquids in equilibrium with these olivines are presented in a later section.

### 4.7.1.1 Comparison with Other Peridotites

To compare the olivine compositions of the Leg 125 peridotites with other peridotites it is useful to plot FeO and MgO against Mg# as these are likely to be the most reliably measured by different laboratories. Other important minor elements such as NiO are closer to the detection limit. MnO has not been measured in the Leg 125 peridotites because of the set up of the electron microprobe (see Appendix A). Ample data exist for the composition of olivines in abyssal peridotites (e.g., Sinton, 1979; Dick, 1989; Komor et al., 1990), rifted continental margins (e.g., Evans and Girardeau 1988; Zipfel and Wörner, 1992), orogenic massifs (e.g., Bodinier et al., 1988, 1990), destructive plate margins (e.g., Bloomer and Hawkins, 1983; Bloomer and Fisher, 1987) and ophiolites (e.g., Browning, 1982; Greenbaum 1977, Jaques and Chappell, 1980).

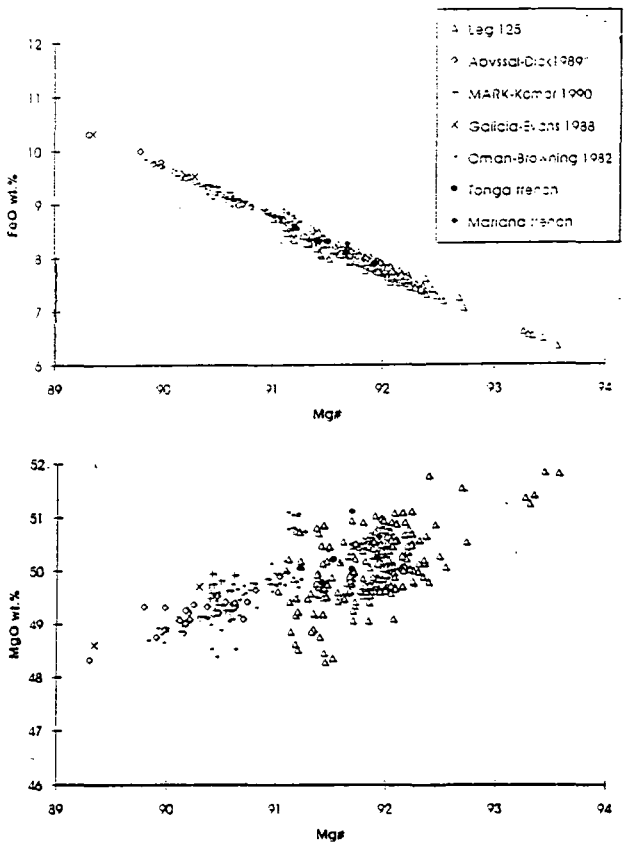


**Fig. 4.9.** Comparative plots of olivines from different tectonic settings on MgO wt.% and FeO wt.% against Mg#. Data for Leg 125 from Ishii et al. (1992), abyssal samples (Dick, 1989; Komor et al., 1990), Galicia margin (Evans and Girardeau, 1988),. Oman ophiolite (Browning, 1982), Tonga trench (Bloomer and Hawkins, 1983) and Tonga trench (Bloomer and Fisher, 1987)

On the two plots (Figure. 4.9), the Leg 125 olivines plot at higher Mg# and at lower FeO and higher MgO than a substantial portion of the other data. Of comparable depletion are data from the Mariana and Tonga Trench and some ophiolitic data (e.g., Papuan samples from Jaques and Chappell, 1980, which are not plotted). There are overlaps in some of the data sets. The data from the Oman ophiolite (Browning, 1982) overlaps the more depleted end of the abyssal field and the less depleted end of the Leg 125 data.

Figure 4.9 shows that there is considerable spread in the data from Oman and Leg 125 compared with the abyssal data set. Temperatures have been calculated from Fabries' (1979) olivine-spinel Fe-Mg exchange thermometer for all the data plotted in Figure 4.9. The Leg 125 and ophiolite data give much lower temperatures for this thermometer (<800 °C) than the abyssal samples. Also, there is a far wider spread in the temperatures for the Leg 125 and ophiolitic samples indicating that these samples have undergone considerable sub-solidus re-equilibration. I interpret the spread in the data as due to the more extensive and variable sub-solidus re-equilibration that these samples have experienced in comparison with most of the abyssal data.

Detailed inspection of the abyssal peridotite data of Dick (1989), shows that these more refractory olivines are from abyssal peridotites associated with hot spots which have undergone higher degrees of partial melting because of elevated mantle potential temperatures (McKenzie and Bickle, 1988). The trend for all the data is that for increases in partial melting from fertile mantle to the ultra-depleted Leg 125 peridotites. A first order approximation from the olivine data is that the Leg 125 peridotites represent residues from high degrees of partial melting.

#### 4.7.1.2 Dunites

Ishii et al., (1992) analysed olivine in dunites in six samples from Conical Seamount. Representative analyses are presented in Table 4.2. They have highly variable forsterite content ranging from 90.60 to 94.10. The lower value is lower than any of the harzburgites whereas two of the dunites have extremely high forsterite contents that are greater than those in the harzburgites. Petrographic evidence suggests that none of the dunites have obvious cumulate textures and often are strongly tectonised, with porphyroclastic olivines. The high Mg# olivines are consistent with the dunites being residues from extremely high degrees of melting, possibly as localised pockets associated with fluid fluxing. Amphibole and small secondary clinopyroxene crystals have been found in some dunite samples so it is possible that some of the dunites with low forsterite content are cumulates from hydrous melts. Because these samples have

been strongly deformed it is difficult to tell on textural grounds whether they are cumulates.

**Table 4.2.** Representative analyses of olivines from Leg 125 dunites (from Ishii et al., 1992). *Total Fe as FeO.

| | Conical Seamount | | | | | |
|---|---|---|---|---|---|---|
| Hole | | | 779A | | | 780C |
| Core | 3R-CC | 14R-2 | 15R-2 | 22R-2 | 25R-1 | 8R-1 |
| Interval | 19-20 | 18-21 | 24-27 | 18-20 | 85-87 | 94-96 |
| Rock | D908 | D934 | D938 | D950 | D954 | D015 |
| Point | 18 | 18 | 147 | 87 | 33 | 41 |
| Analysis | 1 | 46 | 63 | 25 | 41 | 10 |
| $SiO_2$ | 41.14 | 41.75 | 42.51 | 41.12 | 41.27 | 41.37 |
| $TiO_2$ | 0.03 | 0.01 | 0.00 | 0.02 | 0.02 | 0.04 |
| $Al_2O_3$ | 0.00 | 0.00 | 0.00 | 0.00 | 0.00 | 0.01 |
| FeO* | 7.76 | 7.66 | 5.77 | 8.51 | 6.78 | 9.31 |
| MgO | 49.95 | 51.25 | 51.65 | 50.06 | 50.84 | 50.18 |
| CaO | 0.01 | 0.00 | 0.01 | 0.01 | 0.00 | 0.02 |
| $K_2O$ | 0.00 | 0.00 | 0.01 | 0.01 | 0.00 | 0.00 |
| NiO | 0.41 | 0.42 | 0.45 | 0.40 | 0.35 | 0.31 |
| $Cr_2O_3$ | 0.03 | 0.01 | 0.01 | 0.02 | 0.03 | 0.04 |
| Total | 99.33 | 101.10 | 100.41 | 100.15 | 99.29 | 101.28 |
| O=4.000 | | | | | | |
| Si | 1.006 | 1.002 | 1.017 | 1.001 | 1.005 | 0.999 |
| Ti | 0.001 | 0.000 | 0.000 | 0.000 | 0.000 | 0.001 |
| Al | 0.000 | 0.000 | 0.000 | 0.000 | 0.000 | 0.000 |
| $Fe^{2+}$ | 0.159 | 0.154 | 0.115 | 0.173 | 0.138 | 0.188 |
| Mg | 1.820 | 1.833 | 1.842 | 1.816 | 1.845 | 1.805 |
| Ca | 0.000 | 0.000 | 0.000 | 0.000 | 0.000 | 0.001 |
| K | 0.000 | 0.000 | 0.000 | 0.000 | 0.000 | 0.000 |
| Ni | 0.008 | 0.008 | 0.009 | 0.008 | 0.007 | 0.006 |
| Cr | 0.001 | 0.000 | 0.000 | 0.000 | 0.001 | 0.001 |
| Total O | 2.994 | 2.998 | 2.983 | 2.999 | 2.995 | 3.000 |
| Z | 1.007 | 1.002 | 1.017 | 1.001 | 1.005 | 1.000 |
| XY | 1.987 | 1.995 | 1.966 | 1.998 | 1.989 | 2.000 |
| Mg# | 0.920 | 0.923 | 0.941 | 0.913 | 0.930 | 0.906 |

### 4.7.2 Orthopyroxene

Ishii et al., (1992) present a large number of orthopyroxene analyses Table 4.3 lists a reprentative set of analyses for orthopyroxenes from both seamounts. In keeping with the highly forsteritic nature of the olivines, the orthopyroxenes from Leg 125 peridotites are highly enstatitic with Mg# between 91.20 and 93.80.

Figure 4.10 shows the variation of oxides $SiO_2$, $Al_2O_3$, FeO, MgO and CaO with Mg# in orthopyroxenes from the two seamounts. As with the chemistry in other minerals, samples from Conical Seamount show a wide variation in chemistry whereas the samples from Torishima Forearc Seamount have a more restricted compositional range. The ranges of Mg# for the different holes is consistent with their forsterite content. Again, samples from hole 778A have the most refractory compositions. Those from 779A have a wide range of compositions and those from 780C+D plot in the middle of the range. Orthopyroxenes from Torishima Seamount have a more restricted

range of compositions with the majority of the orthopyroxenes from Hole 783A plotting at the lowest Mg#.

**Fig 4.3.** Representative orthopyroxene analyses from Leg 125 harzburgites from Ishii et al. (1992). *Total Fe as FeO..

| | Conical Seamount | | | | | | | Torishima Forearc Seamount | | | |
|---|---|---|---|---|---|---|---|---|---|---|---|
| Hole | 778A | | 779A | | | 780C | | 783A | | 784A | |
| Core | 2R-1 | 3R-CC | 8R-1 | 22R-3 | 26R-3 | 6R-1 | 18R-1 | 16R-CC | 18R-1 | 37R-1 | 45R-1 |
| Interval | 82-84 | 33701 | 41-45 | 55-57 | 102-105 | 67-69 | 65-67 | 14-17 | 100-103 | 33853 | 95-98 |
| Rock | H810 | H815 | H916 | H952 | H958 | H010 | H035 | H325 | H355 | H410 | H460 |
| Point | 13 | 68 | 36 | 87 | 61 | 20 | 44 | 66 | 821 | 334 | 11 |
| Analysis | 1 | 33 | 9 | 9 | 38 | 15 | 40 | 49 | 1 | 39 | 13 |
| $SiO_2$ | 57.53 | 56.61 | 57.84 | 58.00 | 56.38 | 56.75 | 56.09 | 57.59 | 56.27 | 58.12 | 56.55 |
| $TiO_2$ | 0.02 | 0.03 | 0.02 | 0.00 | 0.07 | 0.01 | 0.01 | 0.03 | 0.03 | 0.00 | 0.01 |
| $Al_2O_3$ | 1.00 | 2.06 | 1.03 | 0.53 | 2.75 | 1.05 | 2.20 | 2.31 | 1.91 | 1.83 | 1.25 |
| FeO* | 4.62 | 5.09 | 5.37 | 5.72 | 5.00 | 5.62 | 5.62 | 5.19 | 5.79 | 5.36 | 5.48 |
| MgO | 35.72 | 35.01 | 36.11 | 34.63 | 33.94 | 35.47 | 34.12 | 33.45 | 35.07 | 33.56 | 34.56 |
| CaO | 0.84 | 0.42 | 0.44 | 0.56 | 0.49 | 0.31 | 0.91 | 1.03 | 0.40 | 0.65 | 0.70 |
| $K_2O$ | 0.01 | 0.02 | 0.02 | 0.03 | 0.00 | 0.01 | 0.00 | 0.01 | 0.01 | 0.01 | 0.00 |
| NiO | 0.09 | 0.05 | 0.03 | 0.09 | 0.08 | 0.08 | 0.09 | 0.11 | 0.16 | 0.10 | 0.08 |
| $Cr_2O_3$ | 0.46 | 0.38 | 0.26 | 0.36 | 0.69 | 0.20 | 0.59 | 0.60 | 0.75 | 0.54 | 0.41 |
| Total | 100.29 | 99.67 | 101.12 | 99.92 | 99.40 | 99.50 | 99.63 | 100.32 | 100.39 | 100.17 | 99.04 |
| O=6.000 | | | | | | | | | | | |
| Si | 1.967 | 1.949 | 1.964 | 1.995 | 1.945 | 1.962 | 1.941 | 1.970 | 1.934 | 1.958 | 1.964 |
| Ti | 0.001 | 0.001 | 0.001 | 0.000 | 0.002 | 0.000 | 0.000 | 0.001 | 0.001 | 0.000 | 0.000 |
| Al | 0.040 | 0.084 | 0.041 | 0.021 | 0.112 | 0.043 | 0.090 | 0.093 | 0.077 | 0.074 | 0.051 |
| $Fe^{2+}$ | 0.132 | 0.147 | 0.153 | 0.165 | 0.144 | 0.162 | 0.163 | 0.148 | 0.166 | 0.153 | 0.159 |
| Mg | 1.820 | 1.796 | 1.828 | 1.775 | 1.745 | 1.828 | 1.760 | 1.705 | 1.797 | 1.711 | 1.790 |
| Ca | 0.031 | 0.015 | 0.016 | 0.021 | 0.018 | 0.011 | 0.034 | 0.038 | 0.015 | 0.024 | 0.026 |
| K | 0.000 | 0.001 | 0.001 | 0.001 | 0.000 | 0.000 | 0.000 | 0.000 | 0.000 | 0.000 | 0.000 |
| Ni | 0.002 | 0.001 | 0.001 | 0.002 | 0.002 | 0.002 | 0.003 | 0.003 | 0.004 | 0.003 | 0.002 |
| Cr | 0.012 | 0.010 | 0.007 | 0.010 | 0.019 | 0.005 | 0.016 | 0.016 | 0.020 | 0.015 | 0.011 |
| Total O | 4.006 | 4.004 | 4.011 | 3.990 | 3.988 | 4.014 | 4.006 | 3.975 | 4.016 | 3.968 | 4.004 |
| Z | 2.007 | 2.032 | 2.006 | 2.016 | 2.057 | 2.004 | 2.031 | 2.063 | 2.012 | 2.062 | 2.016 |
| WXY | 1.999 | 1.972 | 2.006 | 1.974 | 1.931 | 2.010 | 1.975 | 1.912 | 2.004 | 1.906 | 1.989 |
| Wo | 0.016 | 0.008 | 0.008 | 0.011 | 0.009 | 0.006 | 0.017 | 0.020 | 0.007 | 0.013 | 0.013 |
| En | 0.918 | 0.917 | 0.916 | 0.906 | 0.915 | 0.913 | 0.900 | 0.902 | 0.908 | 0.906 | 0.906 |
| Fs | 0.067 | 0.075 | 0.076 | 0.084 | 0.076 | 0.081 | 0.083 | 0.078 | 0.084 | 0.081 | 0.081 |
| Mg# | 0.932 | 0.925 | 0.923 | 0.915 | 0.924 | 0.918 | 0.915 | 0.920 | 0.915 | 0.918 | 0.918 |

Obviously there are good correlations between MgO and FeO with Mg#. $Al_2O_3$ has a good negative correlation with Mg#. Orthopyroxenes from hole 778A have much higher values of $Al_2O_3$ for a given Mg# and plot off the main depletion trend of $Al_2O_3$. This again shows samples from hole 778A have subtly different mineral chemistries to the other Leg 125 peridotites. It is possible that the peridotites sampled in hole 778A represent the residue of melting of a slighly different source to the other peridotites or that they have experienced a different melting and re-equilibration history.

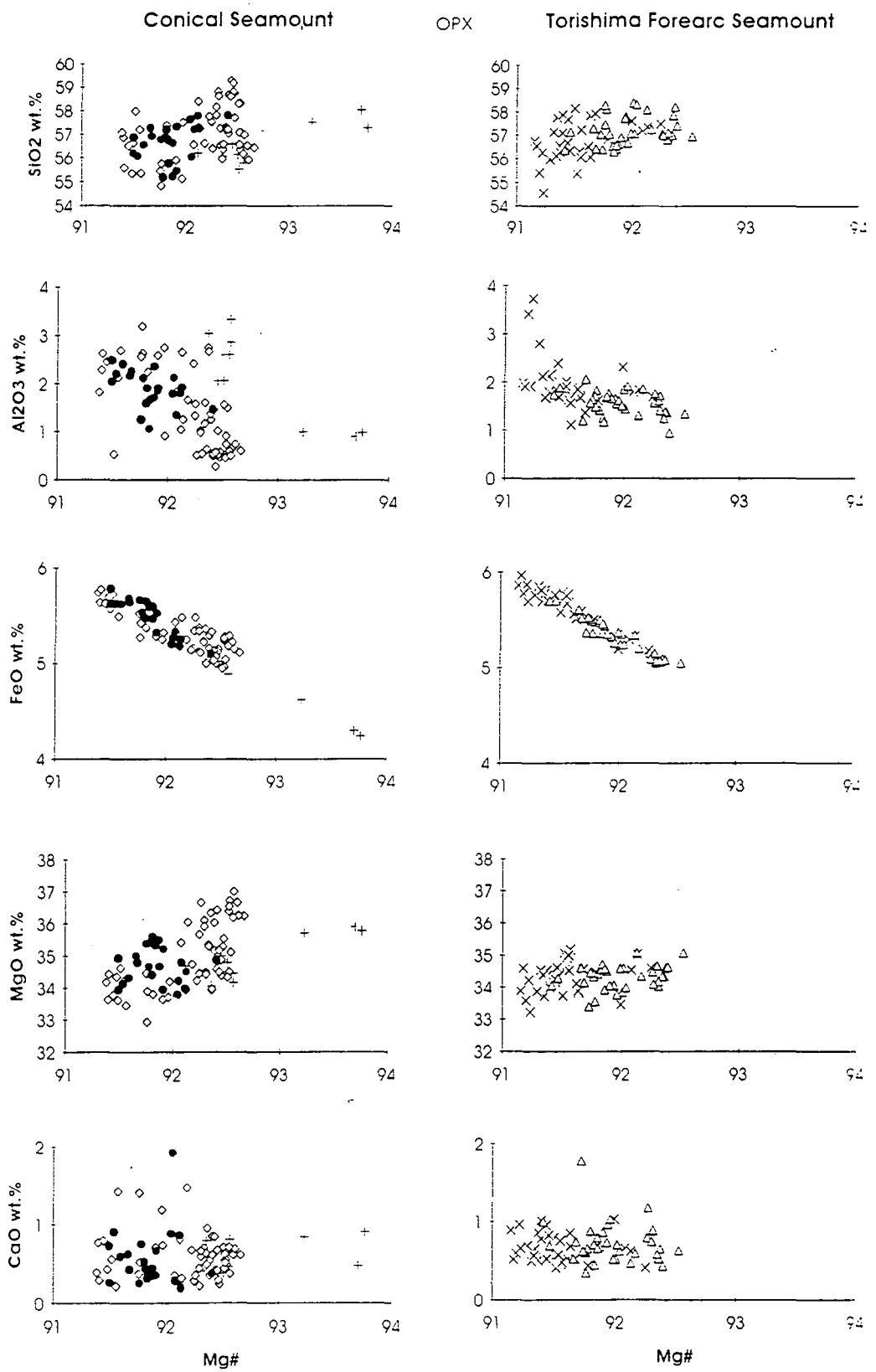


**Figure 4.10**. Plots of wt.% $SiO_2$, $Al_2O_3$, FeO, MgO and CaO versus Mg# in orthopyroxene for the two seamounts. The symbols for each of the holes are the same as in Figure 4.8.

Correlation coefficients between $Mg^{\#}$ and $SiO_2$, $Al_2O_3$, Fe, Mg and CaO are a). for hole 778A 0.7096, 0.7281, 0.9754, 0.7154, 0.2078. b). for hole 779A 0.1432, 0.4454, 0.8814, 0.4084, 0.0103. c). for hole 780C+D 0.1465, 0.2230, 0.7873, 0.0015, 0.0035. d). for hole 783A 0.1839, 0.1281, 0.8410, 0.0876, 0.0822. e). for hole 784A 0.0489, 0.1000, 0.8546, 0.0476, 0.0093. The poor correlation between oxides and $Mg^{\#}$ may reflect the complicated melting history of the peridotites.

#### 4.7.2.1 Comparison With Other Peridotites

In this section orthopyroxenes from Leg 125 are compared with orthopyroxenes from peridotites from different tectonic settings. Bonatti and Michael (1989) have also compared the mineral chemistry of peridotites from different tectonic settings. They use average analyses of minerals from a large data set. Although average analyses emphasise broad differences between the peridotites it became apparent during this study that many subtle differences between the peridotites exist when the available data is studied carefully. The composition of orthopyroxenes from different peridotites emphasises some of these differences.

The same data set that was used to compare the olivine compositions is used here also. Orthopyroxene commonly exsolves clinopyroxene under sub-solidus conditions. This sub-solidus equilibration strongly effects the composition of the coexisting ortho- and clinopyroxenes. To counter this re-equilibration, Dick, (1989) picked both ortho- and clinopyroxenes grains from a large number of ab yssal peridotites and then fused the mineral separates to homogenise the effects of exsolution. This has both beneficial and problematic effects. The bulk analysis is likely to reflect the composition of pyroxenes under magmatic conditions (which is reflected in their two-pyroxene temperatures) but unfortunately makes comparison with most *in situ* electron microprobe studies difficult.

Figure 4.11 shows plots of $Al_2O_3$, FeO, MgO, CaO and $Cr_2O_3$ against Mg# for the various data sets. The effects of Dick's "re-equilibration correction" are apparent to varying extents in all of the plots. The effect of homogenising the orthopyroxenes is to increase the $Al_2O_3$ and CaO concentrations and decrease the FeO and MgO concentrations in the analysis for a given Mg#. This is very well shown in the $Al_2O_3$ plot where Dick's data lie completely off the main depletion trend. The abyssal data from Komor et al. (1990) is *in situ* electon microprobe data and sits nicely on the main depletion trend. The Leg 125 data plot at the depleted end of all diagrams. Again the Oman orthopyroxenes are transitional between the Leg 125 orthopyroxene data and abyssal data. The plots emphasise the need for caution in these types of comparison plots as sub-soldus re-equilibration effects can be substantial. The $Cr_2O_3$ against Mg# diagram should be relatively unaffected by the re-equilibration effects and shows some intersting differences between orthopyroxenes from abyssal peridotites and the more depleted peridotites. $Cr_2O_3$ increases slightly with increasing depletion (increasing Mg#) in the abyssal peridotites. By contrast $Cr_2O_3$ is much lower in the more depleted Leg 125 orthopyroxenes. This suggests that Cr may be behave differently during the

melting history of these peridotites. This point will investigated in more detail later on in this chapter.

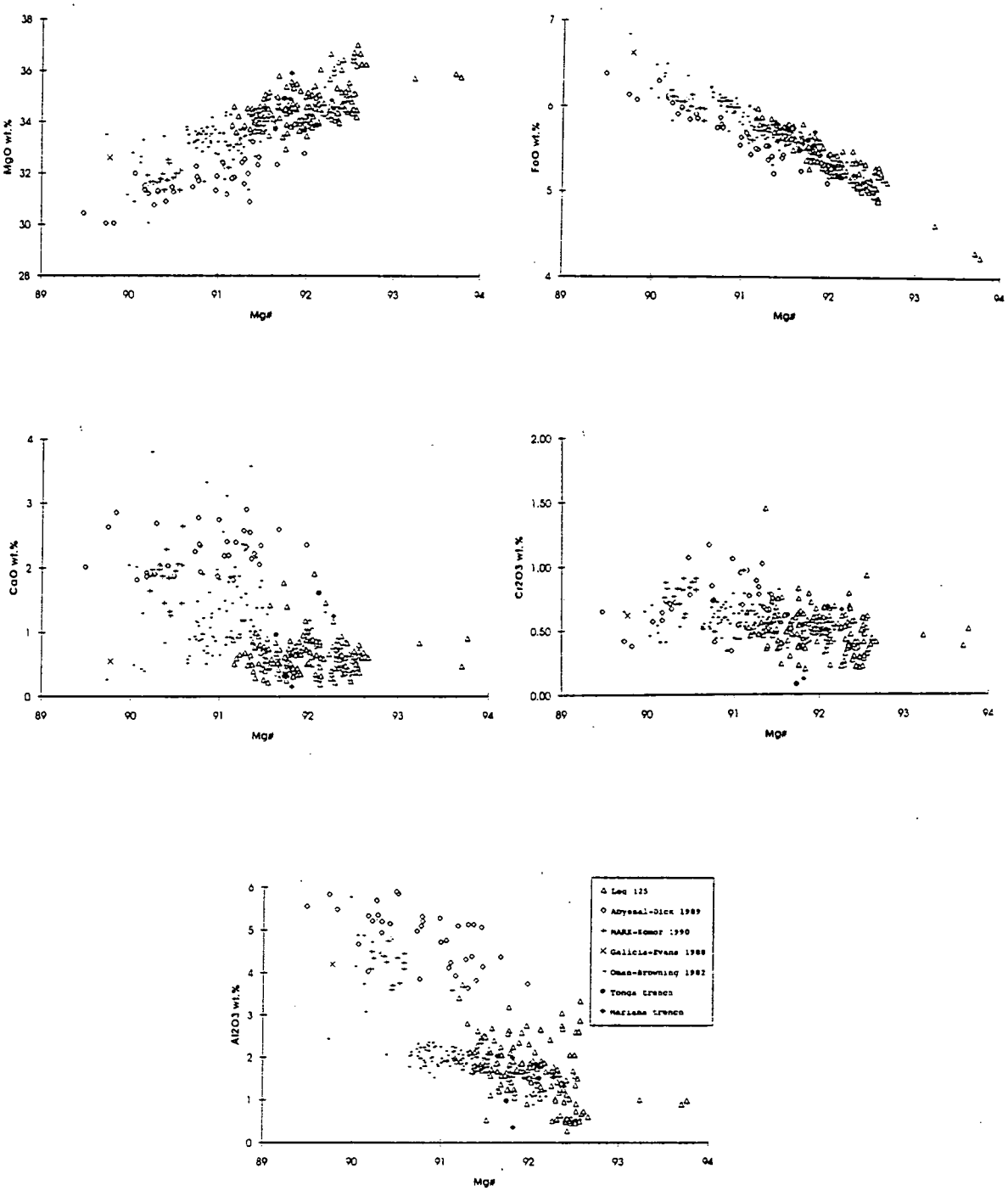


**Figure 4.11.** Plots of selected wt.% oxides against Mg# for orthopyroxenes in peridotites from different tectonic settings. Data source the same as Figure 4.9.

*The trends could be interpreted as either partial melting or fractionation trends depending on whether the rocks are interpreted as melting residues or cumulates. If partial melting had occurred the incompatible oxides would decrease with increasing $Mg^{\#}$. If fractionation had occurred the incompatible oxides would increase with decreasing $Mg^{\#}$ of the mineral. The highly deformed nature of some of the samples makes it difficult to distinguish with complete certainty the actual origin of the peridotites, although the author believes the peridotites are more likely to be melting residues.

*The trends could be interpreted as either partial melting or fractionation trends depending on whether the rocks are interpreted as melting residues or cumulates. If partial melting had occurred the incompatible oxides would decrease with increasing $Mg^{\#}$. If fractionation had occurred the incompatible oxides would increase with decreasing $Mg^{\#}$ of the mineral. The highly deformed nature of some of the samples makes it difficult to distinguish with complete certainty the actual origin of the peridotites, although the author believes the peridotites are more likely to be melting residues.

### 4.7.3 Clinopyroxene

A large number of clinopyroxene analyses are presented in Ishii et al., (1992). Table 4.4 lists a representative set of their analyses for clinopyroxenes from both seamounts. Clinopyroxene analyses are not available for all the samples, because the grains are either too small to analyse or are not represented in the thin section. In accordance with the highly refractory nature of the other ferromagnesian minerals in the peridotites and the very low modal abundance of clinopyroxene, they have extremely magnesian compositions with Mg# between 93.00 and 96.20. The between-hole relationships for Mg# of the clinopyroxenes are similar to those for the olivine and orthopyroxenes, with peridotites from hole 778A having the most refractory compositions. However, there is no obvious distinction between clinopyroxenes from holes 783A and 784A in contrast to the olivine data where they have distinct compositions.

**Table 4.4**. Representative analysis of clinopyroxenes from Leg 125 harzburgites (from Ishii et al., 1992). *Total Fe as FeO.

| | Conical Seamount | | | | | | Torishima Forearc Seamount | | | |
|---|---|---|---|---|---|---|---|---|---|---|
| Hole | 778A | | | 779A | 780C | | 783A | | 784A | |
| Core | 2R-1 | 3R-CC | 8R-1 | 26R-3 | 6R-1 | 18R-1 | 16R-CC | 18R-1 | 37R-1 | 45R-1 |
| Interval | 82-84 | 33701 | 41-45 | 102-105 | 67-69 | 65-67 | 14-17 | 100-103 | 33764 | 95-98 |
| Rock | H810 | H815 | H916 | H958 | H010 | H035 | H325 | H355 | H410 | H460 |
| Point | 11 | 69 | 35 | 66 | 19 | 37 | 67 | 818 | 327 | 9 |
| Analysis | 5 | 42 | 22 | 42 | 25 | 40 | 53 | 11 | 42 | 22 |
| $SiO_2$ | 54.67 | 53.22 | 54.62 | 54.77 | 53.91 | 53.52 | 54.52 | 53.40 | 55.79 | 53.28 |
| $TiO_2$ | 0.02 | 0.10 | 0.04 | 0.14 | 0.03 | 0.03 | 0.06 | 0.02 | 0.02 | 0.04 |
| $Al_2O_3$ | 1.05 | 2.64 | 1.15 | 2.46 | 0.73 | 1.65 | 1.56 | 1.31 | 1.45 | 1.20 |
| FeO* | 1.57 | 1.58 | 1.69 | 1.69 | 1.39 | 1.70 | 1.65 | 1.69 | 1.86 | 1.69 |
| MgO | 18.09 | 17.18 | 18.69 | 16.86 | 17.92 | 17.32 | 17.17 | 17.89 | 17.43 | 17.55 |
| CaO | 23.26 | 23.57 | 24.36 | 22.53 | 25.03 | 24.34 | 24.11 | 24.11 | 23.36 | 24.45 |
| $K_2O$ | 0.00 | 0.02 | 0.02 | 0.02 | 0.00 | 0.00 | 0.00 | 0.01 | 0.01 | 0.00 |
| NiO | 0.12 | 0.05 | 0.06 | 0.10 | 0.11 | 0.05 | 0.12 | 0.08 | 0.08 | 0.09 |
| $Cr_2O_3$ | 0.93 | 0.96 | 0.39 | 0.92 | 0.44 | 0.75 | 0.64 | 0.67 | 0.49 | 0.57 |
| Total | 99.71 | 99.32 | 101.02 | 99.49 | 99.56 | 99.36 | 99.83 | 99.18 | 100.49 | 98.87 |
| O=6.000 | | | | | | | | | | |
| Si | 1.980 | 1.940 | 1.960 | 1.980 | 1.967 | 1.955 | 1.976 | 1.955 | 2.000 | 1.958 |
| Ti | 0.001 | 0.003 | 0.001 | 0.004 | 0.001 | 0.001 | 0.002 | 0.001 | 0.001 | 0.001 |
| Al | 0.045 | 0.113 | 0.049 | 0.105 | 0.031 | 0.071 | 0.067 | 0.057 | 0.061 | 0.052 |
| $Fe^{2+}$ | 0.048 | 0.048 | 0.051 | 0.051 | 0.042 | 0.052 | 0.050 | 0.052 | 0.056 | 0.052 |
| Mg | 0.977 | 0.933 | 1.000 | 0.909 | 0.975 | 0.943 | 0.928 | 0.976 | 0.931 | 0.961 |
| Ca | 0.903 | 0.920 | 0.936 | 0.873 | 0.978 | 0.953 | 0.936 | 0.946 | 0.897 | 0.963 |
| K | 0.000 | 0.001 | 0.001 | 0.001 | 0.000 | 0.000 | 0.000 | 0.000 | 0.000 | 0.000 |
| Ni | 0.003 | 0.001 | 0.002 | 0.003 | 0.003 | 0.001 | 0.003 | 0.002 | 0.002 | 0.003 |
| Cr | 0.027 | 0.028 | 0.011 | 0.026 | 0.013 | 0.022 | 0.018 | 0.019 | 0.014 | 0.017 |
| Total O | 3.983 | 3.988 | 4.010 | 3.951 | 4.010 | 3.998 | 3.980 | 4.007 | 3.962 | 4.007 |
| Z | 2.025 | 2.053 | 2.008 | 2.085 | 1.998 | 2.026 | 2.043 | 2.011 | 2.061 | 2.010 |
| WXY | 1.958 | 1.935 | 2.002 | 1.866 | 2.012 | 1.972 | 1.937 | 1.996 | 1.901 | 1.996 |
| Wo | 0.468 | 0.484 | 0.471 | 0.476 | 0.490 | 0.489 | 0.489 | 0.479 | 0.476 | 0.487 |
| En | 0.507 | 0.491 | 0.503 | 0.496 | 0.488 | 0.484 | 0.485 | 0.495 | 0.494 | 0.487 |
| Fs | 0.025 | 0.025 | 0.026 | 0.028 | 0.021 | 0.027 | 0.026 | 0.026 | 0.030 | 0.026 |
| Mg# | 0.954 | 0.951 | 0.952 | 0.947 | 0.958 | 0.948 | 0.949 | 0.950 | 0.944 | 0.949 |

Figure 4.12 shows plots of the oxides $SiO_2$, $Al_2O_3$, FeO, MgO and CaO against Mg#. These plots show the expected trends for partial melting* with decreasing $Al_2O_3$ and FeO and increasing CaO with increasing Mg#. Again pyroxenes from Hole 778A have

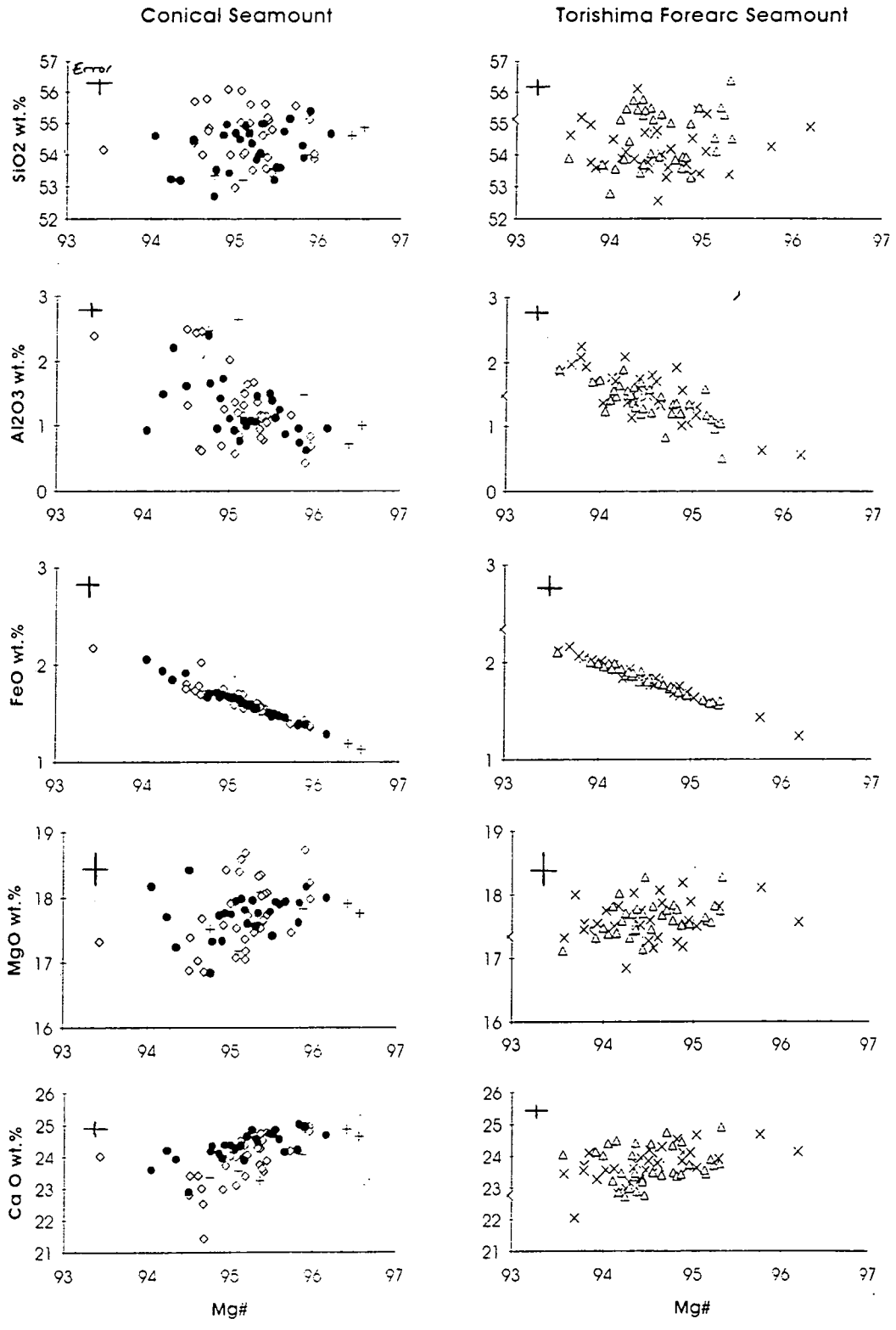


**Figure 4.12.** Plots of selected wt.% oxides against Mg# for clinopyroxenes from the two seamounts. Symbols for the holes are the same as Figure 4.8..

distinct compositions plotting at a relatively high $Al_2O_3$ and low CaO content for a given Mg#.

#### 4.7.3.1 Comparison with Other Peridotites

To compare clinopyroxenes I adopt a similar rationale to that of orthopyroxenes. Plots of $Al_2O_3$, FeO, MgO, CaO and $Cr_2O_3$, against Mg# are shown in Fig 4.13. The abyssal peridotite data of Dick (1989) plot at substantially lower CaO and higher FeO and MgO. These show the effect of homogenising the exsolution lamellae. The data for $Al_2O_3$ do not obviously show the expected trend for homogenisation. The Leg 125 data as a whole again plots at the depleted end of the array, with low $Al_2O_3$ at high Mg#. The $Cr_2O_3$ content of the clinopyroxenes decrease with increasing Mg# which is surprising as Cr is usually compatible with orthopyroxene during partial melting. It is possible that trend on the $Cr_2O_3$ versus Mg# represents some other process than partial melting such as subsolidus re-equilibration with spinel.

### 4.7.4 Spinel

Ishii et al. (1992) present several hundred spinel analysis. Table 4.5 lists representative analyses of spinels from harzburgites from the two seamounts. The Mg# of the spinels has been shown to be a good indicator of partial melting, decreasing with increasing partial melting (Dick, 1977; Browning 1982; Dick and Bullen 1984). Figure 4.14 shows the variation of $Al_2O_3$, $Fe_2O_3$, FeO, MgO and $Cr_2O_3$, with Mg# for harzburgites from the two seamounts. As with the other minerals, data from hole 778A cover the whole range of data from the holes. Hole 779A has a very wide span of compositions, although distinct *en echelon* groups can be seen. Hole 780C+D plot in the middle of the compositional range. Hole 783A and 784A have compositions which plot in the middle of the range but are slightly displaced from the main trend in several of the plots as defined by the hole 779A data.

In detail, $Al_2O_3$ shows a strong positive correlation with Mg# indicating its incompatible behavior with respect to Cr-spinel during partial melting. $Fe_2O_3$ increases slightly with decreasing Mg#, although the correlation is not particulaly strong and possibly reflects the problems in calculating $Fe^{3+}$. However, spinels from Holes 783A and 784A plot at distinctly higher $Fe_2O_3$ for a given Mg# which has implications for the oxygen fugacity under which the peridotite equilibrated (see Oxygen Thermobarometry section). FeO shows a strong antithetic, and MgO a strong sympathetic relationship with Mg#. This is hardly surprising considering that both elements are used to calculate Mg#, but the MgO plot indicates especially well that there are several distinct groups of data, which plot as *en echelon*

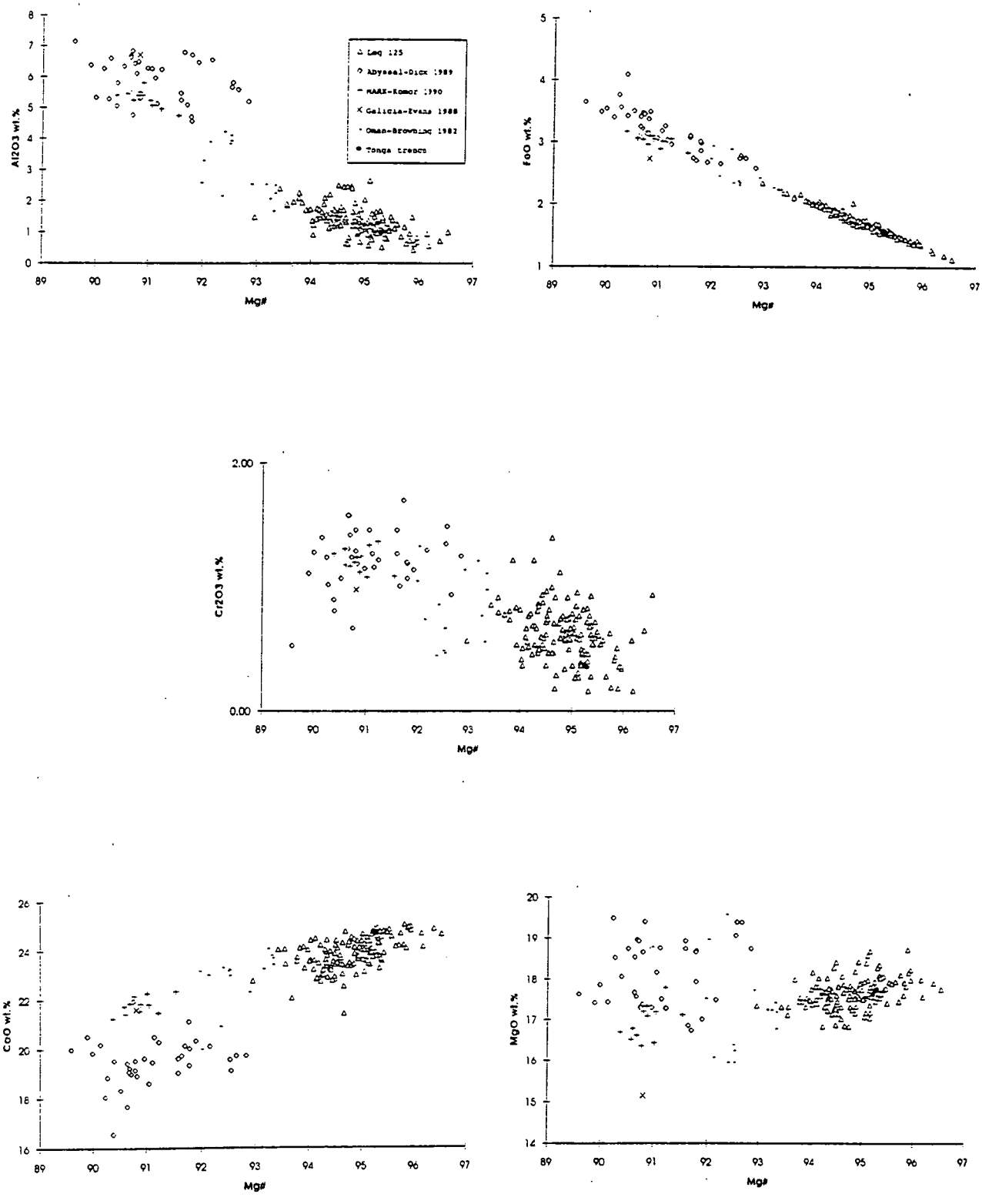


**Fig 4.13.** Comparative plot of clinopyroxenes from different tectonic settings. Data sources as Figure 4.9.

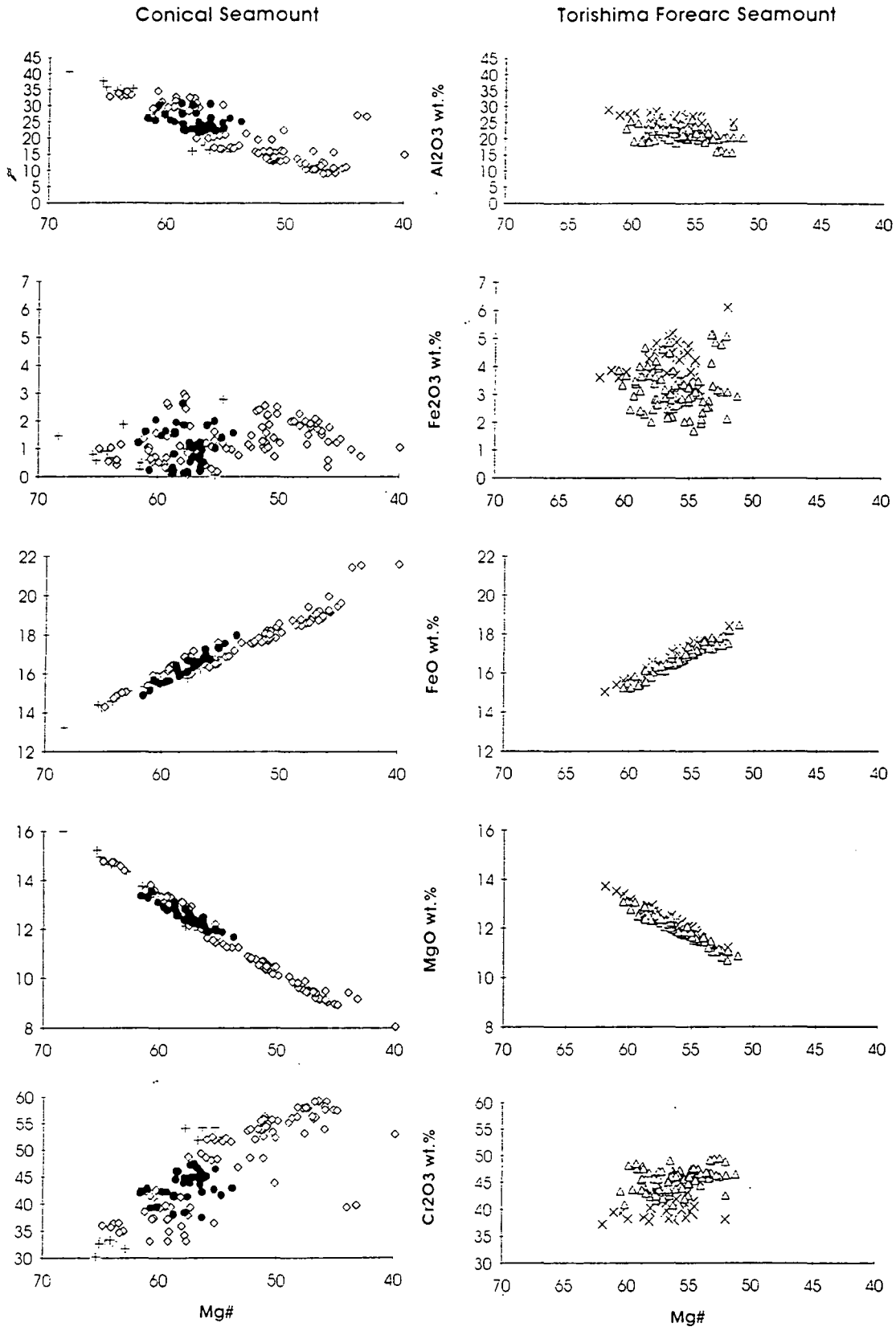


**Fig 4.14.** Selected wt.% major oxides plotted against Mg# for spinels from Conical and Torishima Forearc Seamount.

sets within the main trend for the hole 779A samples. Plots of $SiO_2$, $TiO_2$, $Na_2O$, and NiO against Mg# show no significant correlations which mainly reflects the fact that the concentrations of these elements are close to the detection limit of the electron microprobe. NiO does show a weak negative correlation, but the error in the data is probably as large as the variation with Mg#.

**Table 4.5**. Selected Cr-spinel analyses from harzburgite samples. $Fe_2O_3$ and $Fe^{3+}$ calculated from $AB_2O_4$ stoichiometry. Data from Ishii et al. (1992).

| | Conical Seamount | | | | | | | Torishima Forearc Seamount | | | |
|---|---|---|---|---|---|---|---|---|---|---|---|
| **Hole** | **778A** | | **779A** | | | **780C** | | **783A** | | **784A** | |
| **Core** | **2R-1** | **3R-CC** | **8R-1** | **22R-3** | **26R-3** | **6R-1** | **18R-1** | **16R-CC** | **18R-1** | **37R-1** | **45R-1** |
| **Interval** | **82-84** | **33701** | **41-45** | **55-57** | **102-105** | **67-69** | **65-67** | **14-17** | **100-103** | **33853** | **95-98** |
| **Rock** | **H810** | **H815** | **H916** | **H952** | **H958** | **H010** | **H035** | **H325** | **H355** | **H410** | **H460** |
| **Point** | **1** | **12** | **8** | **77** | **55** | **4** | **24** | **59** | **809** | **330** | **45** |
| **Analysis** | **6** | **28** | **14** | **88** | **81** | **2** | **40** | **1** | **6** | **1** | **29** |
| $SiO_2$ | 0.00 | 0.02 | 0.00 | 0.09 | 0.02 | 0.07 | 0.06 | 0.00 | 0.00 | 0.07 | 0.05 |
| $TiO_2$ | 0.10 | 0.12 | 0.10 | 0.13 | 0.20 | 0.08 | 0.07 | 0.09 | 0.09 | 0.07 | 0.12 |
| $Al_2O_3$ | 16.83 | 35.3 | 20.20 | 10.56 | 33.03 | 24.17 | 30.89 | 27.83 | 21.67 | 24.89 | 18.76 |
| $Fe_2O_3$ | 0.05 | 0.88 | 0.55 | 0.59 | 1.03 | 0.70 | 0.08 | 3.80 | 4.74 | 2.30 | 2.95 |
| FeO | 16.74 | 14.47 | 16.51 | 19.16 | 14.85 | 16.61 | 16.44 | 15.74 | 16.95 | 16.32 | 16.43 |
| MgO | 11.60 | 14.81 | 12.02 | 9.10 | 14.71 | 12.36 | 13.11 | 13.18 | 11.67 | 12.88 | 12.00 |
| CaO | 0.02 | 0.01 | 0.02 | 0.03 | 0.02 | 0.02 | 0.02 | 0.01 | 0.03 | 0.03 | 0.02 |
| $K_2O$ | 0.01 | 0.02 | 0.03 | 0.02 | 0.02 | 0.02 | 0.01 | 0.02 | 0.01 | 0.02 | 0.02 |
| NiO | 0.26 | 0.23 | 0.16 | 0.24 | 0.24 | 0.22 | 0.19 | 0.28 | 0.27 | 0.22 | 0.24 |
| $Cr_2O_3$ | 54.24 | 32.97 | 49.43 | 58.20 | 36.38 | 44.91 | 37.97 | 35.17 | 43.35 | 43.73 | 49.09 |
| **Total** | 99.85 | 98.83 | 99.02 | 98.12 | 100.5 | 99.16 | 98.84 | 99.12 | 98.78 | 100.53 | 99.68 |
| O=4.000 | | | | | | | | | | | |
| Si | 0.000 | 0.001 | 0.000 | 0.003 | 0.001 | 0.002 | 0.002 | 0.000 | 0.000 | 0.002 | 0.002 |
| Ti | 0.002 | 0.003 | 0.002 | 0.003 | 0.004 | 0.002 | 0.002 | 0.002 | 0.002 | 0.002 | 0.003 |
| Al | 0.631 | 1.214 | 0.750 | 0.420 | 1.131 | 0.879 | 1.091 | 0.994 | 0.809 | 0.891 | 0.700 |
| $Fe^{3+}$ | 0.001 | 0.020 | 0.013 | 0.015 | 0.023 | 0.016 | 0.002 | 0.088 | 0.114 | 0.053 | 0.071 |
| $Fe^{2+}$ | 0.445 | 0.353 | 0.435 | 0.541 | 0.361 | 0.429 | 0.412 | 0.399 | 0.449 | 0.414 | 0.435 |
| Mg | 0.550 | 0.644 | 0.564 | 0.458 | 0.637 | 0.569 | 0.586 | 0.595 | 0.551 | 0.583 | 0.567 |
| Ca | 0.001 | 0.000 | 0.001 | 0.001 | 0.001 | 0.001 | 0.001 | 0.000 | 0.001 | 0.001 | 0.001 |
| K | 0.000 | 0.001 | 0.001 | 0.001 | 0.001 | 0.001 | 0.000 | 0.001 | 0.000 | 0.001 | 0.001 |
| Ni | 0.007 | 0.005 | 0.004 | 0.007 | 0.006 | 0.005 | 0.005 | 0.007 | 0.007 | 0.005 | 0.006 |
| Cr | 1.363 | 0.760 | 1.231 | 1.552 | 0.836 | 1.096 | 0.900 | 0.914 | 1.068 | 1.049 | 1.216 |
| **Total O** | 3.000 | 3.000 | 3.001 | 3.000 | 3.000 | 3.000 | 3.000 | 3.000 | 3.002 | 3.000 | 3.002 |
| B | 1.998 | 1.996 | 1.996 | 1.991 | 1.995 | 1.994 | 1.995 | 1.998 | 1.994 | 1.994 | 1.991 |
| A | 1.002 | 1.003 | 1.004 | 1.006 | 1.004 | 1.004 | 1.003 | 1.001 | 1.008 | 1.003 | 1.009 |
| Cr | 0.68 | 0.38 | 0.62 | 0.78 | 0.42 | 0.55 | 0.45 | 0.46 | 0.54 | 0.53 | 0.61 |
| Al | 0.32 | 0.61 | 0.38 | 0.21 | 0.57 | 0.44 | 0.55 | 0.50 | 0.41 | 0.45 | 0.35 |
| $Fe^{3+}$ | 0.00 | 0.01 | 0.01 | 0.01 | 0.01 | 0.01 | 0.00 | 0.04 | 0.06 | 0.03 | 0.04 |
| **Mg#** | 0.55 | 0.65 | 0.56 | 0.46 | 0.64 | 0.57 | 0.59 | 0.60 | 0.55 | 0.58 | 0.57 |
| **Cr#** | 0.68 | 0.39 | 0.62 | 0.79 | 0.42 | 0.55 | 0.45 | 0.48 | 0.57 | 0.54 | 0.63 |

The composition of the spinels within one sample can be very consistent (a 2σ variation of 1% on the major mineral forming elements). However, one or two of the spinel analyses with a thin section may be distinctly different, plotting at much lower Cr×100/(Cr+Al). The difference in the spinel compositions represents two different origins of the spinels. Most of the analyses represent spinels that formed during the partial melting of the peridotite and are the spinels which have been highly deformed and strung out. However, some secondary spinels are formed by incongruent

dissolution of clinopyroxene during the recrystallisation of primary clinopyroxenes and have much lower Cr# (Girardeau and Lagabrielle, 1992).

#### 4.7.4.1 Comparison with Other Peridotites

Dick and Bullen (1984) analysed and collated a large number of spinel analyses from peridotites from many diverse tectonic settings and geological origins. They divided the harzburgite peridotites into three distinct types, I, II, and III, on the basis of their spinel chemistry. Using the rationale of Dick and Bullen (1984), most of the Leg 125 spinels place the peridotites as Type III although some plot at the high-end of Type I (but see below).

The best way of representing spinel analyses for comparison with other peridotites is on a plot of Mg# versus Cr# (Cr#=Cr*100/Cr+Al). Figs 4.15 show all the spinel data for the five Holes on such a plot. Dick and Bullen (1984) synthesised all the abyssal peridotite spinel data to form an often used field for abyssal peridotites which is marked on this plot. Also shown are Cr-spinels from the sources used in the other mineral comparisons. As shown previously the Leg 125 data shows the usual inverse realtionship between Mg# and Cr#. The first thing to note is that although there is some overlap in the Cr# between the abyssal peridotite field and the Leg 125 data, the Leg 125 data all plot at lower Mg# for a given Cr#. To understand the displacement of the Leg 125 data with respect to the Dick and Bullen field it is neccessary to understand the sub-solidus re-equilibration history and its effects on the Fe-Mg exchange between spinel and olivine.

Other mineral chemistry data previously discussed has suggests that the Leg 125 peridotites have undergone higher degrees of partial melting than most of the abyssal peridotites. For the same temperature and ferric-iron content the trend for increasing partial melting runs through and roughly parallel to Dick and Bullen's field to higher Cr# values (Dick 1977). However, as discussed fully in the geothermometry

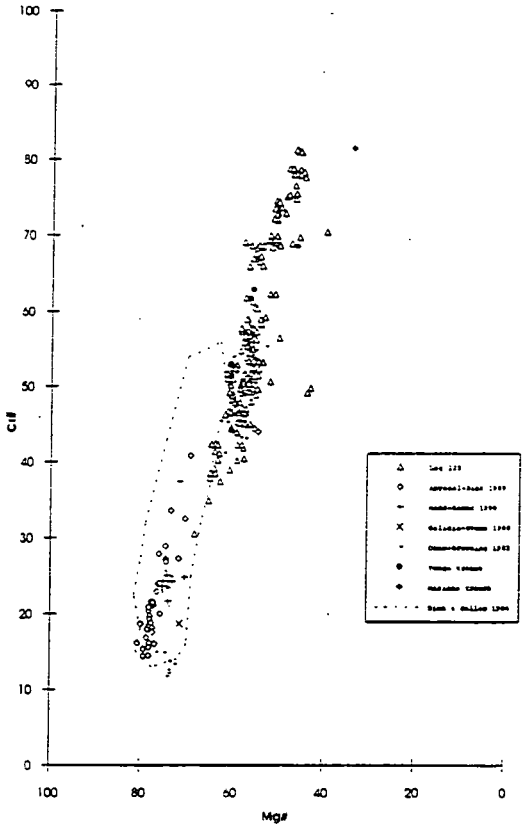


**Fig 4.15.** Spinel compositions from peridotites from different tectonic settings on a Mg# against Cr# plot. Data sources as Figure 4.9.

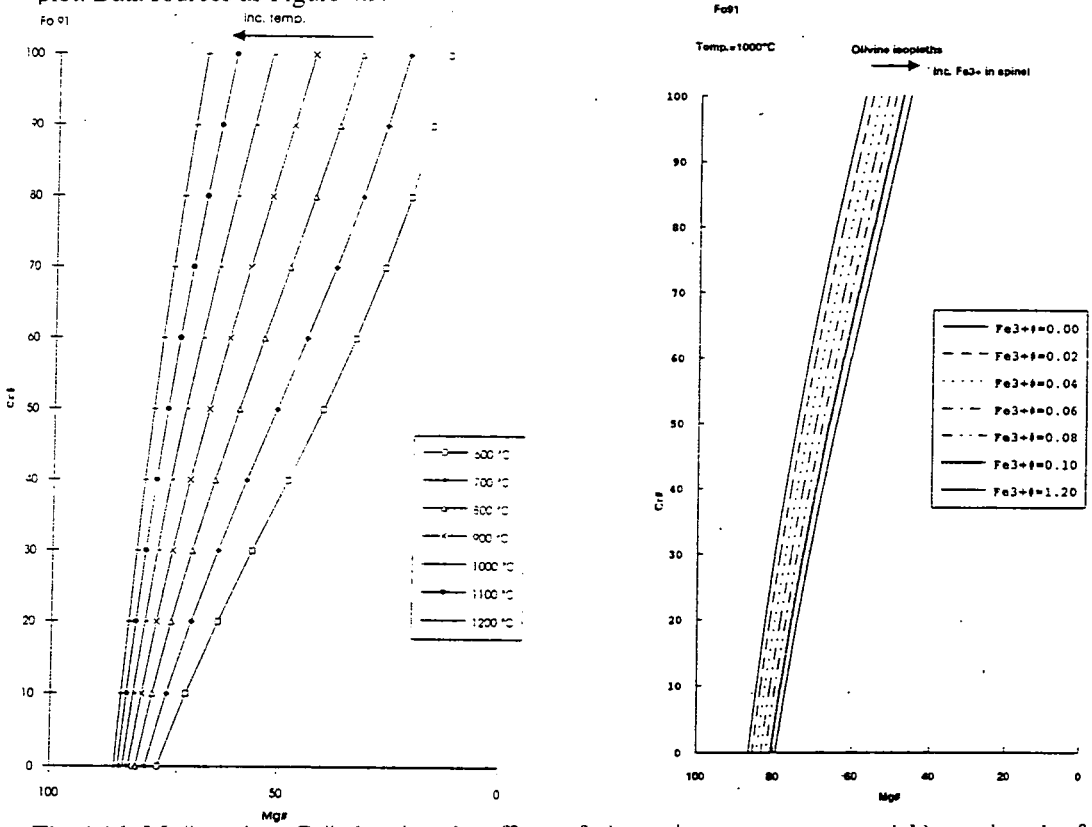


**Fig 4.16.** Mg# against Cr# showing the effects of **a)** varying temperature and **b)** varying the ferric iron content of spinel on the composition of spinel in equilibrium with $Fo_{91}$.

section, the Leg 125 peridotites may have very different cooling histories to abyssal peridotites. By rearranging Fabries' (1979) geothermetric equation (see spinel-olivine geothermometry section), it is possible to contour the Mg# versus Cr# spinel plot with olivine isopleths for a given temperature and ferric-iron content of spinel (e.g., Dick, 1977). The position of these isopleths depends both on the equilibration temperature of the exchange reaction and the ferric-iron content of the spinels. Figure 4.16 shows the effect of changing temperature and ferric-iron content for a single olivine isopleth ($Fo_{91}$). Decreasing the temperature has the effect of moving a given isopleth to lower spinel Mg# values. Increasing the ferric-iron content of the spinel has a similar, but less marked, effect. On this basis, the position of the Leg 125 peridotites relative to the abyssal peridotite field is due to two processes. Firstly, the Leg 125 peridotites have experienced higher degrees of melting (producing higher Cr#), Secondly, they have undergone more sub-solidus re-equilibration with the Fe-Mg exchange between the spinel and olivine taking place to much lower temperatures, so displacing spinels to lower Mg# values. The peridotites from Oman have not partially melted as much as the Leg 125 peridotites and so have lower Cr# than the Leg 125 data. However the Oman data is displaced from the Dick and Bullen field, showing a low temperature sub-solidus equilibration effect similar to that shown by the Leg 125 data. Some of the points that plot to the right of the main Leg 125 field could have been affected by hydrothermal alteration, as a marked increase in the Fe content is a characteristic of the breakdown of spinel to form amphibole and chlorite (Kimball, 1990).

#### 4.7.4.2 Dunites

Dunites have been found in all the cores and spinels from dunites have been analysed by Ishii et al., (1992) from Holes 779A, 780C and 784A. Dunites in ophiolitic sections and from the ocean basins could have two possible origins; as residues from very high degrees of melting or as cumulates from basaltic melts. The Cr-spinels in these dunites have Cr# that vary from 51 up to 83. The variation in Cr# is positively correlated with the Mg# of coexisting olivines. The spinels in 779A 15R-2, 24-27 cm are the most chrome-rich of any of the spinels from the Leg 125 peridotites. As previously mentioned, none of the dunites have obvious cumulate textures and they are interpreted as being residues to localised extremely high degrees of partial melting. However, it should be noted that the strong deformation that has affected some of the dunites would obliterate any cumulate textures, so the interpretation of the dunites as melting residues is not certain.

**Table 4.6.** Representative analysis of chromian spinels from dunites samples from Leg 125. $Fe_2O_3$ and $Fe^{3+}$ calculated from $AB_2O_4$ stoichiometry. Data from Ishii et al. (1992).

| | Conical Seamount | | | | | | Torishima Forearc Seamount |
|---|---|---|---|---|---|---|---|
| Hole | | | 779A | | | 780C | 784A |
| Core | 3R-CC | 14R-2 | 15R-2 | 22R-2 | 25R-1 | 8R-1 | 40R-2 |
| Interval | 19-20 | 18-21 | 24-27 | 18-20 | 85-87 | 94-96 | 33-36 |
| Rock | D908 | D934 | D938 | D950 | D954 | D015 | D425 |
| Point | 27 | 2 | 143 | 72 | 139 | 54 | 1 |
| Analysis | 1 | 71 | 6 | 36 | 53 | 15 | 33 |
| $SiO_2$ | 0.00 | 0.04 | 0.00 | 0.00 | 0.01 | 0.11 | 0.03 |
| $TiO_2$ | 0.20 | 0.11 | 0.11 | 0.10 | 0.12 | 0.10 | 0.17 |
| $Al_2O_3$ | 17.20 | 8.09 | 8.87 | 20.05 | 12.95 | 26.56 | 18.61 |
| $Fe_2O_3$ | 1.77 | 1.87 | 1.94 | 1.75 | 1.33 | 2.36 | 6.07 |
| FeO | 18.99 | 22.86 | 19.65 | 16.02 | 17.97 | 18.94 | 16.24 |
| MgO | 9.99 | 6.48 | 8.67 | 12.32 | 10.22 | 11.33 | 12.27 |
| CaO | 0.04 | 0.03 | 0.01 | 0.01 | 0.02 | 0.02 | 0.03 |
| $K_2O$ | 0.01 | 0.04 | 0.03 | 0.03 | 0.02 | 0.01 | 0.02 |
| NiO | 0.29 | 0.27 | 0.31 | 0.25 | 0.26 | 0.27 | 0.29 |
| $Cr_2O_3$ | 50.61 | 59.03 | 59.47 | 48.99 | 56.09 | 40.63 | 44.00 |
| Total | 99.10 | 98.82 | 99.06 | 99.52 | 98.99 | 100.33 | 97.73 |
| O=4.000 | | | | | | | |
| Si | 0.000 | 0.001 | 0.000 | 0.000 | 0.000 | 0.003 | 0.001 |
| Ti | 0.005 | 0.003 | 0.003 | 0.002 | 0.003 | 0.002 | 0.004 |
| Al | 0.655 | 0.330 | 0.354 | 0.740 | 0.502 | 0.955 | 0.705 |
| $Fe^{3+}$ | 0.044 | 0.049 | 0.050 | 0.042 | 0.033 | 0.055 | 0.149 |
| $Fe^{2+}$ | 0.513 | 0.661 | 0.556 | 0.420 | 0.494 | 0.483 | 0.436 |
| Mg | 0.481 | 0.334 | 0.437 | 0.575 | 0.501 | 0.515 | 0.588 |
| Ca | 0.001 | 0.001 | 0.000 | 0.000 | 0.001 | 0.001 | 0.001 |
| K | 0.000 | 0.002 | 0.001 | 0.001 | 0.001 | 0.000 | 0.001 |
| Ni | 0.008 | 0.008 | 0.008 | 0.006 | 0.007 | 0.007 | 0.007 |
| Cr | 1.293 | 1.613 | 1.591 | 1.213 | 1.458 | 0.980 | 1.118 |
| Total O | 3.000 | 3.001 | 3.001 | 3.001 | 3.000 | 3.000 | 3.010 |
| B | 1.996 | 1.995 | 1.997 | 1.998 | 1.996 | 1.991 | 1.975 |
| A | 1.003 | 1.003 | 1.002 | 1.002 | 1.003 | 1.005 | 1.033 |
| Cr | 0.65 | 0.81 | 0.80 | 0.61 | 0.73 | 0.49 | 0.57 |
| Al | 0.33 | 0.17 | 0.18 | 0.37 | 0.25 | 0.48 | 0.36 |
| $Fe^{3+}$ | 0.02 | 0.02 | 0.03 | 0.02 | 0.02 | 0.03 | 0.08 |
| Mg# | 0.48 | 0.34 | 0.44 | 0.58 | 0.50 | 0.52 | 0.57 |
| Cr# | 0.66 | 0.83 | 0.82 | 0.62 | 0.74 | 0.51 | 0.61 |

### 4.7.5 Amphibole

Ishii et al. (1992) present twelve amphibole analysis from two peridotité samples from Hole 784A. These are presented in Table 4.7. Using the classification scheme of Leake (1978), the amphiboles are all calcic ($(Ca+Na)_B>1.34$) and plot in the fields of magnesio-hornblende and edenitic hornblende (Figures 4.17 and 4.18). Although the amphiboles from both samples are similar those from 784A-45R-CC, 23-27 cm have higher Na contents. Two of the amphiboles from this sample have enough Na to classify the amphiboles as edenitic hornblendes. The amphiboles are both very magnesium- and chrome-rich which is consistent with their being the product of hydration of one of the primary phases in the peridotites. Petrography indicates that the mineral is orthopyroxene. The amphiboles have low concentrations of $K_2O$ and $TiO_2$ which are characersitic of amphibole related to subduction zones (Ozawa, 1988).

**Table 4.7.** Selected analyses of amphiboles from Hole 784A in the Torishima Forearc Seamount. Data from Ishii et al. (1992). *Total Fe as FeO.

| Rock | 784A, 41R-CC, 8-11 (H435) | | | | | | | 784A, 45R-CC, 23-27 (H490) | | | |
|---|---|---|---|---|---|---|---|---|---|---|---|
| Point No. | HB101 | HB102 | HB103 | HB104 | HB105 | HB106 | HB110 | HB111 | HB113 | HB114 | HB115 |
| Analysis No. | 1 | 2 | 3 | 4 | 5 | 6 | 7 | 8 | 9 | 10 | 11 |
| $SiO_2$ | 48.32 | 48.61 | 49.12 | 47.85 | 48.23 | 47.13 | 47.63 | 47.10 | 46.40 | 46.56 | 47.41 |
| $TiO_2$ | 0.15 | 0.16 | 0.15 | 0.14 | 0.14 | 0.14 | 0.14 | 0.14 | 0.09 | 0.08 | 0.16 |
| $Al_2O_3$ | 10.05 | 9.33 | 8.73 | 9.94 | 9.59 | 10.53 | 10.21 | 10.32 | 10.22 | 10.43 | 9.77 |
| FeO* | 2.63 | 2.28 | 2.42 | 2.71 | 2.53 | 2.91 | 3.06 | 2.72 | 2.71 | 2.61 | 2.56 |
| MnO | 0.06 | 0.06 | 0.06 | 0.04 | 0.07 | 0.05 | 0.01 | 0.09 | 0.07 | 0.07 | 0.01 |
| MgO | 19.58 | 19.97 | 20.31 | 19.54 | 20.01 | 19.68 | 19.67 | 19.55 | 19.62 | 19.80 | 19.79 |
| CaO | 12.67 | 12.57 | 13.01 | 12.70 | 12.86 | 12.48 | 12.56 | 12.52 | 12.36 | 12.55 | 12.65 |
| $Na_2O$ | 1.52 | 1.36 | 1.27 | 1.47 | 1.40 | 1.74 | 1.60 | 1.64 | 1.80 | 1.86 | 1.65 |
| $K_2O$ | 0.14 | 0.12 | 0.09 | 0.12 | 0.15 | 0.10 | 0.18 | 0.16 | 0.00 | 0.00 | 0.01 |
| NiO | 0.16 | 0.11 | 0.14 | 0.06 | 0.05 | 0.08 | 0.09 | 0.04 | 0.13 | 0.09 | 0.16 |
| $Cr_2O_3$ | 2.30 | 1.98 | 1.94 | 1.97 | 1.93 | 2.39 | 2.35 | 2.52 | 2.19 | 2.43 | 2.31 |
| Total | 97.58 | 96.55 | 97.24 | 96.54 | 96.96 | 97.23 | 97.50 | 96.80 | 95.59 | 96.48 | 96.48 |
| O=23.000 | | | | | | | | | | | |
| Si | 6.774 | 6.860 | 6.893 | 6.777 | 6.798 | 6.654 | 6.705 | 6.676 | 6.659 | 6.625 | 6.731 |
| Ti | 0.016 | 0.017 | 0.016 | 0.015 | 0.015 | 0.015 | 0.015 | 0.015 | 0.010 | 0.009 | 0.017 |
| Al | 1.661 | 1.552 | 1.444 | 1.659 | 1.593 | 1.752 | 1.694 | 1.724 | 1.729 | 1.749 | 1.635 |
| $Fe^{2+}$ | 0.308 | 0.269 | 0.284 | 0.321 | 0.298 | 0.344 | 0.360 | 0.322 | 0.325 | 0.311 | 0.304 |
| Mn | 0.007 | 0.007 | 0.007 | 0.005 | 0.008 | 0.006 | 0.001 | 0.011 | 0.009 | 0.008 | 0.001 |
| Mg | 4.092 | 4.201 | 4.249 | 4.125 | 4.204 | 4.141 | 4.127 | 4.130 | 4.197 | 4.200 | 4.188 |
| Ca | 1.903 | 1.901 | 1.956 | 1.927 | 1.942 | 1.888 | 1.894 | 1.901 | 1.901 | 1.913 | 1.924 |
| Na | 0.413 | 0.372 | 0.346 | 0.404 | 0.383 | 0.476 | 0.437 | 0.451 | 0.501 | 0.513 | 0.454 |
| K | 0.025 | 0.022 | 0.016 | 0.022 | 0.027 | 0.018 | 0.032 | 0.029 | 0.000 | 0.000 | 0.002 |
| Ni | 0.018 | 0.012 | 0.016 | 0.007 | 0.006 | 0.009 | 0.010 | 0.005 | 0.015 | 0.010 | 0.018 |
| Cr | 0.255 | 0.221 | 0.215 | 0.221 | 0.215 | 0.267 | 0.262 | 0.282 | 0.248 | 0.273 | 0.259 |
| Total | 15.472 | 15.434 | 15.442 | 15.481 | 15.488 | 15.569 | 15.537 | 15.546 | 15.593 | 15.612 | 15.533 |
| Mg# | 0.93 | 0.94 | 0.94 | 0.93 | 0.93 | 0.92 | 0.92 | 0.93 | 0.93 | 0.93 | 0.93 |
| Cr# | 0.13 | 0.12 | 0.13 | 0.12 | 0.12 | 0.13 | 0.13 | 0.14 | 0.13 | 0.14 | 0.14 |

### 4.7.5.1 Comparison With Other Peridotite Amphiboles

Amphiboles are a common and important phase in many peridotites and have been described in numerous continental mantle xenoliths (Kempton, 1987; Menzies et al., 1987) where they are thought to be the product of melt or aqueous fluid metasomatism. In oceanic and ophiolitic peridotites their occurence and chemistry has been described in detail only by Kimball et al. (1985) for the abyssal peridotites, Kornprost and Tabit (1988) for the Galicia margin samples, Roden et al. (1984) for the St. Pauls rocks, Bonatti (1981) for the Red Sea samples and on Japanese ophiolitic samples (Takahashi, 1980; Ozawa, 1988).

The samples from the Galicia Margin, Red Sea and St. Pauls rocks are all thought to represent peridotites formed during incipient rifting of the continental crust and as such are not true oceanic samples. The amphibole they contain is usually Ti-rich pargasite, similar to the amphiboles found in continental xenoliths Kornprost and Tabit (1988).

Kimball et al. (1985) have described the mineralogy of hydrothermally altered abyssal peridotites from the Isla Orcardas Fracture Zone. Here again the amphiboles present

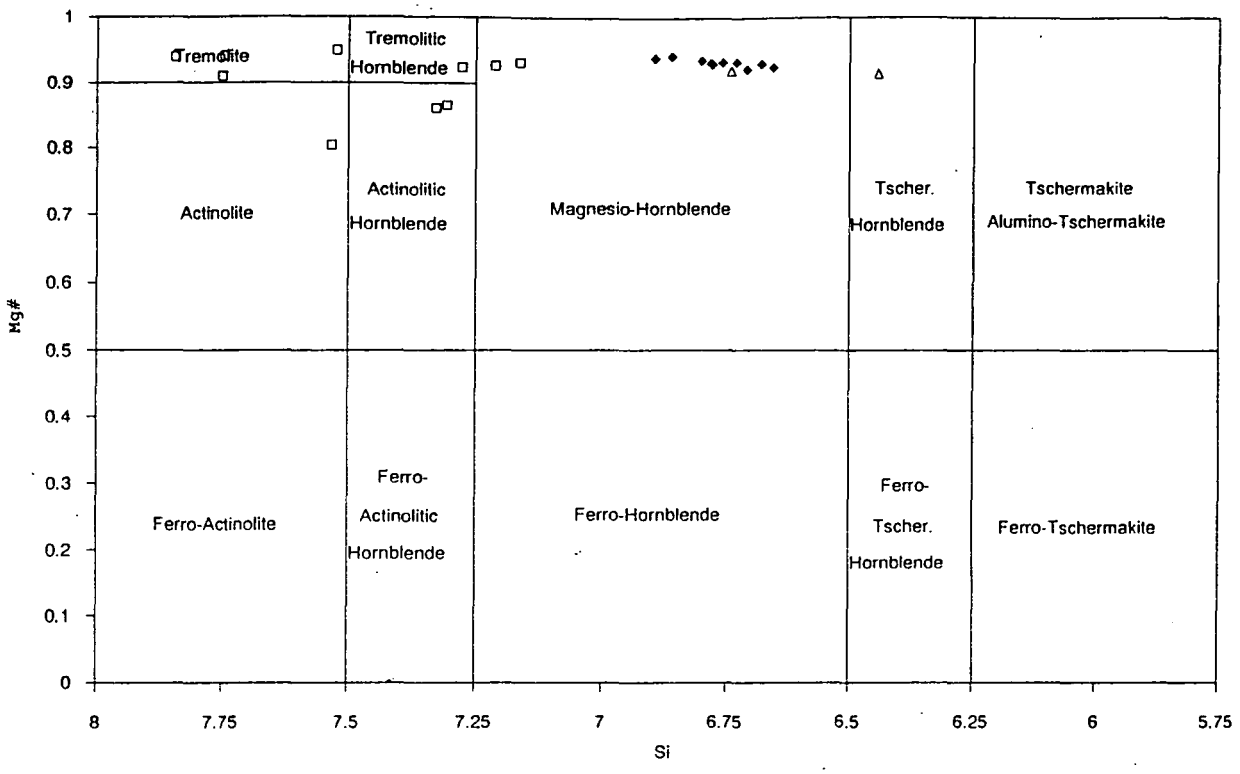


**Fig 4.17.** Leg 125 and other oceanic peridotite amphiboles on Si versus Mg# diagram (after Leake, 1978). Symbols are Leg 125 peridotites (filled diamonds), abyssal peridotites from Kimball et al. (1985) (open squares) and Galicia margin amphiboles from Evans and Girardeau. (1988) (open triangles).

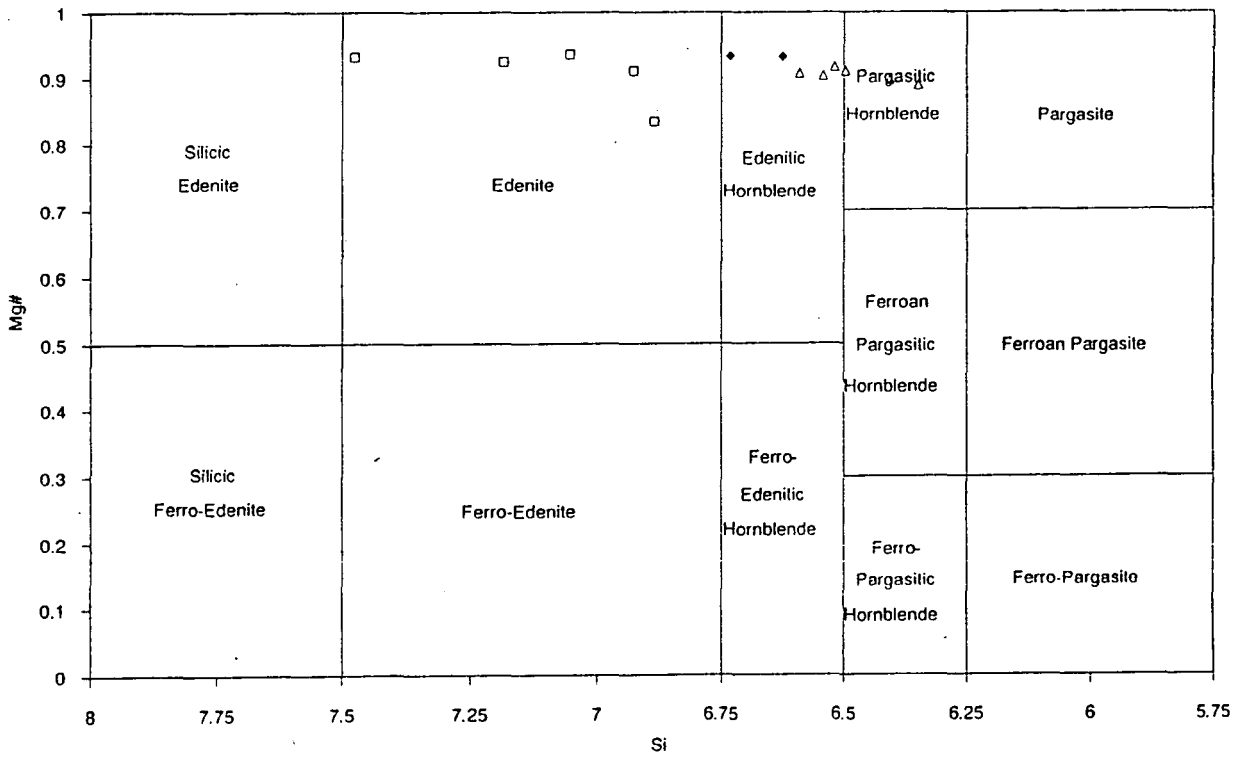


**Figure 4.18.** Leg 125 and other peridotite amphiboles on Si versus Mg# diagram used for more sodic amphiboles. Symbols for peridotites are the same as Figure 4.17.

are distinctive and are shown in Fig. 4.18. They commonly form rims around the edges of clinopyroxene grains where they have a hornblende composition or in cross cutting fractures where they have actinolitic compositions. Kimball et al. (1985) describe the thermal history of the peridotites as a series of hydration reactions between 900°C to 100°C in which the hornblende is the highest temperature alteration mineral and the serpentinization of olivine to mesh-textured lizardite is the lowest temperature alteration mineral formed. Kimball et al. (1985) suggest that seawater is the principal source of the fluid hydration of the primary minerals; they argue that the seawater is heated as it circulates down faults and fractures near the ridge crest.

Amphiboles have been analysed in several of the ophiolites which make up the belt of Japan (Takahashi, 1980; Ozawa, 1988). They have very similar compostions to the amphiboles analysed in the Leg 125 peridotites, being magnesio-hornblendes and edenites (see Figure. 4.18). This is not very surprising as many of these ophiolites have been interpreted as island arc mantle (Ozawa, 1988) and so may have interacted with similar fluids to those which percolated through the Mariana and Izu-Bonin forearcs. Whether the Japanese samples are from island arcs or are forearc peridotites is difficult to tell but they are most certainly related to subduction zones.

### 4.8 Conclusion on Mineral Chemistry

Chemical analy s of the primary phases in the Leg 125 peridotites show that they are probably residues of high degrees of partial melting. Data from individual holes and seamounts show definite characteristics. Minerals from some of the peridotites in hole 778A perodotites plot at the most depleted end of all the trends but may be slightly "enriched" in alumina in some samples. Samples from hole 779A have a very wide range in compositions which spans all the Leg 125 data although more samples have been analysed from this Hole. The spinel data show some interesting effects. Data from hole 779A plot as sets of parallel arrays. These sets represent slightly different thermal histories for the peridotites. The spinels from Torishima Forearc Seamount have consistently higher ferric iron contents which is important for later oxygen fugacity calculations.

Compared with other peridotite data, the Leg 125 peridotites cons istently plot at the depleted end of melting arrays, even when the strong sub-solidus re-equilibration effects are taken into account. This is consistent with Bonatti and Michael's (1989) assertion that the most depleted peridotites are found at destructive plate margins. For comparison with their paper, Mg# of the olivine and alumina content of orthopyroxene are plotted against the Cr# of spinel (Figure 4.19). Strong correlations exist between

these parameters and the Leg 125 data plot at the most depleted end of these plots. However, it should be noted that average mineral compositions are used in the construction of these plots, so they really only emphasise the broad differences that exist between peridotites from different tectonic settings and miss some of the more subtle chemical features of the mineral chemistry and their petrogenetic importance. Some of these features are discussed in the following section.

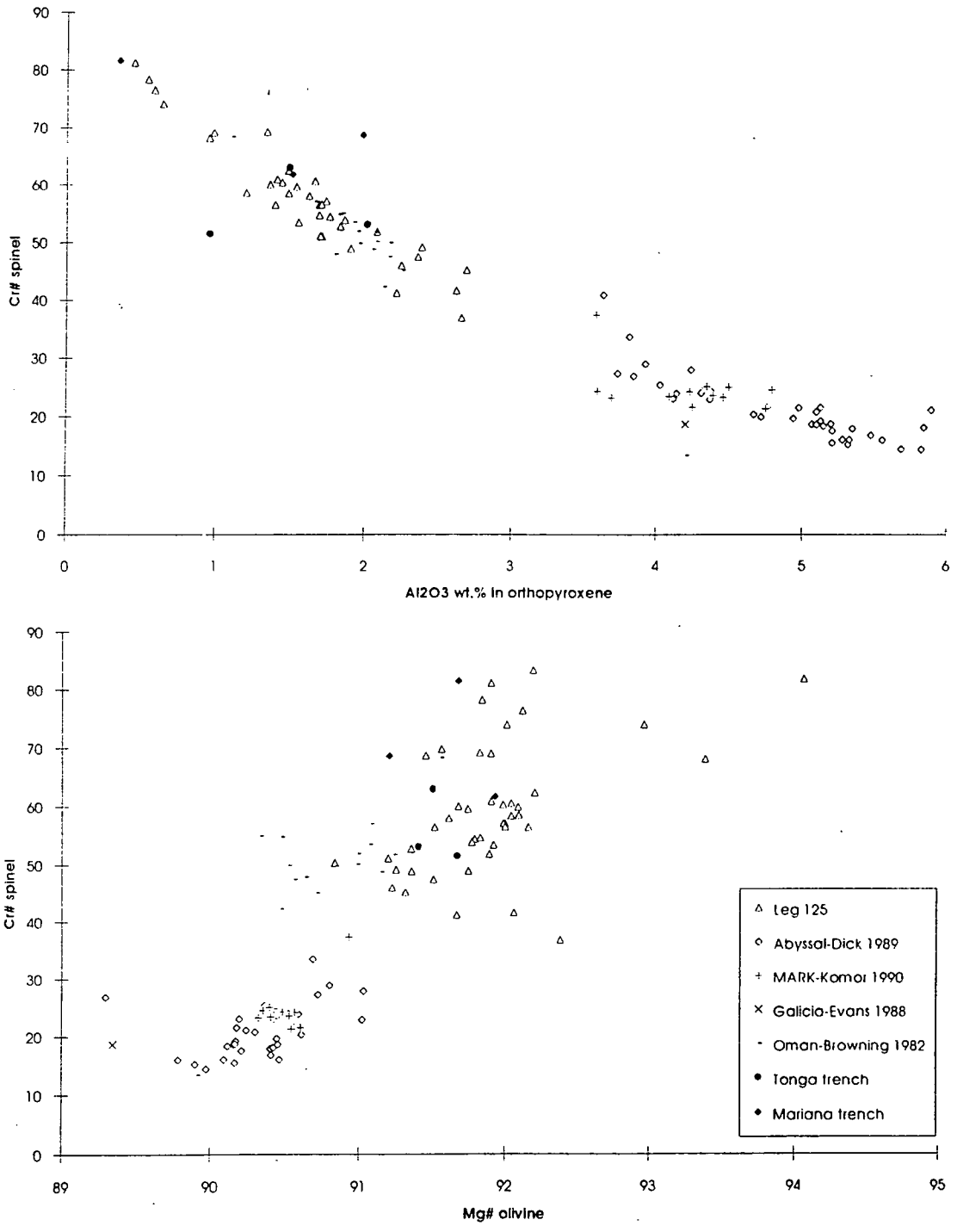


**Fig 4.19.** Cr# in spinel versus Mg# in olivine and alumina in orthopyroxene for peridotites from different tectonic settings.

## 4.9 Petrogenetic Applications of the Mineral Chemistry

### 4.9.1 Geothermometry and Geobarometry

#### 4.9.1.1 Introduction

Ever since Boyd and England (1964) realised that the alumina content of orthopyroxene varied as a function of pressure there has been a plethora of papers published on the geothermometry and geobarometry of peridotites (e.g., Wood and Banno, 1973; Mercier, 1976, 1980; Wells, 1977; Brey and Köhler, 1990; Köhler and Brey, 1990). The types of geothermobarometer can be broadly divided into two types: those based on experimental calibrations where an equilibrium constant is derived as a function of temperature and pressure derived from laboratory experiment and those based on empirical calibrations where an equilibrium constant is derived from analysis of natural rocks and calibrated with temperatures and pressures estimated by other means. Both calibrations have their limitations. The former suffers from the fact that experiments often use synthetic systems such as the CMAS ($CaO$-$MgO$-$Al_2O_3$-$SiO_2$) system and do not take into account important minor components found in natural samples. The latter suffers errors in the external estimation of temperature and pressure. Recently, more experiments have been carried out using natural mineral assemblages and so more accurate geothermobarometers can be derived (e.g. Brey et al. 1990).

In practice it is unlikely that many geothermobarometers give measurements of magmatic temperatures and pressures when applied to peridotites. At best they may give temperatures and pressures of the last time the peridotite equilibrated with a melt, but more likely they reflect sub-solidus re-equilibration temperatures and pressures because elements can still diffuse between minerals and adjust their compositions during the relatively slow cooling of the peridotites (compared to cooling of lavas). To complicate matters, exchange reactions for different mineral pairs often record different equilibration temperatures within the same thin section. This property may be used to elucidate thermal histories of peridotites (e.g. Ozawa, 1983; Zipfel and Wörner, 1992) although more detailed information on diffusion rates of different cations in mantle minerals is needed. Ozawa (1983) showed that different temperatures for the same geothermometer (Fabries' (1979) Fe-Mg olivine-spinel geothermometer) could be found within one thin section, and that the temperature differences could be correlated with the grain size of the spinel and with whether a core or a rim of the mineral was analysed. Ozawa's findings suggest that temperatures derived from geothermometers are a complicated interplay between diffusion rate of cations between minerals, and hence grain size, and the cooling rate of the peridotites. Average core analyses of large minerals in a peridotite tend to give similar temperatures for a given

geothermometer. This temperature may represent the temperature at which the peridotite finally equilbrated . Rim analysis of smaller grains may give information about the cooling or heating histories of the peridotite and, where diffusion coefficients are known, the rates of heating and cooling. For most individual exchange reactions for mineral pairs there seems to be a lower limit or blocking temperature, below which no exchange takes place, so complete cooling histories of peridotites to low temperatures are difficult to attain.

The following section describes and applies some of the more common and useful geothermometers and geobarometers to the Leg 125 mineral chemistry data and on data from other published work. Although there often seems to be decrepencies and inconsistencies between temperatures and pressures derived from individual methods, knowledge of the theory behind any one technique of calculating the temperature or pressure and the petrography of the sample may be used to derive useful information about the petrogenesis of a sample or group of samples.

#### 4.9.1.2 Spinel-Olivine Geothermometry

Irvine (1965; 1967) first undertook a study of the petrogenetic use of chromian spinel and realised that the distribution of iron and magnesium between spinel and olivine was temperature dependent and could be a potential geothermometer. The full equation for the reaction is given by

$$\begin{aligned}&\frac{1}{2}Fe_2SiO_4 + Y^{sp}_{Cr}MgCr_2O_4 + Y^{sp}_{Al}MgAl_2O_4 + Y^{sp}_{Fe^{3+}}MgFe_2O_4 \\ &= \frac{1}{2}Mg_2SiO_4 + Y^{sp}_{Cr}FeCr_2O_4 + Y^{sp}_{Al}FeAl_2O_4 + Y^{sp}_{Fe^{3+}}Fe_3O_4\end{aligned} \qquad (4.1)$$

where

$$Y^{sp}_i = \frac{i}{(Cr + Al + Fe^{3+})} \qquad (4.2)$$

From this Irvine (1965) derived a relationship for a distribution coeffecient, between the Fe-Mg exchange involving the Cr content of the spinel which is given by

$$\ln K_D = \ln \frac{X^{ol}_{Mg} \cdot X^{sp}_{Fe^{2+}}}{X^{ol}_{Fe^{2+}} \cdot X^{sp}_{Mg}} = \ln K_3 + Y^{sp}_{Cr} \ln K_4 + Y^{sp}_{Fe^{3+}} \ln K_5 \qquad (4.3)$$

where $K_3$, $K_4$, and $K_5$, are respectively the equilibrium constants for the following reactions.

$$\frac{1}{2}Fe_2SiO_4 + MgAl_2O_4 = \frac{1}{2}Mg_2SiO_4 + FeAl_2O_4 \quad (4.4)$$

$$MgCr_2O_4 + FeAl_2O_4 = MgAl_2O_4 + FeCr_2O_4 \quad (4.5)$$

$$MgFe_2O_4 + FeAl_2O_4 = MgAl_2O_4 + Fe_3O_4 \quad (4.6)$$

Jackson (1969) first utilised the thermodynamic calculations of Irvine (1965) and calibrated the existing experimental data to derive a geothermometer based on the Fe-Mg exchange between spinel and olivine. Since then there have been several attempts to derive geothermometers for peridotites (Evans and Frost, 1975; Fujii, 1978; Roeder et al. 1979; Fabries, 1979; Engi, 1983). Ozawa (1983) compared the different geothermometers in a detailed study of ophiolitic peridotites and decided that Fabries' geothermometer was the best to use for depleted peridotites. It is also the most commonly used olivine-spinel geothermometer so temperatures in this thesis are calculated using Fabries (1979) formulation.

Fabries (1979) corrected the distribution coeffecient in equation (4.3) to form an apparent distribution coefficient normalised to a ferric-free basis,

$$\ln K_D^0 = \ln K_D - 4.0Y_{Fe^{3+}}^{sp} \quad (4.7)$$

Isotherms plot as straight lines on a plot of $Y_{Cr}^{sp}$ versus $K_D$. Thus, plotting the appropriate experimental data on such a plot Fabries derived a semi-empirical geothermometer, temperatures being calculated by the equation

$$T(^\circ K) = \frac{4250Y_{Cr}^{sp} + 1343}{\ln K_D^0 + 1.825Y_{Cr}^{sp} + 0.571} \quad (4.8)$$

#### 4.9.1.2.1 Results

Figure 4.20 shows the results for the temperatures calculated by Fabries method. Most of the temperatures are in the range 675 to 755°C, with a mean around 710°C. Some of the lower temperatures are from dunite samples. These are low temperatures relative to those from Oman (Browning) and temperatures calculated from the abyssal

data sets of Dick (1989) and Komor et al. (1990). Temperatures from Oman concentrate around 750 °C. Those from abyssal peridotites range from 775 to 975°C with a mean around 850 °C. Ozawa (1983), in his extensive study of olivine-spinel geothermometry in the Miyamori ophiolite recorded temperatures from mineral cores similar to those obtained for the Leg 125 peridotites and temperatures from spinel rims as low as 625°C. Ozawa (1983) proposes that 600 °C is the lowest temperatures likely to be recorded by olivine-spinel pairs as this represents the blocking temperature for Fe-Mg exchange between the two minerals. These data for the Leg 125 peridotites indicate that Fe-Mg have exchanged between olivine and spinel over a large temperature interval from magmatic temperatures (1200°C?) to as low as 625°C.

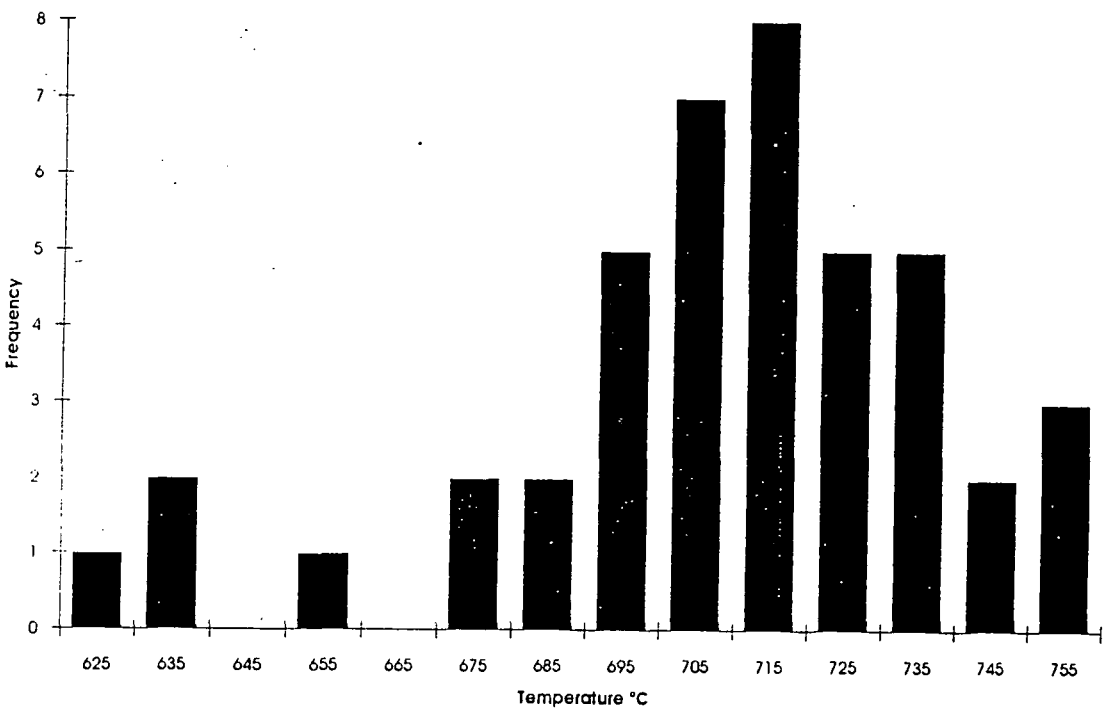


**Figure 4.20.** Temperatures calculated from Fe-Mg exchange between olivine and spinel using formulation of Fabries (1979).

### 4.9.1.3 Pyroxene Geothermometry

The compositions of two coexisting pyroxenes has been used as a geothermobarometer since the work of Boyd and others in the 1960's. Numerous thermometers are based on the exchange of elements such as Fe and Mg between ortho- and clinopyroxene. Discussion of the all the different thermometers is prohibative but experience of using different methods, work of one colleague (D. K. Kostopoulos pers. comm.) and a review paper by Brey and Kohler (1990) are guides to the use of "best" geothermobarometers. Brey et al., (1990) undertook a detailed series of experiments on natural peridotite compositions at different pressures and temperatures to constrain some of the more commonly used geothermobarometers. The two principal pyroxene

geothermometers used here are the method of Wells (1977) and Brey and Köhler (1990). Wells (1977) thermometer is one of the most widespread used, so is useful for comparisons with other studies. Temperatures are also calculated using the Brey and Köhler (1990) Ca-in-orthopyroxene and the two pyroxene thermometer of Bertrand and Mercier (1985/86). Temperatures are also obtained from the exchange of Al and Cr between orthopyroxene and spinel using the formulation of Witt-Eicksesen and Seck (1991). Their geothermometer is useful for detecting low-temperature re-equilibration of pyroxenes with secondary spinels.

**Wells (1977) Geothermometer**

Presented below is the method to calculate temperatures from Wells (1977) geothermometer. The calculations are simple, although care is needed in assigning elements to the M1 and M2 sites of the pyroxenes. Temperatures are calculated using equation (4.9)

$$T(^\circ K) = \frac{7341}{3.355 + 2.44X_{Fe}^{opx} - \ln K} \tag{4.9}$$

where

$$X_{Fe}^{opx} = \frac{Fe^{2+}}{Fe^{2+} + Mg^{2+}} \tag{4.10}$$

and

$$\ln K = \ln\left(\frac{a_{Mg_2Si_2O_6}^{cpx}}{a_{Mg_2Si_2O_6}^{opx}}\right) \tag{4.11}$$

is the natural logarithm of the ratio of the activities of $Mg_2Si_2O_6$ in clinopyroxene and orthopyroxene. Activities are calculated in equation 4.12 using the techniques of Wood and Banno (1973). Methods for assigning Fe and Mg to M1 and M2 sites are provided in Appendix B.

$$a_{Mg_2Si_2O_6} = \left(\frac{Mg^{2+}}{Ca^{2+} + Mg^{2+} + Fe^{2+} + Mn^{2+} + Na^{+}}\right)_{M2} \cdot \left(\frac{Mg^{2+}}{Fe^{3+} + Fe^{2+} + Al^{3+} + Ti^{4+} + Cr^{3+} + Mg^{2+}}\right)_{M1} \quad (4.12)$$

**Brey and Köhler (1990) Method**

Temperatures are calculated from the expression

$$T(^\circ K) = \frac{23664 + (24.9 + 126.3X_{Fe}^{cpx})P}{13.38 + (\ln K_D^*)^2 + 11.59X_{Fe}^{opx}} \quad (4.13)$$

where

$$K_D^* = \frac{(1 - Ca^*)^{cpx}}{(1 - Ca^*)^{opx}} \quad (4.14)$$

and

$$Ca^* = \frac{Ca^{M2}}{1 - Na^{M2}} \quad (4.15)$$

and

$$X_{Fe}^{px} = \frac{Fe^{2+}}{Fe^{2+} + Mg^{2+}} \quad (4.16)$$

Temperatures have also been calculated by the "Ca-in-opx" method of Brey and Kohler (1990) which allows single orthopyroxenes to be used. Temperatures are calculated using equation (4.17)

$$T(^\circ K) = \frac{6425 + 26.4P}{-\ln Ca^{opx} + 1.843} \quad (4.17)$$

where pressures are in kb. A pressure of 15 kb has been used although changing the pressures has little effect on the temperatures calculated.

**Bertrand and Mercier (1985/86)**

Temperatures are calculated by the equation

$$T(^\circ K) = \frac{36273 + 399P}{19.31 - 8.314 \ln K^* - 12.15\left(Ca^*_{cpx}\right)^2} \tag{4.18}$$

where K* is the same as equation (4.14) and Ca*opx is the same as equation (4.15)

$$Ca^*_{cpx} = \left[\frac{X^{M2}_{Ca}}{1 - X^{M2}_{Na}} + \left(-0.77 + 10^{-3}T\right)\frac{Fe}{Fe + Mg}\right]_{cpx} \tag{4.19}$$

and pressure is in GPa. Temperatures are solved by numerical iteration until the temperatures in equation (4.18) and (4.19) converge.

#### 4.9.1.3.1 Results

Figure 4.21 gives the results of the pyroxene thermometry. The error on the temperature calculated varies for each different technique. This is because some of the techniques such as Brey and Köhler Ca-in-orthopyroxene rely principally on an accurate determination of only Ca in the mineral whereas the Wells thermometer uses all the elements from both ortho- and clinopyroxene to assign Fe and Mg to the M1 and M2 sites in the pyroxene. Thus, an accurate determination of all the elements is needed. The minerals were analysed by a wave-length dispersive electron microprobe. Unfortunately Ishii et al. (1992) do not quote errors on their standards. However, the minerals have good totals and using the error estimates of Browning (1982) for his extensive work on electron-microprobe studies of peridotites, the temperatures are thought to be precise to ±50 °C.

The first four plots show the results for each of the individual thermometers and the final plot shows a cumulative frequency plot for all four methods. Temperatures derived by the Wells and the Ca-in-opx methods have a very restricted range of temperatures between 800 and 940 °C with a mean of around 890 °C. Temperatures calculated by the Ca-in-opx method may vary by as much as 150 °C within a single thin section. Browning (1982) reports similar temperature variations for single pyroxene thermometry within a single thin section. Temperatures from the Brey and Köhler (BNK) and Bertrand and Mercier methods have a wide spread of temperatures from 635 °C to 1055 °C although most of the data plots between 700 and 975 °C. There is

no significant difference between the temperatures calculated for the two seamounts or between holes.

Differences in temperature estimates from different pyroxene geothermometers has been widely reported (e.g., Browning, 1982; van der Wal, 1993). From the work of Brey and Köhler (1990), all the methods used should give similar results in the temperature range in question if the coexisting pyroxenes are totally in equilibrium. However in natural samples the oppo unity exists for a wide variety of temperatures to be recorded because of the different diffusion rates of cations in mantle minerals. The temperatures derived from the different techniques have to be assessed individually. The results from the Wells geothermometer suggest that Fe-Mg exchange is rapid and well equilibrated between the pyroxenes until the exchange reaction blocks at just above 800 °C. The Ca-in-orthopyroxene method, which is based solely on the temperature dependence of the Ca content of the orthopyroxene, has a very restricted temperature range. This is thought to be due to the very restricted range of Ca contents in the orthopyroxene, because of the low Ca content of the bulk rock. It is possible that this thermometer is quite compositionally dependent. Temperatures from the BNK and Bertrand and Mercier methods indicate that Ca diffusion in the two pyroxenes is rapid, as there has been substantial re-equilibration down to very low temperatures. This result is not surprising as upon slow cooling Ca is thought to re-equilibrate rapidly in the pyroxenes by *self-diffusion* (van der Wal, 1993 and references therein). The higher temperatures recorded by some samples may reflect faster cooling rates or disequilibrium between pyroxenes.

Temperatures where also calculated for the abyssal peridotite data set to check whether they gave results consistent with mantle temperatures at a spreading ridge. Also to see if there existed the same differences in re-equilibration temperatures that are apparent for the olivine-spinel geothermometer. The data from Dick (1989) gives temperatures around 1150 to 1250 °C which is comparable with upper mantle temperatures at slow spreading ridges from where many of the samples where collected. The data of Komor et al. (1990) gives temperatures of between 950 and 1080 °C. The high temperatures from Dick (1989) show the effect of reconstituting the pyroxenes to get rid of the exsolution lamellae. The data from Komor et al. (1990) reflects sub-solidus re-equilibration temperatures but are consistantly higher then the data from Leg 125. Again, this indicates that there is a substantial difference in the re-equilibration temperatures and may indicate differences in their sub-solidus cooling history.

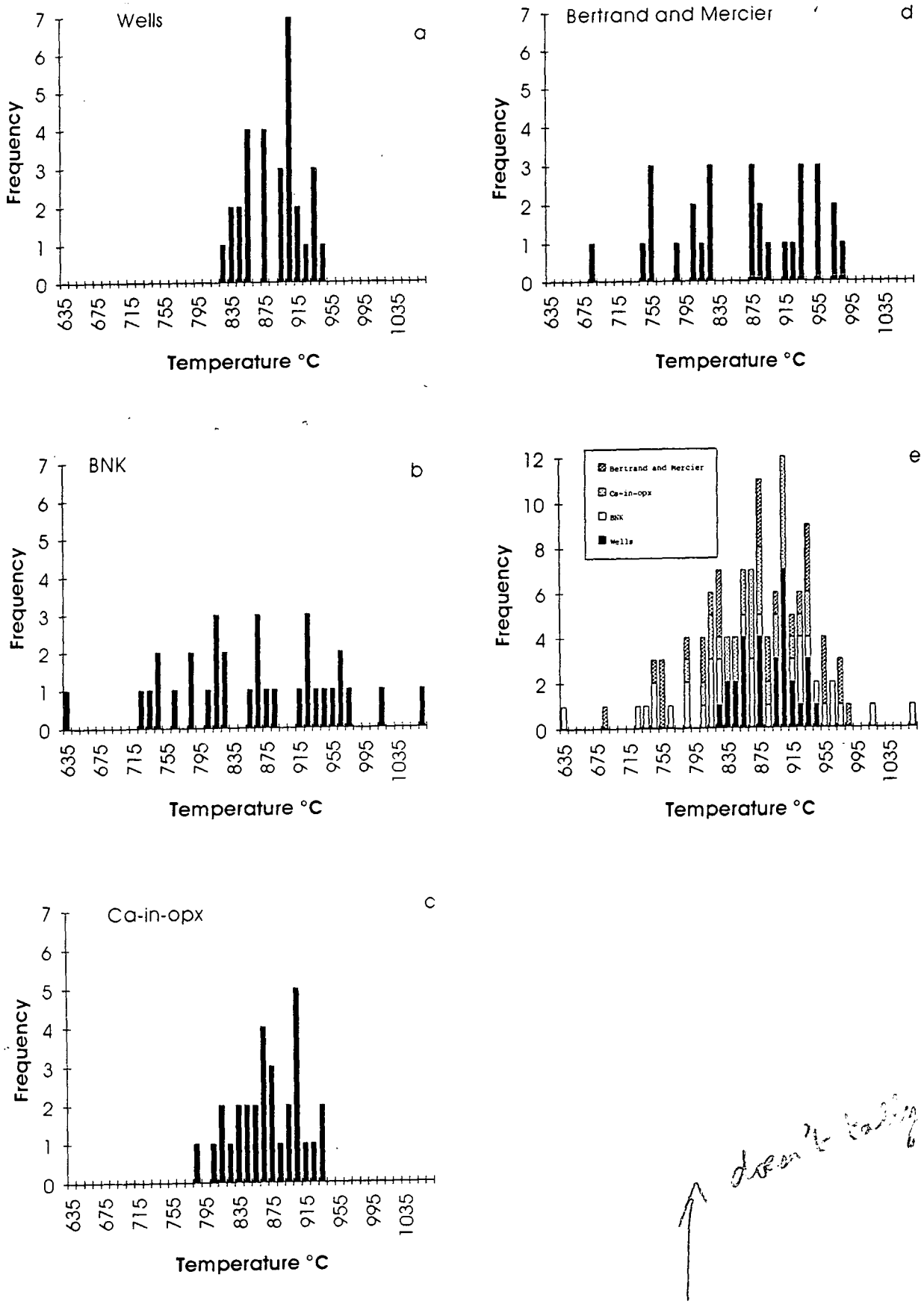


**Fig 4.21.** Temperatures from pyroxene themometry. **a**). Wells (1977), **b**) Bertrand and Mercier, **c**) ,Ca-in-opx, **d**) BNK method and **e**). cumulative frequency of temperatures from all four methods.

### 4.9.1.4 Orthopyroxene-Spinel Geothermometers

Two geothermometer are based on the solubility of alumina in orthopyroxene and the exchange of Cr and alumina between coexisting orthopyroxene and spinel (Witt-Eicksesen and Seck, 1991). Temperatures are calculated using equation (4.20)

$$T(^\circ C) = 2248.25 + 991.58 \ln K_D + 153.32(\ln K_D)^2 + 539.05 Y_{Cr}^{sp} - 2005.74(Y_{Cr}^{sp})^2 \quad (4.20)$$

This expression is useful for assessing the effects of secondary spinel on the distribution of Cr in orthopyroxene at low temperature. In both cases the $K_D$ is calculated by equation (4.21).

$$K_D = \frac{(X_{Fo}^{ol})^2 (X_{Al}^{M1})^{opx}}{(X_{Al}^{sp})^2 (X_{Mg}^{sp})(X_{Mg}^{M1})^{opx}} \quad (4.21)$$

and *YCrsp* is calculated in same manner as for Fabries geothermometer. Witt-Eicksesen and Seck (1991) further calculated a geothermometer based on the alumina and chromium distribution in orthopyroxene with temperatures calculated by

$$T(^\circ C) = 636.54 + 2088.21 X_{Al}^{M1} + 14527.32 X_{Cr}^{M1} \quad (4.22)$$

In all cases alumina is assigned to the M1 site of the orthopyroxene using the method of Carswell (1991).

#### 4.9.1.4.1 Results

Figure 4.22 show the results from calculating temperatures using equation 4.22 (Cr-Al in opx). Temperatures from the Cr-Al thermometer range between 785 to 975 °C with a mean of about 880 °C. The temperatures from Witt-Eickschen and Seck (1991) are not surprisingly similar to the Ca-in-orthopyroxene method, as Witt-Eickschen and Seck (1991) calibrated their thermometer on the later although temperatures are calculated on a different exchange reaction. The results are very similar to those based on two-pyroxene thermometry although they do not record the very low temperatures from some of the Leg 125 perdiotites. The similarity between the results of this thermometer and the pyroxene thermometers is quite surprising, as Cr and Al are thought to diffuse more slowly than Fe, Mg and Cr and temperatures from this thermometer are often higher than those from pyroxene thermometry (van der Wal, 1993). Temperatures were calculated from the re-evaluated Cr-Al thermometer of

Witt-Eickschen and Seck (1991) (equation 4.20), with results varying from negative results to 1100 °C! Witt-Eickschen and Seck (1991) found that xenoliths where secondary spinel was present gave unrealistically high temperures (up to 1900 °C) for this method. Some of the Leg 125 peridotites have secondary spinel and the orthopyroxenes have low Cr contents, which could suggest that there was extensive low-temperature Cr exchange between orthopyroxene and spinel. This has some bearing on some of the arguements for the melting history of the peridotites (see later discussion).

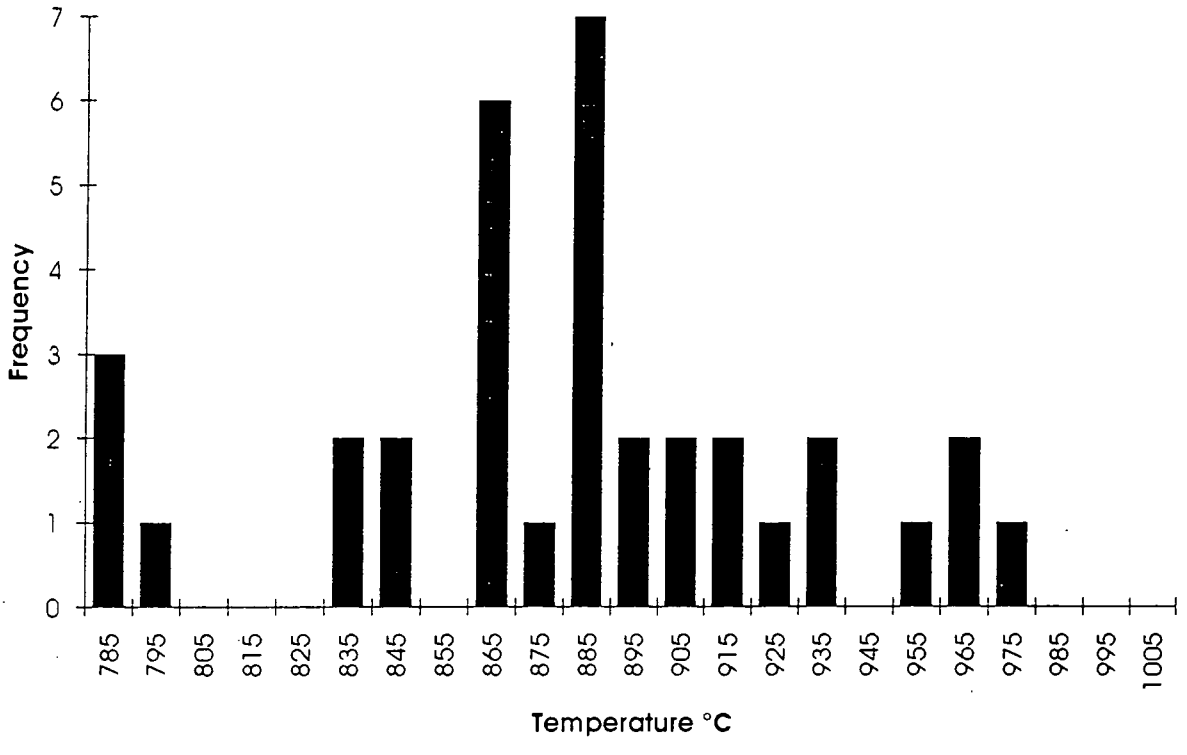


**Figure 4.22.** Temperatures calculated from Cr-Al exchange between orthopyroxene and spinel using the formulation of Witt-Eckschesen and Seck (1991).

### 4.9.2 Geobarometry

Accurate pressure determination for spinel peridotites has been problematical for a long time, because very few of the exchange reactions in spinel peridotites lend themselves to geobarometry. This is because none of the reactions are associated with a large volume change (Spear, 1989). In fact until Köhler and Brey (1990) produced the Ca-in-olivine barometer there was no good barometer for spinel peridotites. Mercier et al. (1984) published a geobarometer applicable to harzburgites. Unfortunately it is only valid to peridotites that equilibrated at magmatic temperatures (>1150 °C) and so cannot be applied to the Leg 125 peridotites. Stroh (1976) derived an empirical formula for calculating pressures in spinel peridotites based on the experimental work of MacGregor (1974). Pressures where calculated by the author for the Leg 125 peridotites using this method and yielded pressures of less than 0.5 kb. However, Stroh's formulation is based on higher pressure experiments and he cautions against using it for rocks which may have equilibrated at very low pressures.

The method of Köhler and Brey (1990) relies on very accurate analysis of Ca in olivine. Even in fertile peridotites Ca has very low concentrations in olivines. In the Leg 125 peridotites, Ca is extremely low (<0.02 wt%) and the precision of the analysis is extremely low. For this reason it is not possible to apply this geobarometer to the Leg 125 peridotites.

Geobarometers have been used with success on mantle xenoliths brought up in alkali basalts and kimberlites. Pressure determinations are based on the 'reliable' orthopyroxene-garnet geobarometer. These xenoliths have been brought to the surface rapidly and so usually retain their high P-T equilibrium assemblage, and pressures and temperatures derived from geothermobarometers are consistent with their genesis inferred by other means. The rationale of applying geobarometers to oceanic mantle samples is questionable. Firstly, the mantle gets to the surface by melting and so re-equilibration during melting is probably efficient owing to grain-size reduction and high diffusion rates in the melt. P-T estimates from samples that retain their magmatic signature should correspond to an advective geotherm related to the potential temperature of the mantle under consideration. Application of the Mercier et al. (1984) geobarometer to the "re-equilibrated" pyroxenes from Dick (1989) gives pressures from 3 to 18 kb. These pressures are consistent with their origin in the upper mantle. However, there is no consistent variation with temperature even though it should be noted that the temperature variation along an advective geotherm for a potential temperature of 1280 °C should be of the order of 100 °C for 13 kb variation in pressure. Data from these reconstituted abyssal pyroxenes thus, suggest that the

geothermal gradient is shallow but are not accurate enough to give information about potential temperatures.

With respect to the pressure of formation of the Leg 125 peridotites, probably the most information can be derived from the petrography of the samples. There is liitle evidence to suggest that garnet was important in the genesis of the peridotites as garnet-spinel symplectites are not present. The trace element content of the clinopyroxenes suggests that garnet had not equilibrated in these samples (see later). Plagioclase is not present, although this does not necessarily mean that the peridotites have not equilibrated at pressures lower than 8 kb as it would be difficult to form plagioclase in such a depleted peridotite (see peridotite facies, chapter 3). Some of the resorption features of the grain boundaries of the orthopyroxenes suggest possible incongruent melting of orthopyroxene, which, according to Morse (1980) is indicative of very low pressures (~3 kb) and high water activity.

### 4.9.3 Thermal History of Leg 125 Peridotites

The main conclusion that can be drawn from the Leg 125 data is that they have a substantial history of sub-solidus thermal re-equilibration, which is in strong contrast to the data from abyssal peridotites. Data from Komor et al. (1990) show that the abyssal peridotites have continued to exchange Ca, Al, Fe and Mg down to 1000 °C with respect to two pyroxene geothermometry and down to 900 °C with respect to Fe-Mg exchange between spinel and olivine. The lower temperature for the later is thought to reflect both lower blocking temperatures for this exchange and the smaller grain-size of the spinels (Ozawa, 1983). The Leg 125 peridotites have re-equilibrated to temperatures between 1000 to 600°C, but predominantly at lower temperatures than the abyssal peridotites. This suggests that they cooled at a relatively slow rate with respect to the diffusion rate of the cations in the minerals. It can be argued that the Leg 125 peridotites cooled at similar rates to the abyssal peridotites, but that diffusion rates were quicker. The evidence for water playing an important rôle in their genesis is strong (Girardeau and Lagabrelle, 1992; Parkinson et al., 1992b). This could increase diffusion rates, although it would also probably increase cooling rates.

I consider that the geothermetric data for the Leg 125 peridotites reflect slower cooling rates. Extensive sub-solidus equilibration is a common feature of ophiolitic peridotites (Dick and Fisher, 1984) and implies that there is a common link in the thermal histories of these peridotites. With respect to the petrogenesis of the Leg 125 peridotites it will be shown in Chapter five that the peridotites are residual to boninite magmatism. Boninites generated in the Arakapas Fault Zone of Cyprus are related to

extension within the fault zone where small volumes of boninites are generated and no large scale spreading centre develops. Residual peridotites to this type of magmatism will have slow cooling and undergo extensive sub-solidus re-equilibration. In contrast, residual peridotites at spreading centres are cooled more quickly by the circulation of cooling seawater through fractures at the ridge crest (Dick and Fisher, 1984).

### 4.9.4 Oxygen Thermobarometry

There have been several attempts in recent years to measure the oxygen fugacities recorded by mantle peridotites. Arculus et al. (1984) used electrochemical methods to determine the $f_{O_2}$ in both spinel peridotites and ilmenite megacrysts. They reported $f_{O_2}$ values from below the IW buffer to above the FMQ buffer. Virgo et al. (1988) suggested that their most reduced values were artifacts of the experimental technique, in that reduced carbon on both mineral surfaces and cracks in the samples would cause drastic reduction of $Fe^{3+}$ to $Fe^{2+}$ during the 1 atm experiments, and so give far too reducing (low) $f_{O_2}$ values.

The most promising and readily available technique for determining the $f_{O_2}$ of mantle peridotites is oxygen thermobarometry. This technique is very powerful because it relies on properties of minerals that are not reset during cooling or affected by normal measuring techniques (Wood et al. 1990).

Several oxygen barometers for spinel peridotites have been proposed in recent years (O'Neill and Wall 1987; Mattioli and Wood 1988; Nell and Wood 1991). These three barometers rely on the fact that mantle minerals contain both ferrous and ferric iron components and that most spinel peridoties contain olivine, orthopyroxene and spinel for which an apparent $f_{O_2}$ may be determined from the equilibrium expression:

$$6Fe_2SiO_4 + O_2 = 6FeSiO_3 + 2Fe_3O_4 \qquad (4.23)$$

To calculate the $f_{O_2}$, it is necessary to measure the concentrations of $Fe_2SiO_4$ in olivine, $FeSiO_3$ in orthopyroxene and $Fe_3O_4$ in spinel and then use thermodynamic calculations utilising the activity-composition relations for the end-member reactions . The measurement of the $Fe_2SiO_4$ and $FeSiO_3$ components in olivine and orthopyroxene are readily accomplished by electron microprobe analysis. However, accurate electron microprobe analysis of the $Fe_3O_4$ component in spinel can be difficult, a point which will be discussed below.

The three papers cited above all recognise that the accuracy of $f_{O_2}$ calculations in mantle peridotites is dependent on the accurate determination of $Fe^{3+}$ in the spinels and the uncertainties in the activity-composition relations of spinel. Wood and Virgo (1989) tackled the first of these problems by separating spinels from mantle xenoliths and then analysing these by Mössbauer spectroscopy to derive their ferric-ferrous iron ratio. Although this technique is not readily available for most studies, by using Mössbauer -analysed spinels as microprobe standards, the ferric iron content of the spinels (and hence $Fe_3O_4$ contents) can be more accurately determined (see Wood and Virgo, 1989 for methodology). The second problem, that of the activity-composition relationships for spinels, is more difficult to resolve although O'Neill and Wall (1987) have tried a theoretical approach and Mattioli and Wood (1988) an experimental approach, both deriving similar results.

To test the validity of the O'Neill-Wall, Mattioli-Wood and Nell-Wood calibrations, Wood (1990) conducted experiments whereby he re-equilibrated olivine ($Fo_{89}$), orthopyroxene ($En_{91}$), and spinel of varying composition at known T and $f_{O_2}$ at 1 atm. He then calculated the $f_{O_2}$ from the three calibrations and compared them to the known $f_{O_2}$ value for the experiments. Figure 4.23 shows plots of the difference between the calculated to observed log $f_{O_2}$ against Cr/(Cr+Al) in the spinel for the three calibrations. The first observation is that $f_{O_2}$ values calculated by the Mattioli-Wood method shows a dependence on the Cr/(Cr+Al) ratio of the spinel. This is not surprising as they used Cr-free spinels in their experiments. As many of the Leg 125 peridotites have Cr/(Cr+Al) ratios greater than 0.6, the Mattioli-Wood calibration would greatly over-estimate the $f_{O_2}$ of the peridotites and so it is not used in the proceeding calculations. The O'Neill-Wall calibrations show no such compositional dependence yet tend to produce calculated $f_{O_2}$ values which are lower than the experimental values by an average of 0.65 log units. The Nell-Wood calibration also produces results with no compositional dependence, on the spinel Cr/(Cr+Al) ratio but produces calculated $f_{O_2}$ values closer to the experimental values, on average 0.35 log units below the expermental results. Given some of the uncertainties used in calculating $f_{O_2}$ values from their calibration, Wood (1990) suggested that, given an accurate $Fe^{3+}/\Sigma Fe$ ratio for the spinel, it is possible to be within 0.6 log units of the actual $f_{O_2}$ value at known temperature and total pressure.

In the following sections, $f_{O_2}$ values for the Leg 125 peridotites are calculated using the Nell-Wood calibration. The equations in Nell and Wood (1991) for calculating cation partioning in spinels are extremely complicated so the simplified parameterisation for calculating $f_{O_2}$ values provided in the Appendix of Wood et al.

(1990) is used to calculate oxygen fugacities in this section. Log $\left(f_{O_2}\right)_{P,T}$ is calculated using the equation:

$$\log\left(f_{O_2}\right)_{P,T} = \log f_{O_2}(FMQ)_{P,T} + \frac{220}{T} + 0.35 - \frac{0.0369P}{T}$$
$$-12\log X_{Fe}^{ol} - \frac{2620}{T}X_{Mg}^{ol\ 2} + 3\log\left(X_{Fe}^{M1}\cdot X_{Fe}^{M2}\right)^{opx} + 2\log a_{Fe_3O_4}^{sp} \qquad (4.24)$$

where $X_{Fe}^{ol}$ and $X_{Mg}^{ol}$ refer to mole fractions of Fe and Mg end-members in olivine, P is pressure in bars, T is temperature in kelvin, and $X_{Fe}^{M1}$, $X_{Fe}^{M2}$ in orthopyroxene refer to the atomic fractions of Fe in the two orthopyroxene sites using an ideal two-site solution. The last term is calulated by the following expression;

$$\log a_{Fe_3O_4}^{sp} = \log\left\{\frac{\left(Fe^{2+}\right)\cdot\left(Fe^{3+}\right)^2}{4}\right\} + \frac{1}{T}\left[406(Al)^2 + 653(Mg)(Al)\right.$$
$$\left.+299(Cr)^2 + 199(Al)(Cr) + 346(Mg)(Cr)\right] \qquad (4.25)$$

where bracketed terms refer to total Mg, Al, Cr, $Fe^{2+}$ and $Fe^{3+}$ cations in the spinel structure on a four oxygen basis.

To help in comparing different data sets, the temperatures used in the equations are all derived from the Wells (1977) two-pyroxene geothermometer for each individual peridotite. Log $f_{O_2}$ values are quoted with respect to the FMQ buffer curve such that values with positive $\Delta f_{O_2}$ values are more oxidising than the FMQ buffer and values with negative $\Delta f_{O_2}$ values more reducing. Presenting the results in this manner is useful because an error of ±100 °C will shift the $\Delta f_{O_2}$ value by 0.2 log units (Wood et al. 1990). Unless otherwise stated the pressure used in the calculations is 15kb which is in the middle of the spinel peridotite stability field. Again, changes in pressure have very little effect on the $\Delta f_{O_2}$ values (Wood et al. 1990).

Unfortunately rather than analysing the ferric-iron content of the spinels by Mössbauer spectroscopy, the ferric-iron content of the spinels in this study are calculated by stoichiometry. However, the errors in calculating the ferric-iron content of the spinels are reduced in high Cr# spinels because the greatest error in the analyses

comes from determining the light elements Al and Mg by electron microprobe. The concentrations of these elements are low in the high Cr# spinels from Leg 125. Estimates of the errors in the determination of the oxygen fugacity are of the order ± 1.0 log units (based on the error calculations in Wood and Virgo, 1989).

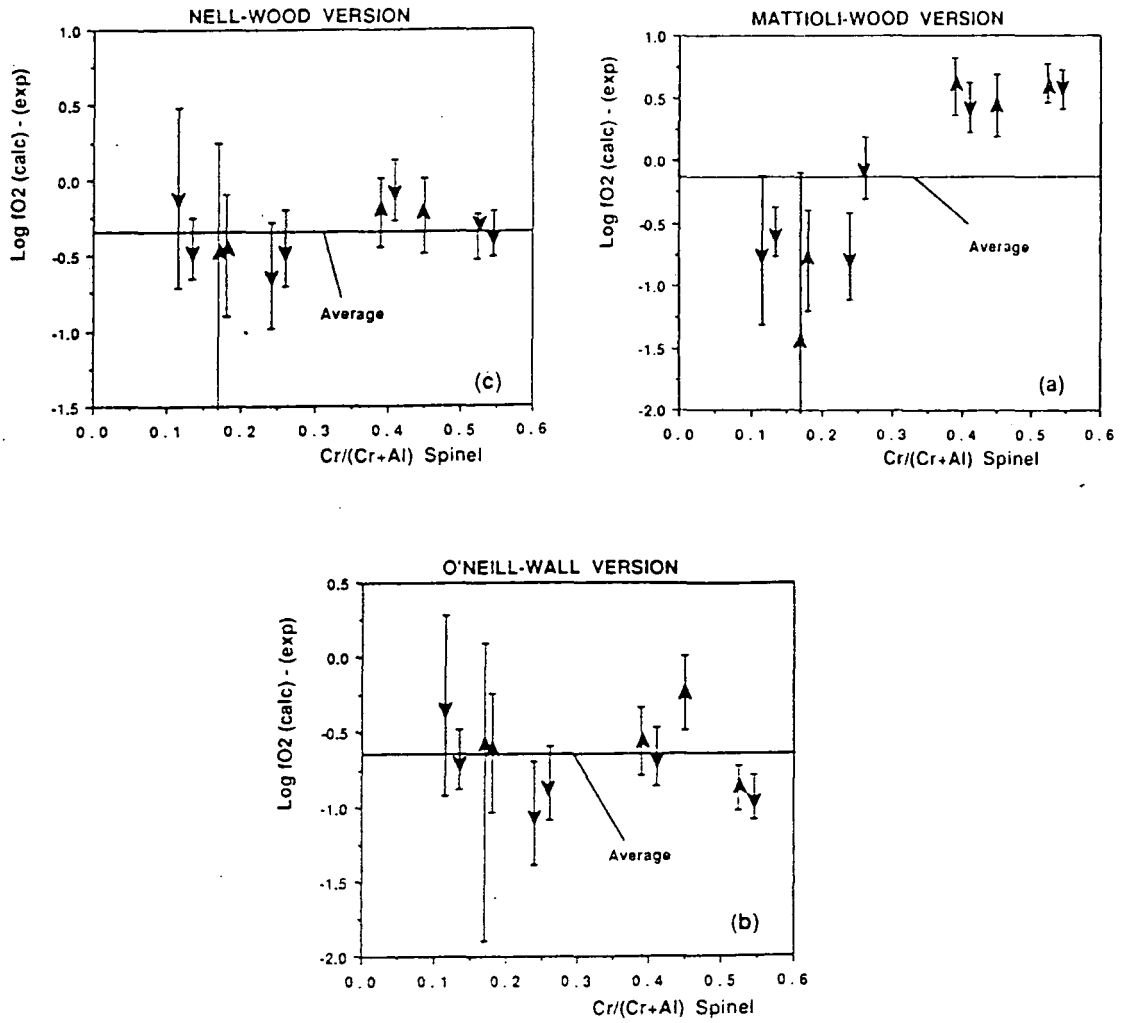


**Figure 4.23** Comparison of the Nell-Wood, Mattioli-Wood and O'Neil-Wall methods of calculating oxygen fugacities. See text for details, (after Wood, 1990).

### 4.9.4.1 Results

Figure 4.24 shows a plots of log $\Delta f_{O_2}$ values versus temperature for the two seamounts. Data from Conical Seamount has a wide range of values. Samples for 778A plot at +2 log units, 779A between -1 and +3.5 log units and 780C+D between +1.5 and +3 log units with respect to the FMQ buffer. Samples from Torishima Forearc Seamount plot at consistently higher log $f_{O_2}$ values than Conical Seamount, forming

two horizontal fields at 3 to 4 log units above the FMQ buffer. Given the errors inherent in calculating oxygen fugacities from spinels with their ferric iron content estimated from stoichiometry, the general result that the Leg 125 samples plot at oxygen fugacities well above the FMQ buffer is outside of the two sigma error in the $f_{O_2}$ values calculated. The elevated oxygen fugacities estimates of this error are in the order of ± 1.0 log units which does not affect the general result that the Leg 125 samples plot at oxygen fugacities well above the FMQ buffer. The samples are heavily serpentinised and many of the chrome-spinels are altered (oxidised) to ferrit-chromit. This could have the effect of producing artificially high oxygen fugacity values. However, detailed examination of the electron microprobe data suggest that the characteristics of ferrit-chromit (high Si) are not present and that fresh chrome-spinels were analysed.

### 4.9.4.2 Discussion

Bryndzia and Wood (1990), Wood et al. (1990) and Draper (1991) compare the oxygen thermobarometry of a series of peridotites from active spreading ridges with those associated with subduction zones. Peridotites from spreading ridges have oxygen fugacitites on average 0.9 log units below the FMQ buffer (Bryndzia and Wood, 1990). Data for peridotites from active or recent subduction zones is more limited. At present only samples from Ichinomegata, Japan (Wood etal., 1990) and Lorena Butte, Washington State (Draper, 1991) have been published. The samples from Japan have oxygen fugacities of 1-2 log units above the FMQ buffer whereas those from the western USA have higher values from 2.3 to 3.9 units above the FMQ buffer. Within error these are similar to the oxygen fugacities in the Leg 125 peridotites. As will be shown later, all three localiti es show a strong relationship between water activity, $f_{O_2}$ and trace element enrichments consistent with models for melt generation in the sub-arc mantle.

## 4.10 Calculating Equilibrium Melt Compositions

The compositions of melts in equilibrium with the residual phases in the peridotites is readily accomplished. The most obvious method is to use the Fe-Mg olivine-liquid equilibria method of Roeder and Emslie (1970). They found that the distribution coefficient

$$K_D = \frac{\left(X_{FeO}^{Ol}\right)\left(X_{MgO}^{Liq}\right)}{\left(X_{FeO}^{Liq}\right)\left(X_{MgO}^{Ol}\right)} \qquad (4.26)$$

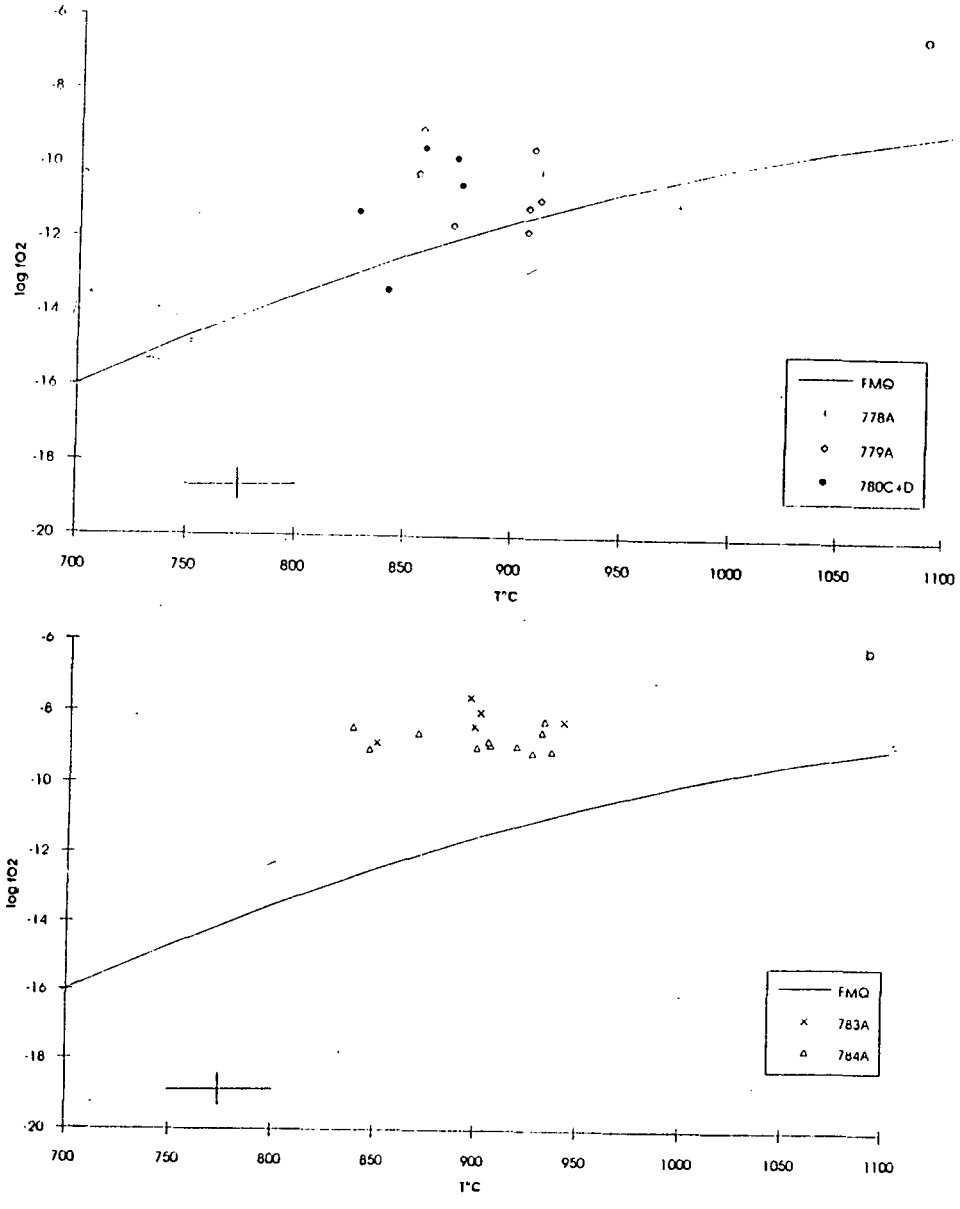


**Figure 4.24.** $f_{O_2}$ calculations for peridotites from a). Conical and B). Torishima Forearc Seamounts. Two sigma error bars are shown (estimated from method of Wood and Virgo, 1989)

relating the distribution of iron and magnesium between olivine and liquid is equal to 0.30 and is independent of temperature. This equation can simply be rearranged to solve for the Fe/Mg ratio of the liquid which is related to the Mg# of the liquid by equation (4.27)

$$Mg\#_{Liq} = \frac{100}{\frac{X^{Liq}_{FeO}}{X^{Liq}_{MgO}} + 1} \tag{4.27}$$

As already discussed the Leg 125 peridotites show very strong evidence of sub-solidus re-equilibration, especially with respect to Fe-Mg exchange between spinel and olivine. To calculate realistic liquid compositions it is neccessary to recalculate the olivine composition back to magmatic temperatures. This is done by rearranging Fabries (1979) geothermetric equation (4.28) to solve for the Fe/Mg ratio in the spinel

$$\frac{X^{sp}_{Fe}}{X^{sp}_{Mg}} = \frac{X^{ol}_{Fe}}{X^{ol}_{Mg}} \exp\left[\left(\frac{4250X^{sp}_{Cr} + 1343}{T°(K)}\right) - 1.825X^{sp}_{Cr} - 0.571 + 4X^{sp}_{Fe^{3+}}\right] \tag{4.28}$$

The new spinel Fe/Mg ratio is then calculated at the magmatic temperature required and the Mg# of the spinel is then calculated. As the Mg# of the spinel changes then the Mg# of the olivine also must change and this is solved by a mass balance calculation for the Mg# of olivine

$$Mg\#_{ol} = \frac{Mg\#_{tot} - Mg\#_{sp} X_{sp/ol}}{1 - X_{sp/ol}} \tag{4.29}$$

where $X_{sp/ol}$ is the relative proportion of spinel to olivine and $Mg\#_{tot}$ is the total mass-balanced Mg# for the system. The value from this is put back into equation (4.28) and a new spinel composition calculated. This is iterated until the spinel composition converges. The calculations assume that olivine exchanges only Fe and Mg with spinel, which seems reasonable as it has been shown that a substantial amount of re-equilibration between the olivine and spinel has occurred (see spinel section). Although the procedure is quite elaborate it is important to correct the olivine composition accurately as will be discussed in the following section.

The section on spinel-olivine Fe-Mg equilibrium showed that, with decreasing temperature, the Mg# of the spinel decreases with a complementary increase in the Mg# of the olivine. Corrections back to a magmatic temperature of 1200 °C produce a decrease of approxiamately 0.50 in the Mg# of the olivine. Figure 4.25 shows a plot of the liquids in equilibrium with a residual ferromagnesian mineral with Mg# ranging from 88 to 100 for various values of $K_D$. Although the value for $K_D$ of 0.30 is

commonly used, peridotite melting experiments (Jaques and Green, 1980; Kinzler and Grove, 1992a) have values ranging from 0.20 to 0.33 which reflect the effects of ferric iron. Assuming values between 0.25 to 0.30 to be realistic, olivines from the Leg 125 peridotites would have been in equilibrium with a melt of Mg# ranging between 70 and 77. The temperature correction for the olivine reduces the Mg# of the melt by 2-3 percent. Primitive MORB glasses have Mg# up to 70 (Elthon, 1992) and boninites and primative arc basalts may have Mg# between 70 and 80.

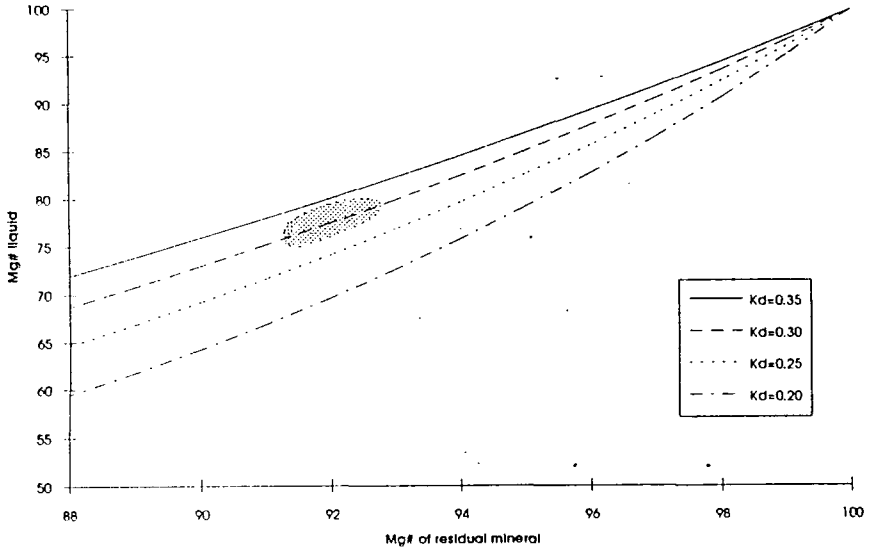


**Figure4. 25** Mg# of liquids (stippled area) in equilibria with the Leg 125 peridotites (see text for detail).

Taken at face value, it is not surprising that very refractory Leg 125 peridotites are in equilibrium with highly magnesian liquids. Furthermore, the compositions of the liquids in equilibrium with the olivines can only be interpreted as representative of the last instantaneous melts to have been in equilibrium with the peridotites. It is difficult to assess from the chemistry of lavas what residue they were in equilibrium with, as they may have been in equilibrium with a range of residues during their melting history. As Johnson et al. (1990) stated with respect to the REE contents of residual diopsides in abyssal peridotites, it is apparent that no MORB's are in equilibrium with these diopsides. This is because the efficient melt extraction and near fractional melting processes at spreading ridges mean that the residues become very depleted fractional residues, whereas the liquids become pooled and have compositions similar to equilibrium batch melts. To, understand the relationship between erupted magmas and their residues it is neccessary to have knowledge of the full melting history of the residues and to intergrate the instantaneous melts produced to arrive at the final liquid compositions. Lack of information means that this calculation is unlikely to be done.

The close spatial relationship of the peridotites with the boninites allows some help in the estimates of the erupted magmas to which the Leg 125 peridotites were possibly residues. Boninites have several characteristics which help in addressing this question. Firstly, there is a consensus view between boninite workers that they represent hydrous (but water-undersatured) melts of a previously variably depleted mantle (Crawford, 1989). Phase-petrology by van der Laan et al. (1989) suggests that they are formed at pressures less than 10 kb. Furthermore they are volumetrically unimportant in both the Western Pacific and in ophiolites with respect to island arc volcanics proper. Geochemical evidence (i.e., Pearce et al., 1992b; Pearce and Parkinson, in press) points to boninites being small degree melts (5-10% absolute maximum) of a depleted source. From this, it is likely that, although the Leg 125 peridotites may have complicated melting histories (see transitional element section, this chapter), the last part of its melting history involved the 5-10% melting to produce magmas with Mg#~70-75 which were probably boninitic in nature.

The compositions of coexisting olivine and orthopyroxene in peridotites may provide constraints on whether melting took place under anhydrous or hydrous conditions or some combination of the two. A study of the published anhydrous melting experiments (von Seckendorff and O'Neill, 1993) shows that the $K_D$ describing iron and magnesium distribution between a liquid and mineral is usually slightly larger for olivine than orthopyroxene. This means residual orthopyroxenes should have higher Mg# than coexisting olivines. This is consistent with experimental studies of Fe-Mg partitioning between these phases (von Seckendorff and O'Neill, 1993). However some experiments where olivine and orthopyroxenes coexist under hydrous conditions (van der Laan et al., 1989) suggest that the $K_D$ values reverse so that residual olivines may have higher Mg# than coexisting orthopyroxenes. To test this hypothesis, data were plotted from the various peridotites used in earlier sections, together with hypothetical "wet" and "dry" residual melting lines (Figure 4.26). It should be noted that the difference between the $K_D$ values is not that large and relies on good electron microprobe data. Also the difference in $K_D$ values should get smaller at higher Mg# (von Seckendorff and O'Neill, 1993). From Figure 4.26 it is not obvious that any of the peridotites have signatures that suggest large amounts of hydrous melting. Many plot on the line for a ratio of one to one units. Although some the olivines in the Leg 125 peridotites do plot at higher olivine Mg#'s than orthopyroxenes, so do some of the peridotites from Leg 106/109 from the Mid-Atlantic ridge.

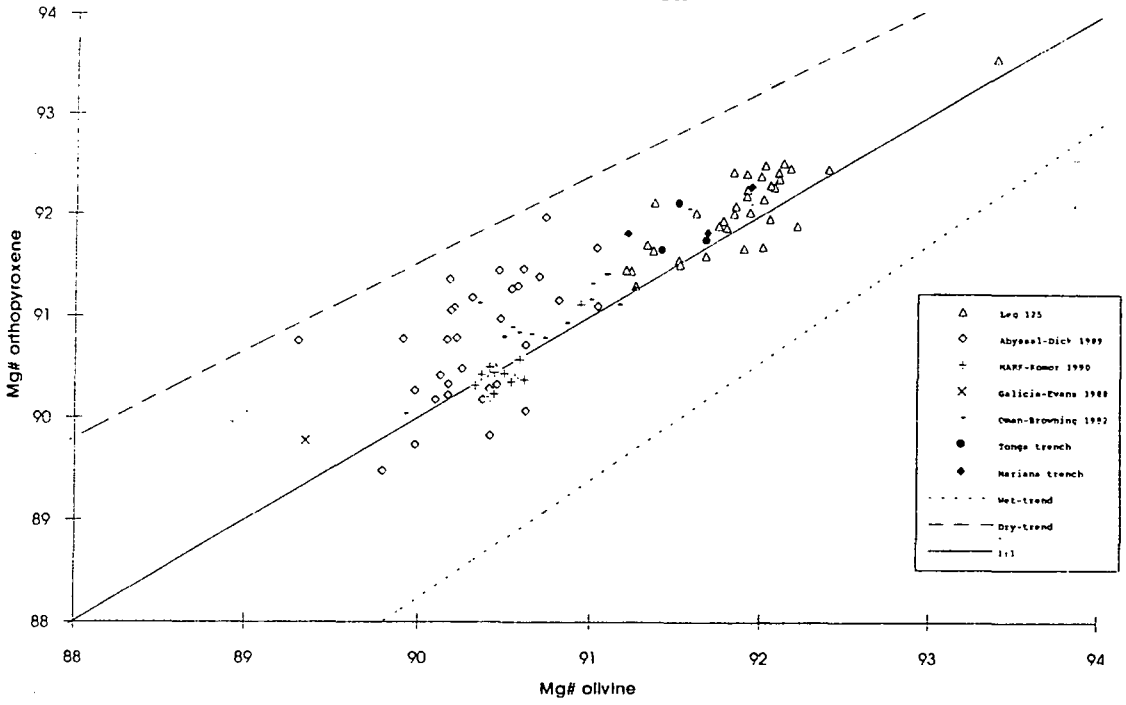


**Figure 4.26.** Plot of Mg# in orthopyroxene against Mg# in olivine from a variety of peridotites, together with lines for "wet" and "dry" melting (see text for details).

## 4.11 Trace Element Analysis of Leg 125 Minerals

Clinopyroxene is the mineral in mantle peridotites which most commonly is analysed for its trace element contents, principally because it is the main inventory for the incompatible trace elements. For this reason, the trace element concentrations of clinopyroxenes have been used to interpret the whole rock trace element patterns (Salters and Shimizu 1989). However, it has recently been shown that orthopyroxene may be important in controlling the whole-rock geochemistry of elements such as Ti and Zr (Rampone et al. 1991; McDonough and Stosch 1992) in clinopyroxene-poor peridotites.

The very low clinopyroxene content of the Leg 125 peridotites together with the fact that, when they do occur, it is usually as exsolution lamellae in orthopyroxene or as very small grains means, that it is virtually impossible to pick clinopyroxene grains for trace element analysis. For this reason clinopyroxenes were analysed *in-situ* for trace element concentrations by ion microprobe. Five samples where analysed on a Cameca 3f ion microprobe at the Geological Institute, University of Tokyo, Japan by Dr Kevin Johnson. He analysed Sr, Zr, Ti, V, Cr, Ni, Hf and the REE in clinopyroxenes, Sr, Zr, Ti, V, Cr, Ni, Hf in orthopyroxenes and Sr, Zr, Ti, V, Cr, Ni, Hf in one olivine grain. Details of the analytical technique are given in Appendix A together with precision and accuracy for the analysis. The full data set is reproduced in Appendix E. While attempting to acquire a Nd isotope ratio for the peridotites, one orthopyroxene

analysis was also obtained for the REE by isotope dilution at the RHBNC isotope laboratory.

| | 784A-42R-1, 7-12 cm | | 784A-45R-1, 101-106 cm | |
|---|---|---|---|---|
| Mineral | Clinopyroxene 1 | Clinopyroxene 2 | Clinopyroxene 1 | Clinopyroxene 2 |
| Ti | 111 | 105 | 131 | 118 |
| V | 107 | 105 | 125 | 114 |
| Cr | 3767 | 3173 | 4594 | 3386 |
| Sr | 5.02 | 5.09 | 0.43 | 0.85 |
| Zr | 0.39 | 0.35 | 0.39 | 0.31 |
| Ce | 0.099 | 0.117 | 0.054 | 0.070 |
| Nd | 0.087 | 0.107 | 0.020 | 0.027 |
| Sm | 0.032 | 0.044 | 0.017 | 0.028 |
| Eu | 0.017 | 0.022 | 0.013 | 0.016 |
| Dy | 0.059 | 0.090 | 0.134 | 0.145 |
| Yb | 0.184 | 0.198 | 0.134 | 0.130 |
| Hf | 0.078 | 0.071 | 0.077 | 0.077 |

**Table 4.8**. Representative trace element contents of clinopyroxenes.

### 4.11.1 REE Geochemistry of Clinopyroxene

In accordance with the depleted major and trace element chemistry of the peridotites the REE concentrations of the clinopyroxenes are very low and represent some of the lowest REE values recorded in peridotite clinopyroxenes (Parkinson et al. 1992a). Figure 4.27 shows the chondrite normalised REE plots for clinopyroxenes in the five samples analysed. The field for the most depleted abyssal peridotites from Johnson et al. (1990) are shown on the same diagram for comparison to emphasise both the depleted character of the Leg 125 peridotites and the different shape of pattern. They have flat to humped HREE to MREE patterns similar to REE patterns in diopsides from abyssal peridotites not associated with hot spots. With the exception of 784A 42R-1, 7-12 cm, all the diopsides show a marked upward inflection in Ce relative to Nd. The diopsides from the Leg 125 peridotites have lower HREE contents than diopsides from the most depleted abyssal peridotites reported in Johnson et al. (1990), but have less fractionated REEs, with $(Ce/Yb)_N$ ratios of 0.018 to 0.15 compared with $(Ce/Yb)_N$ ratios of 0.002 to 0.05 in abyssal peridotites.

### 4.11.2 Other Trace Elements

Of the other trace elements, Sr concentrations in the diopsides range from 0.43 to 5.19 ppm and are high compared to Sr values in diopsides from abyssal peridotites that have a similarly low proportion of modal clinopyroxene. Zr and Ti have very low concentrations, between 0.17 and 0.39 ppm and between 105 and 156 ppm, respectively. However, the Leg 125 peridotites have less fractionated Ti/Zr ratios than abyssal peridotites (300-750 compared with 250-4000). When plotted on extended chondrite-normalised diagrams we found it necessary to change the order of the elements from that proposed by Salters and Shimizu (1988) to take into account

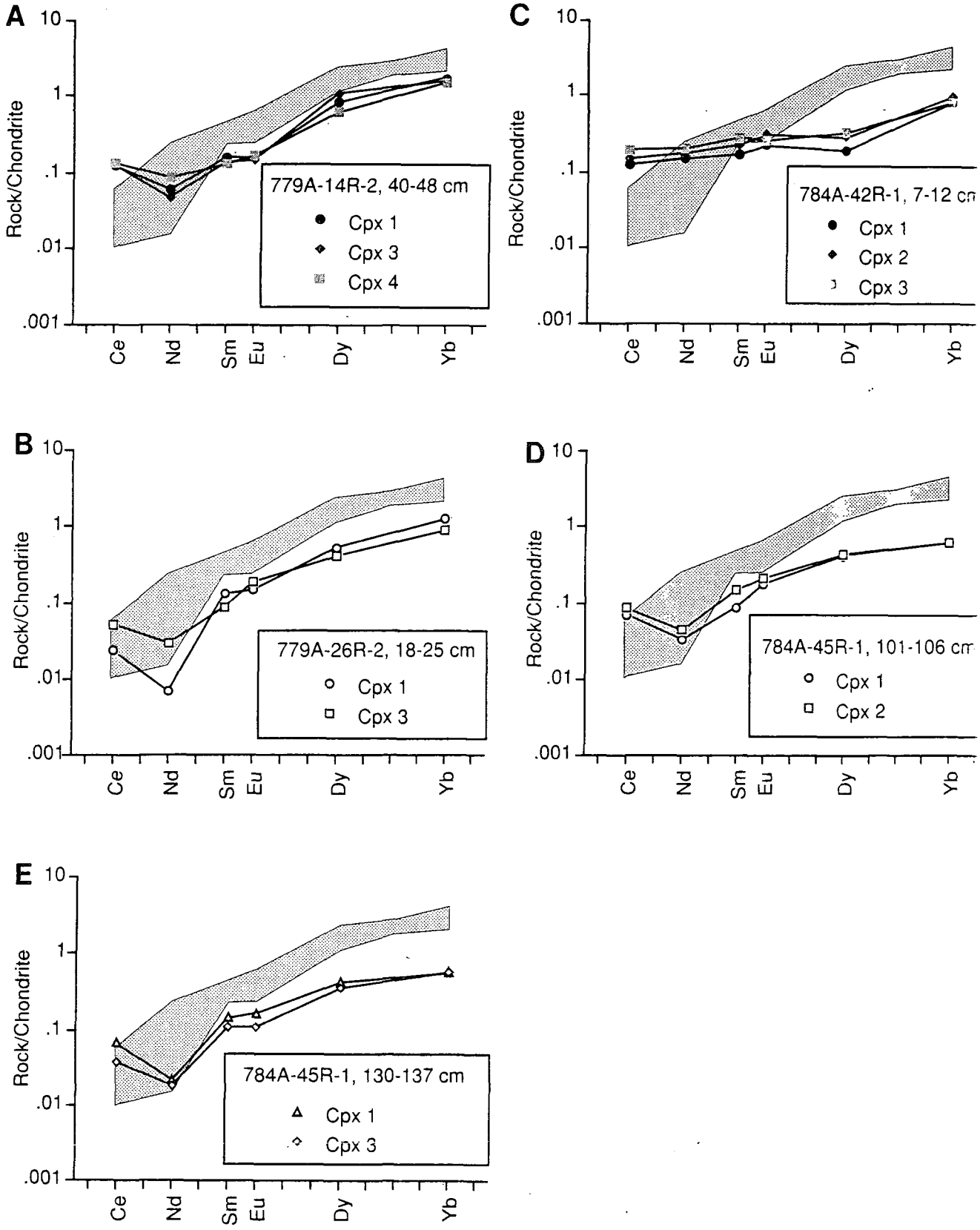


**Figure 4.27** Chondrite normalised REE plots of clinopyroxenes from Leg 125 peridotites. Shaded field represents the most depleted abyssal peridotites from Johnson et al. (1990).

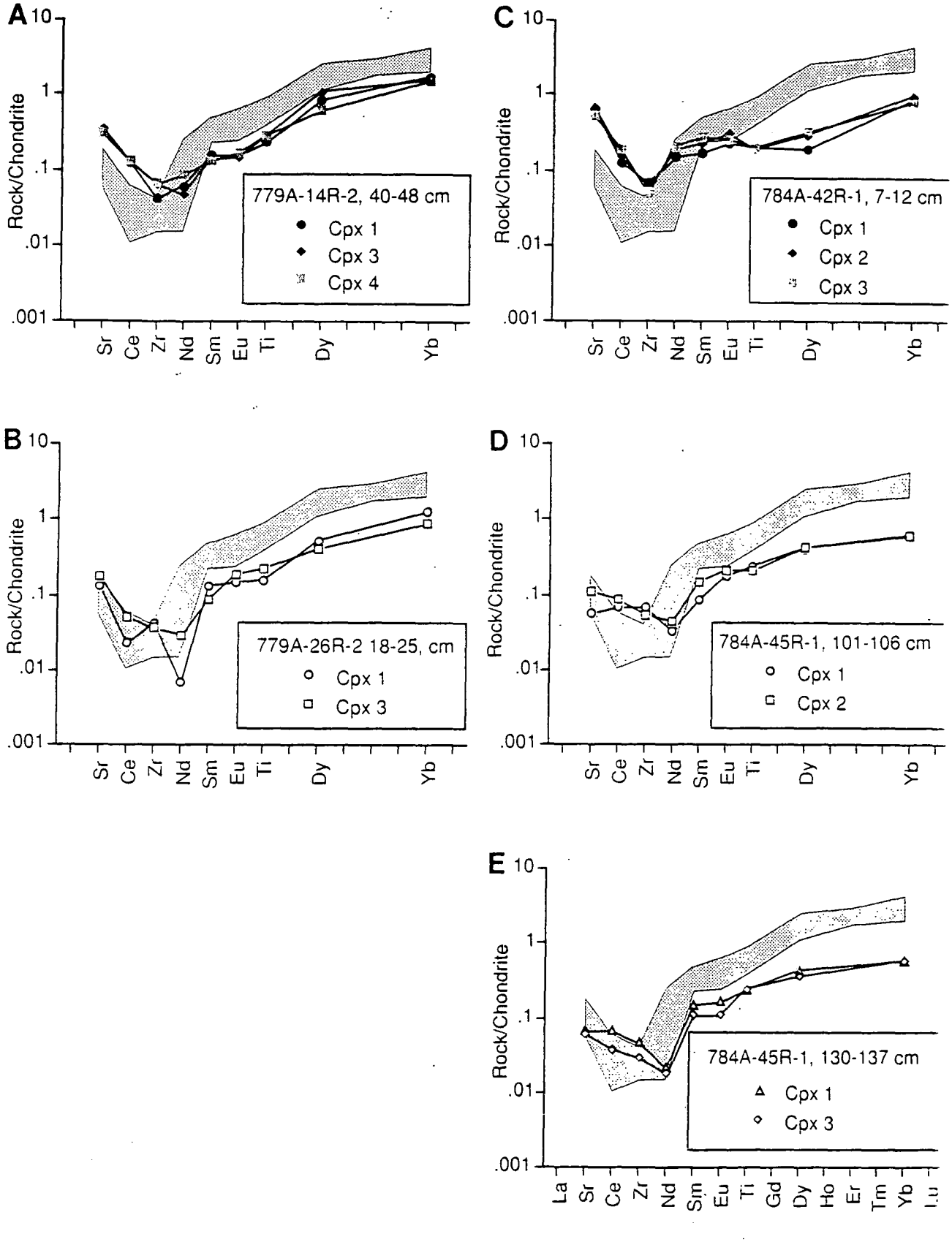


**Fig 4.28.** Extended chondrite-normalised trace element plots for clinopyroxenes from the Leg 125 peridotites. Shaded field represents the most depleted abyssal peridotites from Johnson et al. (1990). See text for element ordering.

compatibility in the system diopside-melt as well as peridotite-melt (see full discussion inand compatibilty in the system diopside-melt as well as peridotite melt (see full discussion in Chapter 5). To do this, and to eliminate the apparent negative anomalies in abyssal peridotite patterns, I have plotted Sr to the left of Ce, Zr between Ce and Nd and Ti between Eu and Sm. Figure 4.28 shows the extended chondrite-normalised plots with the field for the most depleted abyssal peridotites shown. The plots emphasise the enrichments of Sr and Zr with respect to the abyssal peridotites.

Abyssal peridotites commonly show strong depletions in the HFSE's Ti and Zr with respect to their neighbouring REEs in diopsides, to the extent that Salters and Shimizu (1988) suggested that there is a global HFSE-depleted shallow upper mantle. However the revised plot order removes these anomalies for the abyssal peridotites. Johnson et al. (1991) have shown that the degree of negative depletion of HFSE increases with degree of melting. Rampone et al. (1991) have shown that there are corresponding positive anomalies of Zr and Ti in orthopyroxenes which balance the negative anomalies in the clinopyroxenes. The anomalies highlighted by Johnson et al. (1990) reflect the increasing ratio of orthopyroxene to clinopyroxene in the melting residue.

### 4.11.3 Transition Elements

Cr and V were also analysed in the clinopyroxenes. Cr varies between 3133 and 7140 ppm with the higher value almost certainly the effect of a Cr-spinel inclusion (Kevin Johnson written communication, 1991). V has values between 107 and 179 ppm. The concentrations of both Cr and V are much lower than those in clinopyroxenes from abyssal peridotites. This is an important observation which will be discussed further later in this chapter.

### 4.11.4 Petrogenesis from Trace Element Geochemistry

The trace element data from both clinopyroxenes and orthopyroxenes are markedly different from the data from the depleted abysssal peridotites discussed in Johnson et al. (1990) and Johnson and Dick (1992). The following section discusses the petrogenesis of the Leg 125 peridotites in two parts. Firstly the extent and nature of the incompatible element enrichments is determined and evaluated. Secondly, the data for the transition elements Cr and V are discussed in terms of a two stage melting history of the peridotites.

### 4.11.5 Nature and Timing of Trace Element Enrichments

The extended chondrite-normalised patterns provide strong evidence for enrichment of LREE, Sr and Zr relative to Ti and the MREE-HREE in the clinopyroxenes and bulk

peridotites (see Chapter 5). The extent of the enrichment can be calculated for a given peridotite by estimating the composition the peridotite would have had if this enrichment process had not taken place and comparing this with the observed composition. The pre-enrichment composition can be determined by either choosing an unenriched sample with similar modal composition or theoretically by taking a fertile mantle composition and assuming a melting history. To produce a complete model it is necessary to determine whether the enrichment process took place pre- syn or post melting. Here I look at the trace element data from depleted abyssal peridotites and adopt an empirical approach to estimate the extent of the enrichment in the Leg 125 clinopyroxenes.

### 4.11.6 Extent of LREE, Zr, and Sr Enrichment

The extent of the trace element enrichments has been assessed by plotting a series of elements against an element thought not to be affected or the least affected by the enrichment process. Figure 4.28. shows that Ti and the HREEs best satisfy this criteria. Figure 4.29 shows a plot of Yb against Ti for the abyssal peridotite data (Johnson et al., 1990), the Ronda peridotite data of Salters and Shimizu (1988), and the Leg 125 data. The data show a trend from an estimated MORB source within the Ronda field through the abyssal data to the most depleted abyssal peridotites at about 200 ppm Ti. To assist with the interpretation predicted clinopyroxene compositions for fractional, equilibrium batch and incremental melting (with an increment of 1%) are shown, The extreme range of Ti values is best explained by near fractional melting and, as Johnson et al., (1990) pointed out, cannot be explained readily by equilibrium batch melting.

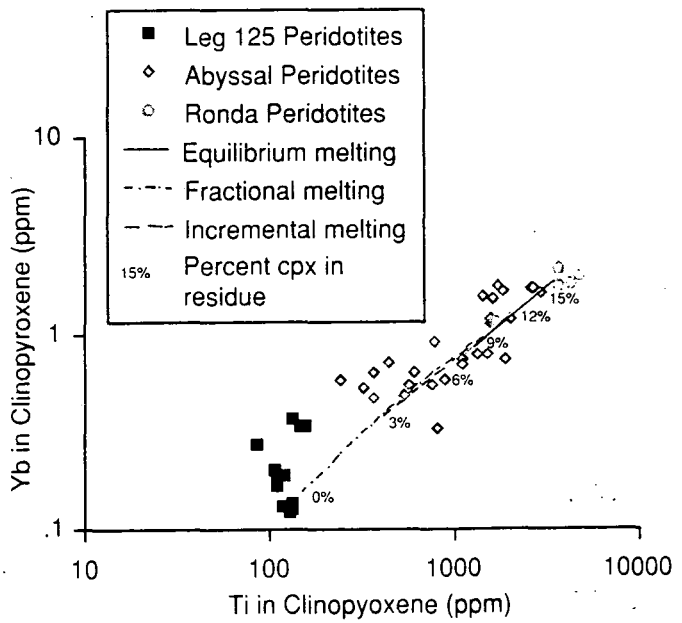


**Figure 4.29.** Ti versus Yb in clinopyroxene for abyssal peridotites, Leg 125 peridotites and peridotites from Ronda. Also shown are the residual clinopyroxene compositions for 0-25% fractional, incremental (0.1% increments) and equilibrium melting.

Fig 4.29 shows that the Leg 125 diopsides plot on an extension of the observed and modelled depletion trends, below even the most depleted abysssal peridotites. This is further evidence that these peridotites are residues from extensive melting. The fact that the Leg 125 data plot on an extension of the melting array has several important implications. Firstly it suggests that the peridotites are the residues from melting, in one or more stages, of a MORB source (see later). Secondly, it indicates that neither Ti or Yb were significantly affected by the event which enrichmed the LREE, Zr and Sr. It is possible that they were both equally enriched but it would have to be in a vector which still allowed them to lie on the melting array, which is unlikely given the smooth HREE to MREE clinopyroxene patterns.

Fig 4.30 shows plots of Sr, Ce, Nd, Zr, Sm, Eu, and Dy against Ti, where Ti rather than Yb is used as the unenriched element because of its considerably better counting precision. Dy is the only element to plot at the end of the melting array defined by Yb and Ti and so is thought also not be enriched in these samples. However, Sr, Ce, Nd, Zr, Sm, and Eu are all displaced to higher values than would be expected for the abyssal peridotite melting trend, confirming that these elements have been added to the peridotites at some stage in their history. The amount of enrichment can be judged by displacement away from the melting trend. Approximate degrees of melting trends are marked on the plots, although it should be noted that some scatter in some elements in the abyssal peridotites is thought to reflect re-enrichment with melts (Johnson and Dick, 1992). The extent of enrichment in the diopsides increases in the order Eu, Sm, Nd, Zr, Ce, Sr. This order in the degree of enrichment does not need to correspond to the bulk-rock enrichment becauses olivine and orthopyroxene may show different enrichment patterns.

The co-variation diagrams shown in Fig 4.30 place strong constraints on the timing of the enrichments. All the elements show variable enrichments that plot at almost constant Ti values. This is explained most simply by the enrichment taking place during or after melting, presumably associated with the second stage melting process. It can be argued that enrichment took place after the first melting event, and the enrichments reflect the residues from the second melting event. However, extremely large enrichments would have to have occurred for some of the highly incompatible elements (Sr, Ce) still to persist after 5% or more melting. We therefore conclude that the diopsides from the Leg 125 peridotites equilibrated with fluid/melt during melting and probably under sub-solidus conditions. The possible compositions of fluids and mechanisms of fluid/mantle interaction are discussed in the next section.

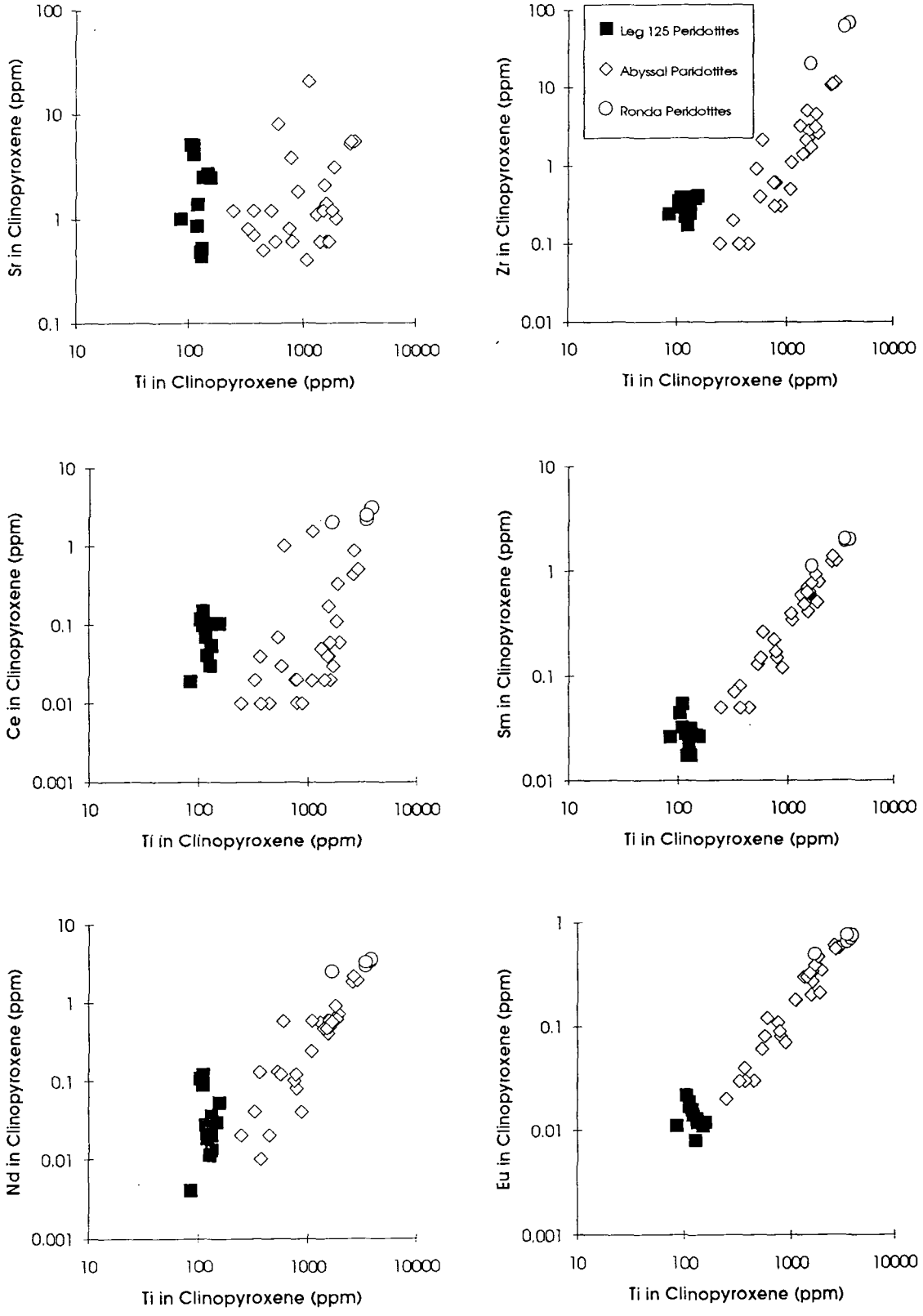


Figure 4.30. Plots of Sr, Ce, Nd, Zr, Sm and Eu versus Ti in clinopyroxene from the abyssal, Leg 125 peridotites and the variability in the highly incompatible element content of both the abyssal and Leg 125 peridotites.

### 4.11.7 Mechanisms of LREE, Zr and Sr Enrichments

Many depleted peridotites are enriched in highly incompatible elements (Frey and Green, 1974; Frey and Prinz, 1978; Stosch and Seck, 1980; Frey, 1984; Kempton, 1987; Menzies, et al., 1987). Furthermore, peridotites which have the greatest depletion in their "basaltic components" are often the most enriched in incompatible elements. This suggests that there could some universal process which causes such enrichments in depleted harzburgites. Obviously, all these harzbugites are rich in olivine and orthopyroxene and by definition poor in clinopyroxene. Bodinier et al. (1990), has used the experimental work of Fujii, et al. (1986) to propose that fluids may percolate more readily through a matrix of olivine and orthopyroxene, than one that contains clinopyroxene. Thus, harzburgites are more likely to interact with an incompatible-element enriched fluid and become enriched. The Leg 125 clinopyroxene trace element data can be tested to see if these peridotites are enriched in this manner. Unfortunately there is very little spread in the Ti (used as a measure of depletion) concentrations of the clinopyroxenes. However, in Figure 4.30 it can be seen that there is no significant correlation between the degree of depletion and the amount of trace element enrichment. Clearly, peridotites with a wider range of modal mineralogies would be needed to test this hypothesis further. However, the distinctive feature of the enrichment in the Leg 125 clinopyroxenes is the variable increase in enriched elements at nearly constant Ti concentration. This suggests that the enrichment event took place during and after the melting event. Before discussing the nature of the enrichment event it is pertinent to look at recent models of melt/mantle interaction to see if they can explain the distinctive trace element content of the Leg 125 clinopyroxenes.

### 4.11.8 Interaction Models

#### 4.11.8.1 Kelemen Reactions

Three different melt/mantle interaction models are discussed with a view to explaining the enrichments in the clinopyroxenes. Firstly, Kelemen and co-workers advocate that harzburgite forms by the reaction of lherzolite with basaltic melts. Kelemen et al. (1990) specifically address this problem in the context of melt/mantle interaction to explain the trace element charactersics of calc-alkaline melts and state that this type of interaction may be prevalent in the mantle wedge.

Kelemen et al. (1992) describe the trace element composition of clinopyroxenes in harzburgites from the Trinity ophiolite, Western USA. Within the harzburgites which they believe to have formed by melt interaction with a lherzolite are clinopyroxenes with a variety of origins. Some clinopyroxenes remain from the original lherzolite, some clinopyroxenes have partially reacted with percolating basaltic melts and some

clinopyroxenes have precipitated from the modified liquid which is formed during the melt/mantle interaction. In the Leg 125 peridotites there are clinopyroxenes with two different origins. Most of the clinopyroxene is Cr-diopside and is associated with orthopyroxene grain boundaries. The trace element geochemistry of these clinopyroxenes indicate that they are the residues from extensive partial melting (~25%) although they are selectively enriched in incompatible elements. In chapter three it was shown that the incompatible element content of the residual clinopyroxenes decreased slightly with increasing harzburgite formation. Therefore, it is difficult to reconcile the trace element characteristics of the Leg 125 clinopyroxenes with those formed during the reactions that Kelemen et al. (1992) describe. However, small crystals of secondary clinopyroxene are present in some peridotite samples (see Figure 4.4c). These have definitely precipitated from a magma which passed through the peridotites. Unfortunately, I have no trace element data for these pyroxenes so it is impossible to comment on their origin and say if they crystallised from the type of modified liquid produced during Kelemen-type reactions. Finally, Kelemen et al. (1992) states that many harzburgites are silica-rich because of excess orthopyroxene, which they crystallise out from the reacting melts in their models. The Leg 125 peridotites are silica-depleted because of the incongruent melting of orthopyroxene (see Chapter 5). Thus there are many features of the Leg 125 peridotites which are incompatible with Kelemen's mantle/melt interaction models.

#### 4.11.8.2 Open System Melting Models

Figure 4.31 shows the Leg 125 clinopyroxenes plotted on a diagram of Ti/Zr against $[Nd/Yb]_N$ along with model open system melting curves for differing amounts of melt trapped. This plot emphasises the difference between the Leg 125 peridotites and the abyssal peridotite data set. Most of the abyssal data lies close to the fractional melting line. However, the Leg 125 data plots at much lower Ti/Zr values and variable $[Nd/Yb]_N$. It is apparent from this diagram that the Leg 125 clinopyroxenes cannot be explained by open system melting with trapping of melts generated in a normal MORB melting column. The data is most readily explained by variable enrichment of Zr and Nd as previously proposed.

#### 4.11.8.3 Melt Percolation Models

Bodinier et al. (1990) has described how melt percolation from a dyke may modify the geochemistry of the wallrock peridotite in which the dyke was intruded. The Leg 125 peridotites have considerable petrographic evidence to suggest that they have interacted with both melts and aqueous fluids (see earlier this chapter). There exists

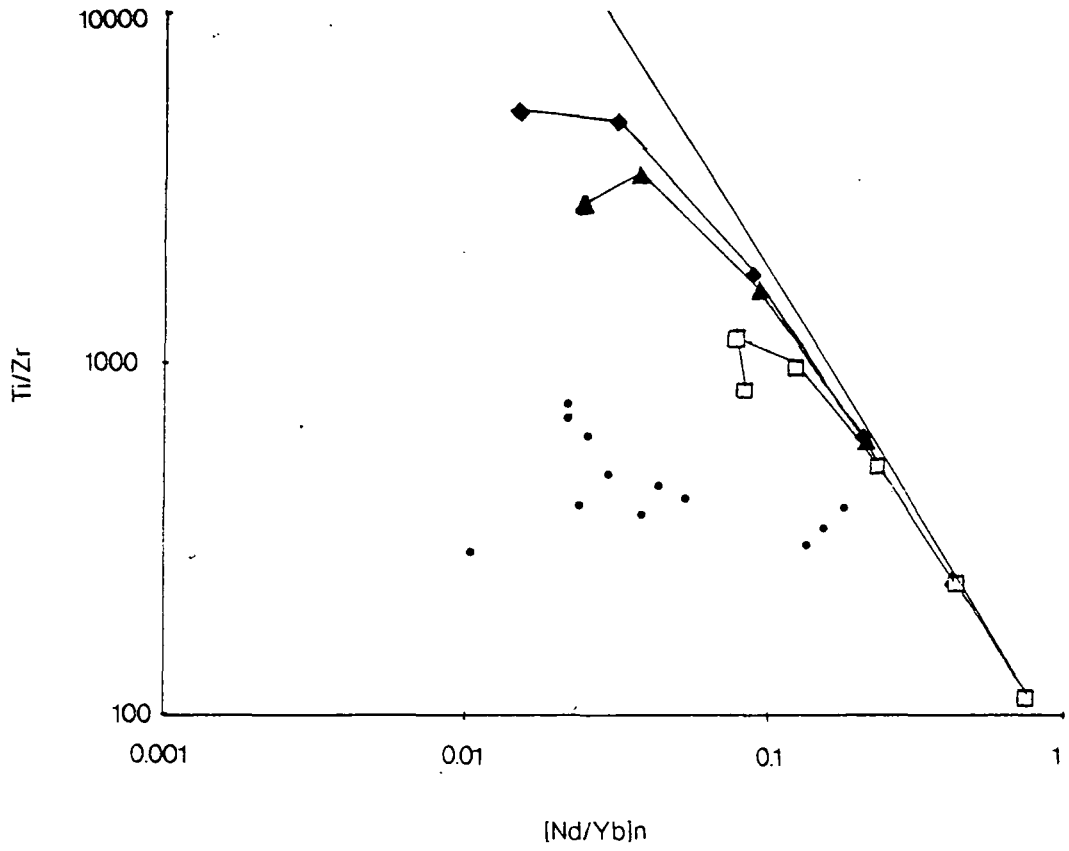


**Figure 4.31**. Plot of Leg 125 clinopyroxenes (filled circles) on a Ti/Zr against $[Nd/Yb]_N$. The lines represent open system melting calculations with fractional melting (solid line), 0.5% trapped melt (solid diamonds), 1% trapped melt (solid triangles) and 5% trapped melt (open squares). The lines represent 0-25% melting. Clearly the Leg 125 data does not fit on any of the melting lines and plots away from the melting trends to lower $[Nd/Yb]_N$ ratios at low Ti/Zr ratios.

some obvious differences between the melt/wallrock interaction that Bodinier et al. (1990) describe and the fluid/mantle interactions that the Leg 125 peridotite record. The amphibole in the Leg 125 peridotites was formed by the reaction of orthopyroxene and an aqueous fluid phase and has not precipitated from a melt phase. Furthermore, the small veinlets of melt present look petrographically like boninites and so represent melt which has not segregated properly rather than a melt which has percolated through the peridotite in the manner that Bodinier et al. (1990) envisage. However, because of the type of samples that the ODP cruise recovered (i.e., very small and with very little 'field' relationships maintained) it is not possible to prove that melts did not percolate from a dyke into the peridotites and affect their trace element geochemistry. From the clinopyroxene data however, it is possible to comment on the composition of both the melt and matrix if melt percolation did cause the incompatible element enrichments in the Leg 125 clinopyroxenes.

The melt must be LREE, Sr and Zr enriched to produce the charateristic trace element content of the clinopyroxenes. Furthermore, if the melt was percolating through a depleted harzburgite matrix similar in modal composition to the Leg 125 peridotites

then the melt would have to be extremely Zr enriched as the harzburgite matrix would hold back Zr relative to its neighbouring REEs. It is therefore difficult to envisage the trace element enrichments seen in the clinopyroxenes being produced by percolation of 'normal' basaltic melts through the mantle wedge. Percolation of more 'exotic' melts and fluids from the underlying subduction zone may be important in generating the characteristic trace element patterns of the Leg 125 diopsides (Parkinson et al., 1992a; Pearce et al., 1992b; Chapter 5).

### 4.12 Nature of the Enrichment

To explain the trace element characteristics of the Leg 125 clinopyroxenes it is necessary to add a LREE, Sr and Zr enriched fluid/melt. Time-integrated enrichment of the lithosphere by small-degree asthenospheric fluids has been suggested as a source for metasomatic enrichment in peridotites (Frey and Green, 1974; McKenzie, 1989). This component is characterised by a composition related to the compatibilty of an element with a garnet lherzolite. A further possibilty with peridotites associated with subduction zones are small melt fractions from an amphibole lherzolite and a phlogopite-bearing lherzolite. Garnet-lherzolite melts have strongly LREE and MREE enriched profiles relative to the HREE. These types of melts are often associated with high Nb concentrations. Small melt fractions from an amphibole-bearing peridotite would have varying compositions depending on the composition of the amphibole and the distribution coeffecients between amphibole and melt. The amphibole distribution coeffecients quoted in McKenzie and O'Nions (1991) would produce a melt with strong Nb, Zr and Ti depletions and relatively depleted in the MREE with respect to the HREE. However, it is apparent that amphiboles have a wide variety of D values (Matthew Thirlwall, pers. comm) and that high Nb and Zr distribution coefficients relative to their neighbouring REE is not a consistent feature of amphiboles.

The models described above for trace element enrichment in the residual diopsides require that the composition of the fluid/melt which causes this enrichment has specific characteristics. Parkinson et al. (1992a) calculated the likely composition of this fluid using simple mass balance calculations assuming that the enriching component had a mass fraction of 1% mass of the peridotite. Fig 4.32 shows calculated compositions for this fluid/melt normalised to a MORB source. Pearce et al. (1992b) undertook similar calculations from the geochemistry of spatially related boninites and produced broadly similar enrichment patterns.

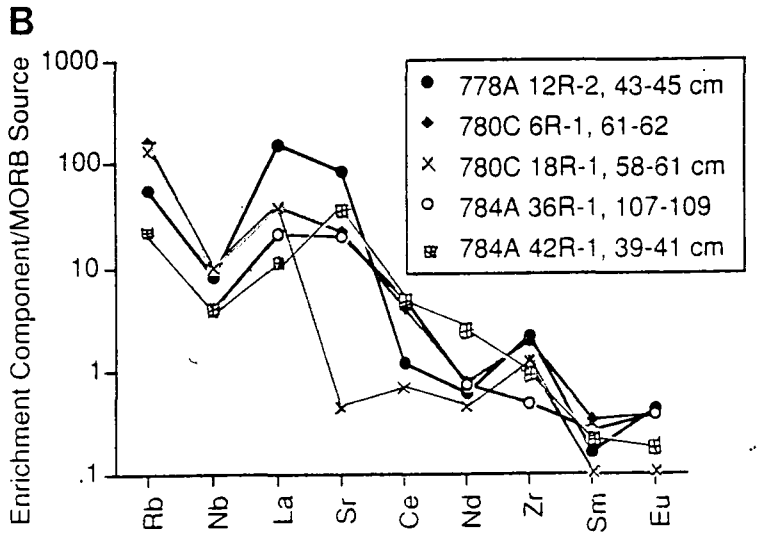


**Fig 4.32.** MORB-source-normalised trace element pattern of the enriching component. The patterns for each peridotite are calculated by mass balance assuming that the enriching component makes up 1% by mass of the peridotite (after Parkinson et al., 1992a).

The charateristics of these enrichment patterns are not consistent with those of 'normal' asthenospheric melts because of the strong Nb depletion and relatively high Zr content. Isotopic work on the boninites (Pearce et al., 1992a) rules out the possibilty of OIB type melts affecting these particular boninites although Stern et al. (1991) and Kostopoulos and Murton (1992) have argued that an OIB type component could be important in the genesis of boninites.

Pearce et al. (1992b) have suggested that granitic melts from the melting of subducting oceanic crust in the amphibolite facies have the requisite composition to produce the characteristic trace element enrichments in the boninites. It is also possible that melts generated during the breakdown of amphibole in the mantle wedge could produce such melts although amphibole-melt partition coefficients would need to be higher than published values. In conclusion the charactersitic enrichments found in the peridotite clinopyroxenes are best explained by interaction with a melt enriched in the LREE, Sr and Zr. Some of the LREE and Sr may have been derived from fluids from the underlying subduction zone whereas the Zr enrichment necessitates the involvement of an melt enriched in Zr relative to the MREE: Melting of the subducting slab in the amphibolite facies may produce this characteristic enrichment (Pearce et al., 1992b).

## 4.13 Transition Element Data-Evidence For Hydrous melting?

The discussion on the variation of Yb (and Dy) with Ti in the diopsides strongly suggests that the Leg 125 peridotites are essentially fractional melting residues from very high degrees of melting. Their position in the forearc and there spatial relationship with boninites makes the common assertion (e.g., Duncan and Green, 1980, 1987) that the peridotites had a two stage melting history, with one stage occuring below a mid-ocean spreading ridge and the other stage above a subduction zone very inviting. However, it can be argued that the abyssal peridotite data set is biased towards peridotites which record lower degrees of melting than residual peridotites that are located directly below the spreading ridge in normal thickness oceanic crust. This arguement is partly valid as many of the analysed abyssal peridotites come from fractures zones located in the slow spreading Atlantic Ocean and so may not be representative of upper most mantle below spreading ridges. Furthermore, if sampled abyssal peridotites essentially represent the residues at the top of the melting column, which represents the total degree of melting in Klein and Langmuir (1987) and Kostopoulos and James (1992) parlance, then peridotites with 10% modal clinopyroxene and 2000 ppm Ti are not the residues from extensive melting in a long melting column. However, some abyssal peridotites are residues to 15-20% partial melting, consistant to the amount of melting thought to produce N-MORB. Bearing this in mind it seems likely that the Leg 125 peridotites must represent either one extremely high (>20%) partial melting event or a two stage (total melting >20%) melting history. The following discussion on the Cr and V data for the Leg 125 peridotites sheds some light on their melting history.

Fig 4.33 shows plots of V and Cr against Ti in the clinopyroxenes from Leg 125. As with the previous section, abyssal peridotite data from Johnson et al. (1990) is also plotted as a reference frame. The Leg 125 clinopyroxenes plot at low V and Cr values relative to the trends defined by the abyssal peridotite data. The plot of V vs Ti is the most interesting as data from Leg 125 not only plot at low concentrations of V but the data from Torishima Forearc Seamount plots at lower values for a given Ti concentration than the clinopyroxenes from Conical Seamount. As discusssed in the distribution coeffecient section of Chapter 3, V is one of the few elements that changes its oxydation state readily within the range of reasonable oxygen fugacity values for terrestrial magma genesis. $V^{3+}$ dominates at oxygen fugacity values around FMQ -1 to +1 log units whereas $V^{4+}$ and $V^{5+}$ dominate at oxygen fugacities corresponding to FMQ +1 through to +4. The effect on the partition coeffecient between clinopyroxene and melt is that V becomes more incompatible with increasing oxygen fugacity.

Oxygen thermobarometry has shown that peridotites from both seamounts have equilibrated under oxidising conditions (generally greater than FMQ+1). Furthermore, the peridotites from Torishima Forearc Seamounts have equilibrated at higher oxygen fugacities than the peridotites from Conical Seamount. The V data can be explained by a two stage melting history. The first melting stage involves the peridotites melting under reducing conditions and V behaves compatibly with respect to clinopyroxene. From the intersection of the two trends in Figure 4.3 the peridotite may have partially melted 15% under dry conditions. This melting event probably occured beneath a spreading centre. The second stage melting event takes place at higher oxygen fugacities (>FMQ+1) and V behaves incompatibly with respect to clinopyroxene. This second melting event partially further melts the peridotite 5 to 10% and is interpreted to have occurred in the mantle wedge above a subduction zone.

The Cr data is also interesting as again the Leg 125 data plot on a completely different trend to the main abyssal array. This time there is no differentiation between the two seamounts. Chromium exists in three common oxidation states, $Cr^{2+}$, $Cr^{3+}$ and $Cr^{6+}$. $Cr^{2+}$ may be important on the moon where conditions are very reducing. $Cr^{3+}$ is the common state for chromium in terrestrial magmas. I know of no study which suggests that $Cr^{6+}$ becomes more stable during terrestrial magma genesis. If the decrease in the Cr content of the Leg 125 clinopyroxenes is explained by partial melting processes then Cr would have to become incompatible with clinopyroxene. However there is no experimental evidence to support this. It could be argued that the systematic decrease in the V and Cr content of the clinopyroxenes and orthopyroxenes (from electron microprobe data) is consistent with formation of secondary spinels which soak up these two elements. Many of the clinopyroxene grains are intimately related to secondary Cr-spinel grains. Girardeau and Lagabrielle (1992) propose that clinopyroxene recrystallises and produces secondary spinel during serpentinisation. During sub-solidus re-equilibration during serpentinisation both V and Cr would be partitioned into the spinel because serpentinisation takes place at low oxygen fugacities (Eckstrand, 1975) and V would be in its trivalent state. Therefore V would be partitioned into spinel and it is unlikely that the two distinct trends shown on the V versus Ti plot in Figure 4.32 would have formed. In conclusion, the low Cr values in the Leg 125 clinopyroxenes are produced by sub-solidus equilibration with secondary spinels. The distinct V trends are formed by melting under oxidising but slightly different oxygen fugacities in the two forearcs, with the peridotites from Torishima forearc having melted under higher oxygen fugacities. The V data provides evidence that the Leg 125 peridotites had a two stage melting history.

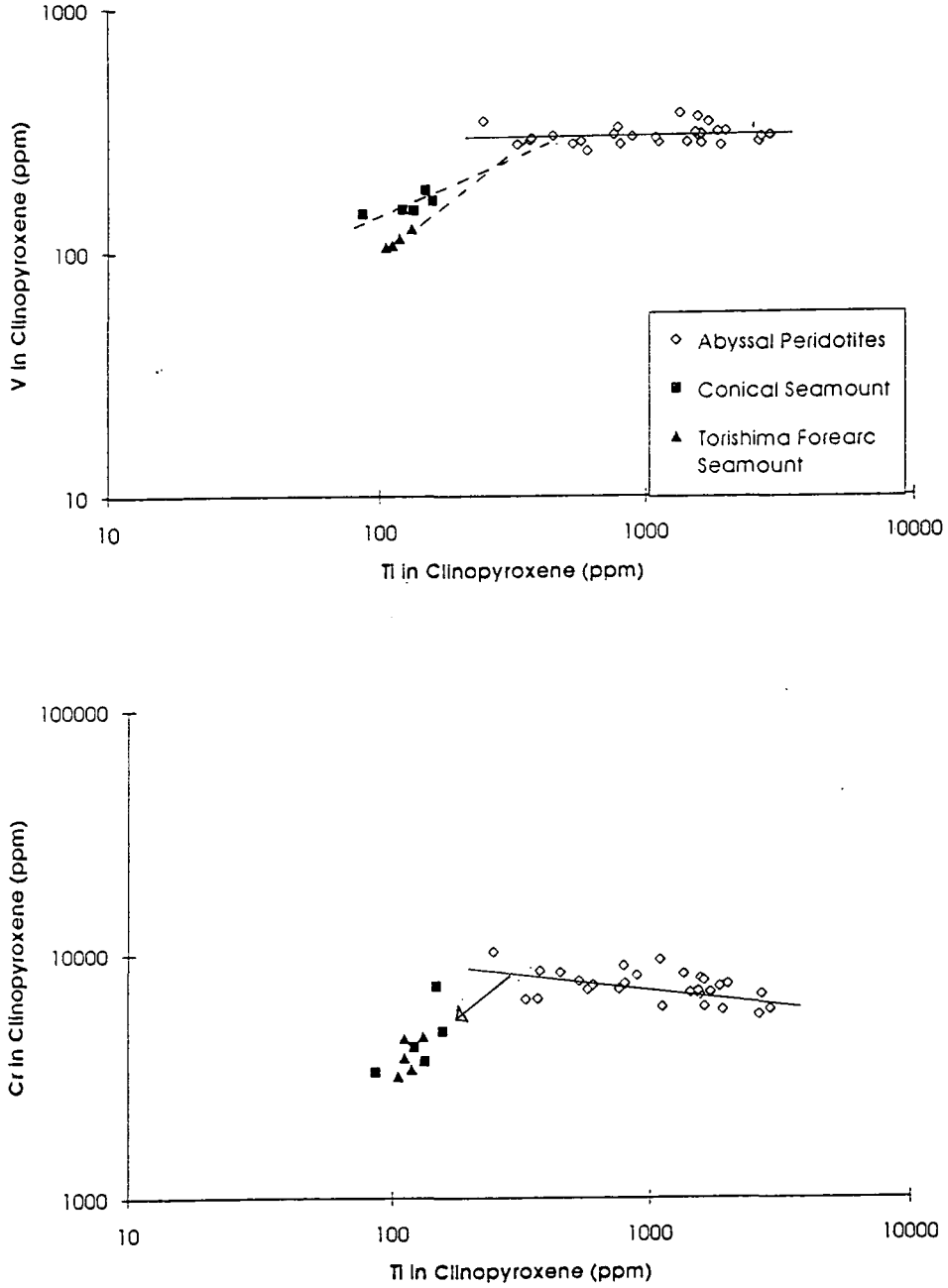


Fig 4.33. V and Cr versus Ti in clinopyroxenes from Leg 125 and abyssal peridotites. Note how the data from the Leg 125 peridotites plots on distinctly different trends to the abyssal data.

Lines indicate 0-15% partial melting of an FNN source using the modelling parameters for melting in the spinel field described in Chapter 3. The two trends in the V versus Ti plot can be best explained by a further 5-10% melting with V behaving slightly incompatibly. The Cr versus Ti data can be explained by sub-solidus re-equilibration with secondary spinel. The arrow shows the effect of decreasing Cr content of the clinopyroxenes during this re-equilibration.

### 4.14 Conclusions For The Chapter

1. The Leg 125 peridotites are depleted harzburgites The mineralogy of the peridotites is 75-80% olivine, 20-25% orthopyroxene, 0-1% clinopyroxene, 1-2% Cr-spinel and 0-5% amphibole.

2. The samples are highly serpentinised, between 20 and 100%. Olivine is serpentinised to lizardite and orthopyroxene to bastite. Clinopyroxene is not serpentinised. Clinopyroxene is often recrystallised with spinel. The rims of many of the Cr-spinels have altered to ferrit-chromit. Late stage chrysotile veins cross-cut many of the samples and in some samples there are complicated histories of veining. Some samples have distinctive alteration with high temperature antigorite replacing some of the olivine. Amphibole is more common in these samples though still rare. Cr-rich chlorite is found as reaction haloes around some spinel grains.

3. The major element mineral chemistry of the minerals shows they are compatible with being residues to high degrees of melting. Olivines are highly forsteritic (Mg# 91.5-93), orthopyroxenes are enstatitic (Mg# 92-94) and spinels highly Cr-rich (Cr# 55-80). on comparative plots with abyssal and ophiolitic data they plot at the depleted end of all the arrays.

4. Many of the different geothermometers consistently give lower temperatures for the Leg 125 peridotites than abyssal peridotites and continental xenolith samples. This is suggestive of an extensive sub-solidus re-equilibration history. Many of the geothermometers record temperatures close to the blocking temperature for the given exchange reaction indicating that cooling was slow.

5. Oxygen geothermobarometry calculations indicate that Leg 125 peridotites equilibrated at high oxygen fugacities between -1 and +4 $\Delta f_{O_2}$ units with respect to the FMQ buffer. These values are higher than abyssal peridotites and within the range of mantle xenoliths associated with subduction zones. Given the tectonic setting of the drilling sites it is likely that the high oxygen fugacities are related to fluxing of water from the underlying subduction zone.

6. Trace element analyses of the clinopyroxene shows they have very low concentrations of incompatible elements, consistent with them being residues to high degrees of partial melting. However, they are selectively enriched in the LREE, Sr, Zr,

Nd, Sm and Eu. The enrichment event occurred during and after the final melting event.

7. Vanadium data from clinopyroxenes lie at distinctly lower levels than data for abyssal peridotites at comparable levels of depletion. This is consistent with V being highly incompatible during mantle melting, which only happens when oxygen fugacities are greater then $10^{-12}$ log units. This is consistent with the oxygen fugacity calculations for the Leg 125 samples and is strongly suggestive of water being important in the genesis of these samples almost certainly related to the underlying subduction zone. Low V levels in mantle minerals, which plot off the trend for abyssal peridotites are a good indicator for characterising subduction related peridotites. However, similar low concentrations in Cr in the clinopyroxene and orthopyroxenes may be a reflection of low temperature equilibration with Cr-spinel.

8. There is evidence to suggest that the peridotites had a two stage melting history, which involved extensive dry melting, presumably at a mid-ocean spreading ridge. This was followed by a smaller episode of hydrous partial melting above a subduction zone. The melts generated were highly magnesian (Mg# ~70-75) and are likely to be the spatially related boninites found in the forearc. Selective trace element enrichment accompanied the melting and possibly continued under sub-solidus conditions producing the distinctive trace element enrichment patterns in the clinopyroxenes.

*In this chapter I have addressed the question of whether alteration processes affect the bulk rock chemistry of the peridotites. All the Leg 125 peridotites are serpentinised (some up to 100%) so that it is important to consider the effects of serpentinisation. I have treated the problem by plotting concentrations of elements (on anhydrous basis) against the loss on ignition value (LOI). This approach is simplistic in that it just approaches the problem by looking for correlations between the amount of water the peridotites have reacted with (and hence degree of serpentinisation) and the concentrations of elements and does not consider the composition of the reacting fluids. For most of the major elements (except $Na_2O$ and $K_2O$) and the immobile trace elements (HFSE, REE) this approach is probably acceptable as the effect of serpentinisation is to increase the volume of the peridotites. In Chapter 2 the possible sources for the serpentinising fluids in the seamounts was discussed. The peridotites could have potentially interacted with fluids from the underlying subducting slab or seawater. When looking at the distribution of the mobile trace elements (principally the LIL elements K, Rb, Sr, Cs and Ba) it is not possible to tell whether these elements have been added from the underlying subduction zone, seawater or have been mobilised by either type of aqueous fluid using the simple element concentration versus LOI plots. In all cases the concentration of the LILE may be affected by secondary (alteration) processes and may not have any petrogenetic significance in the models proposed in this chapter.

*In this chapter I have addressed the question of whether alteration processes affect the bulk rock chemistry of the peridotites. All the Leg 125 peridotites are serpentinised (some up to 100%) so that it is important to consider the effects of serpentinisation. I have treated the problem by plotting concentrations of elements (on anhydrous basis) against the loss on ignition value (LOI). This approach is simplistic in that it just approaches the problem by looking for correlations between the amount of water the peridotites have reacted with (and hence degree of serpentinisation) and the concentrations of elements and does not consider the composition of the reacting fluids. For most of the major elements (except $Na_2O$ and $K_2O$) and the immobile trace elements (HFSE, REE) this approach is probably acceptable as the effect of serpentinisation is to increase the volume of the peridotites. In Chapter 2 the possible sources for the serpentinising fluids in the seamounts was discussed. The peridotites could have potentially interacted with fluids from the underlying subducting slab or seawater. When looking at the distribution of the mobile trace elements (principally the LIL elements K, Rb, Sr, Cs and Ba) it is not possible to tell whether these elements have been added from the underlying subduction zone, seawater or have been mobilised by either type of aqueous fluid using the simple element concentration versus LOI plots. In all cases the concentration of the LILE may be affected by secondary (alteration) processes and may not have any petrogenetic significance in the models proposed in this chapter.

# Chapter 5
# Major and Trace Element Geochemistry

## 5.1 Introduction

This chapter describes the major and trace element whole-rock geochemistry of the Leg 125 and Ojen peridotites. For the Leg 125 peridotites within hole and between hole differences are emphasised. Their petrogenesis is described in terms of melting and melt/mantle interaction models previously described in Chapter 3.

## 5.2 Notes on Analytical Techniques

Depleted mantle peridotites present several analytical problems because of their high concentration of compatible elements and their low to incredibly low concentrations of the incompatible elements. Peridotites in this study have been analysed by several techniques in order to maximize the number of elements analysed and their precision. Details of the analytical techniques are provided in Appendix A.

Major elements where analysed by XRF on glass fusion discs. Cr and Ni where also analysed in this way as they make up 0.6 wt. % between them. Trace elements were analysed by two techniques, XRF on pressed powder pellets and ICP-MS on solutions. For highly incompatible elements such as the REE, ID-MS analysis at RHBNC was undertaken. Although new techniques such as ICP-MS should provide analysis down to less than 0.1 ppm in the rock for elements such as Nb, Zr, Y etc problems w ere still encountered at these low levels because of matrix suppression effects and the lack of high quality standards at such low levels (see details in Appendix A). To give an idea of the problems of analytical quality at such levels, 2σ error bars are provided on the diagrams to assist the reader with interpretations.

## 5.3 Effects of Alteration on Bulk-Rock Chemistry*

### 5.3.1 Serpentinisation

Before primary variations in the geochemistry are described it is necessary to assess the effects of secondary processes such as serpentinisation on the bulk-rock geochemistry of the peridotites. All the peridotites have been extensively serpentinised as previously discussed. To assess the effect of serpentinisation on the geochemistry major and trace

element geochemistry elements are plotted on an anhydrous basis against loss on ignition (LOI) which is used as a measure of serpentinisation.

### 5.3.1.1 Major Elements

Of the major elements only $SiO_2$, $Fe_2O_3$ (total iron as analysed by XRF), MgO and $Na_2O$ show that their distribution is affected by serpentinisation. Figure 5.1 shows plots of these elements against LOI wt.%. $SiO_2$ concentrations are relatively unaffected up to 15 wt.% LOI but drop by 2-3 wt.% at high degrees of serpentinisation. This effect is shown well by the data from hole 779A. $Fe_2O_3$ values are fairly constant up to 15 wt.% LOI but increase by up to 1 wt.% at LOI greater than 15 wt.%. MgO variations with serpentinisation are most pronounced in peridotites from hole 779A. Although there is considerable scatter in the data MgO increases slightly with increasing LOI. Petrological studies in Chapter 3 indicate that olivine is the first mineral to be serpentinised and orthopyroxene is only serpentinised in the very highly serpentinised samples. The variation in the distribution of $SiO_2$ at high LOI values can be explained by the serpentinisation of orthopyroxene as this reaction looses $SiO_2$ to the reacting fluid (Kimball et al., 1985).

Studies of the fluid geochemistry from Leg 125 (Mottl, 1992) have shown that seawater makes up an important component of the serpentinising fluids in the serpentinite seamounts, especially in the fluids sampled at Holes 783A and 784A and to a lesser extent holes 778A and 779A. Even so $Na_2O$ is very low in the Leg 125 peridotites being below 0.8 wt.%. From the plot of $Na_2O$ versus LOI there is a slight increase in $Na_2O$ with LOI but many of the values lie below 0.2 wt.%. Some of the high $Na_2O$ values are from serpentinite muds. Samples from hole 779A can be used to see if there is any variation in the $Na_2O$ values with depth as samples have been collected from throughout this hole. Fig 5.2 shows that there is some cyclicity in the $Na_2O$ content with depth. High $Na_2O$ values are found when serpentinite mud occurs. These muds have similar major element chemistry to the blocks of serpentinised peridotites. The high $Na_2O$ values in these samples possible reflects the stabilisation of Na-bearing minerals when seawater and fresher deep-seated fluids reacted (Fryer and Mottl, 1992; Mottl, 1992).

### 5.3.1.2 Trace Elements

Ultramafic rocks are commonly serpentinised and the effect of serpentinisation on the distribution of trace elements has been a major worry for some workers (Ottonello et al., 1979; Frey, 1984). The effect of serpentinisation on the trace element distribution

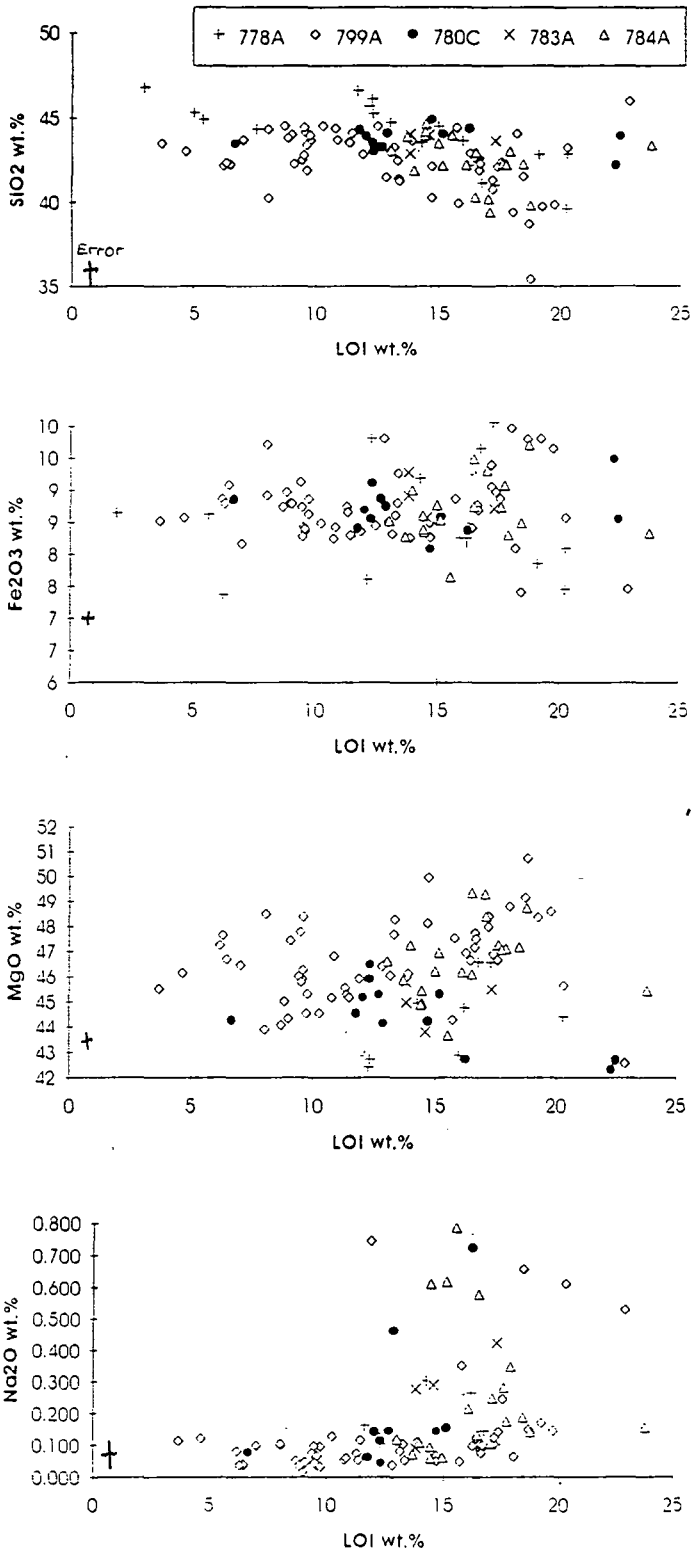


**Figure 5.1.** Plots of wt%. $SiO_2$, $Fe_2O_3$ (total iron as analysed by XRF), MgO and $Na_2O$ against wt.% LOI for peridotites from Conical and Torishima Forearc Seamounts.

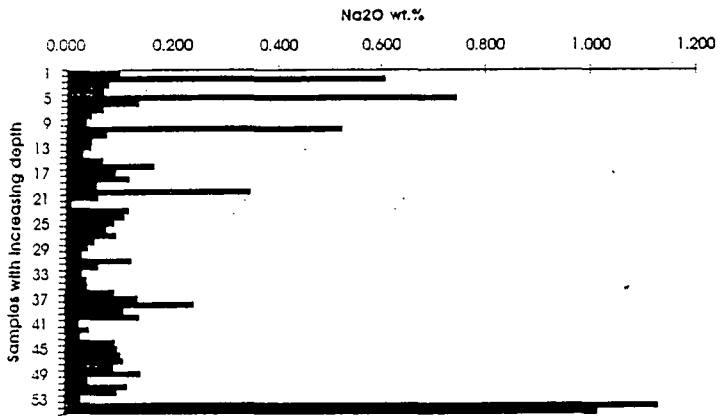


**Figure 5.2.** Downhole variation in wt.% $Na_2O$ in hole 779A.

in ultramafic rocks is not fully understood as no comprehensive investigation has been undertaken (McDonough and Frey, 1989). Empirical studies to date have failed to show any correlation between the degree of serpentinisation and the REE content and pattern shape (e.g. Frey et al., 1985; Prinzhofer and Allègre, 1985). Theoretically, the LREE's and the LILE's should not be incorporated into the serpentinite (lizardite) structure because their large ionic radii are not compatible with the octahedral sites in the serpentinite (Ottonello et al., 1979). However, the elements will be mobile only if the serpentinising fluids are able to transport them out of the system. Tatsumi et al., (1986) produced synthetic serpentinite doped with selected trace elements and found that much of the La was loosely bound onto the surface of the serpentinite and was easily leached with HCl. It is possible, therefore, that any LREE's released by the serpentinisation process are adsorbed by the serpentine, rendering the LREE's effectively immobile.

Menzies et al. (1992) describe a series of experiments on the laboratory serpentinisation of lherzolites and harzburgites with synthetic Pacific seawater which were conducted in order to assess the effects of serpentinisation on Sr isotope and REE distributions. The Sr isotopic composition of the harzburgites is similar to that of the seawater, whereas the lherzolite recorded a Sr isotope composition intermediate to the that of the seawater and the fresh sample suggesting that some unserpentinised

clinopyroxene retained a "primary" Sr isotope composition. The REE distribution does not vary between fresh and serpentinised lherzolites. However, Menzies et al., (1992) reported that the Ce/Yb ratio of the serpentinised harzburgite was lower than its fresh counterpart. This result indicates that Ce may be mobilised during serpentinisation and the LREE as a whole may behave in a similar manner. However, this result is based on one experiment and further experiments have to be carried out before it can be shown that the LREE are mobilised during the serpentinisation of harzburgites.

Again I have plotted elements on an anhydrous basis against LOI to see if trace elements vary systematically with serpentinisation. The LREE, Rb, Sr, Cs and Ba have been shown to be redistributed by alteration processes in basalts (Taylor et al., 1992) so it is important to check whether these elements are redistributed during serpentinisation, as they are elements which are commonly enriched in subduction zone lavas and are important in understanding the petrogenesis of the Leg 125 peridotites.

The pore-fluid geochemistry sampled from the two seamounts has already been described in Chapter 2. The origins of the pore-fluids varied from hole to hole. Pore-fluids from Hole 780C have a large component of deep-seated fluid probably from the underlying subduction zone (Mottl, 1992). In contrast pore-fluids from holes 783A and 784A in Torishima Forearc Seamount is seawater which has been modified by low-temperature serpentinisation reactions. Fluids from holes 778A and 779A are a complex mixture of these two fluid end members. In attempting to understand the effects of serpentinisation on the trace element distribution it is important to also take account of the origin of the serpentinising fluids.

Most of the trace elements (first series transition elements, HREE) show no systematic variation with serpentinisation and it is concluded that the distribution of these elements is not affected by serpentinisation. This is not surprising as these elements are usually considered immobile during alteration of basalts.

However the LILE elements Rb, Sr, Ce and Ba do show some systematic variations with serpentinisation. Figure 5.3 shows the variation of Sr with LOI for Holes 778A, 780C, 783A and 784A. The large number of samples from Hole 779A meant that it was possible to look at the variation of these elements with depth (Figure 5.4). Interestingly, Sr concentrations define three distinct groups with depth, an upper group, a middle group and lower groups. The upper and lower groups have variable but generally high Sr concentration (many over 10 ppm Sr). The middle group have consistently low Sr concentrations between 0.3 and 2 ppm. Figure 5.5 shows Rb, Sr,

Cs and Ba versus LOI for Hole 779A with the samples divided into the three groups previously described.

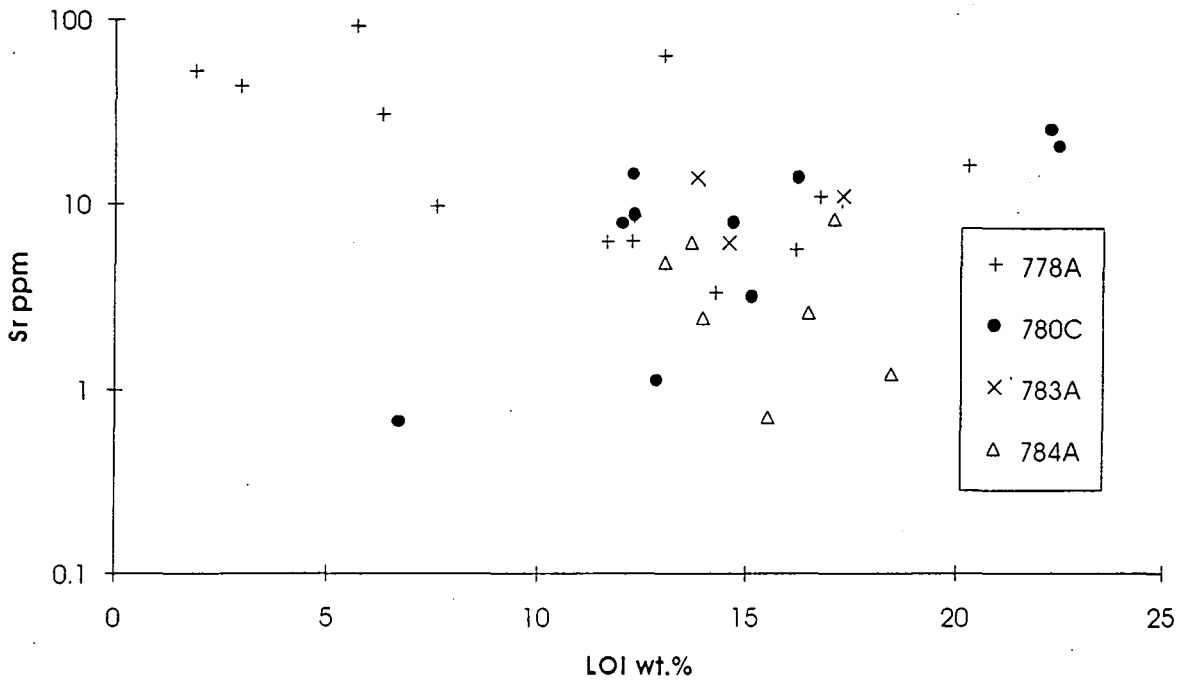


**Figure 5.3.** The variation of Sr with wt.% LOI for Holes 778A, 780C, 783A and 784A.

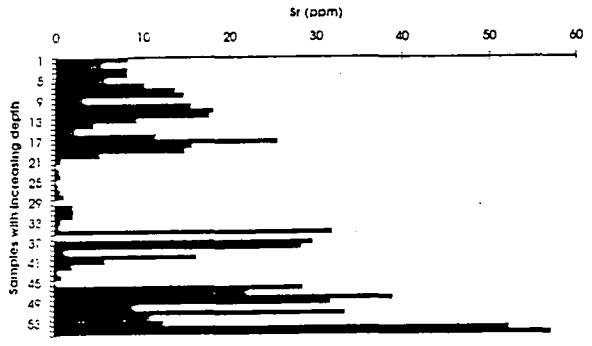


**Figure 5.4.** Downhole variation in Sr in hole 779A. Three groups are defined by their Sr concentration in this hole.

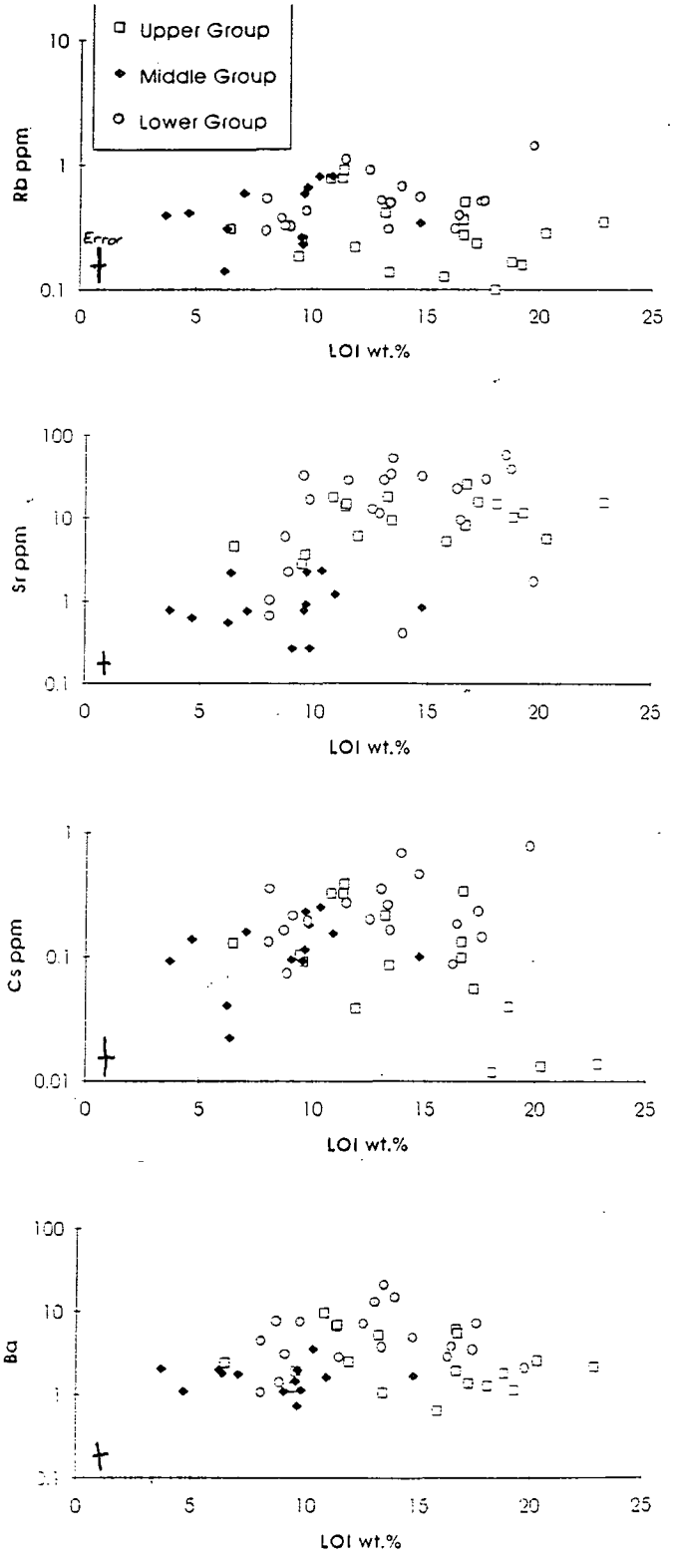


**Figure 5.5**. Rb, Sr, Cs and Ba versus LOI for Hole 779A with the samples divided into upper, middle and lower groups.

The variation of Sr in holes 778A, 780C, 783A and 784A is large but only correlates well with LOI in samples from hole 780C where Sr increases with increasing LOI. This is an interesting observation because the fluids from 780C are generally Sr depleted with respect to seawater because of the deep-seated fluid component (Mottl, 1992). The Sr enrichment in these samples may be caused by serpentinisation, but the Sr may have originated from the underlying slab. Sr in samples from hole 778A tends to decrease with increasing LOI although the scatter in the plot is large so it is possible that Sr may be leached during serpentinisation. Serpentinite muds which are not plotted on these diagrams consistently have very high Sr contents (>100 ppm). These muds also contain aragonite precipitated when seawater reacted with the serpentinising fluids (Fryer and Mottl, 1992). The aragonite tends to fix a large amount of Sr from the fluids

The plots of Rb, Sr, Cs and Ba versus LOI for peridotites from hole 779A show interesting variations. Rb, Sr, Cs and Ba contents of the middle group are similar over a large range of LOI (5-10 wt.%) and so their distribution is not affected by serpentinisation. Rb values for the upper and lower group are very similar to those from the middle group and do not show any consistent variation with LOI and hence degree of serpentinisation. Ba contents of the upper and middle group are generally higher (1-20 ppm) than that of the middle group (1-3 ppm) but are not correlated with LOI. Cs is very low in all the samples (< 1ppm). At high values of LOI (>17 wt.%) the Cs content drops off rapidly and so may be leached at high degrees of serpentinisation. The Sr distribution in the three groups has already been described above. Sr contents in the middle group are unaffected by serpentinisation. In the lower and upper groups there is a slight increase in Sr content with increasing LOI although there is considerable scatter in the data. Therefore, it is possible that some Sr is added to the samples from these groups during serpentinisation (probably from seawater) but the main variations in the Sr content of these groups is caused by some other process. Texturally the peridotites from the different groups are very similar so it is difficult to explain the variation in LILE contents by preferential addition to finer-grained peridotites (e.g., Menzies et al., 1987; Foley, 1992). The different LILE content of the three groups in hole 779A more probably represents variably LILE-enriched peridotites. Reconstruction of the bulk-rock Sr content of two of the peridotites from the ion-micropobe data found that there was excess Sr in the whole-rock, so some of the LILE (and LREE) may reside as grain-boundary films (e.g., Suzuki, 1987; Zindler and Jagoutz, 1988). Therefore, although these peridotites have been in contact with large amounts of fluid with high Sr contents the lack of suitable phases to take-up Sr

(and other incompatible elements with low ionic potential (see Pearce, 1983)) may inhibit the amount that these elements can be added to the peridotite minerals.

### 5.3.2 High Temperature Alteration

Amphibole and the high temperature serpentine mineral antigorite have been described in peridotites from Leg 125 (Chapter 3). Although low temperature serpentinisation dominates the alteration assemblages in most of the samples, some peridotites are predominantly altered to the high temperature alteration minerals. These peridotites were studied to see if any significant difference in their trace elements exist relative to samples which have just been altered at lower temperatures. Peridotites from hole 779A have large variations in their incompatible element contents. However, samples containing amphibole belong to both the high and low Sr groups described earlier in this chapter. Furthermore no peridotite seems to have significant differences in its trace element content irrespective of whether it contains amphibole or antigorite.

### 5.3.3 Further Evidence

Probably the most telling evidence that the trace element ratios studied are not affected significantly by serpentinisation is the good correspondence between the trace element patterns of the bulk rocks and fresh diopsides, as discussed subsequently. This line of evidence has been cited by Downes and Dupuy, (1987), Bodinier et al., (1990) and Menzies et al. (1992) in that the Nd isotope and REE concentrations of clinopyroxenes are good indicators of the whole-rock geochemistry. In summary the principal effect of serpentinisation for most elements is that of dilution. In all of the plots in this chapter, unless specified, the concentration of the elements are recast to an anhydrous basis.

## 5.4 Primary Geochemical Variations in the Leg 125 Peridotites

### 5.4.1 Introduction

In chapter 4 the petrology and mineral chemistry of the Leg 125 peridotites was shown to be compatible with the samples being residues to high degrees of partial melting. Furthermore trace element geochemistry of the clinopyroxenes indicated that there is some selective enrichment in incompatible elements. Other peridotite workers (e.g. Frey and Green, 1974; Stosch and Seck, 1980; Frey et al., 1985; Kempton, 1987) have shown that two princip types of variation occur in peridotite samples which are selectively enriched in incompatible elements. Firstly, variations exist between an indicator of the degree of partial melting such as MgO and elements which are only affected by partial melting such as Si, Al, Ca, first series transition elements and the HREE. Secondly elements like LREE, Sr etc. which are enriched increase in

concentration with increasing degree of depletion (Stosch and Seck, 1980). This variation is obviously not a partial melting effect as LREE, Sr etc are highly incompatible during mantle melting, but is related to some systematic enrichment process.

In the following sections elements are plotted against MgO. The elements are divided up into groups which should behave in a similar manner during partial melting and enrichment processes, principally on their bulk partition coefficient. MgO was chosen as indicator of partial melting instead of Mg# because the small variation in Mg# in these samples (91-93) is disturbed by serpentinisation such that many good correlations between an element and MgO are not shown in a plot of Mg# against the same element. Chapter 4 showed that the variation in modal mineralogy of the Leg 125 peridotites is quite small and that some variation in the olivine and orthopyroxene contents is caused by deformation processes. However, the small but perceivable variation in the Ti and Yb in the clinopyroxenes correlates posivitely with the amount of modal clinopyroxene, even if the amount of clinopyroxene varies between 2% and trace amounts. Although, some of the scatter in the plots presented below may be due to mineralogical effects, many of the trends defined in these plots are continuous with those of Frey et al. (1985) for more fertile peridotites (see later in this Chapter) and so are likely to represent variations caused by very high degrees of melting.

Some elements have very small variations in composition because of the very depleted nature of the peridotites and the small variations in degree of melting. Later in this chapter the Leg 125 data is plotted and compared with data from the Ronda massif (Frey et al., 1985) and the Ojen massif (unpublished) where the geochemical variations in the Leg 125 peridotites are put in the context of partial melting models.

### 5.4.2 Major Elements

Figure 5.6 presents plots of $SiO_2$, $Al_2O_3$, $Fe_2O_3$, MnO, CaO, $Na_2O$, $K_2O$ and $P_2O_5$ with MgO. Strong negative correlations exist between MgO and $SiO_2$, $Al_2O_3$ and CaO. It has already been shown that $SiO_2$ and MgO are affected by serpentinisation, but only at very high degrees of serpentinisation when $SiO_2$ is leached from the peridotites. The negative correlation between these elements is thought to reflect silica's incompatible behaviour during mantle melting. On the plot in Figure 5.6 the samples which are highly serpentinised plot at lower $SiO_2$ off the main trend. The Leg 125 peridotites have very low $Al_2O_3$ and CaO contents (generally less than 1 wt.%) consistent with being residues from high degrees of partial melting. Variation in the $Al_2O_3$ and CaO contents with MgO is thought to reflect variations in partial melting, albeit small

variations in high degrees of partial melting. Some samples from Hole 779A have slightly high $Al_2O_3$ for a given MgO content. Many of these samples are dunites. This aluminium enrichment is a primary feature and is not related to serpentinisation.

Total Fe as $Fe_2O_3$ increases very slightly with MgO although there is considerable scatter in the data. The distribution of $Fe_2O_3$ is affected at very high degrees of serpentinisation. These samples plot above the main trend on Figure 5.6. This plot indicates that iron has behaved slightly compatibly in the Leg 125 peridotites. The behaviour of iron during mantle melting is discussed later in this chapter. MnO shows very little variation with MgO which is compatible with its known behaviour during mantle melting when its has a bulk partition coefficient of approximately one.

The elements $Na_2O$, $K_2O$ and $P_2O_5$ all have very low concentrations in the peridotites, less than 0.8 wt.% for $Na_2O$, less than 0.1 wt.% for $K_2O$ and less than 0.03 wt.% for $P_2O_5$. There is no significant correlation with MgO or between these elements themselves. The extremely low concentrations of $K_2O$ and $P_2O_5$ are a reflection of their highly incompatible nature during mantle melting. As previously discussed some of the variation in $Na_2O$ can be explained by the effects of serpentinisation. All three elements are very close to the detection limit of the XRF which may explain the lack of correlation between these elements.

### 5.4.3 Compatible Transition Elements

The first series transition elements Ni, Cr and Co are known to be compatible with mantle minerals during mantle melting (Irving, 1978; Frey et al., 1985). Therefore their concentrations should increase in peridotites with increasing partial melting. Figure 5.7 shows plots of Ni, Cr, Co and Zn versus MgO. Ni has concentrations between 2000 and 3500 ppm and shows a strong positive correlation with MgO. Samples from Hole 778A however plot on a distinct trend with much higher Ni values for a given MgO content. Although some of these samples are very depleted (in Al and Ca) they are definitely harzburgites and not dunites. It could possibly be explained by a source difference between peridotites from hole 778A and the other holes. However, Ni usually plots very consistently with MgO (see Frey et al., 1985; later this chapter) and the difference in the Ni content of these peridotites is still a mystery. The analyses of Cr in peridotites (especially depleted ones) has always been

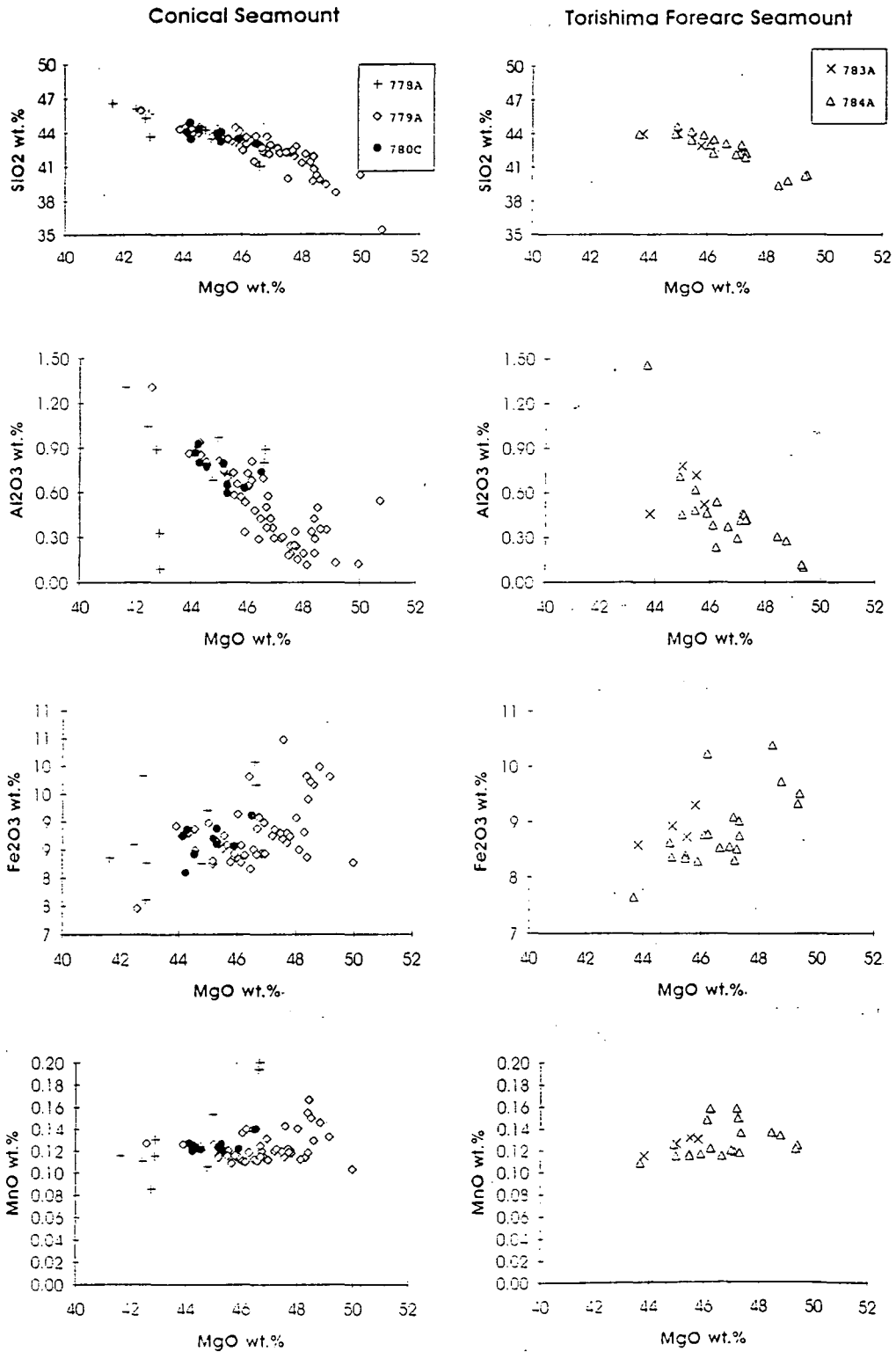


**Figure 5.6**. Plots of wt.% $SiO_2$, $Al_2O_3$, $Fe_2O_3$ and MnO against wt.%MgO for the Leg 125 peridotites.

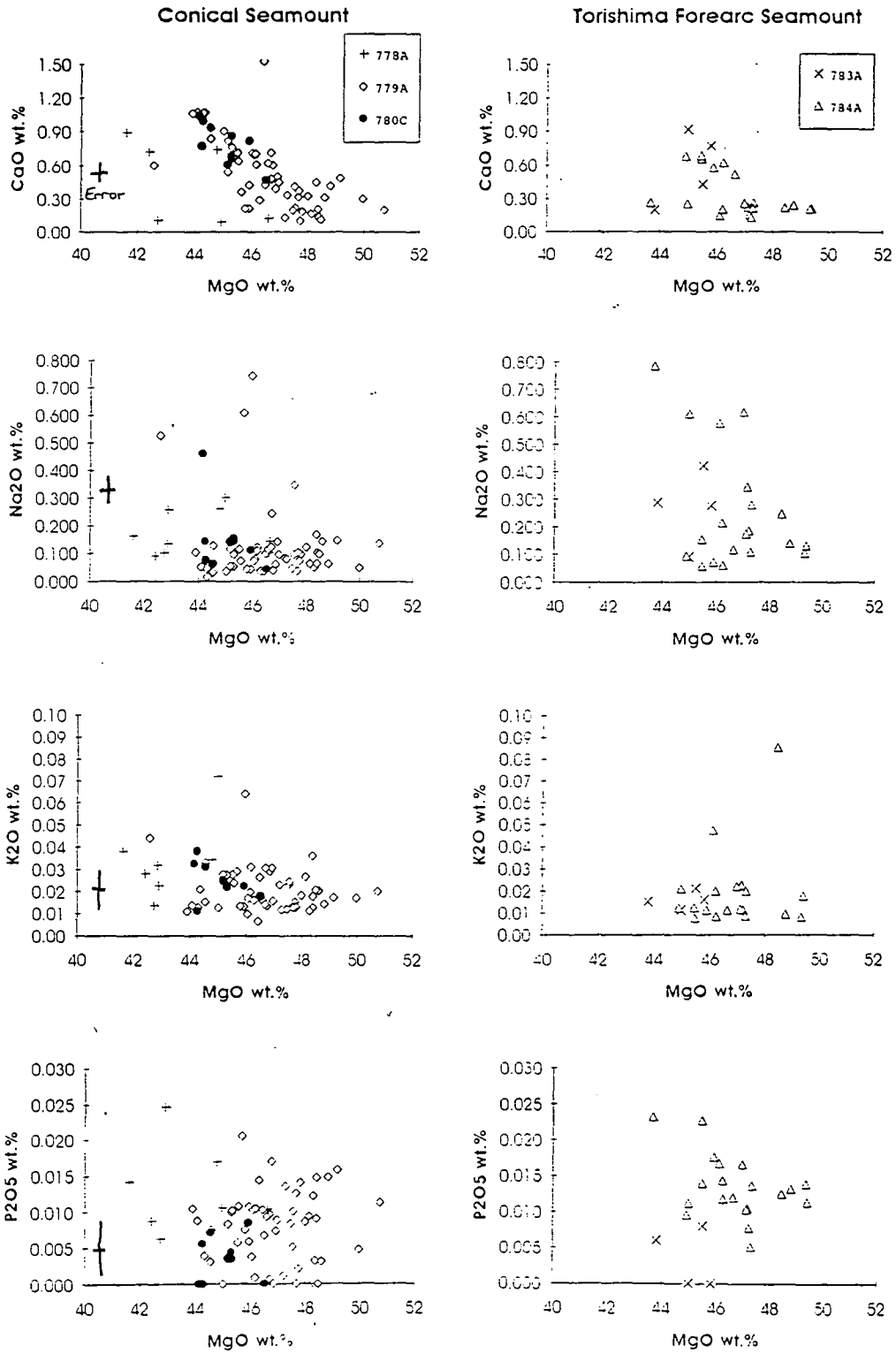


**Figure 5.6.** (cont.) Plots of wt.% CaO, $Na_2O$, $K_2O$ and $P_2O_5$ with wt.% MgO for the Leg 125 peridotites.

a problem (see Appendix A). As noted by several peridotite workers (e.g., Frey et al., 1985) it is often difficult to show a correlation of Cr with other elements even though we can predict the behaviour of Cr during mantle melting from experimental studies. For the Leg 125 peridotites there is considerable scatter on the Cr versus MgO plot. The author thinks the scatter occurs because of heterogeneous distribution of spinel relative to the sample size in agreement with other workers (e.g. Frey et al., 1985). This problem may be enhanced by the strong alignment of spinel during deformation. Co increases slightly with MgO although the correlation is not well defined. Co has concentrations of between 130 and 170 ppm (anhydrous basis). Again samples from hole 778A tend to plot at distinctly different concentrations than peridotites from the other holes. Here, they have higher Co contents for a given MgO content. The reason for this difference is not fully understood but could represent source differences between peridotites sampled in the different holes. Minerals from 778A peridotites often plotted on slightly different chemical trends than samples from the other holes (see Chapter 3) which may indicate some source difference.

Frey et al. (1985) have shown that Zn is a moderately incompatible element during mantle melting and gives a good negative correlation with MgO. In this study Zn behaves very differently. Concentrations range between 35 and 60 ppm. Although there is considerable scatter in the plots in Fig. 5.7, Zn definitely does not behave as an incompatible element in these peridotites and may behave compatibly as the Zn does not decrease with increasing MgO. Data from the Ojen massif also shows very little variation with increasing MgO content (see later this chapter). These samples varying from very fertile to depleted in composition. Although no sulphur analyses have been undertaken, Zn is a chalcophile-element and it is possible that Zn concentrations are buffered by a sulphur-bearing phase. This problem needs further study as reflected light studies for the Leg 125 peridotites have not found any significant sulphide phases.

### 5.4.4 Incompatible Transitional Elements

Sc, Ti, V and Cu are all first series transition elements which are incompatible during mantle melting. Figure 5.8 shows plots of Sc, Ti, V and Cu versus MgO. All four elements show negative correlations with MgO. Sc has concentrations ranging between 9 and 1.5 ppm in one of the dunite samples. There is considerable scatter in the data, especially for samples from Hole 779A. This is thought to be because of the small size of some of the samples, although this will not completely explain the poor correlation between these two elements. Ti has concentrations between 45 and 5 ppm.

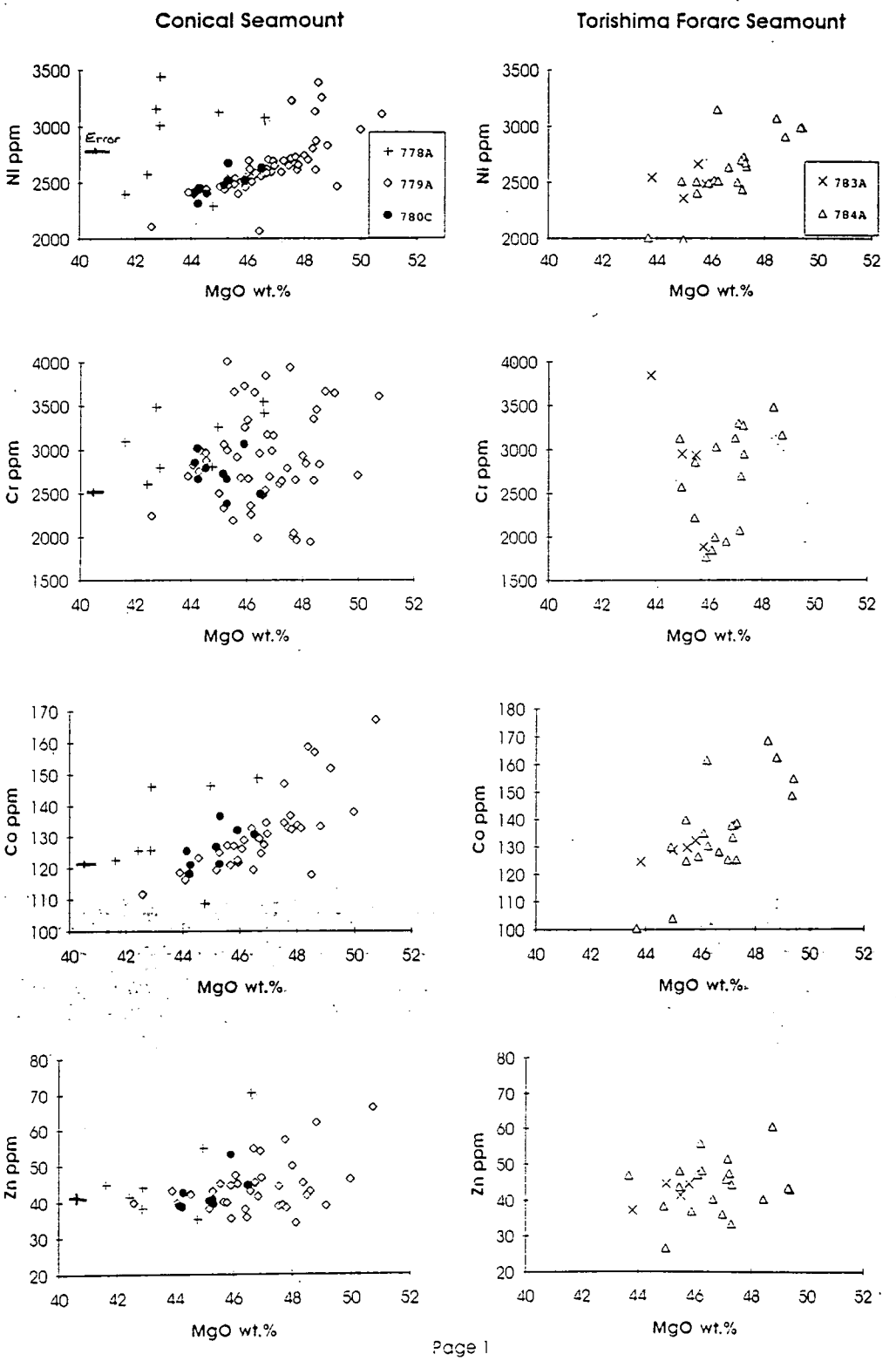




**Figure 5.7.** Plot of Ni, Cr, Co and Zn versus wt.% MgO for peridotites from Leg 125.

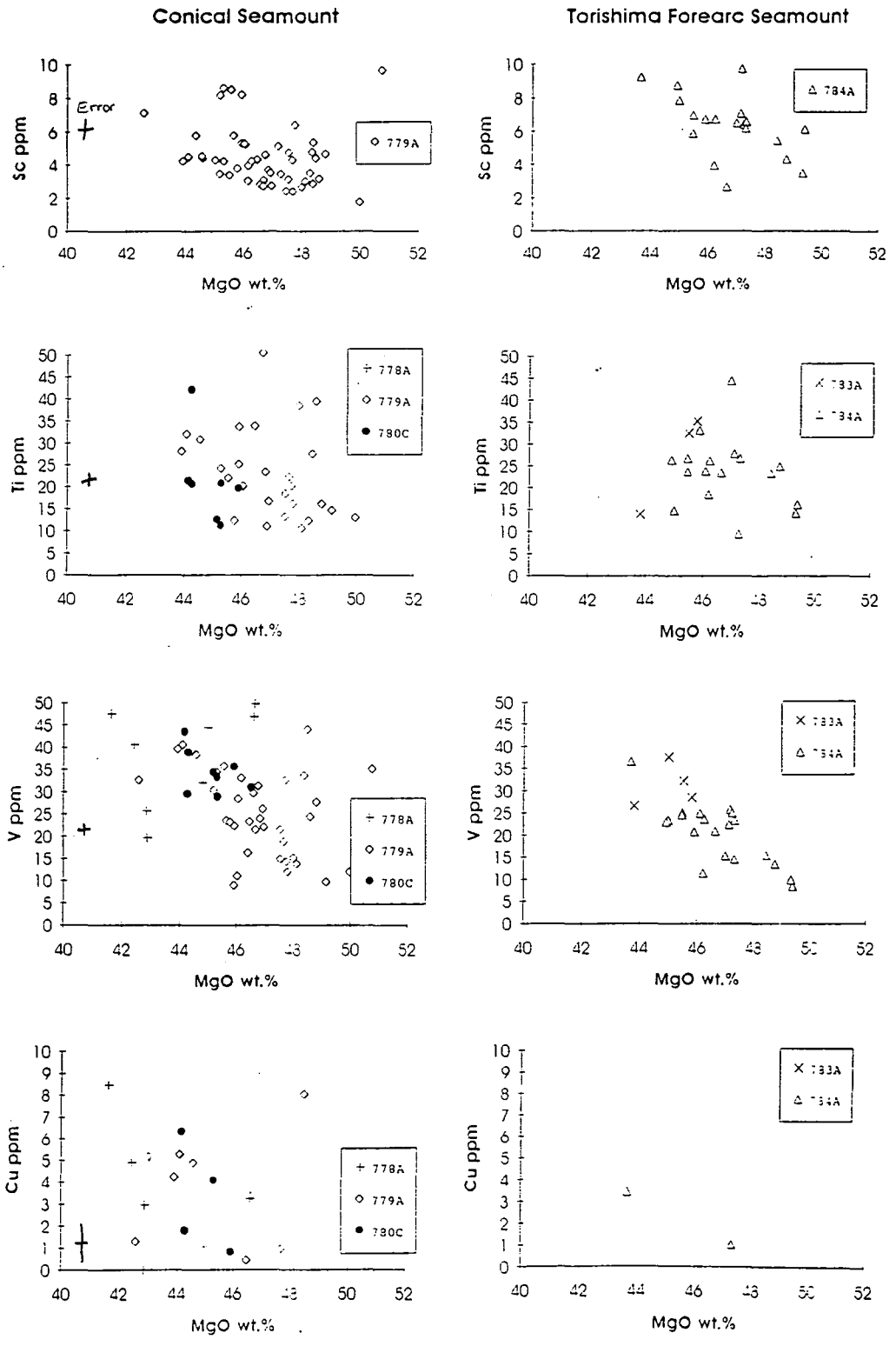


**Figure 5.8.** Plot of Sc, Ti, V and Cu versus wt.% MgO for peridotites from Leg 125.

These are some of the lowest Ti concentrations reported from peridotites. Again, because of the very low concentrations, the correlation between Ti and MgO is poor or absent. Some of the scatter in the data maybe caused because of the difficulty of dissolving Cr-spinel which may contribute 1-2 ppm Ti to the whole rock. V shows a better correlation with MgO decreasing with increasing MgO. Concentrations range between 45 and 5 ppm. Some of the lowest concentrations are in the dunite samples. As was previously discussed in Chapter 3, V may exist in three oxidation states in the mantle depending on the oxygen fugacity. The behaviour of V during mantle melting may vary depending on the oxidation state of the V. As will be discussed later, the scatter in the V data at such low concentrations is in part a reflection of the different melting histories of the peridotites and the degree to which the different samples have melted under different oxidation states. Cu has very low concentrations in these peridotites, generally less than 7 ppm. Many of the peridotite standards such as PCC-1 and DTS-1 have poor Cu determinations and so it is possible that the data is not very precise, especially at low levels. However, in the samples with MgO greater then 48%, Cu is below detection limit indicating that Cu behaves incompatibly in the mantle as suggested by Frey et al. (1985).

### 5.4.5 High Field Strength Elements

The high field strength elements (HFSE) Y, Zr and Nb have very low concentrations in the Leg 125 peridotites. ICP-MS analysis was used to try and analyse the peridotites for these elements. Recent spark source mass spectrometry determinations of Zr and Nb in the peridotite standards PCC-1 and DTS-1 by Jochum et al. (1990) greatly aided the analyses of these elements. Even so Nb was often below detection limit and Y was close to or below detection limit in many samples. In contrast, Zr was detectable in most samples. Y concentrations range between 0.01 and 1 ppm. Zr concentrations are between 0.02 and 0.8 ppm. Nb concentrations are less than 0.1 ppm and some of the samples prepared on the *Joides Resolution* in a tungsten carbide (WC) tema show evidence for Nb contamination. Samples with obvious contamination are excluded from plots involving Nb. Figure 5.9 shows plots of Y and Zr versus MgO. Again samples from Hole 779A are divided into three separate groups as described earlier.

Y does not correlate significantly with MgO. It should decrease with increasing MgO if behaving as an incompatible element, however this is not the case for the Leg 125 data. The paucity in a correlation between Y and MgO is because Y is very close to detection limit in these samples. If the distribution of Zr in the peridotites was controlled only by partial melting, then the concentration of Zr would be expected to decrease with increasing MgO. Clinopyroxenes from the Leg 125 peridotites are

significantly enriched in Zr, suggesting that Zr concentrations in the bulk-rock may also show enrichrichments. Zr is enriched in these samples but does not correlate with MgO values. Samples from the middle group of the hole generally have the lowest Zr contents. The other two groups are indistinguishable from each other on the basis of their Zr contents.

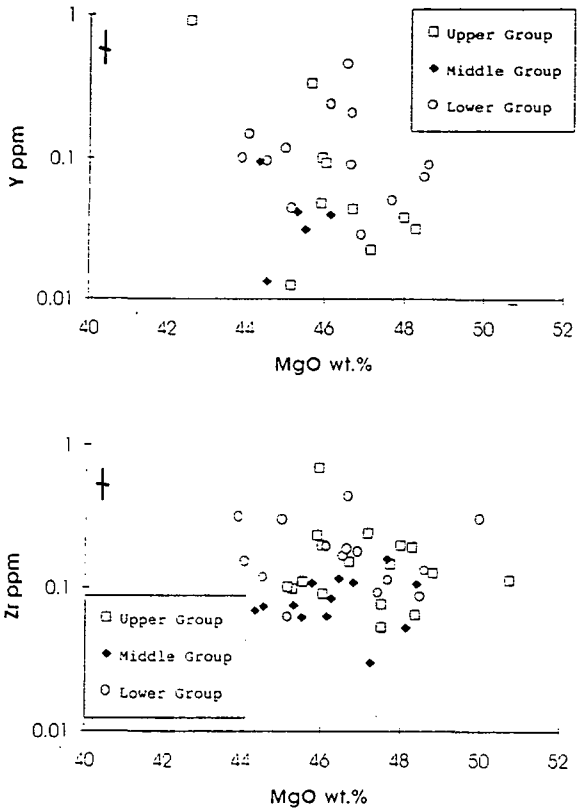


**Figure 5.9** Plots of Y and Zr versus wt.% MgO for peridotites from hole 779A. The samples are divided into an upper, middle and lower group (see text for details).

### 5.4.6 Large Ion Lithophile Elements

Rb, Sr, Cs and Ba have been determined by ICP-MS in many of the samples and Th and U in five samples by ID-MS at the Open University (analyst, Dr F. McDermott). The very depleted nature of the Leg 125 peridotites and the highly incompatible nature of these elements means that they should be at very low concentrations in the peridotites, if the peridotites are melting residues. However, Rb, Sr, Cs and Ba are readily determined in most of the samples and in some cases have higher concentrations than FMM. Thus, some process other than melting must have also operated on the peridotites. Although these elements are commonly thought to be mobile during alteration processes they are also important elements in subduction-zone related magmas so it is important to determine whether their distribution is related to purely alteration or to primary magmatic processes or a combination of both. Because some of the serpentinising fluids sampled from Conical Seamount may have a

component from the underlying subducting slab (Mottl, 1992) separating alteration from magmatic (fluid processes in the mantle wedge) processes is made more difficult. Frey and Green (1974), Stosch and Seck (1980), Kempton (1987) and Bodinier et al. (1989) have all shown that peridotites that are the most depleted in basaltic components are often the most enriched in incompatible elements. Downes et al., (1992) havealso shown that a relationship can also exist between the trace element enrichment and texture of the peridotite samples. In order to separate the different possible origins of the LILE enrichments, it is necessary to study in detail the petrography of the samples in addition to their geochemistry.

The effects of serpentinisation on the distribution of the LILEs have already been discussed in Section 5.3.1.2. With the exception of Sr and Cs serpentinisation cannot be demonstrated to effect the distribution of Rb and Ba and in some cases Sr and Cs. Figure 5.10 shows a plot of Rb, Sr, Cs and Ba against MgO. No significant correlations exist between these variables except for a positive correlation between Sr and MgO for data in the central group, where Sr increases with increasing MgO.

Th and U concentrations in the Leg 125 peridotites are extremely low. Th concentrations vary between 0.55 and 2.43 ppb and U concentrations between 0.39 and 1 ppb. Th/U is quite variable (1.1 to 5.1) and differs from published Th/U ratios in peridotites which are usually less than unity (Jochum et al., 1989).

### 5.4.7 Rare Earth Elements

Five full REE analysis were undertaken by ID-MS at RHBNC radiogenic isotope laboratories. Also analyses of La and Yb were also undertaken on Leg 125 peridotites by ICP-MS at Durham, as their values can exceed the detection limits of the machine. Full details of analytical techniques are provided in Appendix A.

Chondrite-normalised REE patterns for the three harzburgites from Conical Seamount and the harzburgite and dunite from Torishima Seamount are presented in Figure 5.11 using the normalising values of Boynton (1984) (see Appendix B). All the patterns define a pronounced U shape, with LREE having values between 0.01 and 1.6 times chondrite, MREE values between 0.005 and 0.01 times chondrite and HREE values between 0.02 and 0.08 times chondrite. Two of the harzburgites show positive Eu anomalies of 1.7 and 2.6 respectively. Although the peridotites have very low Eu concentrations, these anomalies exceed analytical error. It should also be noted, however, that there was difficulty in reproducing Eu values for the standard PCC-1 (see Appendix A). The samples from Conical Seamount have higher La concentrations

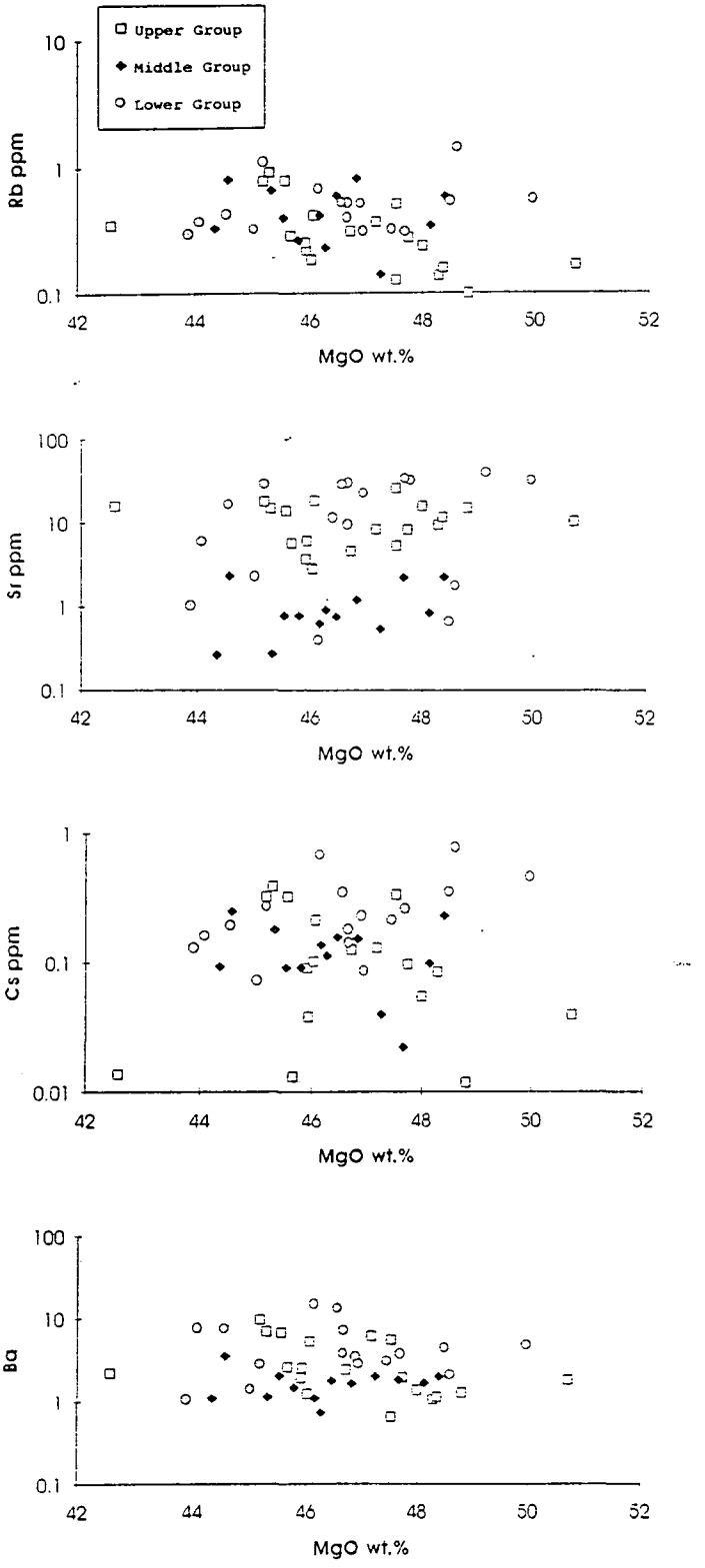


**Figure 5.10** Plot of Rb, Sr, Cs and Ba against MgO for samples from hole 779A.

but lower Ce and Nd concentrations then those from Torishima Forearc Seamount. Sm concentrations are similar in all five of the samples. Also common to all of the samples is a trend of progressive depletion from the HREE's to the MREE's on the chondrite-normalised patterns.

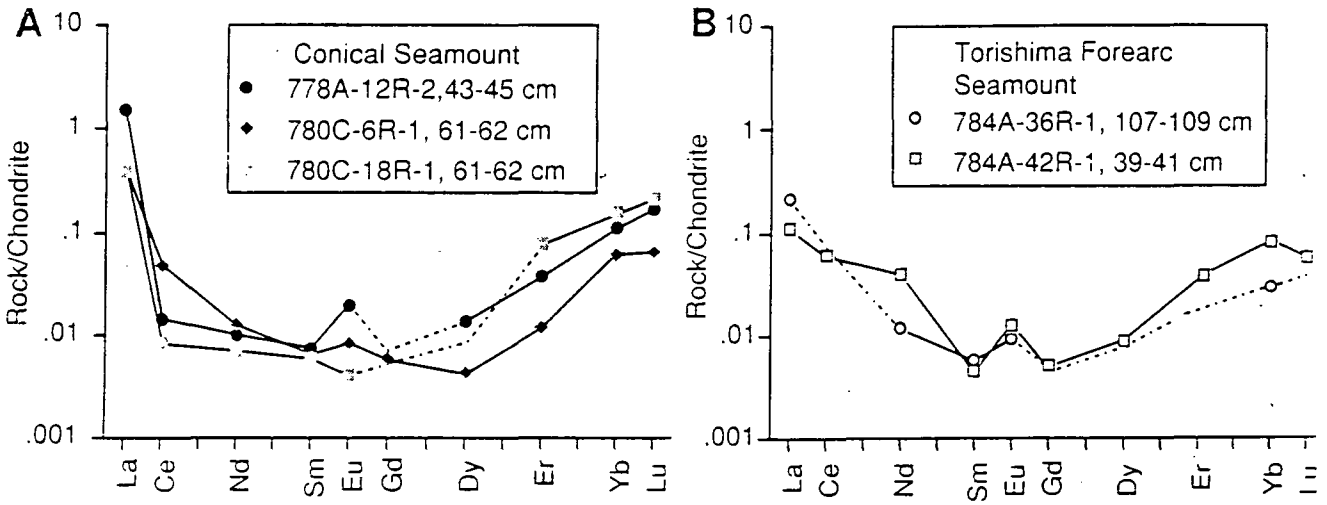


**Figure 5.11**. Chondrite-normalised REE patterns for peridotite from a) Conical Seamount and b) Torishima Forearc Seamount

## 5.5 Petrogenesis

### 5.5.1 Introduction

The previous section has shown that the Leg 125 peridotites have very low incompatible element and high compatible element concentrations, indicating that the peridotites are residues to high degrees of partial melting. However, the peridotites are also enriched in selective incompatible trace elements. It is important, then, to estimate the degree of partial melting the peridotites have undergone, the nature, extent and timing of the trace element enrichments and the types of melts the peridotites could have generated. In Chapter 4 the trace element content of clinopyroxenes was used with success to estimate both the degree of partial melting undergone by the peridotites and important information about the nature, extent and timing of the trace element enrichments. In principle, similar calculations can be undertaken with the bulk-rock data, although the very altered nature of many of the samples means that some elements have to be used judiciously. Similar calculations to those in Chapter 4 are performed for the bulk-rock data to see if the bulk-rock chemistry gave results consistent with those calculated from the clinopyroxene trace element data.

### 5.5.2 Estimates of Degree of Partial Melting in the Leg 125 Peridotites

#### 5.5.2.1 Major Elements

The concentrations of the compatible and incompatible elements not affected by enrichment processes can be used to estimate the degree of partial melting in the peridotites. To help with estimating the degree of partial melting, peridotite analyses from the Ronda massif (Frey et al., 1985) and the Ojen massif (unpublished, see Appendix) are also plotted with the Leg 125 data. Peridotites from the two Spanish massifs have a wide compositional range from fertile garnet lherzolites with the composition of FMM to depleted spinel harzburgites. Unfortunately, there are a limited number of studies which have published the bulk-rock geochemistry of abyssal peridotites (Aumento, 1969: 1970; Shibata and Thompson, 1985) and many of these samples are heavily serpentinised. It is possible that some of the peridotites from Ronda and Ojen could have interacted with melts and continental lithospheric fluids (van der Wal, 1993). While such interaction could affect the incompatible element contents of these peridotites, their melting trends can still be used to provide a useful comparison to the Leg 125 peridotite trends.

The concentration of $SiO_2$, $Al_2O_3$, $Fe_2O_3$, MnO and CaO against MgO are presented in Figure 5.12. These plots are used to provide information about the amount of partial melting undergone by the peridotites, and by using the parameters for partial melting described in Chapter 3, the composition of residues from the fractional melting process have been superimposed on the diagrams. Some of the covariation plots presented earlier in this chapter show considerable scatter for elements that are expected to behave coherently together during partial melting. One of the possible reasons for this scatter is that the modal mineralogy is produced simply by deformation, such that the geochemical variations are controlled by mixing orthopyroxene- and olivine-rich peridotite. To test for this effect, orthopyroxene with a composition of $En_{92}$ and olivine with a composition of $Fo_{92}$ (these are the average composition of orthopyroxene and olivine in the Leg 125 peridotites) are plotted on the diagrams. If the geochemical trends are due to the heterogeneous distribution of these minerals then the data should plot on a mixing line between the two end-member mineral compositions. Serpentinisation and the presence of small quantities of clinopyroxene and spinel in the peridotites may displace the compositions away from the mixing trends. For plots of $SiO_2$ and $Fe_2O_3$ (tot.) the peridotites lie away from the mixing lines. However, for some of the very high MgO (>47 wt.%) samples, $Al_2O_3$ and CaO do lie on the mixing lines. Some of the peridotites might not, therefore, directly represent melting residues. Rather, these samples represent residues which have undergone a subsequent episode

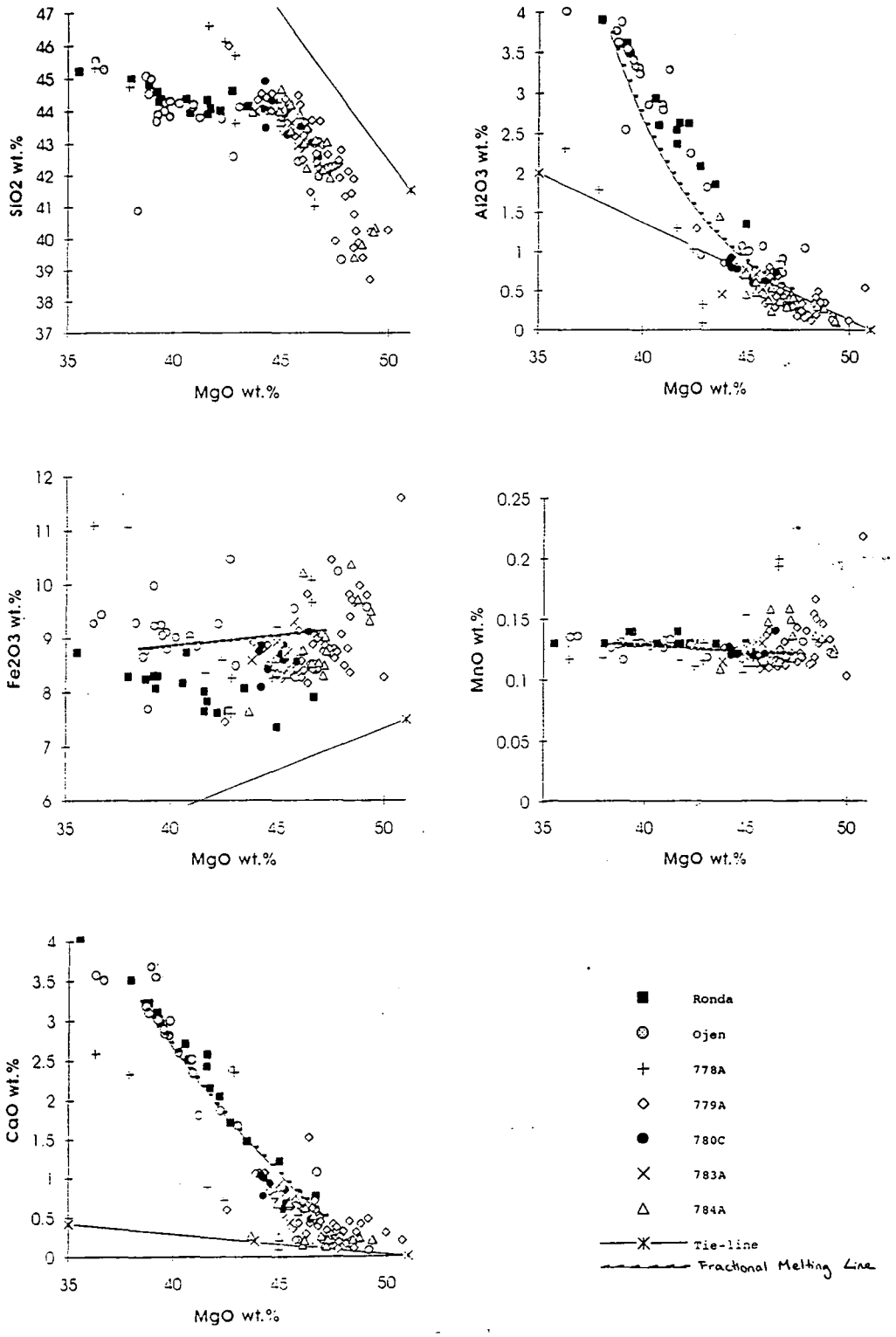


**Figure 5.12.** Plots of $SiO_2$, $Al_2O_3$, $Fe_2O_3$, MnO and CaO against MgO for Leg 125 peridotites. Also data from Ronda (Frey et al., 1985) and the Ojen massif (this study). Composition of residues from fractional melting using the modelling procedures of Chapter 3 is also shown and a tie-line between the composition of $En_{92}$ and $Fo_{92}$.

The melting residues are calculated for melting in the spinel peridotite field using a DMM initial composition and the mineralogy, melting coefficients and mineral/melt partition coefficients specified in Chapter 3 for the spinel field.

of deformation which has led to redistribution of the olivine and orthopyroxene (see section 4.1).

On Figure 5.12 it can be seen that the concentrations of $Al_2O_3$, MnO and CaO in the peridotites are readily explained by ~25% partial melting of a FMM source. This is consistent with estimates of partial melting from the concentration of Ti and Yb in clinopyroxenes (Chapter 4). The reason for displacement of $SiO_2$ and $Fe_2O_3$ off the tie-line is less clear. $SiO_2$ decreases slightly with increasing MgO in the Ronda and Ojen data indicating it is incompatible during mantle melting. However, $SiO_2$ in Leg 125 peridotites decreases more rapidly with increasing MgO. This change in the behaviour of $SiO_2$ during melting indicates that a different type of melting may have influenced these peridotites, at least at high degrees of melting. Textural evidence for the incongruent melting of orthopyroxene in the Leg 125 peridotites was provided in Chapter 4. This melting reaction involves the breakdown of a silica-rich mineral ($SiO_2$ in $En_{92}$ ~56 wt.%) to produce a silica-poor mineral ($SiO_2$ in $Fo_{92}$ ~41 wt.%) and a silica-rich melt. The effect of this process is to decrease $SiO_2$ in the bulk peridotite more rapidly than by normal "dry" mantle melting. The liquids that would be produced by incongruent orthopyroxene melting of a depleted mantle source are low-Ca boninites (van der Laan et al., 1989). It could be argued that the decrease in $SiO_2$ is because of leaching during serpentinisation. However, the samples which have been leached of $SiO_2$ plot offthe main trend defined by the Leg 125 data (see Figure 5.12) at much lower $SiO_2$ concentrations.

$Fe_2O_3$ (tot) increases slightly with increasing MgO in the Leg 125 peridotites although there is considerable scatter in the data. This is in contrast to the Ronda peridotites where total iron decreases with increasing MgO. The distribution of Fe between mantle minerals and melt is strongly controlled by both temperature and oxygen fugacity (Roeder and Emslie, 1970; Hanson and Langmuir, 1978). Pearce and Parkinson (in press) have shown that the bulk-partition coeffecient of total Fe in a spinel peridotite is 0.90 at 1300°C and 1.12 at 1200°C. Thus, Fe will increase slightly in the residue with increasing partial melting at low temperatures. Furthermore, the behaviour of Fe during mantle melting is also pressure dependent; Fe behaves more incompatibly at higher pressures (Klein and Langmuir, 1987; Elliot et al., 1991). As with the trends defined by silica against MgO, the compatible behaviour of iron only applies at high MgO contents.

The $SiO_2$ and $Fe_2O_3$ concentrations in the Leg 125 peridotites suggest that the peridotites have undergone a two stage melting history. It has already been argued on

textural grounds (chapter 4) that the peridotites have petrographic features compatible with a high temperature deformation (and presumably melting) event below a mid-ocean spreading centre and a melting and deformation event in a water-rich environment. From the plots in Figure 5.12, a melting history for the peridotites would be 15-20% melting below a spreading ridge where clinopyroxene dominated the melting mode followed by ~5% melting in the forearc under water-undersaturated conditions where incongruent melting of orthopyroxene was the important process.* From the mineral chemistry described in Chapter 4 the melting in the forearc took place under high oxygen fugacities (>FMQ+1) which is compatible with high water activities.

### 5.5.2.2 Transition Elements

Plots of the first series transition elements Sc, Ti, V, Ni, Co and Zn against MgO are shown in Figure 5.13. Data from the Ronda and Ojen massifs are again plotted, together with the calculated fractional melting trends. The Leg 125 data plots at the end of the melting trends on the Sc, Ti, V, Ni and Co plots. Again the peridotite data represents residues to ~25% partial melting.

Clinopyroxenes from Leg 125 peridotites indicate that the peridotites have experienced a two stage melting history. During the second stage melting, the peridotites melted at high oxygen fugacities so that some tetravalent V became stable, leading to a clinopyroxene/melt partition coeffecient for V of less than one. Although, from Figure 5.13 it is obvious that V is incompatible during mantle melting it might be anticipated that the V in the Leg 125 peridotites would lie off the main melting trend defined by the Ojen and Ronda data because of the high oxygen fugacities during the later part of its melting history. However, the Leg 125 data plots on a continuation of the main melting trend. Samples from Torishima Forearc Seamount melted under higher oxygen fugacities than samples from Conical Seamount, but there is no difference between the two seamounts in the V data. Although the clinopyroxene data highlights the difference in the oxygen fugacity between the seamounts, the change in behaviour of V with respect to clinopyroxene does not change the bulk-partition coeffecient of V by an amount sufficient to deflect the V data from the melting trend.

*The bulk-rock SiO2 and the V content of the clinopyroxene of the Leg 125 peridotites both indicate that they have undergone a two stage melting history. Estimates of the amount of melting in the two different stages of melting vary slightly depending on which element is used. Modelling of both elements is achieved by varying amounts of fractional melting in the spinel peridotite field. Estimates of the amount of melting in each stage using the V data are difficult to constrain because the partition coefficient of V varies with the oxygen fugacity. However, it can be concluded that most of the peridotites have experienced 25% total partial melting of which approximately 15% occurred in the first stage and approximately 5-10% in the second stage during which the incongruent melting of orthopyroxene was important.

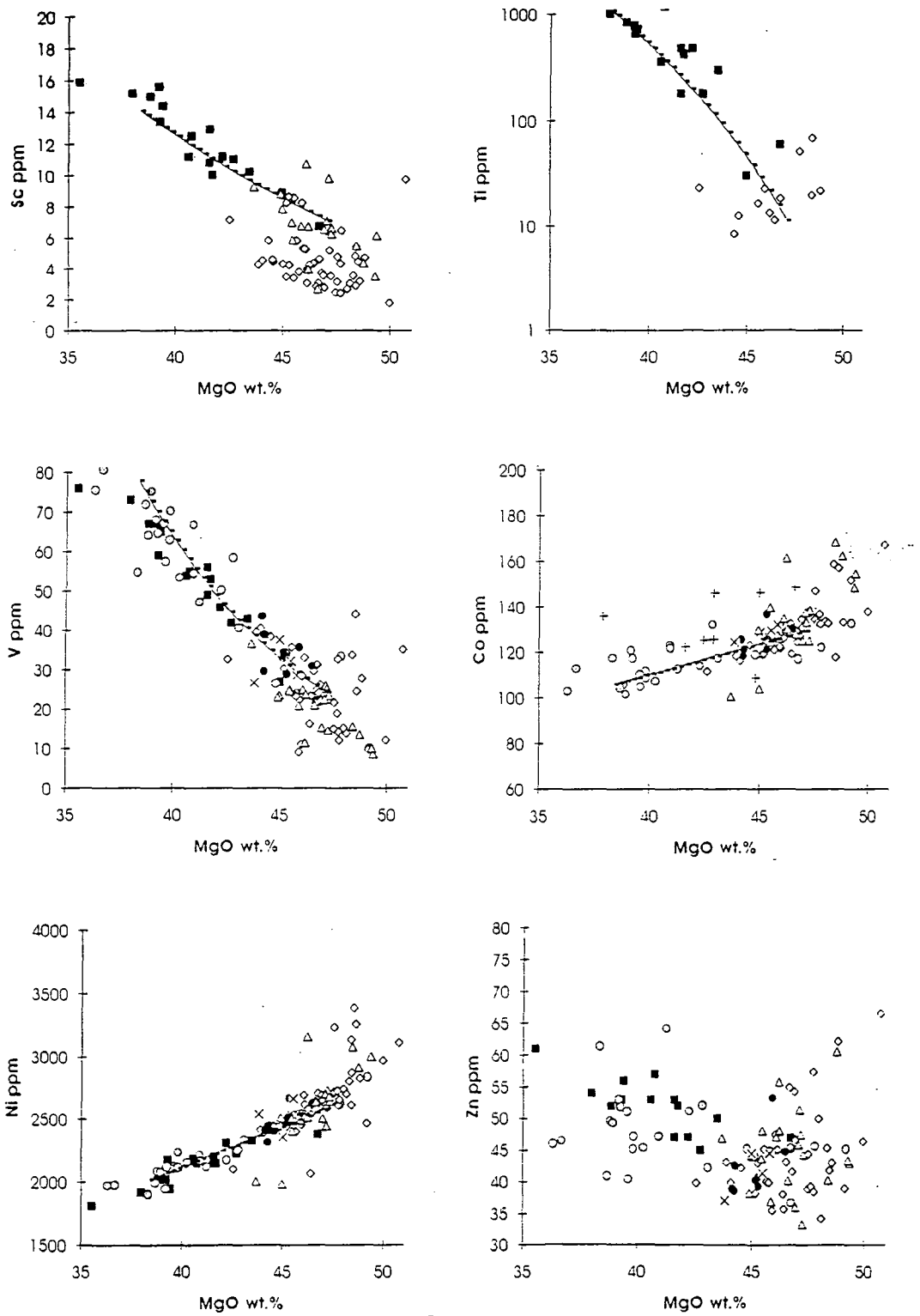


**Figure 5.13.** Plots of Sc, Ti, Co, Ni, V, Zn against wt.% MgO for Leg 125, Ojen and Ronda peridotites. Again the composition of fractional melting residues are plotted.

## 5.6 Petrogenesis of Bulk-Rock Peridotites from Trace Element Data

### 5.6.1 Trace Element Enrichment Patterns

Extended chondrite-normalised diagrams have been used extensively to study the trace-element characteristics of both bulk-rock peridotites and their clinopyroxenes (e.g. Salters and Shimizu, 1988; Salters, 1989). Incompatible elements such as Sr, Zr and Ti are plotted at appropriate points on the patterns so that there is a smooth decrease in incompatibility in the system peridotite-melt from right to left. Conventionally, Sr is plotted between Ce and Nd, Zr between Nd and Sm, and Ti between Gd and Dy. As all the elements were not analysed, abbreviated patterns are presented here, in a form similar to those of McDonough (1991). One problem in constructing these plots is the general inconsistency between the chondrite values for REE's and the values quoted for alkali, alkaline earth and high field strength elements. This may be in part analytical and in part result from the different behaviour of these elements in the fractionation and evolution of the Earth. In consequence, present-day MORB and MORB mantle do not give smooth patterns when published normalising values are used. Normalising values for Rb, Sr, Y, Zr, Nb and Ti were therefore adjusted so that an average N-MORB (from Sun and McDonough, 1989) plots as a smooth pattern on the diagram. Analysis of fertile garnet-lherzolites from the Ojen massif have Rb, Sr, Y, Zr, Nb and Ti contents compatible with the adjusted chondrite-normalising values. Extended chondrite-normalised patterns for five peridotites from Conical and Torishima Seamount are shown in Figure 5.14.

It is apparent from Figure 5.14 that the peridotites from Conical Seamount Zr and Ti have positive anomalies with respect to their adjacent REE's and two of the samples give large positive anomalies in Sr. For Torishima Forearc Seamount, both samples give positive anomalies for Ti and Sr, but no Zr anomaly is apparent. Y gives no anomaly, as would be expected from its similar charge and radius to the adjacent REE's. Rb also shows no anomaly with respect to La.

### 5.6.2 Adjusted Extended Chondrite-Normalised Patterns

It is important to note that anomalies in Zr, Ti and Sr can be created on the type of extended chondrite-normalised pattern described above by partial melting alone. Fig 5.15a shows some synthetic extended chondrite-normalised patterns for varying degrees of partial melting. The patterns are for fractional melting with clinopyroxene disappearing at 25% and using the mineral/liquid partition values from chapter 3. It can be seen that positive Zr and Ti anomalies are developed as the degree of partial melting increases. Sr also gives a positive anomaly at very high degrees of melting. The reason

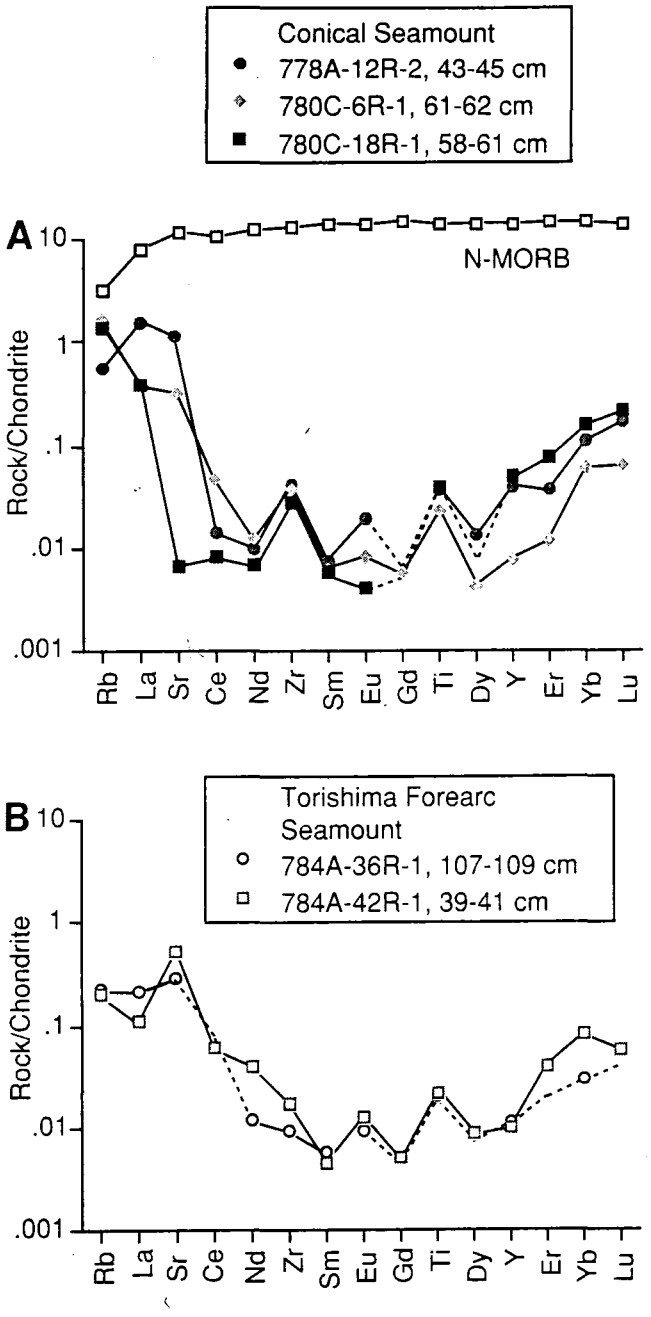


**Figure 5.14** Chondrite-normalised extended REE patterns of peridotite samples from **(A)** Conical Seamount and **(B)** Torishima Forearc Seamount. Element ordering is for a fertile peridotite. The pattern for N-MORB is from Sun and McDonough (1989).

for the positive Zr and Ti anomalies is that the melting residues have increasing orthopyroxene/clinopyroxene ratios with increasing partial melting. In very depleted residues (>20% partial melting) the orthopyroxene/clinopyroxene ratios are typically 20-40 and orthopyroxene is the main host for the incompatible trace elements. Rampone et al., 1991 and McDonough and Stosch, 1992 have recently shown that orthopyroxenes from peridotites have large positive Zr and Ti anomalies, hence in

depleted peridotites the trace element content of orthopyroxenes has a profound effect on the trace element pattern of the bulk-rock peridotite.

To determine an order for the elements that will be independent of the degree of partial melting, and hence enable us to view trace element enrichments of the mantle source, I plotted the variations in the bulk partition coefficients for residues of melting of a MORB source as a function of degree of partial melting (Fig 5.15b). It is apparent that the REE's behave coherently during partial melting, plotting as sub-parallel lines. By contrast, Sr, Zr and Ti form trends that cross the REE lines, indicating that their similarity to a given REE depends on the degree of melting. Although it can be argued that the precise behaviour of these elements will depend on the point of disappearance of clinopyroxene and the partition coefficients chosen, all three elements must experience a shift in behaviour toward the heavier REE's as partial melting proceeds. Thus, although the ordering used by Salters and Shimizu (1988) is correct for fertile peridotites, the order must be changed when plotting depleted peridotites such as the Leg 125 ones. Estimates of the degree of partial melting that the Leg 125 peridotites

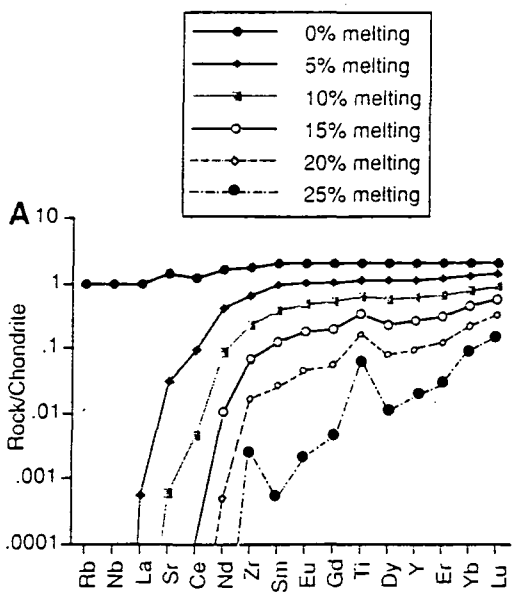

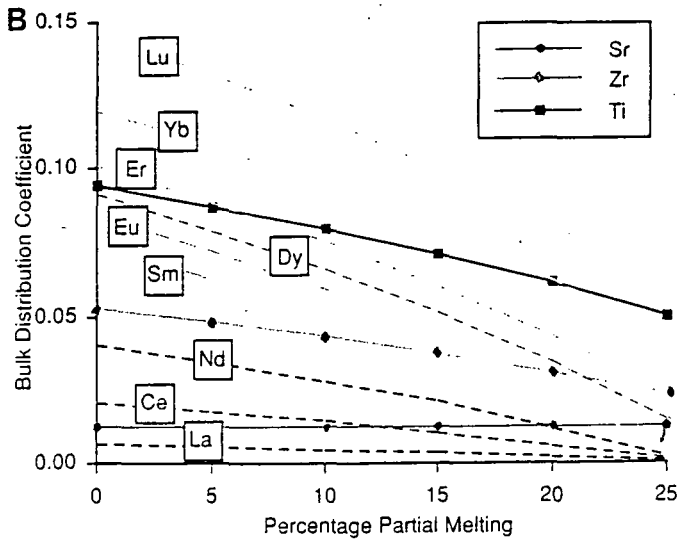


**Figure 5.15** (A) Chondrite-normalised extended REE patterns of modelled peridotites after 0-25% partial melting. Zr and Ti positive anomalies are produced with increasing degree of partial melting. Sr shows a similar positive anomaly at 20-25% partial melting, but is not shown for clarity. (B) Plot of bulk distribution coefficients against percentage of partial melting for REE, Sr, Zr and Ti. The REE behave coherently, whereas Sr, Zr and Ti cross the REE lines with increasing percentage partial melting. Modelling parameters are described in Chapter 3.

have experienced is 20-25% based on the clinopyroxene and bulk-rock data. According to figure 5.15b then, Zr should be plotted between Eu and Gd, Ti should be plotted between Er and Yb and Sr should be plotted between Nd and Sm. However, in changing the order of the elements there are two caveats to consider. Firstly, varying the order of the elements may cause confusion; a rule of thumb would be to plot more fertile peridotites on the normally ordered plots and plot only very depleted harzburgites with the ordering suggested above. Secondly, the new ordering is based purely on the effects of partial melting and relies on the particular behaviour of the elements during melting in the spinel peridotite field. It should be noted that more complicated interaction models such as Kelemen et al. (1992) also produce increases in Zr and Ti relative to their surrounding REE in the bulk-rock peridotite.

Figure 5.16 plots the same five samples as Figure 5.14 on extended chondrite-normalised diagram but with the element order suggested above. Again Sr positive anomalies exist in four of the samples although the size of the anomalies tend to be larger in some samples. However Zr and Ti are markedly affected by the new plot order. Zr now shows positive anomalies in all the samples whereas Ti shows no positive anomalies at all and in some samples gives a negative anomaly. On such a extended chondrite-normalised pattern an unenriched abyssal peridotite would

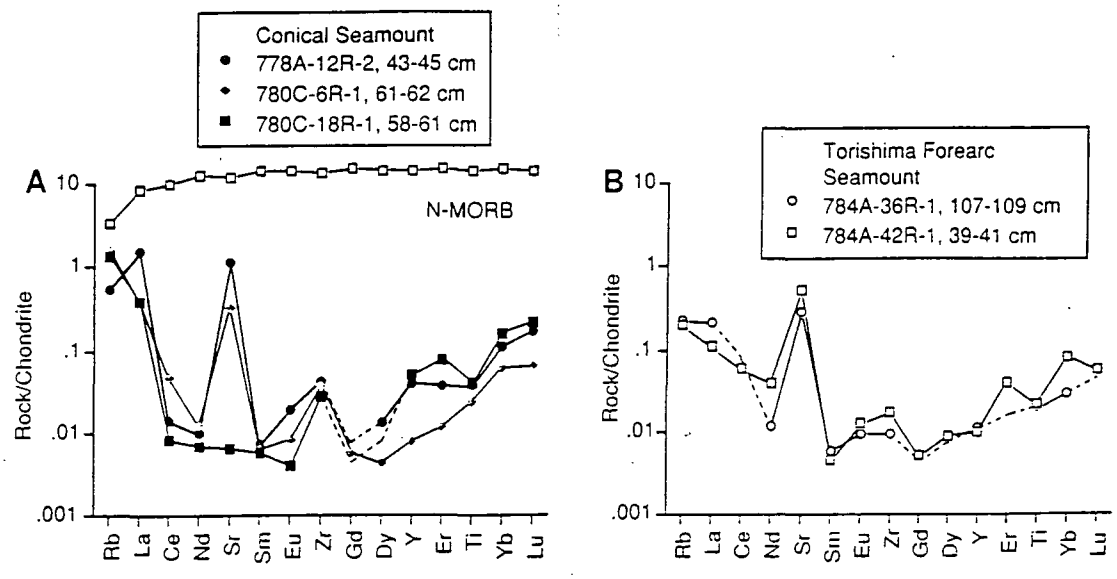


**Figure 5.16** (A) Chondrite-normalised extended REE patterns of peridotites from (A) Conical Seamount and (B) Torishima Forearc Seamount. Element ordering is for a harzburgite mantle. The pattern for N-MORB is from Sun and McDonough (1989).

decrease constantly from the HREE to Rb. From the patterns for the Leg 125 samples and some of plots shown earlier in this chapter a first-order interpretation of the bulk-rock peridotites is that they have been enriched in LREE, Rb, Sr, Zr, Cs, Ba and Eu relative to the MREE and HREE.

### 5.6.3 Nature and Timing of Trace Element Enrichments

The methodology for estimating the extent of the trace element enrichments in the peridotites has been explained previously (Chapter 4). Essentially it is necessary to estimate the composition of the peridotite if it had not been enriched to the observed composition. The pre-enrichment composition can be determined by either choosing an unenriched sample with similar modal composition or calculating the theoretical composition of residues during partial melting. In contrast to the available data for the trace element content of abyssal peridotite clinopyroxenes (e.g. Johnson et al., 1990; Johnson and Dick, 1992), very little data exists for the bulk-rock trace element composition of abyssal peridotites. This is especially true for elements like Zr, Y, Nb and Ti in depleted abyssal peridotites. In the following section data from the Ronda and Ojen massifs are used to compare the extent of trace element enrichment.

### 5.6.4 Extent of Trace Element Enrichment

The extent of trace element enrichment has been assessed by plotting a series of elements against an element thought not to be affected by the enrichment process. As with the plots in section 5.6.1, MgO is used as an indicator of degree of partial melting and is thought not to be affected by enrichment processes. Rb, Sr, Y, Zr, Cs, Ba, La, Ce and Nd are plotted against MgO (Figure 5.17). These plots show that all these elements are enriched in the peridotites relative to calculated fractional melting compositions.* The Leg 125 peridotites are also enriched in Rb, Sr, Cs, Ba, La, Ce and Nd relative to the Ronda and Ojen peridotites. However, the Ojen peridotites plot at higher Rb, Sr, Y, Zr, Cs and Ba than the calculated fractional melting trends and are definitely more Zr enriched than the Leg 125 peridotites for the spinel harzburgite samples. Unfortunately, the lack of published low-level Zr determinations in depleted peridotites makes it difficult to assess how unusual the Zr and Y contents of the Ojen peridotites are. Recent analyses of a large number of depleted peridotites from a variety of tectonic settings on the ICP-MS at Durham, indicate that Zr and Y concentrations in peridotites are highly variable and these two elements (and Nb) do not always behave together in a coherent fashion (J. A. Pearce, pers. comm.). Until a comprehensive study of HFSE, REE and LILE concentrations in peridotites from various tectonic settings (especially abyssal peridotites) is carried out the distribution of Zr and Y in the Ojen peridotites is difficult to explain.

There is considerable scatter in the plots in Figure 5.17 and no significant correlations exist between MgO and the trace element enrichments. However, it is still apparent that the degree of enrichment in the Leg 125 peridotites increases in the order Eu, Sm, Nd, Zr, Ce, Rb, La, Sr, Ba and Cs. The trace element-MgO plots also allow the timing of the enrichments to be constrained. The enrichment episode is explained most simply in terms of enrichment during and after melting. A similar conclusion was reached from the clinopyroxene trace element data (see chapter 4).

Because many of the trace elements are enriched in the Ojen peridotites as well as the Leg 125 peridotites, to quantitatively assess the amount of trace element enrichment in the peridotites it was necessary to undertake calculations using modelled fractional melting trends. Essentially, the concentration of the various trace elements was calculated during fractional melting. The concentrations calculated are then used as an estimate of the pre-enriched composition of the peridotites. Figure 5.18a contrasts the trace element pattern of a typical Leg 125 peridotite and the modelled composition of the peridotite. The relative amount of trace element enrichment is calculated by

***It should be noted that although all these elements are enriched relative to the calculated fractional melting compositions, that some of the enrichments are related to secondary processes. Y, Zr, La, Ce and Nd are related to primary enrichments whereas Rb, Sr, Cs and Ba are more likely related to secondary processes such as serpentinisation.**

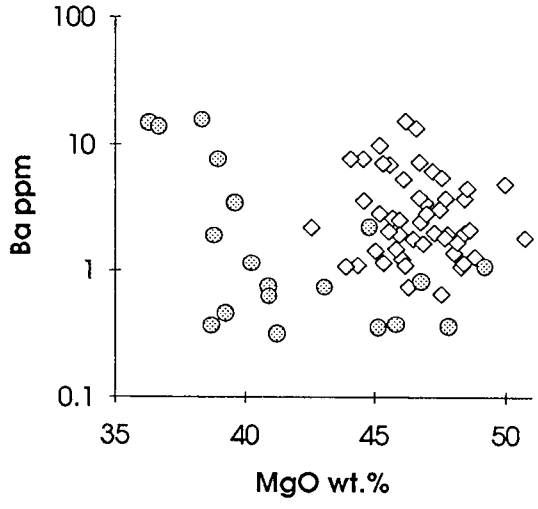
100
10
1
0.1
Ba ppm
35
40
45
50
MgO wt.%

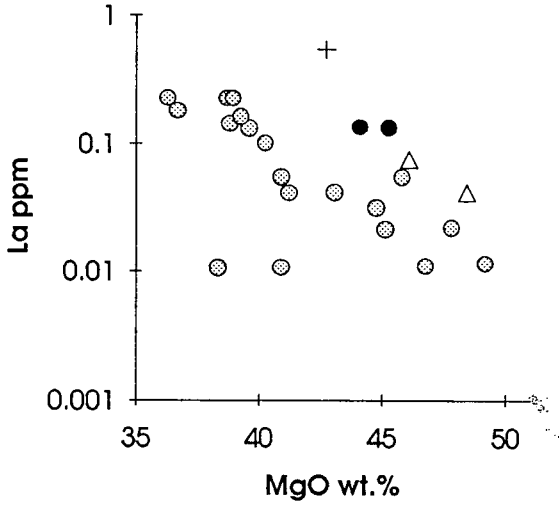
1
0.1
0.01
0.001
La ppm
35
40
45
50
MgO wt.%

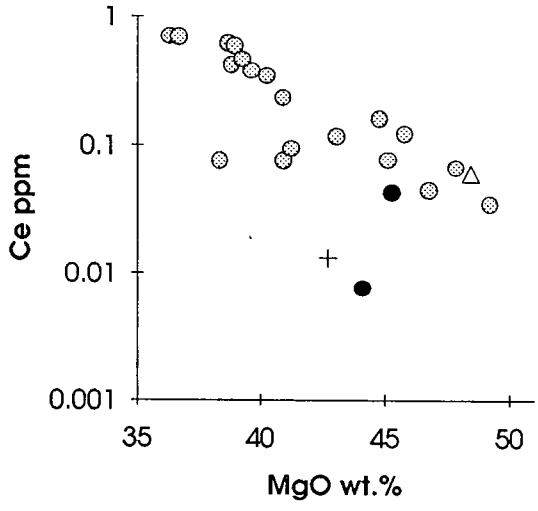
1
0.1
0.01
0.001
Ce ppm
35
40
45
50
MgO wt.%

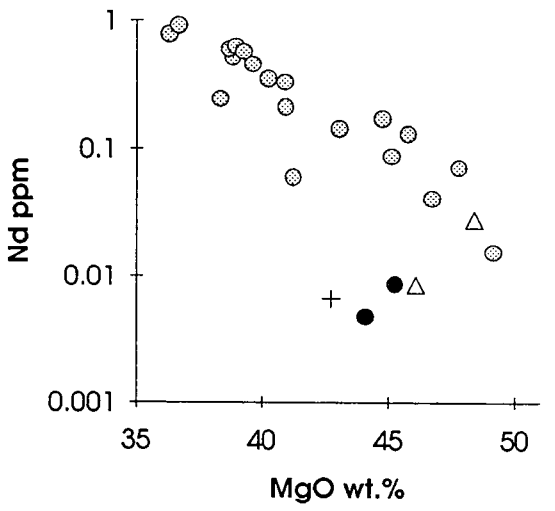
1
0.1
0.01
0.001
Nd ppm
35
40
45
50
MgO wt.%

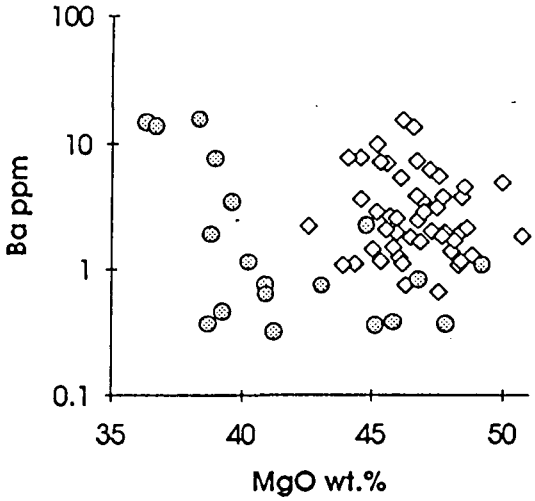
100
10
1
0.1
Ba ppm
35
40
45
50
MgO wt.%

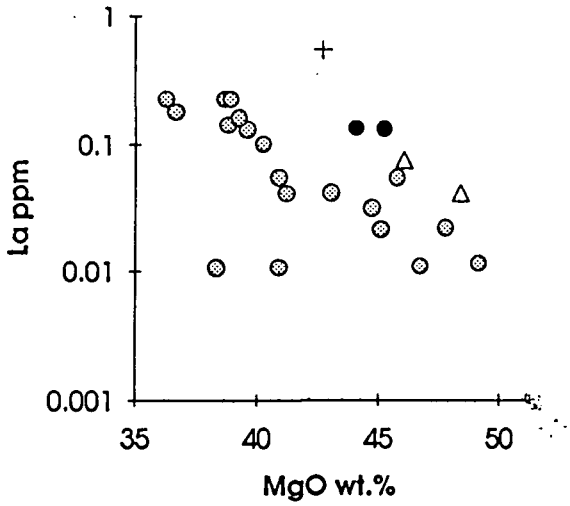
1
0.1
0.01
0.001
La ppm
35
40
45
50
MgO wt.%

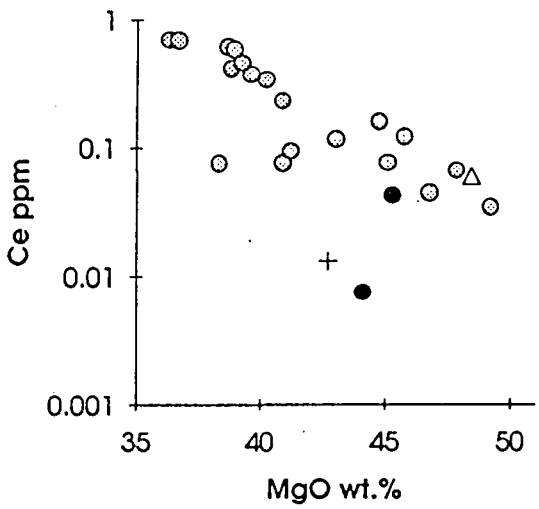
1
0.1
0.01
0.001
Ce ppm
35
40
45
50
MgO wt.%

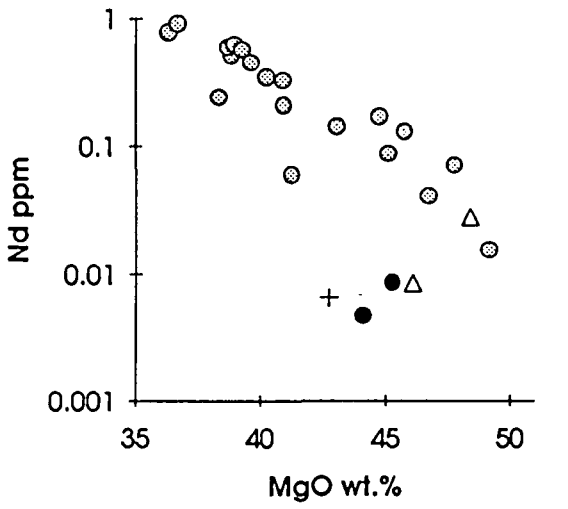
1
0.1
0.01
0.001
Nd ppm
35
40
45
50
MgO wt.%

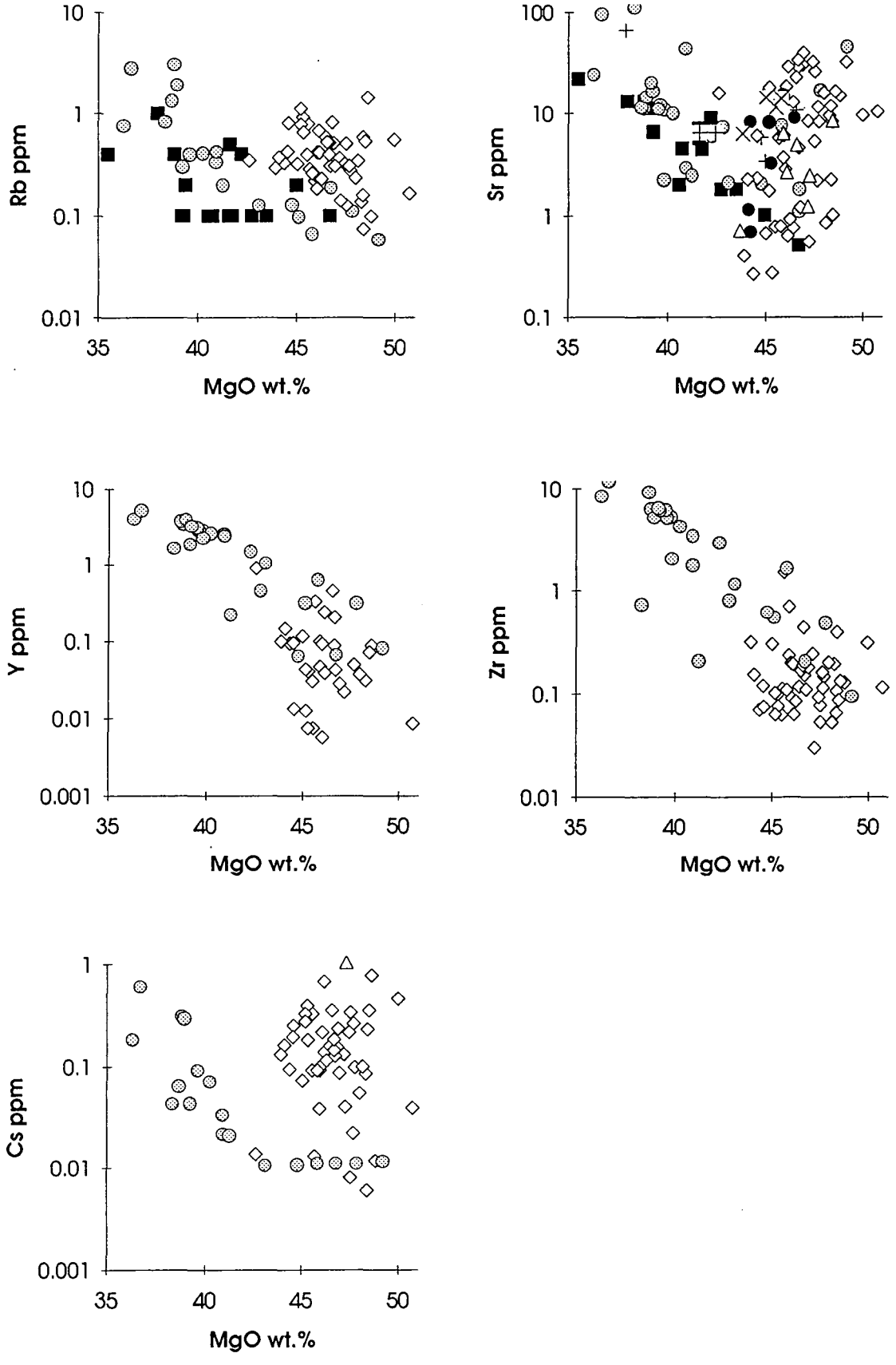


Figure 5.17. Plot of Rb, Sr, Y, Zr, Cs, Ba, La, Ce and Nd against MgO for Leg 125, Ojen and Ronda peridotites. **Key as for figure 5.12.**

matching the forward modelled and observed concentration of an element not enriched (in this case Ti) and using the mass balance equation to calculate the difference between the concentration in the modelled residues and the amount measured in the actual rock. The patterns in Figure 5.18b assume that the mass fraction of the enriching component is 1%. Obviously varying this mass fraction affects the level of the pattern but has little effect on the pattern shape. From Figure 5.18a it can be seen that virtually all of the measured Rb, Sr, La and Ce was introduced by the enriching component. Using the same arguments over 90% of the Zr, Sm and Eu must have been added. There may have been a small enrichment in the HREE.

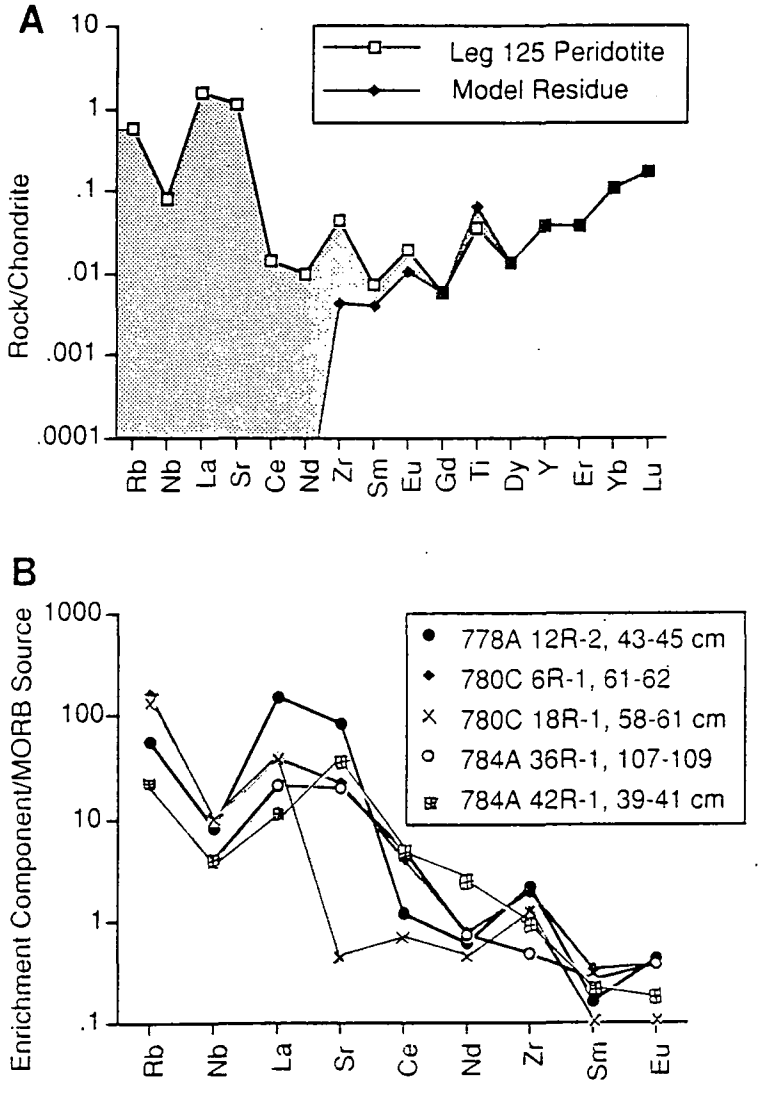


**Figure 5.18** (A) Extended chondrite-normalised REE patterns of a typical Leg 125 peridotite and a forward-modelled (incremental melting) composition of a residual harzburgite for which the HREE values give no enrichment (see text). The shaded area represents the amount of enrichment. The very incompatible elements on the left of the diagram are composed almost totally of the enriched component in the Leg 125 peridotites. (B) MORB-source-normalised trace element pattern for the enriching component. The patterns for each peridotite sample are calculated by mass balance assuming that the enriching component makes up 1% by mass of the peridotite.

*In this paragraph the terms melt and fluids have been used. Here a melt refers to a silicate or carbonate melt and fluid refers to an aqueous fluid phase. Both of these behave as fluids, but an important feature to note is how these "fluids" may travel through the mantle. As McKenzie (1984) suggested, an important network for determining whether a "fluid" forms an interconnecting network along grain edges and is able to move, is the dihedral angle between the "fluid" and the mantle minerals. Dihedral angles below 60 degrees allow the "fluid" to form an interconnected network. The dihedral angle between mantle minerals and silicate and carbonate melts and aqueous fluids is less than 60 degrees, so that these fluids will move readily through the mantle. However, $CO_2$-rich fluids do not form interconnected networks and so may not readily travel through the mantle. However, Bussod and Christie (1991) and Bussod (1991) have shown that deformation of the melting peridotite during decompression melting may enhance the flow of "fluids" and the concept of dihedral angles may not hold. "Fluids" will move upwards driven by their buoyancy (eg. Scott and Stevenson, 1989) and both silicate and carbonate melts and aqueous fluids may be important in causing incompatible element enrichments in peridotites.

*In this paragraph the terms melt and fluids have been used. Here a melt refers to a silicate or carbonate melt and fluid refers to an aqueous fluid phase. Both of these behave as fluids, but an important feature to note is how these "fluids" may travel through the mantle. As McKenzie (1984) suggested, an important network for determining whether a "fluid" forms an interconnecting network along grain edges and is able to move, is the dihedral angle between the "fluid" and the mantle minerals. Dihedral angles below 60 degrees allow the "fluid" to form an interconnected network. The dihedral angle between mantle minerals and silicate and carbonate melts and aqueous fluids is less than 60 degrees, so that these fluids will move readily through the mantle. However, $CO_2$-rich fluids do not form interconnected networks and so may not readily travel through the mantle. However, Bussod and Christie (1991) and Bussod (1991) have shown that deformation of the melting peridotite during decompression melting may enhance the flow of "fluids" and the concept of dihedral angles may not hold. "Fluids" will move upwards driven by their buoyancy (eg. Scott and Stevenson, 1989) and both silicate and carbonate melts and aqueous fluids may be important in causing incompatible element enrichments in peridotites.

### 5.7 Causes of LREE, Zr and LILE Enrichment

Some of the possible causes of trace element enrichments in the clinopyroxenes have been discussed in chapter 4. There are three principal sources of the enrichment; small melt fractionsand $CO_2$-rich fluids from the asthenosphere, melt fractions and related hot fluids from the underlying subduction zone and the low-temperature fluids that caused the serpentinisation.* The origin of the fluids which have serpentinised the Leg 125 peridotites has already been discussed at length in chapter 2, but it possible that some of the serpentinising fluids in Conical Seamount have originated from the slab and so the latter two processes may be interrelated.

From knowledge of the nature of the trace element enrichments it is possible to eliminate some of the possible causes of trace element enrichments. Time integrated enrichment of the lithosphere by small-degree asthenospheric melts is a common cause of metasomatic enrichments in peridotites. Many scientists have suggested that the source of forearc boninites was oceanic lithosphere metasomatised by these fluids, the so called "OIB (ocean island basalt) component" (Crawford 1989 and references therein). As discussed in Chapter 4, the principal characteristic of asthenospheric melts is that the enrichment of a given element is a function of its incompatibility with respect to garnet lherzolite. As a result the OIB components typically exhibit a marked enrichment of MREE relative to HREE. Nb is also strongly enriched, perhaps even more than La. The enrichment pattern in Figure 5.18b shows neither characteristic is a feature of the Leg 125 peridotites, which would be marked by a steady increase in enrichment level from right to left within the pattern. Moreover, as described in Chapter 4, the enrichment did not pre-date the melting event. Thus, it is unlikely that 'normal' asthenospheric fluids were the cause of this enrichment. This conclusion supports the isotopic evidence from the boninites, that none of the isotopic components involved in the enrichment of the boninite source had the composition of asthenospheric fluids of an OIB type.

It is, nonetheless, possible that an asthenospheric melt did invade the peridotites during or after melting if its composition had been fractionated en-route. Navon and Stolper (1987) suggested that the composition of a fluid percolating through the mantle could be fractionated by the chromatographic column effect. In this model, elements travel with a velocity related to their distribution coefficients, the more incompatible elements will move with a faster effective velocity than the more compatible elements. In an amphibole-bearing mantle wedge, elements compatible with amphibole (e.g. Ti, MREE) will be held back and the resultant melt could resemble the enriched component seen in the peridotites. The effect of this fractionation will have a

transient effect on the peridotites in the mantle wedge as the peridotites will eventually have a chance to equilibrate with all the fluid which has passes through the wedge. Equilibration with the peridotites in the mantle wedge depends on the time scale of the percolation and the content of the fluid. However, it is unlikely that amphibole is a stable phase in the mantle wedge during melting unless halogenated-amphiboles are stabilised (Foley, 1991; see Chapter 3).

Alternatively, the enrichment may be derived entirely from the subducted slab. Melted or dehydrated subducted sediments may be the dominant source of subduction components in the Bonin-Mariana region at present. Lead isotopes show that fluids and melts from subducted sediment were also involved in the petrogenesis of Eocene lavas from Chichi-Jima (Dobson and Tilton 1989) and that subducted sediments contribute to the genesis of active arc volcanoes in the Marianas region (Woodhead 1989). The sediment component does not, however, explain the HFSE enrichment seen in the Leg 125 peridotites. A partial melt of amphibolite derived from the subducted slab has also been invoked as a way of explaining the isotope systematics in the Leg 125 boninites (Pearce et al. 1992b). This component explains the absence of a displacement towards a pelagic sediment field on the Pb isotope diagrams and the selective enrichment of elements not retained in residual amphibole (e.g. La, Ce, Zr), relative to others that are compatible with an amphibole-rich residue (e.g. Ti, Zr, Yb). In summary, amphibole would fractionate Sm from Zr and explain the absence of Ti and other HREE enrichment. Further work is needed to evaluate whether chromatographic fractionation or slab melting is involved (J. A. Pearce, ion-microprobe work on amphibolite melting charges currently underway). The enrichment in HFSEs indicates that the enrichment is caused by a melt rather than a fluid, although additional enrichment in some elements may take place by fluids.

It is possible that this occurred after the HFSE enrichment as fluids percolate through the forearc mantle wedge over a prelonged period since the genesis of the boninites.

### 5.8 Relationship Between the Peridotites and Spatially-Related Boninites

In chapter 2 it was shown that boninitic magmatism occurred extensively in the middle to late Eocene in the Western Pacific. Many of these boninites are presently located in the outer forearc and inner trench regions of the Western Pacific. Likewise, peridotites

are extensively exposed in similar localities and it is not unreasonable to expect more than a casual spatial relationship between the boninites and peridotites. The peridotites from Leg 125 are plotted with boninites from their respective forearcs in Figure 5.19a. Data from the Mariana forearc are plotted in Figure 5.19a. REE data from three localities were plotted: DSDP Sites 458 and 459 from the outer forearc basin (Hickey and Frey, 1982), dredge site 28 from the inner trench wall (Stern et al., 1991), and the Facpi and Alutom units on Guam (Hickey and Frey, 1982). The boninites from the DSDP sites are LREE depleted and clearly not cogenetic with the harzburgites from Conical Seamount. The boninites from the inner trench wall and the Guam boninites have U-shaped patterns, but distinctively lower $[La/Sm]_N$ ratios than the harzburgite from Holes 778A and 780C. Data from the Izu-Bonin forearc are plotted in Figure 5.19b. The REE data are from Chichijima (J. A. Pearce, unpubl. data) and the Leg 125

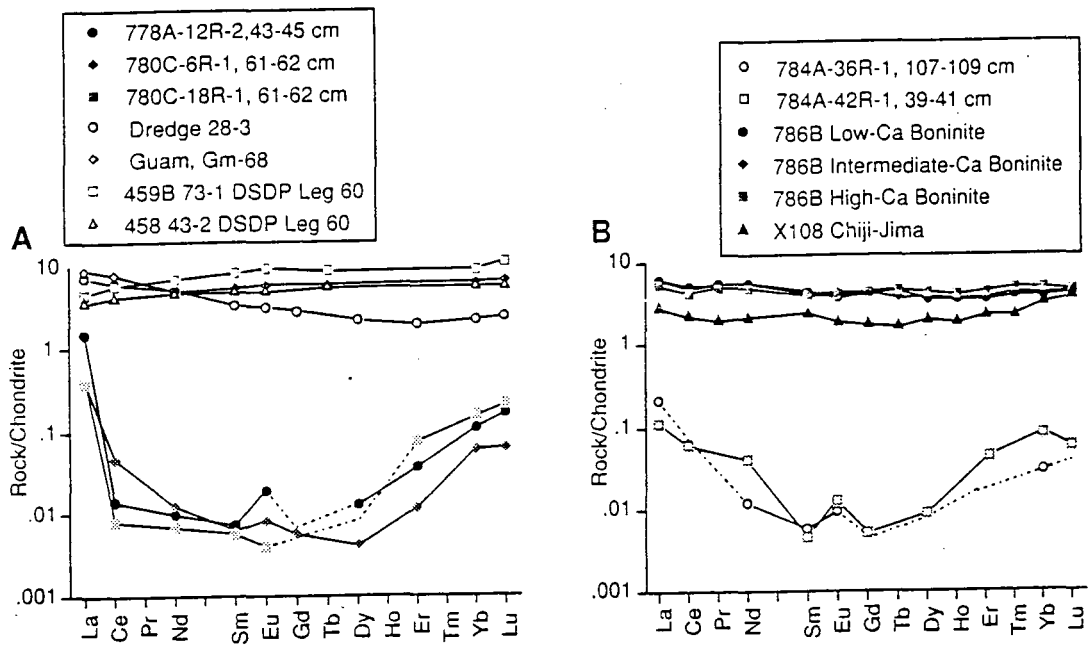


**Figure 5.19** Chondrite-normalised REE patterns of Leg 125 peridotites with spatially related boninites from (A) the Mariana forearc and Guam and (B) the Izu-Bonin forearc. Data for the Marianas boninites are from Hickey and Frey (1982), Hickey-Vargas (1989), Stern et al. (1991); for Izu-Bonin from Murton et al. (1992) and J. A. Pearce (unpubl. data).

sites (Murton et al., 1992). As in Figure 5.19 the degree of LREE enrichment is much greater in the peridotites from the Torishima Forearc Seamount than in the boninites.

Pearce et al, (1992b) argued that the Leg 125 peridotites are unlikely to be average residues from the boninites cored at Hole 786B as they are too refractory to have been in equilibrium with these boninites. Likewise, the calculated melts in equilibrium with

*It could be argued that the similarity in some of the trace element signatures of the spatially associated boninites and the Leg 125 peridotites could be related by the boninites percolating through the peridotites. However, the Leg 125 peridotites are depleted in bulk rock $SiO_2$ at high MgO and show textural evidence for the breakdown of orthopyroxene. This $SiO_2$ depletion is characteristic of the peridotites and is best explained by the incongruent melting of orthopyroxene, This process takes place at low pressure (<3kb) and at high water pressures. These conditions are similar to those calculated for the genesis of boninites (van der Laan et al., 1989). Furthermore the liquids produced by the incongruent melting of orthopyroxene are similar to low-Ca boninites in composition suggesting that some of the Leg 125 peridotites are residual to boninitic melt genesis.

*It could be argued that the similarity in some of the trace element signatures of the spatially associated boninites and the Leg 125 peridotites could be related by the boninites percolating through the peridotites. However, the Leg 125 peridotites are depleted in bulk rock $SiO_2$ at high MgO and show textural evidence for the breakdown of orthopyroxene. This $SiO_2$ depletion is characteristic of the peridotites and is best explained by the incongruent melting of orthopyroxene, This process takes place at low pressure (<3kb) and at high water pressures. These conditions are similar to those calculated for the genesis of boninites (van der Laan et al., 1989). Furthermore the liquids produced by the incongruent melting of orthopyroxene are similar to low-Ca boninites in composition suggesting that some of the Leg 125 peridotites are residual to boninitic melt genesis.

clinopyroxenes from the peridotites have too low trace element contents for the boninites from 786B. To be cogenetic, the peridotites would have to represent the top of the melting column that produced the boninites and would have undergone the most partial melting. However, the $SiO_2$ content of the peridotites* does indicate that they have melted to produce liquids with compositions similar to low-Ca boninites. Because La is more incompatible than Sm during mantle melting, these most residual peridotites should have much lower La/Sm ratios than the extracted melt. As Figure 5.19 shows the observed ratios are much higher than those in the melt. Thus, the peridotites cannot be residues from boninite melting unless further trace element enrichment took place after melting.

Despite this evidence that the Leg 125 peridotites were not in equilibrium with the spatially related boninites, the peridotites and boninites from the Izu-Bonin forearc do exhibit similar patterns of trace element enrichment (Pearce et al., 1992) suggesting that any sub-solidus enrichment involved fluids similar to those involved in the melting episode.

Because we know the nature and timing of the trace element enrichments and the likely type of melting it is possible to illustrate the relationship between the peridotites and their spatially related boninites using melting and enrichment models. To explain the REE patterns in the peridotites, $[La/Sm]_N$ and $[Sm/Yb]_N$ ratios were used to emphasise the LREE to MREE enrichment and MREE to HREE depletion respectively.

A fractional melting model was used to constrain the petrogenesis of the peridotites and the liquids which they produce (Figure 5.20). An FMM source was chosen as a starting composition and the residual compositions for increasing melting are plotted. It is apparent that the resulting compositions have ratios of $[La/Sm]_N$ and $[Sm/Yb]_N$ much too low to be suitable boninite sources. To obtain a suitable boninite source the residues must be re-enriched in the LREE along a vector similar to that shown in the diagram. The vector was modelled from the enrichment component deduced by Hickey and Frey (1982) and is consistent with the enrichment patterns plotted in this paper. To explain the low $[Sm/Yb]_N$ ratios in the boninites, It is necessary to invoke 10-15% melting of the MORB source before enrichment. This amount of source depletion is compatible with the those suggested by Crawford et al. (1989) and Pearce and Parkinson (in press) for boninites from the Western Pacific.

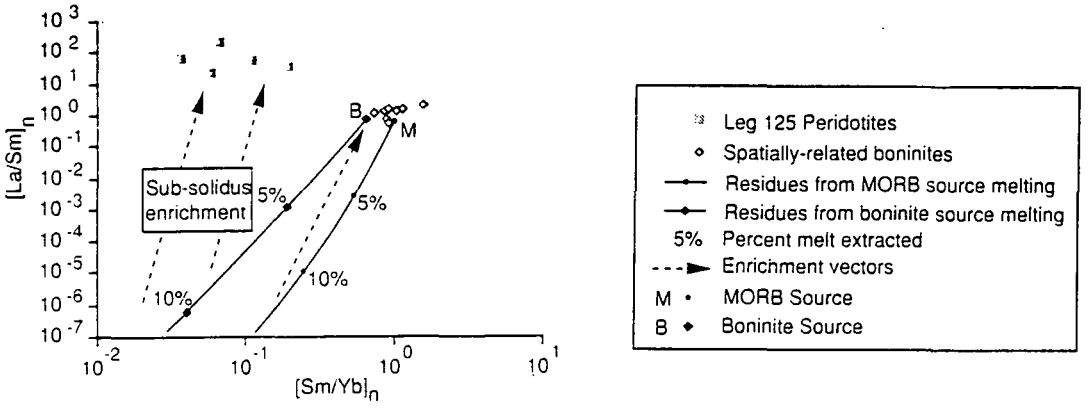


**Figure 5.20.** Plot of $[La/Sm]_N$ vs. $[Sm/Yb]_N$ showing a possible relationship between the Leg 125 peridotites and spatially associated boninites. Solid lines represent depletion trends and dotted lines the enrichment trends. The boninite source represents the residue from 10-15% partial melting of an N-MORB source enriched by the components calculated in Hickey and Frey (1982). Residues from remelting this source are re-enriched under sub-solidus conditions to produce the Leg 125 peridotites.

Partial melting of this enriched mantle source to give boninites will again generate residues with much lower ratios of $[La/Sm]_N$ and $[Sm/Yb]_N$ than those seen in the Leg 125 peridotites. Sub-solidus enrichment must again be invoked to give the observed high $[La/Sm]_N$ ratios. A residue of 10-15% melting of the boninite source enables modelling of the observed chemical variations in the peridotites. Note the spread of $[Sm/Yb]_N$ ratios in the peridotites is explained by variable degrees of depletion. The resulting model is therefore a multistage one of (1) fusion of MORB mantle to form MORB lithosphere, (2) enrichment of this lithosphere in a LREE- and Zr-rich component, (3) fusion of this enriched mantle above a subduction zone at high oxygen fugacities to generate boninites (4) subsolidus enrichment of the most depleted residue from this boninite melting event. This multistage history of the peridotites is compatible with textural, clinopyroxene chemistry and bulk-rock chemistry evidence.

## 5.8 Comparison Between Forearc Peridotites and Supra-Subduction Zone Ophiolite Mantle Sequences

Compared with peridotite xenoliths and Alpine peridotite massifs, there is a relatively small data base of good trace element analyses for depleted peridotites from ophiolite complexes. Representative REE patterns for harzburgites from supra-subduction zone ophiolites are presented in Figure 5.21.

There is a large variation in the apparent REE pattern. HREE values tend to vary by only a factor of 3, whereas the LREE values vary by up to two orders of magnitude, giving a wide range of pattern shapes. Eu anomalies can be positive (e.g., Pindos, Troodos), negative (e.g. New Caledonia), or not detected. The Leg 125 patterns plot within the range of these ophiolitic peridotites, but have steeper LREE profiles (higher $[La/Sm]_N$ ratios) than any of the ophiolite patterns and slightly steeper MREE-HREE profiles ($[Sm/Yb]_N$ ratios). than all but the Bay of Islands harzburgites. As in the case of the Leg 125 peridotites, it is rare for the harzburgites from supra-subduction zone ophiolites to show any obvious relationship to spatially related lavas on the basis of their trace element contents. For example, lavas from Pindos, Troodos, and Semail can have LREE-enriched, flat and LREE-depleted patterns, yet the spatially associated harzburgites have flat to LREE-enriched patterns. In the case of the Semail ophiolite, McCulloch et al., (1980) also showed that this difference in REE pattern was not matched by a corresponding difference in εNd values.

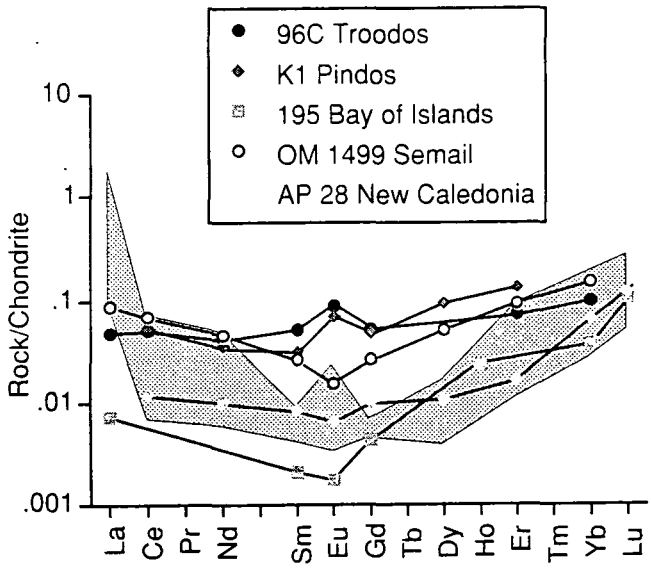


**Figure 5.21.** Chondrite-normalised REE patterns of harzburgites from selected supra-subduction zone ophiolites. The shaded field represents the Leg 125 peridotites. Data from Bay of Islands (Suen et al., 1979), Semail (Lippard et al., 1986), Troodos (Kay and Senechal, 1976), Pindos (Montigny et al., 1973), and New Caledonia (Prinzhofer and Allégre, 1985).

## 5.9 Chapter Summary

Whole-rock data for Leg 125 peridotites have many of the geochemical characteristics of the clinopyroxenes. Major and incompatible trace elements unaffected by enrichment processes indicate that the peridotites are residues from approximately 25% fractional melting. The peridotites are enriched in LREE, and Zr.

This enrichment occurred during and after the final melting event that

affected the peridotites. Based upon petrographic study, mineral chemistry and bulk-rock data, a multi-stage melting and enrichment model has been developed to describe the petrogenesis of the peridotites. The peridotites represent 10-15% melting of an N-MORB source to produce a depleted spinel lherzolite. Enrichment of this lherzolite is followed by a further 10-15% fusion that produces the spatially related boninites. Incongruent melting of orthopyroxene was an important feature of the final stages of melting and generated low Ca-boninites.

The REE patterns of the harzburgites have no obvious equivalents in the harzburgites from SSZ ophiolites which have been analysed to date. Although both can have U-shaped patterns and positive Eu-anomalies, if SSZ ophiolites do represent a forearc setting, it is possible that enrichment and depletion events in this setting are highly variable, and may reflect the residence time of the mantle in question in the forearc.

# Chapter 6
# Discussion and Conclusions

## 6.1 Discussion

### 6.1.1 Melting and Fluid Processes Above Subduction Zones: Evidence from the Leg 125 Peridotites

Recent attempts to model melting processes in the mantle wedge above subduction zones have provided two contrasting models. Davies and Bickle (1991) and Davies and Stevenson (1992) have produced models which are based on the fluxing of the source region for arc magmas with water from the down-going subducting slab. The water generated from the slab hydrates the overlying peridotite in the mantle wedge which then produces melt upon crossing the stability field of pargasitic amphibole. Davies and Bickle (1991) have calculated that the melt generated by this hydrous fluxing process will have the composition of a magnesium andesite and that a maximum of 8-10% melting can be provided by the hydrous fluxing without any decompression melting.

In contrast Plank and Langmuir (1988) describe melting in the mantle wedge in terms of pressure release (decompression) melting whereby the composition of the melts generated is controlled by the length of the melting column. In contrast to a similar study undertaken on melting beneath spreading ridges (Klein and Langmuir, 1987), Plank and Langmuir (1988) found that the thickness of the lithosphere on which the island arc is built principally controlled the length of the melting column rather than the temperature of the mantle. Thus, in areas where an island arc is built on thick lithosphere the melts produced are from small degrees of partial melting and in areas where an island arc was built on thin lithosphere the melts have compositions consistent with higher degrees of partial melting of the mantle. Finally, they found that on average, intraoceanic island arc basalts were the products of a similar amount of partial melting of the mantle to MORB.

A common feature of island arcs is that they are approximately 110 km above the Benioff Zone irrespective of the angle of subduction. This has lead many workers (see Gill, 1981) to propose that a pressure dependent reaction may control the genesis of

island arc basalts. 110 km is equivalent to the pressure of the breakdown of pargasitic amphibole in the mantle (Green, 1973) which gives support to the models of Davies and Bickle (1991). However, the strong correlation between lithospheric thickness and melt chemistry strongly supports the melting column models of Plank and Langmuir (1988).

On the basis of a large geochemical data base of intraoceanic arc basalts and modelling of melting processes, Pearce and Parkinson (in press) propose that aspects of both the hydrous fluxing and decompression melting modles may occur in the mantle wedge. Melt generated during the breakdown of pargasitic amphibole may initiate melting within the wedge. The mantle then decompresses until its dry solidus is crossed and melts in a manner similar to that beneath spreading ridges. Thus in areas where there is a very thin lithosphere the effect of this type of melting model is to have a greater degree of partial melting than beneath a ridge for the same potential temperature (see Chapter 3).

By using elements which are not enriched from the underlying subduction zone Pearce and Parkinson (in press) find that most intraoceanic arc basalts are consistent with being medium to high degrees of partial melting. Furthermore, many samples are melts from variably depleted sources, which are characteristically depleted in the highly incompatible elements.

From the above discussion of melting processes in the mantle wedge it is clear that there are certain processes which are common to mantle melting at intraoceanic destructive plate margins. These are principally that higher degrees of melting than found at normal spreading ridges are common. Also two stage melting processes may also operate, although only one of these melting events may occur in the mantle wedge. Thus any residual peridotites discovered at intraoceanic destructive plate margins may record some of these distinct melting features.

The Leg 125 peridotites provide excellent evidence for both high degrees of partial melting and multistage melting processes. Incompatible element (Ti, Dy and Yb) concentrations in the clinopyroxenes from the Leg 125 peridotites are some of the lowest recorded from oceanic peridotites and are lower than the most depleted abyssal peridotites (Parkinson et al., 1992a). The most depleted abyssal peridotites have REE patterns consistent with some melting in the garnet field, because of the high potential temperature. However, the REE patterns of the Leg 125 peridotites clinopyroxenes show no evidence of being in equilibrium with garnet. Therefore the high degrees of

melting that the peridotites have experienced may well have been due to water from the subduction zone providing the extra amount of melting. As discussed in Chapter 4, the V content of the clinopyroxenes can be explained by a two stage melting history, with the first melting event taking place beneath a spreading centre. Estimates of the amount of melting are ~15%. This is a very large amount of depletion compared with more common amounts of source depletion of 5-10% recorded by intraoceanic arc basalts (Pearce and Parkinson, in press). Therefore, the Leg 125 peridotites represent an extreme example of source depletion in the sub-arc mantle. This amount of depletion is usually associated with boninitic magmatism and is relatively rare (see Section 6.1.2).

Finally, it can postulated that residual peridotites from the sub-arc mantle may record similar amounts of partial melting to the Leg 125 peridotites. However, they may not record the extremely large amounts of first stage melting that the Leg 125 peridotites have experienced. Furthermore, true arc-peridotites may have melted at high oxygen fugacities throughout their melting history and therefore would have lower V contents than the Leg 125 peridotites.

McKenzie and O'Nions (1991) have used inversion theory to propose that residual amphibole is an important mineral in the mantle wedge. Furthermore they suggest that amphibole may produce some of the distinctive trace element characteristics of subduction zone-related magmas such as the fractionation of LILE from HFSEs as magmas percolate through an amphibole-bearing mantle wedge. Unfortunatley the lack of extant sub-arc mantle samples makes it difficult to fully address their proposition. In Chapter 3 phase petrology evidence was cited which indicates that it is unlikely for pargasitic amphibole to be stable in the mantle wedge during decompression melting. McKenzie and O'Nions suggest that K-richterite may be the stable amphibole in the mantle wedge. Certainly the experimental evidence indicates that it is stable at higher temperatures and pressure than pargasitic amphibole (Sudo and Tatsumi, 1989). However, the amphibole characterstic of supra-subduction zone ophiolites and the Leg 125 peridotites are low-K tschermakitic-hornblendes and magnesio-hornblendes (Takahashii, 1980; Ozawa, 1988; this study). Therefore, on the limited evidence available it is unlikely that amphibole is a stable residual phase in the mantle wedge.

In terms of fluid processes within the mantle wedge the Leg 125 peridotites are possibly unique in that they record a complex history of mantle/fluid interaction. Several workers have developed models whereby much of the dehydration of the subducting slab takes place beneath the forearc region (Tatsumi et al., 1983, 1986;

Davies and Stevenson, 1992). The fluid generated by the dehydration reactions in the slab forms amphibole in the overlying mantle wedge. However, in the Mariana and Izu-Bonin forearcs mantle material becomes exposed in the forearc terrane. The geochemical evidence for some of the fluids sampled at Conical Seamount being from the underlying slab has already been described in detail in Chapter 2. Thus, at least some of the fluids produced by dehydration reactions in the slab can make there way through the mantle wedge to the serpentinite seamounts exposed on the sea-floor. The Leg 125 peridotites record some of the characteristic features of subduction zone fluids having high Sr/Nd ratios and low Rb/Cs ratios (Ellam and Hakesworth, 1988; Hart and Reid, 1991). Furthermore, the high oxygen fugacities recorded by the peridotites (>FMQ+1) indicate that this fluid must be $H_2O$-rich and shows that convergent margins are important regions for oxidising the mantle. Mattioli et al. (1989) and Ballhaus, et al. (1990) have proposed that this process has lead to the progressive oxidation of the mantle through geological time. Finally, the presence of retrograde antigorite may be a characteristic feature of convergent margin peridotites (e.g., Eggler, et al., 1973; Peacock, 1987a).

### 6.1.2 Mantle Melting in the Western Pacific in the Eocene

In Chapter 2 a brief summary of tectonomagmatic history of the Western Pacific was provided. One of the remarkable features of the Western Pacific in the middle Eocene times was the eruption of boninitic melts along the length of the Western Pacific (~5000 km along strike). Although volumetrically unimportant boninites represent the shallow melting of a previously depleted peridotite under hydrous, but water-undersaturated conditions. The generation of boninites in the Western Pacific in middle Eocene times indicates that the thermal and tectonic conditions for the production of boninitic melts are met during the initial stages of subduction. Thermal modelling by Peacock (1991) and Pearce et al. (1992b) require both the subducting slab and overlying mantle wedge to be young and very hot and subduction beneath or of an active spreading ridge during the intial stages of subduction may provide the thermal and tectonic conditions to generate boninitic melts (Pearce et al., 1992b). In terms of the melting history of the Leg 125 peridotites it is probable that they first melted beneath an active spreading ridge. Pearce et al. (1992b) have suggested that subduction initiated in the Western Pacific along a transform boundary. Spreading ridges associated with this transform boundary may then be subducted or be subducted under. Fluids, possibly from serpentinite along the transform boundary can flux the hot mantle wedge and initiate melting at shallow pressures. Thus, the Leg 125 peridotites experienced their second melting event in the forearc mantle wedge soon after the first melting event. The melts they generated where boninites. The peridotites then cooled

slowly after magmatism ceased and became selectively enriched in trace elements as the peridotites resided in the mantle wedge.

### 6.2 Further Work

The geochemistry of the Leg 125 peridotite shows that detailed geochemical studies of both the bulk-rock and the minerals can provided detailed information about melting and enrichment history of peridotites. However, the studies in this thesis were hampered by several points. Some of these are more general to melting in the mantle. However one of the principal problems was the small size of the core and whether the material recovered in the core was related to each other stratigraphically. Furthermore it was impossible to know whether a dyke or veins had been intruded close by to where the core was drilled. These problems meant that interpretation was sometimes difficult. In light of the studies in this thesis, below are presented some further work which would help in the interpretation of the Leg 125 peridotites and melting in the mantle wedge in general.

1. There is a real lack in peridotite melting experiments carried out under varying hydrous conditions at the relevant pressures and temperatures for melting in the mantle wedge. Although Green and co-workers (Green, 1973, 1976; Wallace and Green, 1991) have undertaken some experiments (see Chapter 3), there are still considerable experimental problems with undertaking such experiments. The introduction of rhenium capsules rather than platinum may go some way to reducing iron loss during the experiments. However, producing good quenched glasses during the experiments still remains a problem (T. J., Falloon, pers. comm.). However, experiments could be undertaken to quantify the exact amount of extra melt which may be generated by the addition of varying amounts of water. These types of experiments may place constraints on the composition and amount of melt generated by the hydrous fluxing melting that Davies and Bickle (1991) and Davies and Stevenson (1992) have proposed.

2. Recent experiments by Kushiro and co-workers (e.g., Hirose and Kushiro, 1993) have begun to simulate incremental melting. By placing diamond aggregates in their experimental charges, melts which are produced during the experiments rapidly segregate into the diamond aggregate, thus extracting melt fractions after 3-5% melting. This type of technique could be used to simulate decompression melting in the mantle. Fertile mantle could be melted 3-5%. The residue from this first melting event would become the initial composition for the next melting experiment. This procedure could be repeated along the relevant P-T path of a melting adiabat. These types of

experiments will allow us to model the near-fractional polybaric melting in the mantle with considerably more accuracy.

3. Although a large amount of major and trace element data for abyssal peridotite minerals has been published in the last ten years (Dick et al., 1984; Dick, 1989; Johnson et al., 1990; Dick and Johnson, 1992) there still exists a very small data base for bulk-rock analyses of abyssal peridotites. Recent analytical developments (Jochum et al., 1990) mean that the determination of Zr, Y, and Nb at low levels can be readily undertaken. The systematic variation of the spinel composition with the geoid anomaly (Dick et al., 1984) and the trace element content of clinopyroxenes with potential temperature of the mantle (Johnson et al., 1990) indicates that the whole-rock data should also vary systematically with such parameters. However, recent analyses of abyssal peridotites from the Kane Fracture Zone (J. A. Pearce, unpubl. data) and peridotites from a variety of tectonic settings have found that the HFSEs Zr and Y do not behave coherently. Zr can be enriched in many of these samples, therefore the Zr enrichments seen in the Leg 125 data may be more widespread than previously believed.

4. Kelemen and co-workers (Kelemen et al., 1992) propose that the interaction between ascending melts and mantle wallrock may be an important process in the sub-arc mantle. They suggest that calk-alkaline liquids may be generated by the interaction of basaltic melts with a lherzolite to produce a modified calk-alkaline liquid and a harzburgitic residue. Although the data from the Leg 125 peridotites does not support Kelemen's models and the author does not believe that the large volumes of depleted peridotites found in the basal sections of ophiolites represent the reactants from the type of interaction Kelemen proposes, melt/mantle wallrock interaction may be an important process on a local scale around dykes in ophiolites. Detailed ion-microprobe studies of the type undertaken by Kelemen et al., (1992), on ophiolitic peridotites and veins cutting the peridotites will provide a great deal of information on the geochemical consequence of movement of hydrous melts within the sub-arc mantle. One of the main problems in understanding the Leg 125 peridotites was the lack of any proper 'field' relations within core. Geochemical studies of ophiolitic peridotites may find that the distinctive trace element enrichments found in the Leg 125 peridotites are more widespread than previously published. Field studies would help in constraining the origin of trace element enrichments.

## 6.3 Principal Conclusions of the Thesis

Serpentinised tectonised harzburgites and dunites were recovered from Conical Seamount in the Mariana forearc and Torishima Forearc Seamount in the Izu-Bonin forearc. Peridotites from both seamounts are very refractory with high compatible element contents, very low incompatible element contents and are made up of very refractory minerals with olivine (Mg# 91.1-93.6), orthopyroxene (Mg# 91.8-93.2), clinopyroxene (Mg# 93.0-96.2) and spinels (Cr# 39-82). Modelling of the trace element content of both the clinopyroxenes and bulk-rock indicate that the peridotites are the residues to ~25% fractional melting.

However, the peridotites show textural evidence for a two stage melting history. Olivine and spinel petrofabrics indicate that the peridotites where deformed under high temperature (>1000°C) and low stress conditions. Girardeau and Lagabrielle (1992) interpret that this deformation event took place beneath a spreading ridge. A second deformation event took place again at high temperature and low stress conditions, but olivine textures suggest that high water pressures where also indicative of this deformation event. Coupled with the common incongruent melting of orthopyroxene which must take place at low pressures (~3 kb) and high water activities (Morse, 1980) this deformation/melting event took place in the mantle wedge above a subduction zone. A series of heterogeneous deformation events and alteration reactions then took place at progressively lower temperatures. These reactions include the formation of magnesio-hornblende after orthopyroxene at approximately 800 °C, the formation of antigorite serpentine at temperature less than 500 °C, the formation of lizardite after olivine and orthopyroxene and finally the formation of late cross cutting chrysotile veins probably at temperatures lower than 200 °C. This series of hydration reactions is consistent with the peridotites reacting with progressively colder fluids from the underlying subduction zone (Peacock, 1987a and b; Mottl, 1992). However, some of the low temperature serpentinisation of the peridotite from Torishima Forearc Seamount was by seawater (Mottl, 1992).

The geochemistry of the peridotites also provides evidence for a two stage melting history. The V content of the clinopyroxenes is very low and plots on a distinct trend away from the abyssal peridotite trend on a V against Ti plot. The V concentrations of the clinopyroxenes can be modelled most accurately by ~15% partial melting at low oxygen fugacities (FMQ-1) when V will be in its trivalent state and have a clinopyroxene/melt partition coefficient of 1.4, followed by 5-10% partial melting at higher oxygen fugacities (FMQ+1) when V may also exist in its tetravalent state. V has a clinopyroxene/melt partition coefficient of approximately 0.8 during this melting event. An important result from the V data is that clinopyroxenes from Torishima

Forearc Seamount have lower V contents and define a separate melting trend from the Conical Seamount clinopyroxenes. This is consistent with the higher oxygen fugacities recorded by these peridotites (from oxygen thermobarometry) indicating the more incompatible behaviour of V with respect to clinopyroxene. The V concentration in both clinopyroxenes and the bulk-rock is sensitive to the oxygen fugacities that the peridotites melted at. The oxidised nature of many arc-related peridotites (Wood et al., 1990) means that V may be a useful element in discriminating peridotites from destructive plate margins.

Finally, the peridotites are selectively enriched in incompatible trace elements. The clinopyroxenes are enriched in Sr, Ce, Nd, Sm, Eu and Zr. The bulk-rock peridotite have U-shaped REE patterns with $[La/Sm]_N$ ratios of 5.03 to 250.0 and $[Sm/Yb]_N$ ratios of 0.05 to 0.25. The bulk-rock peridotites are also enriched in Rb, Sr, Cs, Ba and Zr. Covariation diagrams based on clinopyroxene and bulk-rock data show that this enrichment event occurred during or after melting. A model is described which proposes that the peridotites have experienced a multistage melting and enrichment history. The peridotites represent 10-15% melting of an N-MORB source to produce a depleted spinel lherzolite. Enrichment of this lherzolite is followed by a further 10-15% fusion that generates the spatially related boninites. The Leg 125 peridotites represent the most depleted residues from that melting event. The peridotites where then enriched again. The enrichment process took place during and after the last melting event. The Leg 125 peridotites have different trace element characteristics from any SSZ ophiolite peridotites. Their unusual compositions may reflect their long residence time in the forearc mantle wedge, during which time they may have interacted with melts and fluids from the underlying subduction zone.

# References

Ahern, J. L., and Turcotte, D. L., 1979. Magma migration beneath an ocean ridge. *Earth. Planet. Sci. Lett.*, **45,** 115-122.

Albarede, F., 1992. How deep do common basaltic magmas form and differentiate? *J. Geophys. Res.*, **97,** 10997-11009.

Allègre C. J., and Minster, J. F., 1978. Quantative models of trace element behaviour in magmatic processes. *Earth. Planet. Sci. Lett.*, **38,** 1-25.

Arculus, R. J., Dawson, J. B., Mitchell, R. H., Gust, D. A., and Holmes, R. D., 1984. Oxidation states of the upper mantle recorded by megacryst ilmenite in Kimberlite and type A and B spinel lherzolites. *Contrib. Mineral. Petrol.*, **85,** 85-94.

Arculus, R. J., Pearce, J. A., Murton, B. J., and van der Laan, S. R., 1992. Igneous stratigraphy and major-element geochemistry of Holes 786A and 786B. *In* Fryer, P., Pearce, J. A., Stokking, L. B., *et al.*, *Proc. ODP, Sci. Results*, 125: College Station, TX (Ocean Drilling program), 143-169.

Aumento, F., and Loubat, H., 1971. The mid-atlantic ridge near 45°N. XVI. Serpentinized ultramafic intrusions. *Can. J. Earth Sci.* **8,** 631-663.

Ballhaus, C., Berry, R. F., and Green, D. H., 1990. Oxygen fugacity controls in the Earth's upper mantle. *Nature*, **348,** 437-440.

Barnes, I., and O'Neil, J. R., 1969. The relationship between fluids in some fresh Alpine-type ultramafics and possible modern serpentinization, Western U.S. *Bull. Geol. Soc. Am.*, **80,** 1947-1960.

Bédard, J. H., 1989. Disequilibrium mantle melting. *Earth. Planet. Sci. Lett.*, **91,** 359-366.

Bell, T. H., Fleming, P. D., and Rubensch, M. J., 1986. Porphyroblast nucleation, growth, and dissolution in regional metamorphic rocks as a function of deformation partitioning during foliation. *J. metamorph. Geol.*, **4,** 37-67.

Bertrand, P., and Mercier, J-C. C., 1985/86. The mutual solubility of coexisting ortho- and clinopyroxene: toward an absolute geothermometer for the natural system? *Earth. Planet. Sci. Lett.*, **76,** 109-122.

Bloomer, S. H., 1983. Distribution and origin of igneous rocks from the landward slopes of the Mariana trench: implications for its structure and evolution. *J. Geophys. Res.*, **88,** 7411-7428.

Bloomer, S. H., and Hawkins, J. W., 1983. Gabbroic and ultramafic rocks from the Mariana trench: an island arc ophiolite. *In* Hayes, D. E. (Ed.), *The Tectonic and Geological Evolution of the Southeast Asian Seas and Islands* (Pt.2). Am. Geophys. Union, Geophys. Monogr. Ser. **27,** 294-317.

Bloomer, S. H., and Fisher, R. L., 1987. Petrology and geochemistry of igneous rocks from the Tonga trench, a non-accreting plate boundary. *J. Geol.*, **95,** 469-495.

Bodinier, J. -L., Dupuy, C., and Dostal, J., 1988. Geochemistry and petrogenesis of Eastern Pyrenean peridotites. *Geochim. Cosmochim. Acta*, **52,** 2893-2907.

Bodinier, J. -L., Vasseur, G., Verniers, J., Dupuy, C., and Fabries, J., 1990. Mechanisms of mantle metasomatism: geochemical evidence from the Lherz orogenic peridotite. *J. Petrol.*, **31,** 597-628.

Bonatti, E., and Michael, P. J., 1989. Mantle peridotites from continental rifts to ocean basins to subduction zones. *Earth. Planet. Sci. Lett.*, **91,** 297-311.

Bowen, N. L., and Andersen, O., 1914. The binary system MgO-$SiO_2$. *Am. J. Sci.*, **37,** 487-500.

Bowin, C. O., Nalwalk, A. J., and Hersey, J. B., 1966. Serpentinised peridotites from the north wall of the Puerto Rico trench. *Bull. Geol. Soc. Am.*, **77,** 257-270.

Boyd, F. R., and England, J. L., 1964. The system enstatite-pyrope. *Yb. Carnegie Inst. Wash.*, **63,** 157-161.

Boynton, W. V., 1984. Cosmochemistry of the rare earth elements: meteorite studies. *In* Henderson, P. (Ed.), *Rare earth element geochemistry*, Amsterdam, (Elsevier), 63-114.

Brenan, J. M., and Watson, E. B., 1991. Partitioning of trace elements between olivine and aqueous fluids at high P-T conditions: implications for the effect of fluid composition on trace element transport. *Earth. Planet. Sci. Lett.*, **107,** 672-688.

Brey, G. P., and Köhler, T., 1990. Geobarometry in four-phase lherzolites II. new thermobarometres, and practical assessment of existing thermobarometers. *J. Petrol.*, **31,** 1353-1378.

Brey, G. P., Köhler, T., and Nickel, K. G., 1990. Geothermobarometry in four-phase lherzolites I. experimental results from 10 to 60 kb. *J. Petrol.*, **31,** 1313-1352.

Browning, P., 1982. *The Petrology, Geochemistry, and Structure of the Plutonic Rocks of the Oman Ophiolite*. Unpublished Ph.D. thesis, Open University, 404 pp.

Bryndzia, L. T., and Wood, B. J., 1990. Oxygen thermobarometry of abyssal spinel peridotites: the redox state and C-O-H volatile composition of the earth's sub-oceanic mantle. *Am. J. Sci.*, **290,** 1095-1116.

Buening, D. K., and Buseck, P. R., 1973. Fe-Mg lattice diffusion in olivine. *J. Geophys. Res.*, **78,** 6852-6862.

Bussod, G. Y., 1991. Melting and mantle flow. *Terra Abstracts*, **3,** 146-147.

Bussod, G. Y., and Christie, J. M., 1991. Textural development and melt topology in spinel lherzolite experimentally deformed at hypersolidus conditions. *J. Petrol.*, Special Lherzolite Issue, 17-39.

Cameron, W. E., McCulloch, M. T., and Walker, D. A., 1983. Boninite petrogenesis: chemical and Nd-Sr isotopic constraints. *Earth. Planet. Sci. Lett.*, **65,** 75-89.

Carlson, R. L., and Mortera-Gutiérrez, C. A., 1990. Subduction hinge migration along the Izu-Bonin-Mariana arc. *Tectonophysics*, **181,** 331-344.

Carswell, D. A., 1991. The garnet-orthopyroxene Al barometer: problematic application to natural garnet lherzolite assemblages. *Min. Mag.*, **55,** 19-31.

Chackraborty, S., amd Ganguly, J., 1990. Compositional zoning and cation diffusion in garnets. *In* Ganguly, J., (Ed.), *Diffusion, Atomic Ordering, and Mass Transport: Selected topics in Geochemistry, Advances in Physical Geochemistry*, Volume **8,** Springer Verlag (New York), 120-175.

Checkmir, A. S., and Epel'baum, M. B., 1991. Diffusion in magmatic melts. *In* Perchuk, L.L., and Kushiro, I., (Eds.), *Physical Chemistry of Magmas, Advances in Physical Geochemistry*, Volume **9**, Springer Verlag (New York), 99-119.

Christie, D. M., Carmichael, I. S. E., and Langmuir, C. H., 1986. Oxidation states of mid-ocean ridge basalt glasses. *Earth. Planet. Sci. Lett.*, **79**, 397-411.

Clark, A. M., and Long, J. V. P., 1971. Anisotropic diffusion of nickel in olivine. *In, Thomas Graham Memorial Symposium on Diffusion Processes*. Gordon & Breach, (New York), 511-521.

Cohen, M., 1971. Self-diffusion during plastic deformation. *Trans. Japan Inst. Metals* **11**, 145-151.

Crank, J., 1956. The Mathematics of Diffusion. Clarendon Press, (Oxford), 347 pp.

Crawford, A. J., (Ed.) 1989. *Boninites and Related Rocks*. Unwin, (London), 465 pp.

Crawford, A. J., Falloon, T. J., and Green, D. H., 1989. Classification, petrogenesis and tectonic setting of boninites. *In* Crawford, A. J., (Ed.) *Boninites and Related Rocks*, Unwin, (London), 1-49.

Daines, M. J., and Kohlstedt, D. L., 1993. A laboratory study of melt migration. *Phil. Trans. R. Soc. Lond.*, **A342**, 43-52.

Davies, J. H., and Bickle, M. J., 1991. Aphysical modelfor the volume and composition of melt produced by hydrous fluxing above subduction zones. *Phil. Trans. R. Soc. Lond.*, **A335**, 355-364.

Davies, J. H., and Stevenson, D. J., 1992. Physical model of source region of subduction zone volcanics. *J. Geophys. Res.*, **97**, 2037-2070.

DePaolo, D. J., 1981. Trace element and isotopic effects of combined wallrock assimilation and fractionation crystallization. *Earth. Planet. Sci. Lett.*, **53**, 189-202.

Dick, H. J. B., 1977. Partial melting in the Josephine peridotite I. The effect on mineral composition and its consequences for geobarometry and geothermometry. *Am. J. Sci.*, **277**, 801-832.

Dick, H. J. B., 1989. Abyssal peridotites, very slow spreading ridges and ocean ridge magmatism. *In* Saunders, A. D., and Norry, M. J., (eds.), *Magmatism in the Ocean Basins. Geol. Soc. Lond. Spec. Publ.*, **42**, 71-105.

Dick, H. J. B., and Bullen, T., 1984. Chromium spinel as a petrogenetic indicator in abyssal and alpine-type peridotites and spatially associated lavas. *Contrib. Mineral. Petrol.*, **86,** 54-76.

Dick, H. J. B., and Fisher, R. L., 1984. Mineralogic studies of the residues of mantle melting: abyssal and alpine-type peridotites. *In* Kornprobst, J., (Ed.), *Kimberlites II: The Mantle and Crust Relations*. Elsevier, (Amsterdam), 295-308.

Dick, H. J. B., Bullen, T., and Bryan, W. B., 1984. Mineralogic variatibility of the uppermost mantle along mid-ocean ridges. *Earth. Planet. Sci. Lett.*, **69,** 88-106.

Dobson, P. F., and O'Neil, J. R., 1987. Stable isotope compositions and water contents of boninites series volcanic rocks from Chichi-jima, Bonin islands, Japan. *Earth. Planet. Sci. Lett.*, **82,** 75-86.

Downes, H., and Dupuy, C., 1987. Textural, isotopic and REE variations in spinel peridotite xenoliths, Massif Central, France. *Earth. Planet. Sci. Lett.*, **82,** 121-135.

Downes, H., Embey-Isztin, E., and Thirlwall, M. F., 1992. Petrology and geochemistry of spinel peridotite xenoliths from the western Pannonian basin (Hungary): evidence for an association between enrichment and texture in the upper mantle. *Contrib. Mineral. Petrol.*, **109,** 340-354.

Draper, D. S., 1991. Spinel lherzolite nodules from Simcoe volcano, southeastern Washington: first mantle xenoliths from the Pacific northwest. *EOS*, **72,** 517.

Duncan, R. A., and Green, D. H., 1980. Role of multi-stage melting in the formation of oceanic crust. *Geology,* **8,** 22-36.

Duncan, R. A., and Green, D. H., 1987. The genesis of refractory melts in the formation of oceanic crust. *Contrib. Mineral. Petrol.*, **96,** 326-342.

Eckstrand, O. R., 1975. The Dumont serpentinite: a model for control of nickeliferous opaque mineral reactions in ultramafic rocks. *Econ. Geol.*, **70,** 183-201.

Eggins, S. M., 1992a. Petrogenesis of Hawaiin tholeiites: 1, phase equilibria constraints. *Contrib. Mineral. Petrol.*, **110,** 387-397.

Eggins, S. M., 1992b. Petrogenesis of Hawaiin tholeiites: 2, aspects of dynamic melt segregation. *Contrib. Mineral. Petrol.*, **110,** 398-410.

Eggler, D. H., 1987. Solubility of major and trace elements in mantle metasomatic fluids: experimental constraints. *In* (Menzies, M. A., and Hawkesworth, C. J., Eds.) *Mantle Metasomatism*, Academic Press, (London), 21-41.

Eggler, D. H., Fahlquist, D. A., and Herndon, J. M., 1973. Ultrabasic rocks from the Cayman Trough, Caribbean Sea. *Bull. Geol. Soc. Am.*, **84,** 2133-2138.

Ellam, R. M., and Hawkesworth, C. J., 1988. Elemental and isotopic variations in subduction related basalts: evidence for a three component model. *Contrib. Mineral. Petrol.*, **98,** 72-80.

Elliot, T. R., Hawkesworth, C. J., and Grönvold, K., 1991. Dynamic melting of the Iceland plume. *Nature*, **351,** 201-206.

Elthon, D., 1992. Chemical trends in abyssal peridotites: refertilization of depleted suboceanic mantle. *J. Geophys. Res.*, **97,** 9015-9025.

Engi, M., 1983. Equilibria involving Al-Cr spinel: Mg-Fe exchange with olivine: experiments, thermodynamic analysis and consequences for geobarometry. *Amer. J. Sci.*, **283-A,** 29-71.

Evans, B. W., and Frost, B. R., 1975. Chrome-spinel in progressive metamorphism - a preliminary analysis. *Geochim. Cosmochim. Acta*, **39,** 959-972.

Evans, C. A., and Girardeau, J., 1988. Galicia Margin peridotites: undepleted abyssal peridotites from the north Atlantic. *In*, Boillet G., Winterer, E. L., et al., *Proc. ODP, Sci. Results*, **103,** College Station, TX (Ocean Drilling Program), 195-207.

Fabries, J., 1979. Spinel-olivine geothermometry in peridotites from ultramafic complexes. *Contrib. Mineral. Petrol.*, **69,** 329-336.

Falloon, T. J., and Green, D. H., 1987. Anhydrous partial melting of MORB pyrolite and other peridotite compositions at 10 kb: implications for the origin of primative MORB glasses. *Miner. Petrol.*, **37,** 181-219.

Falloon, T. J., and Green, D. H., 1988. Anhydrous partial melting of peridotite from 8 to 35kb and the petrogenesis of MORB. *J. Petrol.*, Special lithosphere Issue, 379-414.

Fisk, M. R., 1986. Basalt magma interaction with harzburgite and the formation of high-magnesium andesites. *Geophys. Res. Lett.*, **13,** 467-470.

Foley, S. F., 1991. High-pressure stability of the fluor- and hydroxy-endmembers of pargasite and K-richterite. *Geochim. Cosmochim. Acta*, **55**, 2689-2694.

Foley, S. F., 1992. Vein-plus-wall-rock melting mechanisms in the lithosphere and the origin of potassic alkaline magmas. *Lithos* **28**, 435-453.

Freer, R., 1981. Diffusion in silicate minerals and glasses: a data digest and guide to the literature. *Contrib. Mineral. Petrol.*, **76**, 440-454.

Freer, R., Carpenter, M. A., Long, J. V. P., and Reed, S. J. B., 1982. "Null Result" diffusion experiments with diopsides: implications for pyroxene equilibria. *Earth. Planet. Sci. Lett.*, **58**, 285-292.

Frey, F. A., 1984. Rare earth element abundances in upper mantle rocks. *In* Henderson, P., (Ed.), *Rare earth element geochemistry*. Amsterdam, (Elsevier), 153-203.

Frey, F. A., and Green, D. H., 1974. The mineralogy, geochemistry and origin of some lherzolite inclusions in Victoria basanites. *Geochim. Cosmochim. Acta*, **38**, 1023-1059.

Frey, F. A., and Prinz, M., 1978. Ultramafic inclusions from San Carlos, Arizona: petrologic and geochemical data bearing on their petrogenesis. *Earth. Planet. Sci. Lett.*, **38**, 129-176.

Frey, F. A., Suen, C. J., and Stockman, H. W., 1985. The Ronda high temperature peridotite: geochemistry and petrogenesis. *Geochim. Cosmochim. Acta*, **49**, 2469-2491.

Fryer, P., 1992. A synthesis of Leg 125 drilling of serpentinite seamounts on the Mariana and Izu-Bonin forearcs. *In* Fryer, P., Pearce, J. A., Stokking, L. B., *et al.*, *Proc. ODP, Sci. Results*, **125**, College Station, TX (Ocean Drilling Program), 593-614.

Fryer, P., and Fryer, G. J., 1987. Origin of non-volcanic seamounts in a forearc envirnoment. *In* Keating, B., Fryer, P., Baliza, R. (Eds) *Seamounts, Islands and Atolls:* Washington (Am. Geophys. Union), Mono. Ser., **43**: 61-69.

Fryer, P., and Mottl., M. J., 1992. Lithology, mineralogy, and origin of serpentinite muds recovered from Conical and Torishima Forearc Seamounts: results of Leg 125 drilling. *In* Fryer, P., Pearce, J. A., Stokking, L. B., *et al.*, *Proc. ODP, Sci. Results*, 125: College Station, TX (Ocean Drilling program), 343-362.

Fryer, P., Ambos, E. L., and Hussong, D. M., 1985. Origin and emplacement of Mariana forearc seamounts. *Geology*, **13**, 774-777.

Fryer, P., Haggerty, J., Tilbrook, B., Sedwick, P., Johnson, L. E., Saboda, K. L., Newsom, S. Y., Karig, D. E., Uyeda, S., and Ishii, T., 1987. Results of Alvin studies of Mariana forearc serpentinite diapirism. *EOS. Trans. Am. Geophys. Union*, **68**, 1534. (Abstract).

Fryer, P., Saboda, K. L., Johnson, L. E., Mackay, M. E., Moore, G. F., and Stoffers, P., 1990. Conical Seamount: SeaMARC II, *ALVIN* submersible, and seismic-reflection studies. *In* Fryer, P., Pearce, J. A., Stokking, L. B., *et al.*, *Proc. ODP, Init. Results*, **125**, College Station, TX (Ocean Drilling Program), 69-80.

Fryer, P., Pearce, J. A., Stokking, L. B., et al., 1992. *Proc. ODP, Sci. Results*, 125: College Station, TX (Ocean Drilling program), 716 pp.

Fujii, N., Osamura, K., and Takahashi, E., 1986. Effect of water saturation on the distribution of partial melt in the olivine-pyroxene-plagioclase system. *J. Geophys. Res.*, **91**, 9253-9259.

Fujii, T., 1978. Fe-Mg partitioning between olivine and spinel. *Yb. Carnegie Inst. Wash.*, **77**, 563-569.

Gast, P. W., 1968. Trace element fractionation and origin of tholeiitic and alkaline magma types. *Geochim. Cosmochim. Acta*, **32**, 1057-1086.

Gibson, S. A., Thompson, R. N., Leat, P. T., Morrison, M. A., Hendry, G. L., Dickin, A. P., and Mitchell, J. G., 1993. Ultrapotassic magmas along the flanks of the Oligo-Miocene Rio Grande Rift, USA: monitors of the zone of lithospheric mantle extension and thinning beneath a continental rift. *J. Petrol*, **34**, 187-228.

Gill, J. B., 1981. *Orogenic Andesites and Plate Tectonics*. Springer-Verlag (New York), 390 pp.

Girardeau, J., and Lagabrielle, Y., 1992. Deformation history of peridotites from Mariana forearc, Conical Seamount, Leg 125. *In* Fryer, P., Pearce, J. A., Stokking, L. B., *et al.*, *Proc. ODP, Sci. Results*, **125**, College Station, TX (Ocean Drilling Program), 519-534.

Girardeau, J., Evans, C. A., and Beslier, M. -O., 1988. Structural analysis of plagioclase-bearing peridotites emplaced at the end of continental rifting: Hole 637A,

ODP Leg 103 on the Galicia Margin. *In*, Boillet G., Winterer, E. L., et al., *Proc. ODP, Sci. Results*, **103**, College Station, TX (Ocean Drilling Program), 209-223.

Green, D. H., 1973. Experimental studies on a model upper mantle composition at high pressure under water-saturated and water-undersaturated conditions. *Earth. Planet. Sci. Lett.*, **19**, 37-53.

Green, D. H., 1976. Experimental testing of "equilibrium" partial melting of peridotite under water-saturated, high-pressure conditions. *Can. Min.*, **14**, 255-268.

Green, D. H., and Hibberson, W., 1970. The instability of plagioclase in peridotite at high pressure. *Lithos*, **3**, 209-221.

Green, D. H., and Ringwood, A. E., 1970. Mineralogy of peridotitic compositions under upper mantle conditions. *Phys. Earth Planet. Int.*, **3**, 372-377.

Green, T. H., and Ringwood, A. E., 1968. Genesis of the calkalkaline igneous rock suite. *Contrib. Mineral. Petrol.*, **18**, 163-174.

Haggerty, J., 1987. Geochemistry of carbonate and silicate chimney structures from Conical Seamount collected during *Alvin* dive studies. *EOS*, **68**, 1534.

Hanson, G. N., and Langmuir, C. H., 1978. Modelling of major elements in mantle-melt systems using trace element approaches. *Geochim. Cosmochim. Acta*, **42**, 725-741.

Hart, S. R., and Zindler, A., 1986. In search of a bulk-earth composition. *Chem. Geol.*, **57**, 247-267.

Hart, S. R., and Reid, M. R., 1991. Rb/Cs fractionation: a link between granulite metamorphism and the S-process. *Geochim. Cosmochim. Acta*, **55**, 2379-2383.

Harte, B., 1977. Rock nomencalture with particular relation to deformation and recrystallisation textures in olivine-bearing xenoliths. *J. Geol.* **85**, 279-288.

Hawkesworth, C. J., O'Nions, R. K., Pankhurst, R. J., Hamilton, P. J., and Evenson, N. M., 1977. A geochemical study of island arc and back arc tholeiites from the Scotia Sea. *Earth. Planet. Sci. Lett.*, **36**, 253-263.

Hawkesworth, C. J., Gallagher, K., Hergt, J. M., and McDermott, F. M., 1993. Trace element fractionation processes in the generation of island arc basalts. *Phil. Trans. R. Soc. Lond.*, **A342**, 179-191.

Hickey, R. L., and Frey, F. A., 1982. Geochemical characteristics of boninite series volcanics: implications for their sources. *Geochim. Cosmochim. Acta*, **46,** 2009-2115.

Hickey-Vargas, R. L., 1989. Boninites and tholeiites from DSDP Site 458, Mariana forearc. *In* Crawford, A. J., (Ed.) *Boninites and Related Rocks*, Unwin, (London), 339-356.

Hofmann, A. W., 1980. Diffusion in silicate melts: a critical review. *In* Hargreaves, R. B., (Ed.) *Physics of Magmatic Processes*, Princeton University Press, (Princeton, New Jersey), 385-417.

Hofmann, A. W., and Hart, S. R., 1978. An assessment of local and regional isotopic equilibrium in the mantle. *Earth. Planet. Sci. Lett.*, **38,** 44-62.

Honza, E., and Tamaki, K., 1985. Bonin Arc. *In* Nairn, A. E. M., and Uyeda, S. (Eds.), *The Ocean Basins and Margins*, **Vol. 7.** *The Pacific Ocean:* New York (Plenum Press), 459-499.

Horine, R. L., Moore, G. F., and Taylor, B., 1990. Structure of the outer Izu-Bonin forearc from seismic-reflection profiling and gravity modeling. *In* Fryer, P., Pearce, J. A., Stokking, L. B., *et al.*, *Proc. ODP, Init. Results*, **125,** College Station, TX (Ocean Drilling Program), 81-94.

Huebner, J. S., and Nord, G. L., JR., 1981. Assessment of diffusion in pyroxenes: what we do and do not know. *Lunar Planet. Sci.*, **12,** 479-481.

Hussong, D. M., and Uyeda, S., 1981. Tectonic processes and the history of the Mariana Arc: A synthesis of the results of the Deep Sea Drilling Project Leg 60. *In* Hussong, D. M., Uyeda, S., et al. (Eds), *Init. Repts. DSDP*, **60,** Washington (U. S. Govt. Printing Office), 909-929.

Irvine, T. N., 1965. Chromian spinel as a petrogenetic indicator Part I: Theory. *Can. J. Earth Sci.*, **2,** 648-672.

Irvine, T. N., 1967. Chromian spinel as a petrogenetic indicator Part II: Petrological applications. *Can. J. Earth Sci.*, **4,** 71-103.

Irving, A. J., 1978. A review of experimental studies of crystal/liquid trace element partitioning. *Geochim. Cosmochim. Acta*, **42,** 743-770.

Ishii, T., 1985. Dredged samples from the Ogasawara forearc seamount or "Ogasawara Paleoland"-"forearc ophiolite". *In* Nasu, N., Kobayashi, K., Uyeda, S., Kushiro, I., and

Kagami, H., (Eds), *Formation of Active Ocean Margins*, Tokyo, (Terra Sci. Publ.), 307-342.

Ishii, T., Robinson, P. T., Maekawa, H., and Fiske, R., 1992. Petrological studies of peridotites from diapiric serpentinite seamounts in the Izu-Ogasawara-Mariana forearc, Leg 125. *In* Fryer, P., Pearce, J. A., Stokking, L. B., *et al.*, *Proc. ODP, Sci. Results*, 125: College Station, TX (Ocean Drilling Program), 445-486.

Iwamori, H., 1993. Dynamic disequilibrium melting model with porous flow and diffusion-controllled chemical equilibration. *Earth. Planet. Sci. Lett.*, **114,** 301-313.

Jagoutz, E., Palme, H., Baddenhausen, H., Blum, K., Cendales, M., Dreibus, G., Spettel, B., Lorenz, V., and Wänke, H., 1979. The abundance of major, minor, and trace elements in the earth's mantle as derived from primative ultramafic nodules. *Proc. Lunar. Planet. Sci. Conf.*, **10,** 2031-2050.

Jackson, E. D., 1969. Chemical variation in coexisting chromite and olivine in chromititic zones of the Stillwater comples. *Econ. Geol. Mono.*, **4,** 41-71.

Janecky, D. R., and Seyfreid, W. E., Jr., 1986. Hydrothermal serpentinization of peridotite within the oceanic crust: experimental investigations of mineralogy and major element chemistry. *Geochim. Cosmochim. Acta*, **50,** 1357-1378.

Jaques, A. L., and Chappell, B. W., 1980. Petrology and trace element geochemistry of the Papuan ultramafic belt. *Contrib. Mineral. Petrol.*, **75,** 55-70.

Jaques, A. L., and Green, D. H., 1980. Anhydrous melting of peridotite at 0-15kbar pressure and the genesis of tholeiitic basalts. *Contrib. Mineral. Petrol.*, **73,** 287-310.

Jochum, K. P., McDonough, W. F., Palme, H., and Spettel, B., 1989. Compositional constraints on the continental lithospheric mantle from trace elements in spinel peridotite xenoliths. *Nature*, **340,** 548-550.

Johnson, K. T. M., and Dick, H. J. B., 1992. Open system melting and temporal and spatial variation of peridotite and basalt at the Atlantis II fracture zone. *J. Geophys. Res.*, **97,** 9219-9241.

Johnson, K. T. M., Dick, H. J. B., and Shimizu, N., 1990. Melting in the oceanic upper mantle: an ion microprobe study of diopside in abyssal peridotites. *J. Geophys. Res.*, **95,** 2661-2678.

Johnson, L. E., 1992. Mafic clasts in serpentine seamounts: petrology and geochemistry of a diverse crustal suite from the outer Mariana forearc. *In* Fryer, P., Pearce, J. A., Stokking, L. B., *et al.*, *Proc. ODP, Sci. Results*, 125: College Station, TX (Ocean Drilling program), 401-413.

Johnson, L. E., and Fryer, P., 1988. Oceanic plate material on the Mariana forearc. *EOS. Trans. Am. Geophys. Union,* **69**, 1471.

Karig, D. E., 1975. basin genesis in the Philippine Sea. *In* Ingle, J. C., Karig D. E., et al., *Init. Repts. DSDP*, **31**: Washington (U. S. Govt. Printing Office), 857-879

Kay, R. W., and Senechal, R. G., 1976. The rare earth geochemistry of the Troodos ophiolite complex. *J. Geophys. Res.*, **81,** 964-970.

Kelemen, P. B., 1985. Assimilation of ultramafic rock in subduction-related magmatic arcs. *J. Geol.* **94,** 829-843.

Kelemen, P. B., 1990. Reaction between ultramafic rock and fractionating basaltic magma I. Phase relations, the origin of calc-alkaline magma series, and the formation of discordant dunite. *J. Petrol,* **31,** 51-98.

Kelemen, P. B., Joyce, D. B., Webster, J. D., and Holloway, J. R., 1990. Reaction between ultramafic rock and fractionating basaltic magma II. experimental investigation of reaction between olivine tholeiite and harzburgite at 1150-1050 °C and kb. *J. Petrol,* **31,** 99-134.

Kelemen, P. B., Johnson, K. T. M., Kinzler, R. J., and Irving, A. J., 1990. High-field-strength element depletions in arc basalts due to mantle-magma interaction. *Nature*, **345**, 521-524.

Kelemen, P. B., Dick, H. J. B., and Quick, J. E., 1992. Formation of harzburgite by pervasive melt/rock reaction in the upper mantle. *Nature*, **358**, 635-641.

Kempton, P. D., 1987. Mineralogic and geochemical evidence for differing styles of metasomatism in spinel lherzolite xenoliths: enriched mantle source regions of basalts? *In* (Menzies, M. A., and Hawkesworth, C. J., Eds.) *Mantle Metasomatism*, Academic Press, (London), 45-89.

Kenyon, P. M., 1990. Trace element and isotopic effects arising from magma migration beneath mid-ocean ridges. *Earth. Planet. Sci. Lett.*, **101,** 367-378.

Kimball, K. L., 1990. Effects of hydrothermal alteration on the compositions of chromian spinels. *Contrib. Mineral. Petrol.*, **105,** 337-346.

Kimball, K. L., Spear, F. S., and Dick, H. J. B., 1985. High temperature alteration of abyssal ultramafics from the Isla Orcadas Fracture Zone, South Atlantic. *Contrib. Mineral. Petrol.*, **91,** 307-320.

Kinzler, R. J., and Grove, T. L., 1992a. Primary magmas of mid-ocean ridge basalts 1. Experiments and methods. *J. Geophys. Res.*, **97,** 6885-6906.

Kinzler, R. J., and Grove, T. L., 1992b. Primary magmas of mid-ocean ridge basalts 2. Applications. *J. Geophys. Res.*, **97,** 6907-6926.

Klein, E. M., and Langmuir, C. H., 1987. Global correlation of ocean ridge basalt chemistry with axial depth and crustal thickness. *J. Geophys. Res.*, **92,** 8089-8115.

Klein, E. M., and Langmuir, C. H., 1989. Local versus global variations in ocean ridge basalt composition: a reply. *J. Geophys. Res.*, **94,** 4241-4254.

Kobayashi, K., 1989. *Preliminary Report of Hakuhu Maru Cruise KH87-3*, Ocean Res. Inst., Univ. of Tokyo, 304.

Kobayashi, K., and Nakada, M., 1979. Magnetic anomalies and tectonic evolution of the Shikoku inter-arc basin. *In* Uyeda, S., *et al.*, (Eds), *Advances in Earth and Planet. Sci.*, **6**: 391-402

Köhler, T. P., and Brey, G. P., 1990. Calcium exchange between olivine and clinopyroxene calibrated as a geothermobarometer for natural peridotites from 2 to 60 kb with appications. *Geochim. Cosmochim. Acta*, **54,** 2375-2388.

Komor, S. C., Grove, T. L., and Hégert, R., 1990. Abyssal peridotites from ODP Hole 670A (21°10'N, 45°02'W): residues of mantle melting exposed by non-constructive axial divergence. *In*, Detrick, R., Honnorez, J., Bryan, W. B., Juteau, T., et al., *Proc. ODP, Sci. Results*, **106/109,** College Station, TX (Ocean Drilling Program), 85-101.

Kornprobst, J., and Tabit, A., 1988. Plagioclase-bearing ultramafic tectonites from the Galicia Margin (Leg 103, Site 637): comparison of their origin and evolution with low-pressure ultramafic ultramafic bodies in western Europe. *In*, Boillet G., Winterer, E. L., et al., *Proc. ODP, Sci. Results*, **103,** College Station, TX (Ocean Drilling Program), 253-268.

Kostopoulos, D. K., 1991. Melting of the shallow upper mantle: a new perspective. *J. Petrol.* **32**, 671-699.

Kostopoulos, D. K., and James, S. D., 1992. Parameterization of the melting regime of the shallow upper mantle and the effects of variable lithospheric stretching on mantle modal stratification and trace element concentrations in magmas. *J. Petrol.* **33**, 665-691.

Kostopoulos, D. K., and Murton, B. J., 1992. Origin and distribution of components in boninite genesis: significance of the OIB component. *In* Parsons, L. M., Murton, B. J., and Browning, P., (Eds.), *Ophiolites and their Modern Analogues, Geol. Soc. Lond. Spec. Publ.*, **60**, 133-154.

Kramer, M. J., and Seifert, K. E., 1990. Strain enhanced diffusion in feldspars. *In* Ganguly, J., (Ed.), *Diffusion, Atomic Ordering, and Mass Transport: Selected topics in Geochemistry, Advances in Physical Geochemistry*, Volume **8**, Springer Verlag (New York), 286-303.

Langmuir, C. H., Bender, J. F., Bence, A. E., Hanson, G. N., and taylor, S. R., 1977. Petrogenesis of basalts from the FAMOUS area: Mid-Atlantic Ridge. *Earth. Planet. Sci. Lett.*, **36**, 133-156.

Leake, B. E., 1978. Nomenclature of amphiboles. *Am. Mineral.*, **63**, 1023-1052.

Loubet, M. N., Shimizu, N., and Allègre, C. J., 1975. Rare earth elements in alpine peridotites. *Contrib. Mineral. Petrol.*, **53**, 1-12.

MacGregor, I. D., 1965. Stability fields of spinel and garnet peridotite in the synthetic system MgO-CaO-$Al_2O_3$-$SiO_2$. *Yb. Carnegie Inst. Wash.*, **64**, 126-134.

MacGregor, I. D., 1970. The effect of CaO, $Cr_2O_3$, $Fe_2O_3$, and $Al_2O_3$ on the stability of spinel and garnet peridotites. *Phys. Earth Planet. Int.*, **3**, 372-377.

Macgregor, I. D., 1974. The system MgO-$Al_2O_3$-$SiO_2$: solubility of $Al_2O_3$ in enstatite for spinel and garnet peridotite compositions. *Am. Mineral.*, **59**, 110-119.

Maekawa, H., Shozui, M., Ishii, T., Saboda, K. L., and Ogawa, Y., 1992. Metamorphic rocks from the serpentinite seamounts in the Mariana and Izu-Bonin forearcs. *In* Fryer, P., Pearce, J. A., Stokking, L. B., *et al.*, *Proc. ODP, Sci. Results*, 125: College Station, TX (Ocean Drilling program), 415-443.

Mansolas, I., 1991. *Geochemistry and Petrogenesis of Peridotites, Pindos Ophiolite, NW Greece*. Unpublished Ph.D. thesis, University of Durham, UK.

Maury, R. C., Defant, M. J., and Joron, J. -L., 1992. Metasomatism of the sub-arc mantle inferred from trace elements in Philippine xenoliths. *Nature*, **360,** 661-663.

Mattoili, G. S., and Wood, B. J., 1988. Magnetite activities across the $MgAl_2O_4$ - $Fe_3O_4$ join, with application to thermobarometric estimates of upper mantle oxygen fugacity. *Contrib. Mineral. Petrol.*, **98,** 148-162.

Mattoili, G. S., Baker, M. B., Rutter, M. J., and Stolper, E. M., 1989. Upper mantle oxygen fugacity and its relationship to metasomatism. *J. Geol.*, **97,** 521-536.

McCallister, R. H., Brady, J. B., and Mysen, B. O., 1779. Self-diffusion of Ca in diopside. *Yb. Carnegie Inst. Wash.*, **78,** 574-577.

McDonough, W. F., 1991. Partial melting of subducted oceanic crust and isolation of its residual eclogitic lithology. *Phil. Trans. R. Soc. Lond.*, **A335,** 407-418.

McDonough, W. F., and Frey, F. A., 1989. Rare earth elements in upper mantle rocks. *In* Lipin, B. R., and McKay, G. A. (Eds.), *Geochemistry and mineralogy of rare earth elements*, Reviews in Mineralogy, **21,** 99-145.

McKenzie, D. P., 1984. The generation and compaction of partially molten rock. *J. Petrol*, **25,** 713-765.

McKenzie, D. P., 1985a. $^{230}Th$-$^{238}U$ disequilibria and the melting processes beneath ridge axes. *Earth. Planet. Sci. Lett.*, **72,** 149-157.

McKenzie, D. P., 1985b. The extraction of magma from the crust and mantle. *Earth. Planet. Sci. Lett.*, **74,** 81-91.

McKenzie, D. P., 1989. Some remarks on the movement of small melt fractions in the mantle. *Earth. Planet. Sci. Lett.*, **95,** 53-72.

McKenzie, D. P., and Bickle, M. J., 1988. The volume and composition of melt generated by extension of the lithosphere. *J. Petrol*, **29,** 625-679.

McKenzie, D. P., and O'Nions, R. K., 1991. Partial melt distributions from inversion of rare earth element concentrations. *J. Petrol*, **32,** 1021-1091.

Meen, J. K., Eggler, D. H., and Ayers, J. C., 1989. Experimental evidence for very low solubility of rare-earth elements in $CO_2$-rich fluids at mantle conditions. *Nature*, **340**, 301-303.

Meijer, A., 1983. The origin of low-K rhyolites from the Mariana frontal arc. *Contrib. Mineral. Petrol.*, **83**, 45-51.

Menzies, M. A., 1973. Mineralogy and partial melt textures within an ultramafic-mafic body, Greece. *Contrib. Mineral. Petrol.*, **42**, 273-285.

Menzies, M. A., 1991. Oceanic peridotites. *In* Floyd, P. A., (Ed.), *Oceanic Basalts*, Blackie, Glasgow, 363-385.

Menzies, M. A., and Allen, C., 1974. Plagioclase lherzolite residual mantle relationships within two eastern Mediterranean ophiolites. *Contrib. Mineral. Petrol.*, **45**, 197-213.

Menzies, M. A., Rodgers, N. W., Tindle, A., and Hawkesworth, C. J., 1987. Metasomatic and enrichment processes in lithospheric peridotites, an effect of asthenosphere-lithosphere interaction. *In* (Menzies, M. A., and Hawkesworth, C. J., Eds.) *Mantle Metasomatism*, Academic Press, (London), 313-361.

Mercier, J-C. C., 1976. Single-pyroxene geothermometry and geobarometry. *Am. Min.*, **61**, 603-615.

Mercier, J-C. C., 1980. Single pyroxene thermobarometry. *Tectonophysics* , **70**, 1-37.

Mercier, J-C. C., and Nicolas, A., 1975. Textures and fabrics of upper-mantle peridotites as illustrated by xenoliths from basalts. *J. Petrol.* **16**, 454-487.

Mercier, J-C. C., Benoit, V., and Giradeau, J., 1984. Eqilibrium state of diopside-bearing harzburgites from ophiolites: geobarometric and geodynamic implications. *Contrib. Mineral. Petrol.*, **85**, 391-403.

Michael, P. J., 1988. The concentration, behavior and storage of $H_2O$ in the suboceanic upper mantle: implications for mantle metasomatism. *Geochim. Cosmochim. Acta*, **52**, 555-566.

Mitchell, J. G., Peate, D. W., Murton, B. J., Pearce, J. A., Arculus, R. J., and van der Laan, S. R., 1992. K-Ar dating of samples from Sites 782 and 786 (Leg 125): the Izu-Bonin forearc region. *In* Fryer, P., Pearce, J. A., Stokking, L. B., *et al.*, *Proc. ODP, Sci. Results*, **125**, College Station, TX (Ocean Drilling program), 203-210.

Montigny, R., Bougault, H., Bottinga, Y., and Allègre, C. J., 1973. Trace element geochemistry and the genesis of the Pindus ophiolite suite. *Geochim. Cosmochim. Acta*, **37**, 2135-2147.

Moody, J. B., 1976. An experimental study on the serpentinization of iron-bearing olivines. *Can. Min,*, **14**, 462-478.

Morioka, M., 1980. Cation diffusion in olivine-I. Cobalt and magnesium. *Geochim. Cosmochim. Acta*, **44**, 759-762.

Morioka, M., 1981. Cation diffusion in olivine-II. Ni-Mg, Mn-Mg, Mg, and Ca. *Geochim. Cosmochim. Acta*, **45**, 1573-1580.

Morioka, M., 1981. Cation diffusion in olivine-III. $Mn_2SiO_4$ system. *Geochim. Cosmochim. Acta*, **47**, 2275-2279.

Morioka, M., and Nagasawa, N., 1990. Ionic diffusion in olivine. *In* Ganguly, J., (Ed.), *Diffusion, Atomic Ordering, and Mass Transport: Selected topics in Geochemistry, Advances in Physical Geochemistry*, Volume **8**, Springer Verlag (New York), 176-197.

Morse, S. A., 1980. Basalts and Phase Diagrams. Springer-Verlag, New York, 493 pp.

Mottl, M. J. 1992. Pore water waters from serpentinite seamounts in the Mariana and Izu-Bonin forearcs, Leg 125: evidence for volatiles from the subducting slab. *In* Fryer, P., Pearce, J. A., Stokking, L. B., *et al.*, *Proc. ODP, Sci. Results*, **125**, College Station, TX (Ocean Drilling program), 373-386.

Murton, B. J., Peate, D. W., Arculus, R. J., Pearce, J. A., and van der Laan, S. R., 1992. Trace-element geochemistry of volcanic rocks from Site 786: the Izu-Bonin forearc. *In* Fryer, P., Pearce, J. A., Stokking, L. B., *et al.*, *Proc. ODP, Sci. Results*, 125: College Station, TX (Ocean Drilling program), 211-235.

Myers, J., and Eugster, H. P., 1983. The system Fe-Si-O: oxygen buffer calibrations to 1500K. *Contrib. Mineral. Petrol.*, **82**, 75-90.

Mysen, B. O., and Kushiro, I., 1977. Compositional variations of coexisting phases with degree of melting of peridotite in the upper mantle. *Am. Min.*, **62**, 843-856.

Natland, J. H., and Tarney, J., 1981. Petrologic evolution of the Mariana arc and backarc basin system- a synthesis of drilling results in the South Philippine Sea. *In*

Hussong, D. M., Uyeda, S., et al. (Eds), *Init. Repts. DSDP*, **60**: Washington (U. S. Govt. Printing Office), 877-908.

Navon, O., and Stolper, E., 1987. Geochemical consequences of melt percolation: the upper mantle as a chromatographic column. *J. Geol.* **95,** 285-307.

Nell, J., and Wood, B. J., 1991. High temperature thermopower and electrical conductivity measurements on Cr-bearing spinels and development of a thermodynamic model. *Am. Mineral.*

Newman, S., and Van der Laan, S. R., 1992. Volatile contents of Izu-Bonin forearc volcanic glasses. *In* Fryer, P., Pearce, J. A., Stokking, L. B., *et al.*, *Proc. ODP, Sci. Results*, **125,** College Station, TX (Ocean Drilling program), 131-139.

Nickel, K. G., 1986. Phase equilibria in the system $SiO_2$-MgO-$Al_2O_3$-CaO-$Cr_2O_3$ (SMACCR) and their bearing on spinel/garnet lherzolite relationships. *Neus. Jahrb. Miner. Abh.*, **155,** 259-287.

Nicolas, A., 1986. Structure and petrology of peridotites: clues to their geodynamic environments. *Rev. Geophys.* **24,** 875-895.

Niu, Y., and Batiza, R., 1991. An empirical method for calculating melt compositions produced beneath mid-ocean ridges: application for axis and off-axis (seamounts) melting. *J. Geophys. Res.*, **96,** 21753-21777.

O'Hara, M. J., 1967. Mineral facies in ultramafic rocks. *In* Wyllie, P. J., (Ed.) *Ultramafic and Related Rocks*, Wiley, New York, 7-18.

O'Hara M. J., 1985. The importance of the "shape" of the melting regime during partial melting of the mantle. *Nature*, **314,** 58-62.

O'Hara, M. J., Richardson, S. W., and Wilson, G., 1971. Garnet-peridotite stability and occurrence in crust and mantle. *Contrib. Mineral. Petrol.*, **32,** 48-68.

O'Neill, H. St. C., 1981. The transition between spinel lherzolite and garnet lherzolite, and its use as a geobarometer. *Contrib. Mineral. Petrol.*, **77,** 185-194.

O'Neill, H. St. C., and Wall, V. J., 1987. The olivine-spinel oxygen goebarometer, the nickel precipitation curve and the oxygen fugacity of the upper mantle. *J. Petrol,* **28,** 1169-1192.

O'Nions, R. K., and Pankhurst, R. J., 1974. Petrogenetic significance of isotope and trace element variations in volvanic rocks from the Mid-Atlantic. *J. Petrol*, **15,** 603-634.

Obata, M., 1980. The Ronda peridotite: garnet-, spinel-, and plagioclase-lherzolite facies, and the P-T trajectories of a high-temperature mantle intrusion. *J. Petrol*, **21,** 533-572.

Onuma, N., Higuchi, H., Wakida, H., and Nagasawa, H., 1968. Trace element partitioning between two pyroxenes and host lava. *Earth. Planet. Sci. Lett.*, **5,** 47-51.

Ottonello, G., Piccard, G. B., and Ernst, W. G., 1979. Petrogenesis of some Lingurian peridotites-II. Rare earth element chemistry. *Geochim. Cosmochim. Acta*, **43,** 1273-1284.

Ozawa, K., 1983. Evaluation of olivine-spinel geothermometry as an indicator of thermal history for peridotites. *Contrib. Mineral. Petrol.*, **82,** 52-65.

Ozawa, K., 1988. Ultramafic tectonite of the Miyamori ophiolite complex in the Kitakami mountains, northeast Japan: hydrous upper mantle in an island arc. *Contrib. Mineral. Petrol.*, **99,** 159-175.

Pallister, J. A., and Knight, R. J., 1981. Rare earth element geochemistry of the Semail Ophiolite near Ibra, Oman. *J. Geophys. Res.*, **86,** 2673-2697.

Parkinson, I. J., Pearce, J. A., Thirlwall, M. F., Johnson, K. T. M., and Ingram, G., 1992a. Trace element geochemistry of peridotites from the Izu-Bonin-Mariana forearc, Leg 125. *In* Fryer, P., Pearce, J. A., Stokking, L. B., *et al., Proc. ODP, Sci. Results*, **125,** College Station, TX (Ocean Drilling program), 487-506.

Parkinson, I. J., Hall, G. E. M., Pearce, J. A., 1992b. Palladium, platinum, and gold distribution in serpentinite seamounts in the Mariana and Izu-Bonin forearcs: evidence from Leg125 fluids and serpentinites. *In* Fryer, P., Pearce, J. A., Stokking, L. B., *et al., Proc. ODP, Sci. Results*, **125,** College Station, TX (Ocean Drilling program), 507-518.

Peacock, S. M., 1987a. Serpentinization and infiltration metasomatism of the Trinity peridotite, Klamath province, northern California: implications for subduction zones. *Contrib. Mineral. Petrol.*, **95,** 55-70.

Peacock, S. M., 1987b. Thermal effects of metamorphic fluids in subduction zones. *Geology*, **15,** 1057-1060.

Peacock, S. M., 1989. Thermal modeling of metamorphic pressure-temperature-time paths: a forward approach. *Short Courses in Geology*, **7**, American Geophysical Union (Washington, D. C.), 57-102.

Peacock, S. M., 1991. Numerical simulation of subduction zone pressure-temperature-time paths: constraints on fluid production and arc magmatism. *Phil. Trans. R. Soc. Lond.*, **A335**, 341-353.

Pearce, J. A., 1982. Trace element characteristics of lavas from destructive plate boundaries. *In* Thorpe, R. S., (Ed.), *Andesites: Orogenic Andesites and Related Rocks*, John Wiley & Sons (New York), 525-546.

Pearce, J. A., 1983. Role of the sub-continental lithosphere in magma genesis at active plate margins. *In* Hawkesworth, C. J., and Norry, M. J., (Eds.), Shiva Publishing Limited, (Natwich), 230-249.

Pearce, J. A., Lippard, S. J., and Roberts, S., 1984. Characteristics and tectonic significance of supra-subduction zone ophiolites. *In* Kokelaar, B. P., and Howells, M. F. (Eds.), *Marginal Basin Geology, Geol. Soc. Lond. Spec. Publ.*, **16**, 77-94.

Pearce, J. A., Thirlwall, M. F., Ingram, G., Murton, B. J., Arculus, R. J., and van der Laan, S. R., 1992a. Isotopic evidence for the origin of boninites and related rocks drilled in the Izu-Bonin (Ogasawara) forearc, Leg 125. *In* Fryer, P., Pearce, J. A., Stokking, L. B., *et al.*, *Proc. ODP, Sci. Results*, **125**, College Station, TX (Ocean Drilling program), 237-261.

Pearce, J. A., van der Laan, S. R., Arculus, R. J., Murton, B. J., Ishii, T., Peate, D. W., and Parkinson, I. J., 1992b. Boninite and harzburgite from Leg 125 (Bonin-Mariana forearc): a case syudy of magma genesis during the initial stages of subduction. *In* Fryer, P., Pearce, J. A., Stokking, L. B., *et al.*, *Proc. ODP, Sci. Results*, 125: College Station, TX (Ocean Drilling Program), 623-674.

Pearce, J. A., and Parkinson, I. J., *in press*. Trace element models for mantle melting: applications to volcanic arc petrogenesis. *Ian Gass Memorial Volume*.

Plank, T., and Langmuir, C. H., 1988. An evaluation of the global variations in the major element chemistry of arc basalts. *Earth. Planet. Sci. Lett.*, **90**, 349-370.

Plank, T., and Langmuir, C. H., 1992. Effects of the melting regime on the composition of the oceanic crust. *J. Geophys. Res.*, **97**, 19748-19770.

Powell, R, 1978. Equilibrium Thermodynamics in Petrology. An Introduction. Harper and Row, London, 284 pp.

Prinzhofer, A., and Allègre, C. J., 1985. Residual peridotites and the mechanisms of partial melting. *Earth. Planet. Sci. Lett.*, **74,** 251-265.

Qin, Z., 1992. Disequilibrium partial melting model and its implications for trace element fractionations during mantle melting. *Earth. Planet. Sci. Lett.*, **112,** 75-90.

Quick, J., 1981. Petrology and petrogenesis of the Trinity peridotite, an upper mantle diapir in the eastern Klamath Mountains, northern California. *J. Geophys. Res.*, **86,** 11837-11864.

Rampone, E., Bottazi, P., and Ottolini, L., 1991. Complementary Ti and Zr anomalies in orthopyroxene and clinopyroxene from mantle peridotites. *Nature*, **354,** 518-520.

Rampone, E., Piccardo, G. B., Vannucci, R., Bottazzi, P., and Ottolini, L., *in press.* Subsolidus reactions monitered by trace element partitioning: the spinel- to plagioclase- facies transition in mantle peridotites. *Contrib. Mineral. Petrol.*

Reagan, M., and Meijer, A., 1984. Geology and geochemistry of early arc volcanic rocks from Guam. *Geol. Soc. Am. Bull.*, **95,** 701-713.

Richter, F. M., 1986. Simple models for trace element fractionation during melt segregation. *Earth. Planet. Sci. Lett.*, **77,** 333-344.

Roden, M. K., Hart, S. R., Frey, F. A., and Melson, W. G., 1984. Sr, Nd, and Pb isotopic and REE geochemistry of St. Paul's Rocks: the metamorphic and metasomatic development of an alkali basalt mantle source. *Contrib. Mineral. Petrol.*, **85,** 376-390.

Roeder, P. L., and Emslie, R. F., 1970. Olivine-liquid equilibrium. *Contrib. Mineral. Petrol.*, **29,** 275-289.

Roeder, P. L., Campbell, I. H., and Jamieson, H. E., 1979. A re-evaluation of the olivine-spinel geothermometer. *Contrib. Mineral. Petrol.*, **68,** 325-334.

Rucklidge, J. C., 1972. Chlorine in partially serpentinized dunite. *Econ. Geol.*, **67,** 38-40.

Rucklidge, J. C., and Patterson, G. C., 1977. The role of chlorine in serpentinization. *Contrib. Mineral. Petrol.*, **65,** 39-44.

Sakai, R., Kusuakabe, M., Noto, M., and Ishii, T., 1990. Origin of waters responsible for serpentinization of the Izu-Ogasawara-Mariana forearc seamounts in view of hydrogen and oxygen isotope ratios. *Earth. Planet. Sci. Lett.*, **100,** 291-303.

Salters, V. J. M., and Shimizu, N., 1988. World-wide occurence of HFSE-depleted mantle. *Geochim. Cosmochim. Acta.*, **52,** 2177-2182.

Sawyer, E. W., 1991. Disequilibrium melting and the rate of melt-residuum separation during migmatization of mafic rocks from the Greville Front, Quebec. *J. Petrol*, **32,** 701-738.

Scott, D. R., and Stevenson, D. J., 1989. A self-consistent model of melting, magma migration and buoyancy-driven circulation beneath mid-ocean ridges. *J. Geophys. Res.*, **94,** 2973-2988.

Seitz, M. G., 1973. Uranium and thorium diffusion in diopside and fluoroapitite. *Yb. Carnegie Inst. Wash.*, **72,** 586-588.

Seno, T., Moriyama, T., and Stern, S., 1987. Redetermination of Philippine Sea plate motion. *EOS. Trans. Am. Geophys. Union,* **68**: 1474. (Abstract).

Shaw, D. M., 1970. Trace element fractionation during anatexis. *Geochim. Cosmochim. Acta*, **34,** 237-243.

Shcherbakov, S. A., and Savelyeva, G. N., 1984. Structures of ultramafic rocks of the Mariana Trench and the Owen Fracture Zone. *Geotectonics*, **18,** 159-167.

Shervais, J. W., 1982. Ti-V plots and the petrogenesis of modern and ophiolitic lavas. *Earth. Planet. Sci. Lett.*, **59,** 101-118.

Shibata, T., and Thompson, G., 1986. Peridotites from the mid-atlantic ridge at 43°N and their petrogenetic relation to abyssal tholeiites. *Contrib. Mineral. Petrol.*, **93,** 144-159.

Shipboard Scientific Party, 1990a. Site 778. *In* Fryer, P., Pearce, J. A., Stokking, L. B., *et al.*, *Proc. ODP, Init. Results*, 125: College Station, TX (Ocean Drilling Program), 97-114.

Shipboard Scientific Party, 1990b. Site 779. *In* Fryer, P., Pearce, J. A., Stokking, L. B., *et al.*, *Proc. ODP, Init. Results*, 125: College Station, TX (Ocean Drilling Program), 115-145.

Shipboard Scientific Party, 1990c. Site 780. *In* Fryer, P., Pearce, J. A., Stokking, L. B., *et al.*, *Proc. ODP, Init. Results*, 125: College Station, TX (Ocean Drilling Program), 147-178.

Shipboard Scientific Party, 1990d. Site 783. *In* Fryer, P., Pearce, J. A., Stokking, L. B., *et al.*, *Proc. ODP, Init. Results*, 125: College Station, TX (Ocean Drilling Program), 253-272.

Shipboard Scientific Party, 1990e. Site 784. *In* Fryer, P., Pearce, J. A., Stokking, L. B., *et al.*, *Proc. ODP, Init. Results*, 125: College Station, TX (Ocean Drilling Program), 273-305.

Shipboard Scientific Party, 1990f. Explanatory Notes. *In* Fryer, P., Pearce, J. A., Stokking, L. B., *et al.*, *Proc. ODP, Init. Results*, 125: College Station, TX (Ocean Drilling Program), 15-40.

Sinton, J. M., 1979. Petrology of alpine-type peridotites from site 395, DSDP Leg 45. *In* Melson, W. G., Rabinowitz, P. D., et al., *Init. Repts., DSDP*, 45, Washington (U. S. Govt., Printing Office), 595-602.

Sobolev, A. V., and Shimizu, N., 1991. The direct evidence for existence of ultra-depleted melts in the oceanic mantle: SIMS data on the composition of melt inclusion in olivine from MORB. *EOS*, **72,** 544-545.

Sneeringer, M., Hart, S. R., and Shimizu, N., 1984. Strontium and samarium diffusion in diopside. *Geochim. Cosmochim. Acta*, **48,** 1589-1608.

Spear, F. S. 1989. Petrological determination of metamorphic pressure-temperature-time paths. *Short Courses in Geology*, **7,** American Geophysical Union (Washington, D. C.), 1-55.

Spiegelman, M., 1993. Physics of melt extraction: theory, implications and applications. *Phil. Trans. R. Soc. Lond.*, **A342,** 23-41.

Spiegelman, M., and McKenzie, D. P., 1987. Simple 2-D models for melt segregation at mid-ocean ridges and island arcs. *Earth. Planet. Sci. Lett.*, **83,** 137-152.

Spiegelman, M., and Kenyon, P., 1992. The requirements for chemical disequilbrium during magma migration. *Earth. Planet. Sci. Lett.*, **109,** 611-620.

Stern, R. J., Smoot, N. C., and Rubin, M., 1984. Unzipping of the volcanic arc, Japan. *Tectonophysics*, **102**: 153-174.

Stern, R. J., Morris, J., Bloomer, S. H., and Hawkins, J. W., 1991. The source of the subduction component in convergent margin magmas: trace element and radiogenic isotope evidence from Eocene boninites. *Geochim. Cosmochim. Acta*, **55**, 1467-1481.

Stolper, E. M., and Newman, S., *in press*. The role of water in the petrogenesis of Mariana Trough Magmas. *Earth. Planet. Sci. Lett.*

Stosch, H. -G., 1981. Sc, Cr, Co and Ni partitioning between inerals from spinel peridotite xenoliths. Mattoili, G. S.,Stosch, H. -G., 1982. Rare earth element partioning between minerals from anhydrous spinel peridotite xenoliths. *Geochim. Cosmochim. Acta*, **46**, 793-811.

Stosch, H., -G., and Seck, H. A., 1980. Geochemistry and mineralogy of two spinel peridotite suites from Dreiser Weiher, West Germany. *Geochim. Cosmochim. Acta*, **44**, 457-470.

Streckeisen, A. L., 1976. To each plutonic rock its proper name. *Earth-Sci. Rev.*, **12**, 1-33.

Stroh, J. M., 1976. Solubility of alumina in orthopyroxene plus spinel as a geobarometer in complex systems. Applications to spinel-bearing Alpine-type peridotites. *Contrib. Mineral. Petrol.*, **54**, 173-188.

Sudo, A., and Tatsumi, Y., 1990. Phlogopite and K-amphibole in the upper mantle: Implications for magma genesis in subduction zones. *Geophys. Res. Lett.*, **17**, 29-32.

Suen, C. J., Frey, F. A., and Malpas, J., 1979. Bay of Islands ophiolite suite, Newfoundland: petrologic and geochemical characteristics with emphasis on the rare earth element geochemistry. *Earth. Planet. Sci. Lett.*, **45**, 337-348.

Sun, S. -s., and Nesbitt, R. W., 1978. Geochemical regularities and genetic significance of ophiolitic basalts. *Geology*, **6**, 689-693.

Sun, S. -s., and McDonough, W. F., 1989. Chemical and isotopic systematics of oceanic basalts: implications for mantle composition and processes. *In* Saunders, A. D., and Norry, M. J., (eds.), *Magmatism in the Ocean Basins. Geol. Soc. Lond. Spec. Publ.*, **42**, 313-345.

Taira, A., and Pickering, K. T., 1991. Sediment deformation and fluid activity in the Nanlai, Izu-Bonin and Japan forearc slopes. *Phil. Trans. R. Soc. Lond.*, **A335**, 341-353.

Takahashi, E., 1980. Thermal history of lherzolite xenoliths-I. Petrology of lherzolite xenoliths from the Ichinomegata crater, Oga peninsula, northeast Japan. *Geochim. Cosmochim. Acta*, **44,** 1643-1658.

Takahashi, E., and Kushiro, I., 1983. Melting of a dry peridotite at high pressures and basalt magma genesis. *Am. Min.*, **68,** 859-879.

Takahashi, N., 1992. Evidence for melt segregation towards fractures in the Horoman mantle peridotie complex. *Nature*, **359,** 53-55.

Takazawa, E., Frey, F. A., Shimizu, N., Obata, M., and Bodinier, J. -L., 1992. geochemical evidence for melt migration and reaction in the upper mantle. *Nature*, **359,** 55-58.

Tatsumi, Y., 1989. Migration of fluid phases and genesis of basalt magmas in subduction zones. *J. Geophys. Res.*, **94,** 4697-4707.

Tatsumi, Y., 1991. Origin of subduction zone mamas based on experimental petrology. *In* Perchuk, L.L., and Kushiro, I., (Eds.), *Physical Chemistry of Magmas, Advances in Physical Geochemistry*, Volume **9,** Springer Verlag (New York), 268-301.

Tatsumi, Y., and Nakamua, N., 1986. Composition of aqueous fluid from serpentinite in the subducted lithosphere. *Geochem. J.*, **20,** 191-196.

Tatsumi, Y., and Isoyama, H., 1988. Transportation of beryllium with $H_2O$ at high pressures: implications for magma genesis in subduction zones. *Geophys. Res. Lett.*, **15,** 180-183.

Tatsumi, Y., Sakuyama, M., Fukuyama, H., and Kushiro, I., 1983. Generation of arc basalt magmas and thermal structure of the mantle wedge in subduction zones. *J. Geophys. Res.*, **88,** 5815-5825.

Tatsumi, Y., Hamilton, D. L., and Nesbitt, R. W., 1986. Chemical characteristics of fluid phase released from a subducted lithosphere and the origin of arc magmas: evidence from high-pressure experiments and natural rocks. *J. Volcan. Geotherm. Res.* **29,** 293-309.

Taylor, B., 1992. Rifting and the volcanic-tectonic evolution of the Izu-Bonin-Mariana Arc. *In* Taylor, B., Fujioka, K., *et al.*, *Proc. ODP, Sci. Results*, **126,** College Station, TX (Ocean Drilling Program), 627-651.

Taylor, R. N., Lapierre, H., Vidal, P., Nesbitt, R. W., and Croudace, I. W., 1992. Igneous geochemistry and petrogenesis of the Izu-Bonin forearc basin. *In* Taylor, B., Fujioka, K., *et al.*, *Proc. ODP, Sci. Results*, **126,** College Station, TX (Ocean Drilling Program), 405-430.

Thirlwall, M. F., 1982. A triple-filament method for the rapid and precise analysis of rare-earth elements by isotope dilution. *Chem. Geol.*, **35,** 155-166.

Trommsdorff, V., and Evans, B. W., 1974. Alpine metamorphism of peridotite rocks. *Schweiz. Mineral. Petrogr. Mitt.*, **54,** 333-354.

Turner, F. J., and Verhoogen, J., 1960. *Igneous and Metamorphic Petrology*, McGraw-Hill (New York), 672pp.

van der Laan, S. R., Flower, M. F. J., and koster van Groos, A. F., 1989. Experimental evidence for the origin of boninites: near-liquidus phase relations to 7.5 kbar. *In* Crawford, A. J., (Ed.) *Boninites and Related Rocks*. Unwin, (London), 112-147.

van der Wal, D. 1993. Deformation processes in Mantle Peridotites. *Geologica Ultraiectina,* **No.102,** 180pp.

Vasseur, G., Vernières, J., and Bodinier, J. -L., 1991. Modelling of trace element transfer between mantle melt and heterogranular peridotite matrix. *J. Petrol.*, Special Lherzolite Issue, 41-54.

Viereck, L. G., Flower, M. F. J., Hertogen, J., Schminke, H. U., and Jenner, G. A., 1989. The genesis and significance of N-MORB sub-types. *Contrib. Mineral. Petrol.*, **102,** 112-126.

Virgo, D., Luth, R. W., Moats, M. A., and Ulmer, G. C., 1988. Constraints on the oxidation state of the mantle: an electrochemical and $^{57}$Fe Mössbauer study of mantle-derived ilmenites. *Geochim. Cosmochim. Acta*, **52,** 1781-1794.

von Seckendorff, V., and O'Neill, H. St. C., 1993. An experimental study of Fe-Mg partitioning between olivine and orthopyroxene at 1173, 1273 and 1423 K and 1.6 GPa. *Contrib. Mineral. Petrol.*, **113,** 196-207.

Waff, H. S., and Bulau, J. R., 1979. Equilibrium fluid distribution in an ultramafic partial melt under hydrostatic stress conditions. *J. Geophys. Res.*, **84,** 6109-6114.

Walker, D. A., and Cameron, W. E., 1983. Boninite primary magmas: evidence from the Cape Vogel Peninsula, PNG. *Contrib. Mineral. Petrol.*, **83,** 150-158.

Wallace, M. E., and Green, D. H., 1991. The effect of bulk rock composition on the stability of amphibole in the upper mantle: implications for solidus positions and mantle metasomatism. *Miner. Petrol.*, **44,** 1-19.

Watson, E. B., and Baker, D. R., 1991. Chemical diffusion in magmas; an overview of experimental results and geochemical applications. *In* Perchuk, L.L., and Kushiro, I., (Eds.), *Physical Chemistry of Magmas, Advances in Physical Geochemistry*, Volume **9,** Springer Verlag (New York), 120-151.

Wells, P. R. A., 1977. Pyroxene thermometry in simple and complex systems. *Contrib. Mineral. Petrol.*, **62,** 129-139.

Wicks, F. J., and Whittaker, E. J. W., 1977. Serpentine textures and serpentinization. *Can. Min.*, **15,** 459-488.

Williams, R. W., and Gill, J. B., 1989. Effects of partial melting on the uranium decay series. *Geochim. Cosmochim. Acta*, **53,** 1607-1619.

Witt-Eickschen, G., and Seck, H. A., 1991. Solubility of Ca and Al in orthopyroxenes from spinel peridotites: an improved version of an empirical geothermometer. *Contrib. Mineral. Petrol.*, **106,** 431-439.

Wood, B. J., 1990. An experimental test of the spinel peridotite oxygen barometer. *J. Geophys. Res.*, **95,** 15845-15851.

Wood, B. J., 1991. Oxygen barometry of spinel peridotites. *In* Lindsley, D. H., (Ed.), *Oxide Minerals: Petrologic and Magnetic Significance.* Reviews in Mineralogy, **25,** 417-431.

Wood, B. J., and Banno, S., 1973. Garnet-orthopyroxene and orthopyroxene-clinopyroxene relationships in simple and complex systems. *Contrib. Mineral. Petrol.* , **42,** 109-124.

Wood, B. J., and Virgo, D., 1989. Upper mantle oxidation state: ferric iron contents of lherzolite spinels by $^{57}$Fe Mössbauer spectroscopy and resultant oxygen fugacities. *Geochim. Cosmochim. Acta*, **53,** 1277-1291.

Wood, B. J., Bryndzia, L. T., and Johnson, K. E., 1990. Mantle oxidation state and its relationship to tectonic environment and fluid speciation. *Science*, **248,** 337-345.

Wood, D. A., 1979. Dynamic partial melting: its application to the petrogenesis of basalts erupted in Iceland, the Faeroe Islands, the Isle of Skye (Scotland) and the Troodos Massif (Cyprus). *Geochim. Cosmochim. Acta*, **43**, 1031-1046.

Yund, R. A., Smith, B. M., and Tullis, J., 1981. Dislocation-assisted diffusion of oxygen in albite. *Phys. Chem. Minerals*, **7**, 185-189.

Zindler, A., and Hart, S. R., 1986. Chemical Geodynamics. *Ann. Rev. Earth. Planet. Sci.*, **14**, 493-571.

Zipfel, J., and Wörner, G., 1992. Four- and five-phases peridotites from a continental rift system: evidence for upper mantle uplift and cooling at the Ross Sea margin (Antartica). *Contrib. Mineral. Petrol.*, **111**, 24-36.

# Appendix A
# Analytical Techniques

During the period of research, several major changes have occurred in the facilities for sample preparation and geochemical analysis at Durham University, including the installation of new crushing and milling equipment, the purchase of the Philips X40 Alpha on-line software for the XRF and the building of two new geochemistry laboratories.

## A.1 Sample Preparation

Samples for this study were prepared in several ways. A number of the samples were prepared on the *Joides Resolution* for shipboard X-ray Fluorescence (XRF) analysis. Samples on the *Joides Resolution* are usually crushed in a Spex 8510 Shatterbox, using a tungsten carbide barrel (Shipboard Scientific Party 1990e). However, because of the Ta and W contamination produced by this technique, and the fact that many of the shipboard powders were going to be analysed onland for these elements, most of the samples were crushed using an agate-lined barrel. Although the shipboard analyst stated the crushing history of each of the samples, it was found that running the samples for W by ICP-MS was the easiest way of telling how the samples were crushed. Crushing in the tungsten carbide barrel not only produces Ta and massive W contamination, but also seems to produce some minor Nb contamination, as samples which had been crushed in tungsten carbide showed contamination of up to 0.2 ppm in the rock.

All the rest of the ODP samples, plus all the samples collected from California and Troodos were prepared in Durham. Samples were washed before crushing to remove any extraneous material and were then crushed in a Fritsch Pulverisette jaw crusher (type 01-704). To avoid any cross contamination from other peoples samples, the jaw crusher was scrupulously cleaned before any crushing took place with a wire brush and absolute alcohol. The plates for the jaw crusher were cleaned thoroughly between each sample, and no one else was allowed to crush samples during the period that the peridotites were being crushed. Because of the small size of the ODP samples, only 30-60g of samples was usually crushed. Samples were then milled in agate pots in a Frisch agate ball mill tema for about 10-15 minutes until a fine powder was produced.

Samples from Ronda were either crushed, or crushed and milled at the University of Grenada, Spain. These samples were prepared by first cutting of the surface alteration with a diamond saw to leave the apparently fresher cores, and then washed with distilled water in an ultrasonic bath. The samples were then crushed in a hardened-iron jaw-crusher. Half the samples were milled at the University of Grenada in a ring mill made of titanium carbide. The other half of the samples were milled in agate at the University of Durham as above.

### A.2 X-ray Fluorescence (XRF)

All the samples were analysed for major and some trace elements by XRF at the University of Durham, using fusion discs. Powders were first heated at 900 °C for two hours in porcelain crucibles to derive the loss on ignition (LOI). Fusion discs were prepared by weighing accurately 0.45g ±0.001g of the LOI powder, followed by 2.25g ±0.001g of dried lithium metaborate and lithium tetraborate (Spectroflux 100B) into a platinum crucible. After thorough mixing the powder, the crucibles were placed in a furnace set at 1050 °C for 20 minutes. This was deemed long enough for the Cr-spinels to dissolve in the flux, but not too long to drive of the volatile elements such as sodium. The molten mixture was then poured into moulds on a hot plate set at 250°C. The mixture was quenched with a metal plunger, and then left to cool for 20 minutes before being labelled, bagged and stored in a desiccator.

Pressed powder pellets were made by roughly measuring out 9g of samples, adding 10 drops or less of Mowiol binder, thoroughly mixing and then pressing for 15 seconds at 10-15bars. The pellets are dried at 110°C and labelled and bagged.

Elements were measured on a Philips PW 1500 spectrometer with a Rhodium anode tube. Because of the very low concentrations of the incompatible elements, long count times where employed for these elements. For elements like Ti a count time of 200 seconds were used. For the minor elements Mn, Ca and Al count times of 100 seconds were used. Because there are very few good low level standards, peridotites from the Ojen Massif where used as calibration standards as we have good trace element analyses for these samples by ICP-MS. These samples were especially useful for the low level dtermination of Zr, Y and Nb. For the major element runs an internal monitor was run every six samples to check for drift in MgO and $SiO_2$. This monitor was run over a period of 18 months and its composition is accurately known. For trace element runs the standard PCC-1 and three of the Ojen samples were run as monitors.

### A.3 Inductively Coupled Plasma Mass Spectrometry (ICP-MS)

Ti, Rb, Sr, Y, Zr, Nb, La, Ce and Yb were analysed by inductively coupled plasma mass spectrometry on a VG Elemental Plasmaquad at Durham. Samples of 0.1±0.001g were digested with 4ml of 48% hydrofluoric acid and 1 ml of nitric acid in a Savillex bomb for 24 hr. The samples were evaporated to dryness and then taken up in 1 ml of nitric acid and again evaporated to dryness. A further 1 ml of nitric was added and the product again evaporated to dryness to effect quantitative removal of the hydrofluoric acid and form nitrate salts. The samples were redissolved with 20 ml of deionised water and 2,5 ml of nitric acid and boiled for 1 hr. The cooled solutions were spiked with 1.25 ml of a 2-ppm Rh, Re and Bi spike solution and made up accurately to 50 ml. The samples were run on a VG Elemental Plasmaquad with long peak dwell times (320 ms per mass unit) over the the mass unit range 84 to 105. Calibration is done manually and involves a drift correction, a blank correction and calibration using international standards. Detection limits for Ti, Rb, Sr, Y, Zr, Nb, La, Ce and Yb are 0.5, 0.03, 0.01, 0.02, 0.02, 0.02, 0.02 and 0.02 ppm respectively, as calculated as an average blamk plus ten times the standard deviation of the blank (approximately three times the average blank). Precision is estimated at about 10% at ten times the detection limit. Accuracy is better than 20% with respect to the recommended values of the USGS standard PCC-1. Detection limits for Sc, Cr, V, Ni and Co are all less than 1 ppm, well below their concentrations in the peridotites.

### A.4 Isotope Dilution REE Analysis

Because of their very low concentrations in the Leg 125 peridotites, the REE were analysed by isotope dilution mass spectrometry. The USGS standard, PCC-1, a depleted harzburgite also having low REE values, was included in the run to provide an independent check on the accuracy of our analyses. These analyses were conducted using a VG 354, 5 collector mass spectrometer at the Department of Geology, Royal Holloway and Bedford New College, University of London. The technique is, with slight modifications, that described by Thirlwall (1982) and is described below.

0.03 g of mixed very dilute REE spike was added to 0.2 g of sample, which was then digested with 8 ml of 40% hydrofluoric and 4 ml 15 *M* nitric acid in a Savillex bomb for 36 hours. The solutions were then evaporated to dryness. As found by other analysers of ultrabasic rocks (e.g. Prinzhofer and Allègre, 1985), the Cr-spinels resisted dissolution and left a small black residue in all cases. However, Cr-spinels have the lowest REE concentrations of minerals in ultramafic rocks (Stosch, 1982), and make up less than 1% of the peridotites. This residue is unlikely to have any significant effect

on the bulk rock concentrations. The solutions were dissolved in a 75% acetic acid, 25% 5 *M* nitric acid mixture, centrifuged and loaded onto the first of the ion-exchange columns, washed with a 90% acetic acid, 10% 5 *M* nitric acid mixture and eluted with 0.05 *M* nitric acid. To remove Ba and other impurities, the resulting solutions were loaded onto a second set of smaller diameter columns and collected in the same manner as that previously described. These solutions were evaporated to dryness and taken up in 1 mL of ultra-high quality water. The solutions then were loaded onto the two outside filaments of a Ta-Re-Ta triple bead assembly, and analysed for REEs using a multi-collector mass spectrometer (Thirlwall, 1982).

After the first set of samples were run in December 1990, it was decided to run a blank through the whole of the REE analysis procedure, as it was thought that the blank could make up a significant proportion of the concentration measured in the actual sample. All the samples were blank corrected using this procedure blank.

The PCC-1 standard, a depleted harzburgite that has low REE values was included in the run to provide an independent check on the accuracy of the analyses. The values for PCC-1 are lie within he published range of values for this standard. However, we had difficulty in reproducing the Eu value despite obtaining apperently good values on the unknown samples. The reason for this is not known.

**A.5 Ion Microprobe Analysis**

*In situ* trace element analyses of discrete mineral phases in polished thin section were carried out on a Cameca IMS-3f ion microprobe at Tsukuba University, Japan, by Dr Kevin Johnson. Clinopyroxene, orthopyroxene and olivines were chosen, mainly on the basis of freshness and size by observation under a petrographic microscope, and the polished samples were then evaporation-coated with gold to a thickness of approximately 20 nm for analysis. Measurements were made with a 10-20 na primary beam of mass filtered $^{16}O^-$ accelerated to 14.5 keV and focused to a 20μm (for Ti, V, Cr, Sr, and Zr measurements) or a 40μm (for REE and Hf) spot diameter. Energy filtering of secondary positive ions was employed to eliminate isobaric molecular ion interferences: secondary ions of REE and Hf were accelerated to 4.44 keV (energy filter of -60 eV), while secondary ions of the other elements were accelerated to 4.41 keV (energy filter of -90 eV). The exit slit was adjusted to its maximum opening corresponding to a mass resolution ($m/\Delta m$) of ~500. Secondary ions were detected by a 17-stage electron multiplier in pulse counting mode and the energy bandpass of the secondary ion analyser was adjusted to ± 10 eV.

Secondary ion intensities were measured for 10 to 15 seconds each on the peak tops of isotopes $^{30}Si$, $^{51}V$, $^{52}Cr$, $^{88}Sr$, $^{90}Zr$, $^{140}Ce$, $^{146}Nd$, $^{147}Sm$, $^{153}Eu$, $^{163}Dy$, $^{174}Yb$, and $^{180}Hf$, run in ascending sequence by changing the magnetic field stepwise. The sequence was repeated 10 to 20 times per point, depending on the count rates encountered. Average elemental intensity ratios against $^{30}Si$ were calculated based on 10 to 20 sets of doubly time-interpolated ratios for each element at each analysis point. Concentrations were determined using empirical relationships between secondary ion intensity ratios and concentration (working curves) established for mineral and glass standards. Accuracy of the concentrations reported in the thesis is primary a function of the working curves, which generally have been determined to ±1%-10% uncertainty, but are higher for Dy and Hf. The most important uncertainty in the measurements is the counting error, which, at the lower abundance's encountered, can be quite high; Analysis of some of Kevin Johnson's samples has been carried out on both the ion microprobe at Tsukuba University and on the ion microprobe at the Massachusetts Institute of Technology (MIT), the results being very similar (Kevin Johnson, pers. comm. 1991).

### A.6 X-ray Diffraction (XRD)

Serpentine samples where run on the Phillips XRD in the Department of Geological Sciences, Durham using a copper tube. Serpentine samples were crushed in an agate pessle and mortar and then spread on to a glass slide in acetone using some nichrome wire.

# Appendix B
# Values

This appendix gives details of all the values used in the thesis. These include terms such as magnesium number (Mg#) and site allocation of cations for calculation in geothermometres and geobarometres and values for chondrite normalisation.

## B.1 Chondrite Normalisation Values

1. REE normalising values used in this thesis are from Boynton (1984).

| | |
|---|---|
| La | 0.310 |
| Ce | 0.808 |
| Pr | 0.122 |
| Nd | 0.600 |
| Sm | 0.195 |
| Eu | 0.0735 |
| Gd | 0.259 |
| Tb | 0.0474 |
| Dy | 0.322 |
| Ho | 0.0718 |
| Er | 0.210 |
| Tm | 0.0324 |
| Yb | 0.209 |
| Lu | 0.0322 |

## B.2 Cation Site Allocation

Much of the geothermometry and geobarometry used in chapter x relies on the accurate assignment of cations to their sites within the minerals. This most strongly applies to two pyroxene geothermobarometry.

### B.2.1 M1 and M2 Site Allocation in Pyroxenes.

The formula for both ortho- and clinopyroxenes is (Mg, Fe, Ca, Mn, Na, Ti, Cr, Al)$_2$ (Si, Al)$_2$ O$_6$. Pyroxenes have three sites for the cations within their structure. A tetrahedral site occupied by the Si and some Al and two octahedral sites, M1 and M2. The M2 site is the larger and so is occupied by the large cations Ca, Na and Mn plus some Fe and Mg. The smaller M1 site is occupied by Ti, Cr and the Al not occupied on the tetrahedral site plus the remaining Fe and Mg (Wood and Banno, 1973). After the microprobe analysis of a pyroxene has been converted to a six oxygen basis the sum of the cations should be four. The formula for the pyroxene can be then written as (Ti, Cr, Al, Fe, Mg)$^{M1}$ (Ca, Na, Mn, Fe, Mg)$^{M2}$ (Si, Al)$_2^{TET}$ O$_6$. The pyroxene geothermometres based on Fe-Mg exchange between ortho- and clinopyroxene such as Wood and Banno (1973) and Wells (1977) rely on knowledge of the Mg allocated to the M1 and M2 sites. Follows is a simple method for calculating the site occupancy of Mg and $Fe^{2+}$ on the M1 and M2 sites in pyroxenes similar to the one presented in Powell (1978). The first assumption is that the Fe/Mg ratio on the sites is the same as the ratio of the mineral such that

$$\frac{Fe^{2+}}{Mg}M1 = \frac{Fe^{2+}}{Mg}M2 = \frac{Fe^{2+}}{Mg}Mineral$$

The number of cations allocated to the tetrahedal site is two so the Al on the tetrahedral site is

$$Al^{IV} = 2 - Si$$

and the Al on the M1 site is

$$Al^{VI} = Al - (2 - Si)$$

the total number of cation allocated to the M1 site is one so

$$1 = Fe^{2+} + Mg + Ti + Cr + Al^{VI}$$

substituting eq x and rearranging for the amount of Fe and Mg to be allocated leaves

$$Fe + Mg = 1 - Ti - Cr - (Al - (2 - Si))$$

which simplifies to leave

$$Fe + Mg = 3 - Ti - Cr - Al - Si$$

the Fe and Mg must be assigned in the same Fe/Mg ration as XFe/XMg so

$$MgM1 = \frac{3 - Ti - Cr - Al - Si}{\frac{Fe}{Mg} + 1}$$

and

$$FeM1 = \frac{3 - Ti - Cr - Al - Si}{\frac{Mg}{Fe} + 1}$$

from this it follows that the Mg and Fe on the M2 sites area as follows

$$MgM2 = Mg - MgM1$$

and

$$FeM2 = Fe\text{-}FeM1$$

**B.3 Mg#**

Magnesium numbers for peridotites from XRF data are calculated by the following equation.

$$Mg\# = \frac{\frac{MgO}{40.3}}{\frac{MgO}{40.3} + 0.95\frac{Fe_{tot}}{79.80}}$$

# Appendix C
# Calculations

## Melting Equations

The following section reproduces melting equations from the literature as well as some new equations derived during the course of this study. For completness equations for both modal and non-modal melting are given. Table 1 gives definitions of the symbols used throughout the equations.

## Equilibrium Batch Melting

Shaw (1970) gives expressions for both modal and non-modal equilibrium batch melting. For modal melting the composition of the liquids is given by the equation

$$C^L = \frac{C_0}{D_0 + F(1 - D_0)} \tag{C1}$$

the composition of the residual solid is simply

$$C_X^S = D_X C_X^L \tag{C2}$$

but can be written as the continuous expression

$$C^S = \left[\frac{D_0 - D_0 F}{1 - F}\right]\left[\frac{C_0}{D_0 + F(1 - D_0)}\right] \tag{C3}$$

the composition of any of the residual minerals is given by

$$C^{min} = C_0\left[\frac{D^{min/l}}{D_0 + F(1 - D_0)}\right] \tag{C4}$$

| | |
|---|---|
| $C^L$ | The concentration of an element in a liquid. |
| $C_X^L$ | The concentration of an element in a liquid after $X$ degrees of partial melting. |
| $\overline{C^l}$ | The concentration of an element an aggregated liquid. |
| $C^{min}$ | Concentration of an element in a mineral. |
| $C_0^{min}$ | Initial concentration of an element in a mineral. |
| $C_X^{min}$ | Concentration of an element in a mineral after $X$ degrees of partial melting. |
| $C_0$ | The initial concentration of an element in the solid. |
| $C^S$ | The concentration of an element in a solid. |
| $C_X^S$ | The concentration of an element in the residue after $X$ degrees of partial melting. |
| $D_0$ | The initial bulk distribution coeffecient of an element in the solid. |
| $D^{min/l}$ | The distribution coeffecient of an element between mineral and liquid. |
| $D_X$ | The bulk distribution coeffecient after $X$ degrees of partial melting. |
| $F$ | The degree of partial melting. |
| $f$ | Mass of fluid fraction in the pore space. |
| $I$ | The mass fraction of the liquid in each melting increment. |
| $n$ | The number of solid phases. |
| $\phi$ | Porosity or fluid fraction (by volume). |
| $P_0$ | The initial bulk distribution coeffecient of the solids entering the melt phase. |
| $P_X$ | The bulk distribution coeffecient of the solids entering the melt phase after $X$ degrees of partial melting. |
| $\rho_f$ | Density of the fluid. |
| $\rho_s$ | Density of the solid. |
| $v_e$ | Melt extraction rate. |
| $v_m$ | Melting rate. |
| $X_M^{min}$ | Mass fraction of a mineral in the residue. |
| $X_P^{min}$ | Mass fraction of mineral entering the melt phase. |

**Table C1**. Table of symbols used in the equations in this section.

for some types of modelling the following form may be more useful

$$C^{min} = C_0^{min}\left[\frac{D_0}{D_0 + F(1-D_0)}\right] \quad \text{(C5)}$$

For non-modal melting the compostion of the liquid is given by

$$C^L = \frac{C_0}{D_0 + F(1-P_0)} \quad \text{(C6)}$$

The composition of the solid is simply equation A2 or can be written as the continuous equation

$$C^S = \left[\frac{D_0 - P_0F}{1-F}\right]\left[\frac{C_0}{D_0 + F(1-P_0)}\right] \quad \text{(C7)}$$

Johnson et al. (1990) derived equations for the composition of the residual minerals during equilibrium batch melting

$$C^{min} = C_0\left[\frac{D^{min/l}}{D_0 + F(1-P_0)}\right] \quad \text{(C8)}$$

for some types of modelling equation A6 of Johnson et al. (1990) maybe more useful

$$C^{min} = C_0^{min}\left[\frac{D_0}{D_0 + F(1-P_0)}\right] \quad \text{(C9)}$$

**Fractional melting**

Again Shaw (1970) gives expressions for both modal and non-modal fractional melting. For modal melting the composition of the instantaneous liquid is given by

$$C^L = \frac{C_0}{D_0}[1-F]\left[\frac{1}{D_0} - 1\right] \quad \text{(C10)}$$

and the composition of the aggregated liquids by

$$\overline{C^l} = \frac{C_0}{F}\left[1-(1-F)^{\left(\frac{1}{D_0}\right)}\right] \tag{C11}$$

the composition of the solid is simply equation C2 or can be written in the continuous form as

$$C^S = C_0(1-F)^{\left(\frac{1}{D_0}-1\right)} \tag{C12}$$

the composition of any residual mineral is given by

$$C^{\min} = C_0[1-F]^{\left[\frac{1}{D_0}\right]}\left[\frac{D^{\min/l}}{D_0 - D_0F}\right] \tag{C13}$$

or for types of modelling may be written as

$$C^{\min} = C_0^{\min}[1-F]^{\left[\frac{1}{D_0}-1\right]} \tag{C14}$$

For non-modal melting the composition of the liquid is given by

$$C^L = \frac{C_0}{D_0}\left[1-\frac{P_0F}{D_0}\right]^{\left[\frac{1}{P_0}-1\right]} \tag{C15}$$

For aggregated fractional liquids after any degree of melting

$$\overline{C^l} = \frac{C_0}{F}\left[1-\left(1-\frac{P_0F}{D_0}\right)^{\frac{1}{P}}\right] \tag{C16}$$

the solid is simply equation C2 again or can be written in a continuous form as

$$C^S = \frac{C_0}{1-F}\left[1-\frac{P_0F}{D_0}\right]^{\frac{1}{P_0}} \qquad \text{(C17)}$$

Johnson et al. (1990) derive equations for the composition of the minerals in the residue as follows

$$C^{\min} = C_0\left[1-\frac{P_0F}{D_0}\right]^{\frac{1}{P_0}}\left[\frac{D^{\min/l}}{D_0-P_0F}\right] \qquad \text{(C18)}$$

for some modelling equation A4 of Johnson et al. (1990) maybe more useful

$$C^{\min} = \left[1-\frac{P_0F}{D_0}\right]^{\left[\frac{1}{P_0}-1\right]} \qquad \text{(C19)}$$

**Disequilibrium Melting**

Prinzhofer and Allègre (1985) derive equations for disequilibrium melting which involve melting through three different peridotite facies. Simpler equations for melting in one facies (i.e. a single $P_0$ and $D_0$ are used) are presented here. The concentration of an element in the liquid is simply a function of the melting mode and independent of the degree of melting and is given by

$$C^L = \sum_{i=1}^{i=n} X_{Pi}^{\min} C_{0i}^{\min} \qquad \text{(C20)}$$

The concentration of an element in the original mineral is simply given by

$$C_0^{\min} = C_0\frac{D^{\min/l}}{D_0} \qquad \text{(C21)}$$

Expression C20 can be simplified by substituting equation C21 into equation C20 to obtain

$$C^L = \frac{C_0 P_0}{D_0} \tag{C22}$$

The concentration of an element in the residue is dependent on the degree of melting and is given by

$$C^S = \sum_{i=1}^{i=n} X_{Mi}^{\min} C_{0i}^{\min} \tag{C23}$$

This expression for the residue can be written in a continuous form by rearranging the mass balance equation for $C^S$ to give

$$C^S = \frac{C_0 - \left(\frac{C_0 P_0}{D_0}\right) F}{1 - F} \tag{C24}$$

Obviously as the minerals melt out with their own composition the concentration of an element in any mineral is independent of F and will always equal the original composition as defined by equation X.

**Incremental Melting**

Wood (1979) derived equations for this type of melting. Essentially equation C1 is used but is incremented over the the mass fraction of interest. The concentration in the residual solid after each increment is taken as the starting composition for the next melt increment. This type type of modelling is most easily done with a simple computer program which can iterate the calculation over whatever increment is needed. The composition of the instantaneous liquid is given by the equation

$$C_X^L = \frac{C_{X-1}^S}{D_X + I(1 - D_X)} \tag{C25}$$

where for the first increment $C_{X-1}^S = C_0$ and $D_X = D_0$. The concentration of the aggregate liquid is simply the sum of the instantaneous liquids divided by the number of increments (degrees of partial melting).

$$\overline{C^l} = \frac{1}{F}\sum_{i=0}^{i=F} C_{Xi}^{L} \tag{C26}$$

the residue is simply equal to equation C2. The concentration in a residual mineral is

$$C_X^{\min} = C_{X-1}^{S}\left[\frac{D^{\min/l}}{D_X + l(1-D_X)}\right] \tag{C27}$$

or some types of modelling the form

$$C_X^{\min} = C_{X-1}^{\min}\left[\frac{D_X}{D_X + l(1-D_X)}\right] \tag{C28}$$

**Dynamic Melting**

McKenzie (1985) gives descriptions of equations for what he describes as dynamic melting. This type of melting is best described as melting with a residual porosity. After using McKenzie's equations it became apparent that there are problems with mass balancing the system, a point which Qin (1992) has also recently shown. The composition of the instaneous liquids (dynamic) is given by the expression

$$C^L = GC_0(1-F)^{G(1-D_0)} \tag{C29}$$

the composition of the aggregate (continuous) liquids

$$\overline{C^l} = \frac{1}{F}GC_0\left[\frac{1-(1-F)^{G(1-D_0)+1}}{G(1-D_0)+1}\right] \tag{C30}$$

the composition of the residue is given by

$$C^S = GC_0(1-F)^{G(1-D_0)} \tag{C31}$$

where $G$

$$G = \frac{\rho_f\varphi + \rho_s(1-\varphi)}{\rho_f\varphi + \rho_s(1-\varphi)D_0} \tag{C32}$$

**Melting with Diffusion**

Qin (1992) has recently described a melting model in which the diffusion of elements through the melting minerals is taken into account. He terms this type of melting disequilibrium melting although in practice it is very different to the disequilibrium melting that Bedard (1989) describes. Qin argues that because the melting rate of minerals in the mantle is likely to be rapid compared with solid diffusion rate of elements through the mineral grains it is unlikely that the distribution of elements between liquid and solid will be described by Qin describes a simple system in which a spherical mineral grain melts at a given rate, $v_m$, and the melt is extracted at a given rate, $v_e$.

To model melting with with diffusion in the mineral grains the problem has to be solved numerically and can be readily accomplished using finite difference methods which are described in detail below.

**Finite Difference Modelling**

Qin (1992) shows that the solutions he derives can be solved analytically when either the melting rate greatly exceeds the diffusion rates, when the solutions simplify to disequilibrium modal melting, or when the diffusion rates greatly exceed the melting rates when the solutions simplify to modal equilibrium batch melting equations. However, for many elements in the mantle these end member conditions are not met, and solutions need to be solved numerically. Qin (1992) solves his modal melting solutions using a Crank-Nicolson finite difference method, whereas I solve similar non-modal melting solutions using explicit finite difference methods. Details of these solutions and the finite difference methods are shown below for completness.

**Explicit Finite Difference Models**

Peacock (1989) gives details of finite difference models used in thermal modelling of metamorphic Pressure-Temperature-time (P-T-t) paths. The equations used for the thermal modelling contain thermal diffusivity terms which describe the transfer of heat through solids. In practice the thermal diffusivity terms can be changed to chemical diffusivity terms and the equations can be used to describe the movement of elements through mineral grains.

For ease of computing an explicit finite difference method has been used to compute the concentrations of elements in the mantle minerals during melting. The grains of

mantle minerals are assumed to be spherical. Crank (1947) defines the equation for diffusion in a sphere by the following expression

$$\frac{\partial C^S}{\partial t} = \kappa\left(\frac{\partial^2 C^S}{\partial r^2} + \frac{2}{r}\frac{\partial C^S}{\partial r}\right) \qquad \text{(C33)}$$

For ease of computing this expression has been simplified to the linear flow equation, (C37) which describes the one-dimensional, time-dependant transfer of an element through a solid

$$\frac{\partial C^S}{\partial t} = \kappa\frac{\partial^2 C^S}{\partial x^2} \qquad \text{(C34)}$$

from this equation forward, backward and central difference equations for first order derivatives can be approximated from the continuous partial differential equation. Also a central difference equation for second order derivatives can be derived. This equation is the basis of the explicit finite difference modelling and is reproduced in equation (C38). This is similar to equation (13) of Peacock (1989).

$$\frac{\partial^2 C^S}{\partial x^2} = \frac{C^S_{i+1} - 2C^S_i + C^S_{i-1}}{(\Delta x)^2} + O\left\{(\Delta x)^2\right\} \qquad \text{(C35)}$$

In the explicit finite difference method a time and distance dependent equation is derived from the forward and backward difference first order derivative equations and the central difference second order derivative equations to give an equation of the form

$$\frac{C^{Sn+1}_i - C^S_i}{\Delta t} = \kappa\left[\frac{C^{Sn}_{i+1} - 2C^{Sn}_i + C^{Sn}_{i+1}}{(\Delta x)^2}\right] + O\left\{\Delta t, (\Delta x)^2\right\} \qquad \text{(C36)}$$

this is equavalent to equation (14) of Peacock (1989). The subscripts describe spatial grid points and the superscripts describe time grid points. By rearranging equation (A**) and dropping the truncation error yields equation (C40) which is similar to equation (15) of Peacock (1989)

$$C_i^{Sn+1} = C_i^{Sn} + \kappa\Delta t\left[\frac{C_{i+1}^{Sn} - 2C_i^{Sn} + C_{i-1}^{Sn}}{(\Delta x)^2}\right] \quad \text{(C37)}$$

which expresses the concentration of an element at point i after one time step $\left(C^{Sn+1}\right)$ as a function of concentrations at neighbouring points at the beginning of the time step $\left(C^{Sn}\right)$. When using explicit finite difference equations the size of the time step $(\Delta t)$ is very important to keep the calculations mathematically stable. Peacock (1989) defines the limits of the stability of the equations by

$$\Delta t \leq \frac{1}{2}\frac{(\Delta x)^2}{\kappa} \quad \text{(C38)}$$

thus for a mineral grain of 0.5 cm divided into a hundred grid points and a diffusion rate of $10^{-10}$ $cm^2s^{-1}$ the maximum time step equals 0.396yr so a time step of 0.3yr is used.

In both mine and Qin's (1992) model the initial condition is

$$C^S(r,0) = C_0 \text{and} 0 \leq r \leq R_0 \quad \text{(C39)}$$

and the boundary conditions are that

$$C^S(0,t) = \text{finite} \quad \text{(C40)}$$

and

$$C_b = D_x C^L(t) \quad \text{(C41)}$$

The grain radius, R(t) changes with time by the relationship

$$R(t) = R_0\left(1 - \frac{V_m t}{V_0}\right)^{\frac{1}{3}} \quad \text{(C42)}$$

which simplifies to

$$R(t) = R_0(1 - vt)^{\frac{1}{3}} \tag{C43}$$

where $V_0$, the initial volume equals

$$V_0 = \frac{4}{3}\pi R_0^3 \tag{C44}$$

and v, a normalised melting rate, equals

$$v = \frac{V_m}{V_0} \tag{C45}$$

Qin (1992) defines the concentration of the instantaneous (residual) melt with time as

$$\frac{d(V^L C^L)}{dt} = -4\pi R^2 \kappa \frac{\partial C^s}{\partial r}\Big|_{r=R(t)} + v_m C_b - v_e C^L \tag{C46}$$

and the concentration of the segregated melt with time as

$$\overline{C^l}(t) = \frac{1}{V^l}\int_0^t v_e C^L(t)dt \tag{C47}$$

**Kelemen Models**

Models developed by Kelemen and co-workers (Kelemen, 1985; Kelemen, 1990; Kelemen et al., 1990; Kelemen et al., 1992) model the interaction between basaltic melts and peridotite wall rock using the approach of DePaolo's 1981 assimilation-fractional crystallization (AFC) models. It is not always apparent what Kelelmen actually computes in his papers-the Kelemen et al., (1992) *Nature* paper is littered with typographic errors in the table of values he uses in his calculations. The following section tries to clarify the exact nature of the calculations.

DePaolo (1981) derived a series of equations which describe a magma chamber in which both the magma can crystallization phases and assimilate the wallrock. The solutions for the equations can be seperated into two forms, ones where the rate of wallrock assimilated ($M_a$) equals the rate of phases crystallizing ($M_c$) and ones where

$M_a$ does not equal $M_c$ and the magma mass either decreases or increases. The equations have limitation in that they use constant $D$ values for the crystallizing phases and the concentration of the assimilant ($C_a$) stays constant. To get round this fact the equations can be iterrated over small steps so that $D$ and $C_a$ may be varied. For the simply case where the ratio $M_a/M_c$ equals one an adjusted version of equation (3) from DePaolo (1981) is used

$$C_m = C_{m-1}\left[\left(\frac{C_a}{DC_{m-1}}\right)\left[1-\exp\left(\frac{-DM_a}{M_m}\right)\right]+\exp\left(\frac{-DM_a}{M_m}\right)\right] \qquad \text{(C48)}$$

For the case where the ratio $M_a/M_c$ does not equal one an adjusted version of equation (6a) from DePaolo (1981) is used

$$C_m = C_{m-1}\left[F^{-z}+\left(\frac{r}{r-1}\right)\frac{C_a}{zC_{m-1}}\left(1-F^{-z}\right)\right] \qquad \text{(C49)}$$

where the ratio $r = M_a/M_c$ is a constant and

$$z = \frac{r+D-1}{r-1} \qquad \text{(C50)}$$

and $F$ is the relative mass of the magma remaining which depends on the value of $r$ and step used in the iteration.

Follows is a step by step approach to doing one of the calculations. One of the common reactions Kelemen et al., (1992) describes is the reaction of lherzolite with melt to form harzbugite plus a modified liquid. At its simplest form this involves the assimilation of clinopyroxene and the precipitation of olivine and orthopyroxene. In fact in Kelemen et al., (1992) his "best fit" reaction is more complicated with assimilation of clinopyroxene and spinel and the precipitation of olivine and orthopyroxene and a value for $r$ of about 0.97. In the simple case the the phase proportions of the lherzolite are adjusted for each step so that the $P$ for clinopyroxene equals -1 and $P$ for olivine and orthopyroxene equals 1 (in Kelemen's calculations about five times as much olivine is precipitated with respect to orthopyroxene). The $D$ values are calculated for the proportion of olivine and orthopyroxene crystallizing and usually stays constant in the calculations. $C_a$ is the concentration of the clinopyroxene

from the previous step. For each step the concentration of the bulk peridotite can be calculated by mass balance (assuming a closed system) and the new concentration of the phases in the peridotite may calculated from equation (C21), in the case of the clinopyroxene becoming the new value for $C_a$.

# Appendix D
# Major and Trace Element Data

The following section gives the major and trace element composition of the bulk-rock peridotites. The major element data and some of the trace element data are from XRF. The low level trace element data (e.g., Nb, Y, Zr, Cs, Ba) are by ICP-MS. The REE analyses are by ID-MS as is the U and Th data. Many of the elements are the average of both ICP-MS and XRF runs.

# Appendix D

| Hole | 778A | 778A | 778A | 778A | 778A | 778A | 778A | 778A | 778A | 778A |
|---|---|---|---|---|---|---|---|---|---|---|
| Core | 1R-2 | 1R-3 | 1R-4 | 2R-1 | 2R-1 | 2R-1 | 3R-CC | 3R-CC | 5R-1 | 7R-2 |
| Interval | 0-5 | 15-20 | 135-140 | 20-25 | 81-84 | 89-92 | 1-7 | 4-7 | 7-10 | 14-22 |
| Rock | s. mud | s. mud | s. mud | s. mud | s.t. harz | s.t. harz | s.t. harz | s.t. harz | met. bas. | p. s. |
| SiO2 | 42.86 | 42.84 | 39.61 | 42.16 | 45.68 | 43.62 | 46.59 | 46.10 | 58.99 | 44.24 |
| TiO2 | 0.054 | 0.033 | 0.068 | 0.143 | 0.011 | 0.009 | 0.022 | 0.019 | 0.330 | 0.011 |
| Al2O3 | 0.89 | 0.78 | 1.00 | 2.73 | 0.33 | 0.09 | 1.31 | 1.04 | 14.98 | 0.68 |
| Fe2O3 | 8.11 | 7.86 | 7.46 | 8.19 | 7.61 | 8.27 | 8.36 | 8.59 | 8.66 | 8.26 |
| MnO | 0.09 | 0.10 | 0.13 | 0.13 | 0.12 | 0.13 | 0.12 | 0.11 | 0.17 | 0.11 |
| MgO | 44.43 | 40.51 | 38.08 | 40.22 | 42.87 | 42.89 | 41.61 | 42.42 | 7.36 | 44.77 |
| CaO | 0.63 | 4.90 | 10.16 | 2.98 | 2.36 | 4.23 | 0.89 | 0.72 | 3.14 | 0.74 |
| Na2O | 0.885 | 1.396 | 0.948 | 1.378 | 0.135 | 0.258 | 0.163 | 0.091 | 6.122 | 0.263 |
| K2O | 0.124 | 0.058 | 0.046 | 0.161 | 0.032 | 0.023 | 0.038 | 0.028 | 0.202 | 0.034 |
| P2O5 | 0.023 | 0.019 | 0.026 | 0.042 | 0.036 | 0.025 | 0.014 | 0.009 | 0.046 | 0.017 |
| NiO | 0.30 | 0.28 | 0.28 | 0.26 | 0.38 | 0.44 | 0.31 | 0.33 | 0.01 | 0.29 |
| Cr2O3 | 0.42 | 0.38 | 0.39 | 0.33 | 0.41 | 0.13 | 0.45 | 0.38 | 0.02 | 0.41 |
| Total | 98.81 | 99.15 | 98.19 | 98.73 | 99.96 | 100.09 | 99.87 | 99.84 | 100.00 | 99.83 |
| LOI | 20.26 | 19.08 | 20.24 | 16.17 | 12.12 | 15.95 | 11.65 | 12.26 | 1.88 | 16.17 |
| Mg# | 91.95 | 91.49 | 91.41 | 91.10 | 92.15 | 91.54 | 91.21 | 91.15 | 63.92 | 91.87 |
| Sc | | | | | | | | | | |
| Ti | 151.4 | 137.8 | 272.7 | 647.2 | 18.8 | 15.9 | 81.5 | 64.3 | 1828.6 | 12.2 |
| V | 18.9 | 19.5 | 25.9 | 37.8 | 22.7 | 16.6 | 42 | 35.6 | 186.5 | 26.9 |
| Cr | 2840 | 2612 | 2658 | 2289 | 2796 | 865 | 3097 | 2605 | 105 | 2805 |
| Co | 85.5 | 62.6 | 73.4 | 78.8 | 110.5 | 122.8 | 108.2 | 110.2 | 40.6 | 91.1 |
| Ni | 2326 | 2201 | 2169 | 2007 | 3008 | 3439 | 2399 | 2571 | 65 | 2291 |
| Cu | 2.5 | 5.3 | 5.9 | 14.4 | 0.0 | 2.5 | 7.5 | 4.3 | 294.8 | 0.0 |
| Zn | 47.0 | 41.6 | 142.6 | 162.4 | 33.6 | 37.0 | 39.6 | 36.4 | 55.0 | 29.6 |
| Ga | | | | | | | | | | |
| Rb | | | | | | | | | | 0.08 |
| Sr | 13.2 | 1058.2 | 1426 | 111.9 | 310.6 | 642.2 | 5.6 | 5.6 | 52 | 4.8 |
| Y | | | | | | | | | | |
| Zr | | | | | | | | | | |
| Nb | | | | | | | | | | |
| Cs | | | | | | | | | | |
| Ba | | | | | | | | | | |
| La | | | | | | | | | | |
| Ce | | | | | | | | | | |
| Nd | | | | | | | | | | |
| Sm | | | | | | | | | | |
| Eu | | | | | | | | | | |
| Gd | | | | | | | | | | |
| Dy | | | | | | | | | | |
| Er | | | | | | | | | | |
| Yb | | | | | | | | | | |
| Lu | | | | | | | | | | |
| Th | | | | | | | | | | |
| U | | | | | | | | | | |

# Appendix D

| Hole | 778A | 778A | 778A | 778A | 778A | 778A | 778A | 778A | 778A | 778A |
|---|---|---|---|---|---|---|---|---|---|---|
| Core | 7R-CC | 8R-1 | 8R-1 | 9R-CC | 11R-1 | 11R-1 | 11R-1 | 12R-2 | 13R-1 | 13R-1 |
| Interval | 7-13 | 36-44 | 41-44 | 9-12 | 0-3 | 5-8 | 50-55 | 43-45 | 9-12 | 12-14 |
| Rock | s.t. harz | s.t. harz | s.t. harz | met. bas. | serp. | serp. | p. s. | s.t. harz | met. bas. | met. bas. |
| SiO2 | 43.53 | 41.14 | 41.01 | 48.20 | 46.78 | 45.31 | 44.74 | 45.26 | 44.91 | 44.34 |
| TiO2 | 0.010 | 0.011 | 0.013 | 0.977 | 2.290 | 0.128 | 0.088 | 0.012 | 1.206 | 1.178 |
| Al2O3 | 0.97 | 0.89 | 0.80 | 16.20 | 6.59 | 2.31 | 1.79 | 0.89 | 12.94 | 13.20 |
| Fe2O3 | 9.21 | 9.67 | 10.08 | 8.63 | 18.81 | 11.09 | 11.06 | 9.83 | 12.75 | 11.61 |
| MnO | 0.15 | 0.20 | 0.19 | 0.18 | 0.26 | 0.12 | 0.12 | 0.09 | 0.26 | 0.25 |
| MgO | 44.96 | 46.60 | 46.57 | 7.33 | 10.95 | 36.25 | 37.88 | 42.74 | 6.89 | 16.29 |
| CaO | 0.09 | 0.13 | 0.12 | 12.80 | 9.53 | 2.58 | 2.33 | 0.11 | 18.13 | 11.02 |
| Na2O | 0.304 | 0.145 | 0.103 | 1.576 | 4.219 | 0.942 | 0.842 | 0.103 | 2.317 | 1.208 |
| K2O | 0.072 | 0.014 | 0.015 | 3.146 | 0.022 | 0.060 | 0.038 | 0.014 | 0.323 | 0.844 |
| P2O5 | 0.011 | 0.010 | 0.010 | 0.087 | 0.266 | 0.019 | 0.026 | 0.006 | 0.126 | 0.120 |
| NiO | 0.40 | 0.39 | 0.39 | 0.01 | 0.05 | 0.36 | 0.37 | 0.40 | 0.01 | 0.01 |
| Cr2O3 | 0.48 | 0.50 | 0.52 | 0.02 | 0.02 | 0.52 | 0.55 | 0.51 | 0.03 | 0.04 |
| Total | 100.18 | 99.70 | 99.83 | 99.15 | 99.78 | 99.69 | 99.82 | 99.96 | 99.88 | 100.09 |
| LOI | 14.27 | 16.74 | 17.25 | 5.65 | 2.94 | 4.99 | 13.01 | 12.31 | 5.38 | 7.55 |
| Mg# | 91.05 | 90.95 | 90.60 | 63.91 | 54.82 | 87.20 | 87.72 | 90.06 | 52.98 | 74.53 |
| Sc | | | | | | | | 10.65 | | |
| Ti | 13.4 | 16.8 | 15.7 | 5083.8 | 12534.9 | | 328.3 | 19.8 | | 6301.9 |
| V | 38.1 | 41.5 | 38.8 | 224.4 | 427.7 | | 33.9 | 46 | | 222.2 |
| Cr | 3258 | 3417 | 3550 | 132 | 124 | 3584 | 3729 | 3487 | 177 | 247 |
| Co | 125.5 | 123.8 | 123.2 | 43.9 | 72.9 | | 118.2 | 116.0 | | 46.7 |
| Ni | 3125 | 3048 | 3076 | 54 | 427 | 2806 | 2899 | 3156 | 53 | 110 |
| Cu | 0.9 | 2.9 | 2.7 | 26.2 | 43.5 | | 9.2 | 9.0 | | 36.6 |
| Zn | 47.2 | 58.4 | 58.5 | 72.6 | 85.8 | | 43.3 | 42.0 | | 90.8 |
| Ga | | | | | | | | | | |
| Rb | | | 0.076 | | | | | 0.1 | | |
| Sr | 2.9 | 9.3 | 8.7 | 87.9 | 42.7 | | 56.7 | 7.602 | | 9 |
| Y | | | | | | | | 0.078 | | |
| Zr | | | | | | | | 0.246 | | |
| Nb | | | | | | | | | | |
| Cs | | | | | | | | | | |
| Ba | | | | | | | | | | |
| La | | | | | | | | 0.4866 | | |
| Ce | | | | | | | | 0.0116 | | |
| Nd | | | | | | | | 0.0058 | | |
| Sm | | | | | | | | 0.0014 | | |
| Eu | | | | | | | | 0.0014 | | |
| Gd | | | | | | | | | | |
| Dy | | | | | | | | 0.0044 | | |
| Er | | | | | | | | 0.008 | | |
| Yb | | | | | | | | 0.0229 | | |
| Lu | | | | | | | | 0.0054 | | |
| Th | | | | | | | | 1.39 | | |
| U | | | | | | | | 0.75 | | |

# Appendix D

| Hole | 778A | 778A | 779A | 779A | 779A | 779A | 779A | 779A | 779A | 779A |
|---|---|---|---|---|---|---|---|---|---|---|
| Core | 13R-2 | 13R-CC | 4R-1 | 4R-1 | 5R-2 | 5R-2 | 5R-3 | 8R-1 | 8R-1 | 8R-1 |
| Interval | 8-11 | 4-6 | 27-30 | 45-50 | 40-43 | 63-72 | 8-13 | 29-33 | 45-48 | 49-55 |
| Rock | met. vol. | met. bas. | s.t. harz | s. mud | s.t. harz | s. dun | s. mud | s.t. harz | s.t. harz | s.t. harz |
| SiO2 | 52.39 | 44.47 | 40.75 | 43.21 | 42.63 | 41.90 | 42.82 | 35.39 | 43.54 | 43.50 |
| TiO2 | 0.046 | 1.409 | 0.010 | 0.026 | 0.012 | 0.010 | 0.013 | 0.011 | 0.010 | 0.011 |
| Al2O3 | 4.90 | 10.20 | 0.29 | 0.66 | 0.30 | 0.24 | 0.53 | 0.55 | 0.58 | 0.64 |
| Fe2O3 | 7.37 | 10.76 | 9.41 | 8.59 | 8.76 | 8.78 | 8.37 | 11.61 | 8.75 | 8.67 |
| MnO | 0.19 | 0.25 | 0.17 | 0.11 | 0.12 | 0.12 | 0.11 | 0.22 | 0.12 | 0.12 |
| MgO | 24.20 | 23.96 | 48.41 | 45.66 | 47.17 | 47.74 | 45.93 | 50.73 | 45.56 | 45.29 |
| CaO | 8.89 | 6.70 | 0.12 | 0.36 | 0.13 | 0.10 | 0.43 | 0.20 | 0.64 | 0.66 |
| Na2O | 0.936 | 1.666 | 0.104 | 0.608 | 0.083 | 0.074 | 0.746 | 0.139 | 0.073 | 0.052 |
| K2O | 0.046 | 0.033 | 0.013 | 0.029 | 0.023 | 0.015 | 0.064 | 0.020 | 0.024 | 0.022 |
| P2O5 | 0.019 | 0.150 | 0.009 | 0.021 | 0.001 | 0.002 | 0.011 | 0.011 | 0.011 | 0.010 |
| NiO | 0.08 | 0.01 | 0.36 | 0.31 | 0.33 | 0.33 | 0.32 | 0.40 | 0.32 | 0.32 |
| Cr2O3 | 0.13 | 0.01 | 0.39 | 0.43 | 0.38 | 0.39 | 0.48 | 0.53 | 0.54 | 0.59 |
| Total | 99.18 | 99.61 | 100.03 | 100.00 | 99.93 | 99.70 | 99.82 | 99.79 | 100.16 | 99.87 |
| LOI | 6.27 | 14.97 | 17.19 | 20.29 | 16.61 | 16.62 | 11.89 | 18.78 | 11.32 | 11.38 |
| Mg# | 87.25 | 82.28 | 91.47 | 91.73 | 91.83 | 91.89 | 91.97 | 90.11 | 91.56 | 91.60 |
| Sc | | | 4.4 | 4.6 | 4.3 | 5.3 | 4.7 | 7.8 | 7.5 | 7.6 |
| Ti | 229.5 | | | 101.2 | | 16.8 | 29.7 | | 19.5 | 21.5 |
| V | 64.8 | | | 18.8 | | 11.9 | 19.7 | 28.5 | 31.7 | 30.5 |
| Cr | 887 | 71 | 2652 | 2918 | 2614 | 2654 | 3256 | 3612 | 3661 | 4011 |
| Co | 51.6 | | | 96.4 | | 114.1 | 107.2 | 135.8 | 112.8 | 110.7 |
| Ni | 590 | 42 | 2868 | 2400 | 2589 | 2609 | 2544 | 3108 | 2535 | 2530 |
| Cu | 0.0 | | | 0.0 | | 0.0 | 0.0 | 0.0 | 0.0 | 0.0 |
| Zn | 41.7 | | | 31.9 | | 47,8 | 31.3 | 54.0 | 40.0 | 38.1 |
| Ga | | | | | | | | | | |
| Rb | | | 0.061 | 0.228 | 0.304 | 0.230 | 0.194 | 0.136 | 0.691 | 0.805 |
| Sr | 29 | | 6.87 | 4.54 | 6.91 | 6.86 | 5.31 | 8.38 | 12.26 | 13.09 |
| Y | | | | 0.26 | 0.02 | | 0.09 | 0.01 | 0.01 | 0.01 |
| Zr | | | 0.32 | 1.21 | 0.20 | 0.12 | 0.61 | 0.09 | 0.10 | 0.09 |
| Nb | | | | | | | | | | |
| Cs | | | 0.000 | 0.010 | 0.109 | 0.082 | 0.034 | 0.032 | 0.288 | 0.345 |
| Ba | | | 3.09 | 2.08 | 5.10 | 1.61 | 2.22 | 1.48 | 6.06 | 6.21 |
| La | | | | | | | | | | |
| Ce | | | | | | | | | | |
| Nd | | | | | | | | | | |
| Sm | | | | | | | | | | |
| Eu | | | | | | | | | | |
| Gd | | | | | | | | | | |
| Dy | | | | | | | | | | |
| Er | | | | | | | | | | |
| Yb | | | | | | | | | | |
| Lu | | | | | | | | | | |
| Th | | | | | | | | | | |
| U | | | | | | | | | | |

# Appendix D

| Hole | 779A | 779A | 779A | 779A | 779A | 779A | 779A | 779A | 779A | 779A |
|---|---|---|---|---|---|---|---|---|---|---|
| Core | 8R-1 | 9R-1 | 9R-2 | 9R-2 | 9R-2 | 10R-1 | 10R-1 | 10R-1 | 11R-1 | 12R-1 |
| Interval | 90-93 | 43-48 | 11-15 | 23-26 | 52-54 | 17-21 | 40-43 | 106-110 | 94-96 | 18-23 |
| Rock | s.t. harz | s. mud | s.t. harz | s.t. harz | s.t. harz | s.t. harz | s. dun? | s.t. harz | s. dun? | s.t. harz |
| SiO2 | 44.17 | 45.97 | 43.22 | 44.35 | 41.41 | 42.23 | 42.47 | 39.71 | 42.27 | 41.32 |
| TiO2 | 0.063 | 0.169 | 0.011 | 0.012 | 0.013 | 0.016 | 0.015 | 0.009 | 0.009 | 0.013 |
| Al2O3 | 0.34 | 1.30 | 0.65 | 0.74 | 0.34 | 0.58 | 0.73 | 0.42 | 0.19 | 0.19 |
| Fe2O3 | 8.44 | 7.46 | 8.33 | 8.25 | 8.81 | 9.09 | 9.14 | 9.82 | 8.70 | 9.07 |
| MnO | 0.11 | 0.13 | 0.11 | 0.12 | 0.11 | 0.12 | 0.14 | 0.15 | 0.11 | 0.14 |
| MgO | 45.92 | 42.58 | 46.06 | 45.18 | 48.29 | 46.72 | 46.03 | 48.37 | 47.52 | 48.00 |
| CaO | 0.22 | 0.60 | 0.69 | 0.82 | 0.45 | 0.60 | 0.71 | 0.21 | 0.41 | 0.32 |
| Na2O | 0.043 | 0.527 | 0.081 | 0.053 | 0.052 | 0.038 | 0.074 | 0.169 | 0.098 | 0.123 |
| K2O | 0.013 | 0.044 | 0.017 | 0.025 | 0.011 | 0.013 | 0.010 | 0.036 | 0.023 | 0.018 |
| P2O5 | 0.006 | 0.032 | 0.010 | 0.004 | 0.012 | 0.017 | 0.004 | 0.003 | 0.005 | 0.009 |
| NiO | 0.31 | 0.27 | 0.33 | 0.31 | 0.36 | 0.34 | 0.34 | 0.40 | 0.35 | 0.35 |
| Cr2O3 | 0.54 | 0.33 | 0.39 | 0.34 | 0.28 | 0.46 | 0.49 | 0.68 | 0.19 | 0.43 |
| Total | 100.17 | 99.41 | 99.90 | 100.21 | 100.13 | 100.23 | 100.14 | 99.98 | 99.88 | 99.98 |
| LOI | 9.56 | 22.86 | 13.16 | 10.78 | 13.35 | 6.48 | 9.41 | 19.24 | 16.67 | 17.18 |
| Mg# | 91.90 | 92.25 | 92.02 | 91.95 | 91.95 | 91.46 | 91.31 | 91.13 | 91.93 | 91.69 |
| Sc | 7.4 | 5.5 | 4.5 | 7.3 | 3.0 | 4.3 | 4.8 | 3.8 | 2.6 | 2.2 |
| Ti | 22.8 | 894.0 | 17.5 | | | 47.3 | | 9.9 | 11.0 | 32.0 |
| V | 8.17 | 25.2 | 24.7 | 27.1 | | 29.3 | 10.02 | 27.2 | 12.5 | 12.6 |
| Cr | 3727 | 2241 | 2671 | 2330 | 1939 | 3174 | 3340 | 4661 | 1328 | 2933 |
| Co | 110.8 | 86.1 | 109.5 | 106.4 | | 116.6 | | 128.2 | 112.1 | 110.8 |
| Ni | 2456 | 2108 | 2616 | 2469 | 2800 | 2705 | 2692 | 3131 | 2714 | 2739 |
| Cu | 0.0 | 1.0 | 0.0 | 0.0 | | 17.7 | | 0.0 | 0.0 | 0.0 |
| Zn | 40.4 | 30.7 | 41.2 | 34.1 | | 42.5 | | 36.6 | 32.4 | 41.4 |
| Ga | | | | | | | | | | |
| Rb | 0.227 | 0.268 | 0.359 | 0.689 | 0.119 | 0.287 | 0.168 | 0.128 | 0.421 | 0.195 |
| Sr | 3.29 | 12.11 | 15.81 | 15.85 | 8.18 | 4.28 | 2.56 | 9.41 | 21.47 | 13.08 |
| Y | 0.04 | 0.70 | 0.01 | 0.01 | 0.03 | 0.04 | 0.08 | | | 0.03 |
| Zr | 0.21 | 13.10 | 0.08 | 0.09 | 0.17 | 0.14 | 0.18 | 0.05 | 0.04 | 0.17 |
| Nb | | 1.70 | | | | | | | | |
| Cs | 0.083 | 0.011 | 0.186 | 0.290 | 0.073 | 0.119 | 0.094 | 0.005 | 0.281 | 0.046 |
| Ba | 1.74 | 1.68 | 4.59 | 8.71 | 0.92 | 2.26 | 1.11 | 0.92 | 4.56 | 1.14 |
| La | | | | | | | | | | |
| Ce | | | | | | | | | | |
| Nd | | | | | | | | | | |
| Sm | | | | | | | | | | |
| Eu | | | | | | | | | | |
| Gd | | | | | | | | | | |
| Dy | | | | | | | | | | |
| Er | | | | | | | | | | |
| Yb | | | | | | | | | | |
| Lu | | | | | | | | | | |
| Th | | | | | | | | | | |
| U | | | | | | | | | | |

# Appendix D

| Hole | 779A | 779A | 779A | 779A | 779A | 779A | 779A | 779A | 779A | 779A |
|---|---|---|---|---|---|---|---|---|---|---|
| Core | 13R-1 | 13R-1 | 14R-2 | 14R-2 | 16R-1 | 16R-1 | 16R-2 | 16R-2 | 17R-2 | 17R-3 |
| Interval | 2-5 | 55-60 | 21-24 | 40-48 | 19-23 | 36-43 | 84-89 | 128-133 | 14-17 | 77-80 |
| Rock | s.t. harz | s. mud | s. dun | s.t. harz | s. dun | s.t. harz | s.t. harz | s.t. harz | s.t. harz | s.t. harz |
| SiO2 | 39.39 | 39.92 | 42.10 | 43.99 | 43.03 | 43.49 | 43.64 | 42.16 | 43.70 | 43.67 |
| TiO2 | 0.009 | 0.010 | 0.009 | 0.012 | 0.014 | 0.013 | 0.011 | 0.012 | 0.011 | 0.011 |
| Al2O3 | 0.35 | 0.24 | 0.12 | 0.85 | 0.68 | 0.73 | 0.70 | 0.30 | 0.43 | 0.43 |
| Fe2O3 | 9.99 | 10.47 | 8.50 | 8.81 | 8.58 | 8.52 | 8.64 | 8.87 | 8.17 | 8.43 |
| MnO | 0.15 | 0.14 | 0.11 | 0.12 | 0.14 | 0.12 | 0.12 | 0.12 | 0.11 | 0.11 |
| MgO | 48.81 | 47.53 | 48.13 | 44.34 | 46.16 | 45.52 | 45.32 | 47.25 | 46.46 | 46.82 |
| CaO | 0.42 | 0.22 | 0.16 | 1.07 | 0.61 | 0.71 | 0.76 | 0.33 | 0.42 | 0.39 |
| Na2O | 0.063 | 0.348 | 0.066 | 0.015 | 0.122 | 0.114 | 0.096 | 0.081 | 0.099 | 0.060 |
| K2O | 0.014 | 0.024 | 0.027 | 0.021 | 0.031 | 0.028 | 0.027 | 0.012 | 0.026 | 0.029 |
| P2O5 | 0.015 | 0.010 | 0.009 | 0.004 | 0.011 | 0.006 | 0.010 | 0.014 | 0.007 | 0.000 |
| NiO | 0.36 | 0.41 | 0.34 | 0.31 | 0.32 | 0.32 | 0.31 | 0.34 | 0.32 | 0.33 |
| Cr2O3 | 0.54 | 0.58 | 0.42 | 0.44 | 0.33 | 0.32 | 0.44 | 0.39 | 0.43 | 0.39 |
| Total | 100.10 | 99.91 | 99.99 | 99.98 | 100.02 | 99.88 | 100.07 | 99.88 | 100.18 | 100.67 |
| LOI | 18.03 | 15.78 | 14.69 | 9.00 | 4.66 | 3.69 | 9.77 | 6.20 | 7.04 | 10.86 |
| Mg# | 91.06 | 90.44 | 92.19 | 91.30 | 91.82 | 91.76 | 91.62 | 91.74 | 92.23 | 92.05 |
| Sc | 3.8 | 4.0 | 2.6 | 5.3 | 3.8 | 3.3 | 3.8 | 3.2 | 4.0 | 3.3 |
| Tl | 13.2 | 15.6 | 9.1 | | | | | | 31.5 | 20.8 |
| V | 22.7 | 18.2 | 11.8 | | | | | | 21.7 | 21.4 |
| Cr | 3663 | 3940 | 2843 | 2987 | 2253 | 2188 | 2995 | 2646 | 2959 | 2694 |
| Co | 109.3 | 123.8 | 113.3 | | | | | | 111.0 | 113.6 |
| Ni | 2824 | 3229 | 2697 | 2451 | 2547 | 2483 | 2474 | 2691 | 2551 | 2592 |
| Cu | 0.0 | 0.0 | 0.0 | | | | | | 0.4 | 0.0 |
| Zn | 50.9 | 37.4 | 29.2 | | | | | | 33.2 | 37.1 |
| Ga | | | | | | | | | | |
| Rb | 0.081 | 0.107 | 0.294 | 0.298 | 0.394 | 0.381 | 0.587 | 0.133 | 0.553 | 0.719 |
| Sr | 12.28 | 4.47 | 0.72 | 0.24 | 0.60 | 0.74 | 0.24 | 0.51 | 0.70 | 1.06 |
| Y | | | | 0.09 | 0.04 | 0.03 | 0.04 | | | |
| Zr | 0.10 | 0.06 | 0.04 | 0.06 | 0.06 | 0.06 | 0.07 | 0.03 | 0.11 | 0.10 |
| Nb | | | | | | | | | | |
| Cs | 0.010 | 0.007 | 0.085 | 0.086 | 0.131 | 0.088 | 0.163 | 0.038 | 0.147 | 0.137 |
| Ba | 1.05 | 0.55 | 1.43 | 1.00 | 1.04 | 1.96 | 1.03 | 1.86 | 1.65 | 1.46 |
| La | | | | | | | | | | |
| Ce | | | | | | | | | | |
| Nd | | | | | | | | | | |
| Sm | | | | | | | | | | |
| Eu | | | | | | | | | | |
| Gd | | | | | | | | | | |
| Dy | | | | | | | | | | |
| Er | | | | | | | | | | |
| Yb | | | | | | | | | | |
| Lu | | | | | | | | | | |
| Th | | | | | | | | | | |
| U | | | | | | | | | | |

Appendix D

| Hole | 779A | 779A | 779A | 779A | 779A | 779A | 779A | 779A | 779A | 779A |
|---|---|---|---|---|---|---|---|---|---|---|
| Core | 19R-2 | 19R-2 | 19R-2 | 19R-2 | 19R-3 | 22R-2 | 22R-3 | 22R-3 | 24R-1 | 24R-1 |
| Interval | 19-23 | 97-99 | 108-113 | 132-140 | 17-21 | 18-20 | 49-55 | 55-57 | 36-38 | 43-48 |
| Rock | s.t. harz | s. dun | s.t. harz | s.t. harz | s. dun | s. dun | s.t. harz | s. dun | s. dun | s.t. harz |
| SiO2 | 44.38 | 42.33 | 44.52 | 41.87 | 43.41 | 44.46 | 42.27 | 42.76 | 42.09 | 42.38 |
| TiO2 | 0.010 | 0.011 | 0.013 | 0.011 | 0.009 | 0.010 | 0.010 | 0.011 | 0.009 | 0.010 |
| Al2O3 | 0.94 | 0.25 | 0.79 | 0.19 | 0.48 | 0.57 | 0.18 | 0.15 | 0.36 | 0.37 |
| Fe2O3 | 8.87 | 8.80 | 8.49 | 8.37 | 8.40 | 8.28 | 8.80 | 8.74 | 8.99 | 8.88 |
| MnO | 0.13 | 0.12 | 0.12 | 0.12 | 0.12 | 0.12 | 0.12 | 0.12 | 0.13 | 0.13 |
| MgO | 44.29 | 47.66 | 44.56 | 48.39 | 46.27 | 45.78 | 47.45 | 47.79 | 46.90 | 46.67 |
| CaO | 1.07 | 0.32 | 0.84 | 0.14 | 0.29 | 0.22 | 0.20 | 0.18 | 0.49 | 0.48 |
| Na2O | 0.047 | 0.036 | 0.127 | 0.066 | 0.037 | 0.045 | 0.047 | 0.097 | 0.141 | 0.245 |
| K2O | 0.013 | 0.013 | 0.033 | 0.018 | 0.016 | 0.013 | 0.012 | 0.013 | 0.031 | 0.031 |
| P2O5 | 0.000 | 0.013 | 0.008 | 0.015 | 0.014 | 0.008 | 0.008 | 0.014 | 0.007 | 0.010 |
| NiO | 0.31 | 0.34 | 0.31 | 0.33 | 0.33 | 0.32 | 0.34 | 0.34 | 0.34 | 0.33 |
| Cr2O3 | 0.40 | 0.29 | 0.42 | 0.49 | 0.53 | 0.39 | 0.41 | 0.29 | 0.44 | 0.56 |
| Total | 100.45 | 100.17 | 100.22 | 100.00 | 99.90 | 100.21 | 99.82 | 100.50 | 99.93 | 100.09 |
| LOI | 15.70 | 6.32 | 10.28 | 9.62 | 9.60 | 9.51 | 9.09 | 9.49 | 17.38 | 17.55 |
| Mg# | 91.24 | 91.86 | 91.63 | 92.34 | 91.99 | 92.02 | 91.84 | 91.94 | 91.58 | 91.64 |
| Sc | | 4.0 | 3.9 | 2.6 | 3.8 | 3.4 | 2.2 | | 2.9 | 2.5 |
| Ti | | 20.9 | | | | 11.2 | | 14.6 | 9.1 | |
| V | | 17.7 | | | | 21 | | 10.9 | 21.6 | |
| Cr | 2750 | 2004 | 2876 | 3349 | 3658 | 2680 | 2791 | 1959 | 2991 | 3844 |
| Co | | 124.6 | | | | 115.0 | | 119.9 | 111.2 | |
| Ni | 2440 | 2668 | 2403 | 2611 | 2577 | 2510 | 2648 | 2654 | 2688 | 2618 |
| Cu | | 0.9 | | | | 0.0 | | 0.0 | 0.0 | |
| Zn | | 36.8 | | | | 36.1 | | 34.8 | 44.8 | |
| Ga | | | | | | | | | | |
| Rb | | 0.288 | 0.717 | 0.526 | 0.209 | 0.237 | 0.291 | | 0.423 | 0.425 |
| Sr | | 2.06 | 2.07 | 2.03 | 0.83 | 0.70 | 29.13 | | 24.63 | 23.58 |
| Y | | | 0.01 | | | | | | | 0.17 |
| Zr | | 0.15 | 0.07 | 0.10 | 0.08 | 0.10 | 0.08 | | | 0.36 |
| Nb | | | | | | | | | | |
| Cs | | 0.021 | 0.225 | 0.209 | 0.103 | 0.084 | 0.195 | | 0.192 | 0.118 |
| Ba | | 1.70 | 3.20 | 1.80 | 0.67 | 1.33 | 2.79 | | 2.85 | 5.94 |
| La | | | | | | | | | | |
| Ce | | | | | | | | | | |
| Nd | | | | | | | | | | |
| Sm | | | | | | | | | | |
| Eu | | | | | | | | | | |
| Gd | | | | | | | | | | |
| Dy | | | | | | | | | | |
| Er | | | | | | | | | | |
| Yb | | | | | | | | | | |
| Lu | | | | | | | | | | |
| Th | | | | | | | | | | |
| U | | | | | | | | | | |

# Appendix D

| Hole | 779A | 779A | 779A | 779A | 779A | 779A | 779A | 779A | 779A | 779A |
|---|---|---|---|---|---|---|---|---|---|---|
| Core | 25R-1 | 26R-1 | 26R-2 | 26R-2 | 26R-2 | 26R-2 | 26R-3 | 26R-3 | 26R-3 | 28R-3 |
| Interval | 80-82 | 4-9 | 18-25 | 28-33 | 50-52 | 103-107 | 3-9 | 101-103 | 118-124 | 26-28 |
| Rock | s.t. harz | s.t. harz | s.t. harz | s.t. harz | s.t. harz | s.t. harz | s.t. harz | s.t. harz | s.t. harz | s.t. harz |
| SiO2 | 44.07 | 39.86 | 43.98 | 44.51 | 43.80 | 40.23 | 44.32 | 43.62 | 42.95 | 42.92 |
| TiO2 | 0.013 | 0.012 | 0.012 | 0.013 | 0.011 | 0.010 | 0.012 | 0.025 | 0.029 | 0.009 |
| Al2O3 | 0.76 | 0.36 | 0.81 | 0.88 | 0.82 | 0.50 | 0.86 | 0.81 | 0.70 | 0.30 |
| Fe2O3 | 8.31 | 9.67 | 8.87 | 8.75 | 8.98 | 9.72 | 8.93 | 8.27 | 8.51 | 8.43 |
| MnO | 0.11 | 0.13 | 0.12 | 0.12 | 0.13 | 0.15 | 0.13 | 0.11 | 0.11 | 0.11 |
| MgO | 45.18 | 48.60 | 44.54 | 44.08 | 45.02 | 48.49 | 43.90 | 46.14 | 46.56 | 46.94 |
| CaO | 0.54 | 0.31 | 0.93 | 1.07 | 0.91 | 0.11 | 1.06 | 0.70 | 0.62 | 0.45 |
| Na2O | 0.116 | 0.144 | 0.032 | 0.050 | 0.035 | 0.099 | 0.104 | 0.110 | 0.115 | 0.097 |
| K2O | 0.028 | 0.020 | 0.015 | 0.014 | 0.013 | 0.021 | 0.011 | 0.020 | 0.016 | 0.016 |
| P2O5 | 0.008 | 0.003 | 0.003 | 0.009 | 0.000 | 0.000 | 0.011 | 0.001 | 0.009 | 0.009 |
| NiO | 0.31 | 0.41 | 0.31 | 0.30 | 0.31 | 0.43 | 0.31 | 0.32 | 0.33 | 0.34 |
| Cr2O3 | 0.45 | 0.41 | 0.43 | 0.41 | 0.37 | 0.51 | 0.39 | 0.34 | 0.36 | 0.46 |
| Total | 99.88 | 99.93 | 100.06 | 100.22 | 100.38 | 100.26 | 100.03 | 100.47 | 100.31 | 100.07 |
| LOI | 11.47 | 19.74 | 9.75 | 8.70 | 8.85 | 8.06 | 8.05 | 13.89 | 13.01 | 16.25 |
| Mg# | 91.90 | 91.29 | 91.28 | 91.31 | 91.27 | 91.23 | 91.11 | 92.08 | 91.94 | 92.07 |
| Sc | 3.1 | 2.5 | 4.1 | 4.1 | 3.9 | 4.0 | 3.9 | 2.6 | 2.4 | 2.3 |
| Ti | | 31.7 | 27.8 | 29.3 | | 25.4 | 25.8 | 101.1 | 124.3 | 14.0 |
| V | | 19.6 | 34.6 | 37 | | 40.5 | 36.4 | 28.5 | 25.8 | 18.5 |
| Cr | 3059 | 2832 | 2966 | 2825 | 2501 | 3457 | 2697 | 2360 | 2477 | 3164 |
| Co | | 126.0 | 111.2 | 106.1 | | 108.3 | 108.9 | 111.0 | 113.0 | 109.7 |
| Ni | 2438 | 3253 | 2443 | 2394 | 2463 | 3382 | 2416 | 2504 | 2578 | 2648 |
| Cu | | 0.0 | 4.4 | 4.8 | | 7.4 | 3.9 | 0.0 | 0.0 | 0.0 |
| Zn | | 34.5 | 38.1 | 36.4 | | 38.4 | 39.6 | 38.8 | 37.5 | 39.1 |
| Ga | | | | | | | | | | |
| Rb | 0.976 | 1.140 | 0.381 | 0.340 | 0.293 | 0.490 | 0.274 | 0.577 | 0.454 | 0.257 |
| Sr | 1.55 | 13.18 | 5.36 | 2.06 | 0.60 | 0.94 | 0.37 | 24.77 | 19.61 | 32.81 |
| Y | 0.04 | 0.07 | 0.09 | 0.13 | 0.11 | 0.07 | 0.09 | 0.20 | 0.39 | 0.02 |
| Zr | 0.06 | 0.11 | 0.11 | 0.14 | 0.27 | 0.08 | 0.29 | 0.17 | 0.15 | 0.15 |
| Nb | | | | | | | | | | |
| Cs | 0.241 | 0.627 | 0.176 | 0.148 | 0.066 | 0.325 | 0.121 | 0.587 | 0.305 | 0.072 |
| Ba | 2.51 | 1.69 | 6.86 | 6.97 | 1.29 | 4.10 | 0.98 | 12.94 | 11.49 | 2.38 |
| La | | | | | | | | | | |
| Ce | | | | | | | | | | |
| Nd | | | | | | | | | | |
| Sm | | | | | | | | | | |
| Eu | | | | | | | | | | |
| Gd | | | | | | | | | | |
| Dy | | | | | | | | | | |
| Er | | | | | | | | | | |
| Yb | | | | | | | | | | |
| Lu | | | | | | | | | | |
| Th | | | | | | | | | | |
| U | | | | | | | | | | |

| Hole | 779A | 779A | 779A | 779A | 779A | 779A | 779A | 779B | 779B | 780C |
|---|---|---|---|---|---|---|---|---|---|---|
| Core | 28R-3 | 32R-3 | 34R-1 | 35R-1 | 35R-1 | 36R-2 | 37R-1 | 1R-1 | 1R-5 | 1R-1 |
| Interval | 106-115 | 18-22 | 52-58 | 103-107 | 109-112 | 99-104 | 125-130 | 125-130 | 134-139 | 88-93 |
| Rock | s.t. harz | s.t. harz | s.t. harz | s.t. harz | s.t. harz | s. mud | s. mud | s. mud | s. mud | s. mud |
| SiO2 | 38.70 | 40.26 | 42.66 | 42.45 | 41.45 | 44.48 | 41.25 | 41.52 | 44.05 | 41.10 |
| TiO2 | 0.010 | 0.010 | 0.015 | 0.013 | 0.015 | 0.168 | 0.606 | 0.025 | 0.304 | 0.123 |
| Al2O3 | 0.13 | 0.12 | 0.50 | 0.34 | 0.29 | 6.99 | 12.13 | 0.50 | 6.09 | 1.64 |
| Fe2O3 | 9.81 | 8.28 | 8.42 | 8.62 | 9.82 | 8.46 | 9.28 | 7.41 | 8.10 | 8.03 |
| MnO | 0.13 | 0.10 | 0.12 | 0.12 | 0.14 | 0.16 | 0.37 | 0.19 | 0.15 | 0.12 |
| MgO | 49.15 | 49.97 | 46.66 | 47.69 | 46.40 | 31.47 | 33.49 | 39.38 | 24.91 | 41.43 |
| CaO | 0.48 | 0.30 | 0.71 | 0.37 | 1.53 | 6.54 | 1.63 | 9.17 | 13.21 | 4.27 |
| Na2O | 0.147 | 0.049 | 0.122 | 0.103 | 0.036 | 1.136 | 1.022 | 0.654 | 1.720 | 0.971 |
| K2O | 0.017 | 0.017 | 0.014 | 0.013 | 0.007 | 0.035 | 0.031 | 0.081 | 0.290 | 0.144 |
| P2O5 | 0.016 | 0.005 | 0.001 | 0.000 | 0.010 | 0.042 | 0.096 | 0.027 | 0.073 | 0.026 |
| NiO | 0.31 | 0.38 | 0.33 | 0.35 | 0.26 | 0.19 | 0.02 | 0.32 | 0.19 | 0.26 |
| Cr2O3 | 0.53 | 0.40 | 0.37 | 0.30 | 0.29 | 0.32 | 0.03 | 0.36 | 0.24 | 0.34 |
| Total | 99.44 | 99.87 | 99.92 | 100.35 | 100.24 | 99.98 | 99.95 | 99.64 | 99.32 | 98.46 |
| LOI | 18.69 | 14.70 | 16.42 | 13.31 | 12.83 | 12.51 | 13.40 | 18.45 | 18.19 | 22.47 |
| Mg# | 91.26 | 92.64 | 92.03 | 92.02 | 90.78 | 88.59 | 88.27 | 91.72 | 86.51 | 91.49 |
| Sc | | 1.5 | 2.3 | 2.1 | | 8.2 | 9.3 | | | |
| Ti | 11.9 | 11.1 | 55.0 | | 72.3 | 23.7 | 24.3 | 56.7 | 1231.9 | |
| V | 7.9 | 10.3 | 18 | 28.3 | 14.2 | 6.6 | 7.5 | 21.3 | 62.1 | |
| Cr | 3647 | 2708 | 2540 | 2044 | 1991 | 2156 | 205 | 2494 | 1625 | 2354 |
| Co | 123.5 | 117.6 | 108.2 | | 115.7 | | | 109.6 | 61.1 | |
| Ni | 2464 | 2967 | 2583 | 2726 | 2068 | 1522 | 176 | 2518 | 1503 | 2076 |
| Cu | 0.0 | 0.0 | 0.0 | | 0.0 | 218.2 | 228.0 | 2.8 | 35.6 | |
| Zn | 31.7 | 39.5 | 45.9 | | 33.2 | 72.7 | 101.7 | 108.3 | 95.6 | |
| Ga | | | | | | | | | | |
| Rb | | 0.473 | 0.330 | 0.265 | | 0.797 | 0.428 | | | |
| Sr | 26.00 | 8.16 | 28.09 | 9.89 | 11.10 | 46.03 | 49.70 | 1148.5 | 1473.5 | |
| Y | | | 0.07 | 0.04 | | 7.37 | 23.94 | | | |
| Zr | | 0.26 | 0.16 | 0.10 | | 10.94 | 67.16 | | | |
| Nb | | | | | | | | | | |
| Cs | | 0.394 | 0.152 | 0.226 | | 0.173 | 0.141 | | | |
| Ba | | 4.12 | 3.17 | 3.24 | | 6.26 | 18.34 | | | |
| La | | | | | | | | | | |
| Ce | | | | | | | | | | |
| Nd | | | | | | | | | | |
| Sm | | | | | | | | | | |
| Eu | | | | | | | | | | |
| Gd | | | | | | | | | | |
| Dy | | | | | | | | | | |
| Er | | | | | | | | | | |
| Yb | | | | | | | | | | |
| Lu | | | | | | | | | | |
| Th | | | | | 2.43 | | | | | |
| U | | | | | 0.47 | | | | | |

| Hole | 780C | 780C | 780C | 780C | 780C | 780C | 780C | 780C | 780C | 780C |
|---|---|---|---|---|---|---|---|---|---|---|
| Core | 1R-3 | 2R-1 | 2R-CC | 5R-1 | 6R-1 | 6R-1 | 8R-1 | 8R-1 | 10R-1 | 13R-1 |
| Interval | 100-105 | 33-38 | 0-5 | 29-34 | 61-62 | 95-101 | 98-101 | 120-124 | 13-16 | 45-50 |
| Rock | s. mud | s. mud | s. mud | s. mud | s.t. harz | s.t. harz | s. dun | s.t. harz | s.t. harz | s.t. harz |
| SiO2 | 43.90 | 43.90 | 42.16 | 44.33 | 44.03 | 44.89 | 43.89 | 42.99 | 44.28 | 43.24 |
| TiO2 | 0.089 | 0.089 | 0.086 | 0.093 | 0.010 | 0.014 | 0.009 | 0.009 | 0.009 | 0.012 |
| Al2O3 | 1.40 | 1.40 | 1.20 | 1.34 | 0.59 | 0.93 | 0.79 | 0.74 | 0.77 | 0.65 |
| Fe2O3 | 8.57 | 8.57 | 9.50 | 8.37 | 8.60 | 8.09 | 8.70 | 9.12 | 8.42 | 8.87 |
| MnO | 0.12 | 0.12 | 0.13 | 0.12 | 0.12 | 0.12 | 0.12 | 0.14 | 0.12 | 0.13 |
| MgO | 42.69 | 42.69 | 42.31 | 42.72 | 45.30 | 44.23 | 45.17 | 46.48 | 44.54 | 45.29 |
| CaO | 1.38 | 1.38 | 1.05 | 0.96 | 0.68 | 0.77 | 0.61 | 0.47 | 0.93 | 0.86 |
| Na2O | 0.905 | 0.905 | 1.251 | 0.722 | 0.153 | 0.143 | 0.141 | 0.043 | 0.062 | 0.143 |
| K2O | 0.116 | 0.116 | 0.062 | 0.047 | 0.022 | 0.038 | 0.025 | 0.018 | 0.031 | 0.023 |
| P2O5 | 0.023 | 0.023 | 0.021 | 0.024 | 0.003 | 0.006 | 0.003 | 0.000 | 0.007 | 0.004 |
| NiO | 0.29 | 0.29 | 0.29 | 0.29 | 0.34 | 0.29 | 0.31 | 0.33 | 0.31 | 0.32 |
| Cr2O3 | 0.38 | 0.38 | 0.39 | 0.41 | 0.35 | 0.44 | 0.40 | 0.36 | 0.41 | 0.39 |
| Total | 99.86 | 99.86 | 98.44 | 99.42 | 100.19 | 99.96 | 100.16 | 100.71 | 99.89 | 99.93 |
| LOI | 22.27 | 16.22 | 15.13 | 14.69 | 12.04 | 12.32 | 11.76 | 12.67 | 12.30 | 6.67 |
| Mg# | 91.22 | 91.22 | 90.28 | 91.41 | 91.66 | 91.93 | 91.54 | 91.40 | 91.69 | 91.41 |
| Sc | | | | | | | | | | |
| Ti | | 390.7 | 399.7 | 471.8 | 11.2 | 42.1 | 12.6 | | | 20.8 |
| V | | 29.3 | 31.2 | 32.4 | 25.4 | 25.9 | 30.3 | 27 | | 31 |
| Cr | 2583 | 2583 | 2664 | 2824 | 2382 | 3015 | 2724 | 2491 | 2789 | 2662 |
| Co | | 89.9 | 95.1 | 97.3 | 120.2 | 103.6 | 111.8 | 114.1 | | 113.1 |
| Ni | 2285 | 2285 | 2254 | 2245 | 2665 | 2315 | 2475 | 2628 | 2400 | 2510 |
| Cu | | 3.8 | 12.4 | 4.7 | 0.0 | 0.0 | 0.0 | 0.0 | | 3.8 |
| Zn | | 74.0 | 140.2 | 43.7 | 34.6 | 33.8 | 35.5 | 39.0 | | 38.0 |
| Ga | | | | | | | | | | |
| Rb | | | | | 0.289 | | | | | |
| Sr | | 17.4 | 21.9 | 12 | 2.8 | 7 | 7 | 7.7 | | |
| Y | | | | | 0.015 | | | | | |
| Zr | | | | | 0.214 | | | | | |
| Nb | | | | | | | | | | |
| Cs | | | | | | | | | | |
| Ba | | | | | | | | | | |
| La | | | | | 0.1182 | | | | | |
| Ce | | | | | 0.0374 | | | | | |
| Nd | | | | | 0.0075 | | | | | |
| Sm | | | | | 0.0013 | | | | | |
| Eu | | | | | 0.0006 | | | | | |
| Gd | | | | | 0.0015 | | | | | |
| Dy | | | | | 0.0014 | | | | | |
| Er | | | | | 0.0025 | | | | | |
| Yb | | | | | 0.0128 | | | | | |
| Lu | | | | | 0.0021 | | | | | |
| Th | | | | | 0.551 | | | | | |
| U | | | | | 0.39 | | | | | |

| Hole | 780C | 780C | 780C | 783A | 783A | 783A | 783A | 783A | 783A | 783A |
|---|---|---|---|---|---|---|---|---|---|---|
| Core | 16R-1 | 18R-1 | 18R-1 | 1R-1 | 1R-2 | 1R-3 | 1R-5 | 2R-1 | 4R-3 | 5R-1 |
| Interval | 53-59 | 54-57 | 58-61 | 98-103 | 140-145 | 15-20 | 140-145 | 135-140 | 135-140 | 135-140 |
| Rock | s.t. harz | s.t. harz | s.t. harz | v. clay | v. clay | s. mud | v. clay | v. clay | v. clay | v. clay |
| SiO2 | 43.49 | 43.46 | 44.04 | 63.01 | 61.78 | 43.18 | 62.61 | 58.45 | 57.86 | 64.64 |
| TiO2 | 0.011 | 0.012 | 0.011 | 0.741 | 0.630 | 0.011 | 0.697 | 0.634 | 0.635 | 0.742 |
| Al2O3 | 0.63 | 0.80 | 0.87 | 15.95 | 14.88 | 0.40 | 16.52 | 15.07 | 15.09 | 16.26 |
| Fe2O3 | 8.56 | 8.86 | 8.75 | 7.45 | 7.09 | 8.35 | 7.53 | 6.07 | 6.12 | 7.07 |
| MnO | 0.12 | 0.12 | 0.13 | 0.10 | 0.16 | 0.12 | 0.13 | 0.27 | 0.27 | 0.15 |
| MgO | 45.90 | 44.26 | 44.13 | 2.23 | 2.76 | 47.04 | 3.35 | 3.05 | 2.62 | 2.57 |
| CaO | 0.82 | 1.00 | 1.04 | 2.79 | 5.06 | 0.23 | 2.50 | 10.67 | 10.59 | 2.44 |
| Na2O | 0.113 | 0.075 | 0.461 | 4.207 | 4.135 | 0.041 | 3.879 | 3.689 | 3.534 | 3.982 |
| K2O | 0.022 | 0.011 | 0.033 | 2.316 | 2.508 | 0.031 | 2.738 | 2.347 | 2.274 | 2.737 |
| P2O5 | 0.009 | 0.000 | 0.000 | 0.126 | 0.113 | 0.003 | 0.138 | 0.130 | 0.126 | 0.116 |
| NiO | 0.32 | 0.31 | 0.31 | 0.00 | 0.01 | 0.34 | 0.00 | 0.00 | 0.01 | 0.00 |
| Cr2O3 | 0.45 | 0.39 | 0.42 | 0.01 | 0.01 | 0.42 | 0.01 | 0.01 | 0.01 | 0.01 |
| Total | 100.44 | 99.30 | 100.18 | 98.94 | 99.13 | 100.16 | 100.11 | 100.39 | 99.14 | 100.71 |
| LOI | 12.86 | 11.09 | 11.00 | 8.69 | 11.56 | 8.91 | 21.65 | 8.71 | 14.29 | 9.21 |
| Mg# | 91.79 | 91.24 | 91.32 | 38.43 | 44.80 | 92.15 | 48.12 | 51.18 | 47.16 | 43.11 |
| Sc | | | | | | | | | | |
| Ti | 19.6 | 20.6 | 21.4 | 3841.6 | 3879.1 | 22.3 | 3265.2 | 2785.0 | 1955.1 | 3057.9 |
| V | 31 | 34.5 | 38.7 | 104.3 | 108.9 | 22.1 | 101.2 | 69.9 | 70.2 | 110.3 |
| Cr | 3064 | 2660 | 2856 | 69 | 62 | 2842 | 71 | 56 | 66 | 71 |
| Co | 115.1 | 107.5 | 111.5 | 16.9 | 17.8 | 110.9 | 19.4 | 14.4 | 13.2 | 15.8 |
| Ni | 2516 | 2447 | 2410 | 37 | 48 | 2696 | 38 | 35 | 41 | 38 |
| Cu | 0.7 | 1.6 | 5.6 | 69.1 | 70.3 | 0 | 65.8 | 61.1 | 86.1 | 46.1 |
| Zn | 46.3 | 37.8 | 34.6 | 95.9 | 99.1 | 42.2 | 96.9 | 114.0 | 87.3 | 89.3 |
| Ga | | | | | | | | | | |
| Rb | | | 0.25 | | | | | | | |
| Sr | 12.8 | 0.6 | 0.05 | 148.8 | 149 | 1 | 151.9 | 134.6 | 321.2 | 132.4 |
| Y | | | 0.1 | | | | | | | |
| Zr | | | 0.16 | | | | | | | |
| Nb | | | | | | | | | | |
| Cs | | | | | | | | | | |
| Ba | | | | | | | | | | |
| La | | | 0.1212 | | | | | | | |
| Ce | | | 0.0067 | | | | | | | |
| Nd | | | 0.0042 | | | | | | | |
| Sm | | | 0.0011 | | | | | | | |
| Eu | | | 0.0003 | | | | | | | |
| Gd | | | | | | | | | | |
| Dy | | | | | | | | | | |
| Er | | | 0.0157 | | | | | | | |
| Yb | | | 0.0321 | | | | | | | |
| Lu | | | 0.0069 | | | | | | | |
| Th | | | 1.14 | | | | | | | |
| U | | | 1 | | | | | | | |

# Appendix D

| Hole | 783A | 783A | 783A | 783A | 783A | 783A | 784A | 784A | 784A | 784A |
|---|---|---|---|---|---|---|---|---|---|---|
| Core | 7R-1 | 8R-1 | 16R-1 | 17R-1 | 18R-1 | 18R-1 | 3R-2 | 4R-2 | 6R-4 | 8R-4 |
| Interval | 135-140 | 124-129 | 45-50 | 65-70 | 64-71 | 119-124 | 135-140 | 135-140 | 135-140 | 135-140 |
| Rock | v. clay | v. clay | s. mud | s. mud | s. t. harz | s. t. harz | v. clay | v. clay | v. clay | v. ash |
| SiO2 | | 62.34 | 43.98 | 43.61 | 42.89 | 44.02 | 64.51 | 62.51 | 62.95 | 61.70 |
| TiO2 | | 0.702 | 0.011 | 0.013 | 0.013 | 0.017 | 0.635 | 0.749 | 0.716 | 0.777 |
| Al2O3 | | 16.44 | 0.46 | 0.72 | 0.52 | 0.78 | 15.50 | 15.81 | 14.95 | 15.40 |
| Fe2O3 | | 7.53 | 8.58 | 8.73 | 9.30 | 8.93 | 6.11 | 8.04 | 7.85 | 8.69 |
| MnO | | 0.14 | 0.12 | 0.13 | 0.13 | 0.13 | 0.13 | 0.23 | 0.29 | 0.16 |
| MgO | | 3.38 | 43.81 | 45.50 | 45.79 | 44.99 | 1.93 | 2.83 | 2.72 | 2.41 |
| CaO | | 2.52 | 0.20 | 0.43 | 0.77 | 0.91 | 2.65 | 3.62 | 3.56 | 3.77 |
| Na2O | | 4.033 | 0.288 | 0.421 | 0.277 | 0.091 | 5.055 | 4.027 | 4.630 | 3.970 |
| K2O | | 2.751 | 0.015 | 0.021 | 0.016 | 0.011 | 2.472 | 2.111 | 2.002 | 2.018 |
| P2O5 | | 0.152 | 0.006 | 0.008 | 0.000 | 0.000 | 0.122 | 0.109 | 0.136 | 0.129 |
| NiO | | 0.00 | 0.32 | 0.34 | 0.32 | 0.30 | 0.00 | 0.00 | 0.00 | 0.00 |
| Cr2O3 | | 0.01 | 0.56 | 0.43 | 0.27 | 0.43 | 0.01 | 0.01 | 0.01 | 0.01 |
| Total | | 99.99 | 98.34 | 100.34 | 100.29 | 100.60 | 99.12 | 100.02 | 99.80 | 99.04 |
| LOI | 8.58 | 9.67 | 14.58 | 17.28 | 13.81 | 13.82 | 8.38 | 7.90 | 8.85 | 8.14 |
| Mg# | | 48.34 | 91.41 | 91.58 | 91.13 | 91.31 | 39.71 | 42.30 | 41.90 | 36.64 |
| Sc | | | | | | | | | | |
| Ti | 3494.4 | 3350.1 | 12.0 | 26.9 | 30.4 | 53.9 | 3227.9 | 3939.6 | 3704.3 | 4085.7 |
| V | 110.1 | 119.3 | 22.8 | 26.7 | 24.6 | 32.4 | 90.7 | 123.3 | 110 | 156.1 |
| Cr | 0 | 40 | 3838 | 2935 | 1880 | 2948 | 48 | 46 | 50 | 44 |
| Co | 17.0 | 17.6 | 106.3 | 107.1 | 113.9 | 110.8 | 14.4 | 21.5 | 17.5 | 20.7 |
| Ni | 0 | 4 | 2541 | 2663 | 2486 | 2356 | 22 | | 16 | 22 |
| Cu | 72.4 | 68.4 | 0.0 | 0.0 | 0.0 | 0.0 | 76.3 | 65.9 | 68.1 | 107.9 |
| Zn | 94.6 | 88.4 | 31.7 | 34.2 | 38.3 | 38.3 | 87.9 | 115.1 | 99.4 | 98.7 |
| Ga | | | | | | | | | | |
| Rb | | | | | | | | | | |
| Sr | 149.4 | 141.3 | 5.3 | 9.2 | 11.9 | 12.1 | 153.3 | 141.1 | 147.4 | 151.6 |
| Y | | | | | | | | | | |
| Zr | | | | | | | | | | |
| Nb | | | | | | | | | | |
| Cs | | | | | | | | | | |
| Ba | | | | | | | | | | |
| La | | | | | | | | | | |
| Ce | | | | | | | | | | |
| Nd | | | | | | | | | | |
| Sm | | | | | | | | | | |
| Eu | | | | | | | | | | |
| Gd | | | | | | | | | | |
| Dy | | | | | | | | | | |
| Er | | | | | | | | | | |
| Yb | | | | | | | | | | |
| Lu | | | | | | | | | | |
| Th | | | | | | | | | | |
| U | | | | | | | | | | |

# Appendix D

| Hole | 784A | 784A | 784A | 784A | 784A | 784A | 784A | 784A | 784A | 784A |
|---|---|---|---|---|---|---|---|---|---|---|
| Core | 9R-3 | 12R-1 | 13R-1 | 16R-5 | 19R-2 | 22R-3 | 24R-6 | 26R-1 | 29R-4 | 36R-1 |
| Interval | 0-5 | 135-140 | 18-20 | 135-140 | 115-120 | 131-134 | 103-107 | 110-113 | 109-113 | 60-65 |
| Rock | v. clay | v. clay | v. clay | v. clay | v. clay | v. clay | v. clay | v. clay | v. clay | s. mud |
| SiO2 | | 63.02 | 37.59 | 62.46 | 64.86 | 62.68 | 63.34 | 64.98 | | |
| TiO2 | | 0.716 | 0.010 | 0.663 | 0.695 | 0.698 | 0.704 | 0.700 | | |
| Al2O3 | | 16.19 | 0.33 | 16.21 | 16.95 | 16.52 | 16.09 | 16.08 | | |
| Fe2O3 | | 6.97 | 10.32 | 7.09 | 7.42 | 7.45 | 7.06 | 7.04 | | |
| MnO | | 0.10 | 0.15 | 0.11 | 0.11 | 0.15 | 0.11 | 0.10 | | |
| MgO | | 2.50 | 48.91 | 2.58 | 2.85 | 2.72 | 2.45 | 2.33 | | |
| CaO | | 2.66 | 0.35 | 3.02 | 1.92 | 2.35 | 2.40 | 1.99 | | |
| Na2O | | 4.066 | 0.203 | 3.940 | 3.613 | 3.749 | 3.726 | 3.706 | | |
| K2O | | 2.444 | 0.017 | 2.273 | 2.865 | 2.619 | 2.447 | 2.723 | | |
| P2O5 | | 0.104 | 0.010 | 0.109 | 0.104 | 0.099 | 0.108 | 0.106 | | |
| NiO | | 0.00 | 0.38 | 0.00 | 0.01 | 0.01 | 0.01 | 0.00 | | |
| Cr2O3 | | 0.01 | 1.52 | 0.01 | 0.01 | 0.01 | 0.01 | 0.00 | | |
| Total | | 98.78 | 99.78 | 98.48 | 101.39 | 99.05 | 98.45 | 99.75 | | |
| LOI | 9.41 | 9.36 | 19.26 | 8.92 | 7.90 | 10.50 | 10.12 | 10.86 | 9.48 | 16.96 |
| Mg# | | 42.79 | 90.81 | 43.14 | 44.47 | 43.22 | 41.98 | 40.78 | | |
| Sc | | | | | | | 18.2 | 18.4 | 22.2 | 6.3 |
| Ti | 3238.1 | 3685.7 | 15.8 | 2420.1 | 2347.8 | 2285.1 | 3345.2 | 3071.1 | 3216.6 | 24.2 |
| V | 84.9 | 136.2 | 27 | 78.4 | 82.7 | 89 | 133.4 | 111 | 136.7 | 19.7 |
| Cr | | 46 | 10371 | 73 | 74 | 60 | 51 | 0 | 0 | 0 |
| Co | 16.6 | 17.0 | 128.5 | 16.9 | 15.6 | 17.7 | 21.7 | 20.7 | 22.3 | 95.3 |
| Ni | | 37 | 2991 | 32 | 46 | 45 | 85 | 0 | 0 | 0 |
| Cu | 50.6 | 103.3 | | 49.8 | 39 | 67 | 373.2 | 103.3 | 73.5 | 0 |
| Zn | 87.7 | 98.4 | 56.8 | 85.5 | 88.2 | 90.9 | 103.2 | 96.2 | 103 | 35.9 |
| Ga | | | | | | | | | | |
| Rb | | | | | | | | | | |
| Sr | 143.8 | 140.9 | | 24.8 | 25.6 | 21.3 | 26 | 26 | 25 | |
| Y | | | | | | | | | | |
| Zr | | | | | | | | | | |
| Nb | | | | | | | | | | |
| Cs | | | | | | | | | | |
| Ba | | | | | | | | | | |
| La | | | | | | | | | | |
| Ce | | | | | | | | | | |
| Nd | | | | | | | | | | |
| Sm | | | | | | | | | | |
| Eu | | | | | | | | | | |
| Gd | | | | | | | | | | |
| Dy | | | | | | | | | | |
| Er | | | | | | | | | | |
| Yb | | | | | | | | | | |
| Lu | | | | | | | | | | |
| Th | | | | | | | | | | |
| U | | | | | | | | | | |

# Appendix D

| Hole | 784A | 784A | 784A | 784A | 784A | 784A | 784A | 784A | 784A | 784A |
|---|---|---|---|---|---|---|---|---|---|---|
| Core | 36R-1 | 38R-1 | 38R-1 | 38R-1 | 38R-2 | 38R-CC | 39R-2 | 40R-1 | 40R-2 | 40R-2 |
| Interval | 107-109 | 45-50 | 66-68 | 73-78 | 72-77 | 13-19 | 72-79 | 85-90 | 22-25 | 41-43 |
| Rock | s.t. harz | s. mud | s.t. harz | s.t. harz | s.t. harz | s.t. harz | s. mud | s. mud | s.t. harz | s.t. harz |
| SiO2 | 42.98 | 43.96 | 43.02 | 42.25 | 42.28 | 42.23 | 41.89 | 42.16 | 42.21 | 40.33 |
| TiO2 | 0.009 | 0.060 | 0.021 | 0.018 | 0.011 | 0.012 | 0.011 | 0.015 | 0.011 | 0.011 |
| Al2O3 | 0.38 | 1.46 | 0.46 | 0.46 | 0.42 | 0.41 | 0.42 | 0.30 | 0.23 | 0.10 |
| Fe2O3 | 8.76 | 7.65 | 8.31 | 8.50 | 8.76 | 9.09 | 9.02 | 8.55 | 10.22 | 9.51 |
| MnO | 0.15 | 0.11 | 0.16 | 0.15 | 0.14 | 0.12 | 0.12 | 0.12 | 0.16 | 0.13 |
| MgO | 46.09 | 43.68 | 47.14 | 47.20 | 47.30 | 47.09 | 47.27 | 46.96 | 46.20 | 49.37 |
| CaO | 0.15 | 0.27 | 0.16 | 0.13 | 0.27 | 0.22 | 0.22 | 0.26 | 0.21 | 0.21 |
| Na2O | 0.577 | 0.785 | 0.346 | 0.187 | 0.280 | 0.174 | 0.109 | 0.617 | 0.214 | 0.132 |
| K2O | 0.048 | 0.218 | 0.023 | 0.011 | 0.020 | 0.012 | 0.009 | 0.022 | 0.020 | 0.018 |
| P2O5 | 0.017 | 0.023 | 0.011 | 0.008 | 0.014 | 0.010 | 0.005 | 0.017 | 0.014 | 0.011 |
| NiO | 0.32 | 0.26 | 0.31 | 0.35 | 0.34 | 0.34 | 0.34 | 0.32 | 0.40 | 0.38 |
| Cr2O3 | 0.27 | 0.80 | 0.30 | 0.39 | 0.43 | 0.48 | 0.48 | 0.46 | 0.29 | 0.14 |
| Total | 99.75 | 99.27 | 100.26 | 99.65 | 100.25 | 100.20 | 99.89 | 99.79 | 100.18 | 100.35 |
| LOI | 16.49 | 15.51 | 17.89 | 18.44 | 17.58 | 17.73 | 13.97 | 15.13 | 16.08 | 16.46 |
| Mg# | 91.65 | 92.25 | 92.20 | 92.05 | 91.85 | 91.53 | 91.62 | 91.97 | 90.41 | 91.54 |
| Sc | 8.9 | 7.8 | 8 | 5.2 | 5.4 | 5.8 | 5.3 | 5.5 | 3.3 | 5.1 |
| Ti | 19.9 | 293.1 | 78.7 | 61.9 | 22.1 | 23.0 | 8.2 | 37.8 | 15.5 | 13.6 |
| V | 20.9 | 31 | 21.3 | 20.5 | 19.3 | 18.5 | 12.5 | 13 | 9.6 | 7.1 |
| Cr | 1847 | 5487 | 2072 | 2696 | 2946 | 3296 | 3274 | 3131 | 1997 | 987 |
| Co | 112.7 | 84.9 | 109.5 | 112.5 | 114.3 | 113.2 | 107.7 | 106.2 | 135.5 | 129.2 |
| Ni | 2521 | 2007 | 2441 | 2733 | 2643 | 2700 | 2677 | 2505 | 3155 | 2996 |
| Cu | 0 | 2.9 | 0.0 | 0.0 | 0.0 | 0.0 | 0.9 | 0.0 | 0.0 | 0.0 |
| Zn | 39.3 | 39.6 | 42.2 | 38.7 | 36.5 | 37.7 | 28.7 | 30.6 | 46.8 | 35.9 |
| Ga | | | | | | | | | | |
| Rb | 0.041 | | | | | | | | | |
| Sr | 2.2 | 0.6 | | 1 | | | 2.125 | | | |
| Y | 0.022 | | | | | | | | | |
| Zr | 0.055 | | | | | | | | | |
| Nb | | | | | | | | | | |
| Cs | | | | | | | | | | |
| Ba | | | | | | | | | | |
| La | 0.0639 | | | | | | | | | |
| Ce | | | | | | | | | | |
| Nd | 0.0071 | | | | | | | | | |
| Sm | 0.0011 | | | | | | | | | |
| Eu | 0.0007 | | | | | | | | | |
| Gd | | | | | | | | | | |
| Dy | | | | | | | | | | |
| Er | 0.0001 | | | | | | | | | |
| Yb | 0.006 | | | | | | | | | |
| Lu | | | | | | | | | | |
| Th | | | | | | | | | | |
| U | | | | | | | | | | |

# Appendix D

| Hole | 784A | 784A | 784A | 784A | 784A | 784A | 784A | 784A | 784A | 784A |
|---|---|---|---|---|---|---|---|---|---|---|
| Core | 40R-2 | 41R-1 | 42R-1 | 42R-1 | 42R-1 | 42R-1 | 45R-1 | 45R-1 | 45R-2 | 45R-CC |
| Interval | 70-75 | 45-50 | 5-8 | 7-12 | 39-41 | 47-50 | 98-100 | 130-137 | 33-38 | 7-10 |
| Rock | s.t. harz | s.t. harz | s.t. harz | s.t. harz | s.t. harz | s.t. harz | s.t. harz | s.t. harz | s.t. harz | s.t. harz |
| SiO2 | 40.20 | 44.66 | 43.98 | 44.19 | 39.40 | 39.81 | 43.89 | 43.09 | 43.38 | 43.47 |
| TiO2 | 0.010 | 0.010 | 0.012 | 0.012 | 0.011 | 0.012 | 0.012 | 0.011 | 0.011 | 0.012 |
| Al2O3 | 0.12 | 0.45 | 0.71 | 0.62 | 0.31 | 0.28 | 0.46 | 0.37 | 0.48 | 0.54 |
| Fe2O3 | 9.33 | 8.37 | 8.63 | 8.40 | 10.39 | 9.73 | 8.29 | 8.53 | 8.34 | 8.78 |
| MnO | 0.12 | 0.12 | 0.13 | 0.12 | 0.14 | 0.13 | 0.12 | 0.12 | 0.12 | 0.12 |
| MgO | 49.31 | 44.98 | 44.91 | 45.47 | 48.43 | 48.75 | 45.89 | 46.62 | 45.46 | 46.23 |
| CaO | 0.21 | 0.26 | 0.68 | 0.66 | 0.22 | 0.24 | 0.58 | 0.52 | 0.69 | 0.62 |
| Na2O | 0.105 | 0.611 | 0.094 | 0.058 | 0.247 | 0.139 | 0.072 | 0.119 | 0.155 | 0.060 |
| K2O | 0.008 | 0.021 | 0.012 | 0.008 | 0.086 | 0.009 | 0.011 | 0.011 | 0.012 | 0.008 |
| P2O5 | 0.014 | 0.011 | 0.010 | 0.014 | 0.012 | 0.013 | 0.018 | 0.012 | 0.023 | 0.012 |
| NiO | 0.38 | 0.25 | 0.32 | 0.31 | 0.39 | 0.37 | 0.32 | 0.34 | 0.32 | 0.32 |
| Cr2O3 | 0.18 | 0.38 | 0.46 | 0.42 | 0.51 | 0.46 | 0.26 | 0.28 | 0.32 | 0.44 |
| Total | 99.98 | 100.11 | 99.93 | 100.27 | 100.14 | 99.94 | 99.91 | 100.02 | 99.31 | 100.62 |
| LOI | 17.01 | 14.45 | 14.42 | 14.44 | 17.08 | 18.75 | 13.69 | 13.04 | 23.75 | 14.97 |
| Mg# | 91.68 | 91.81 | 91.56 | 91.86 n=1 | 90.67 | 91.27 | 92.03 | 91.93 | 91.91 | 91.65 |
| Sc | 2.9 | 6.7 | 7.5 | 5 | 4.5 | 3.5 | 5.8 | 2.3 | 5.3 | 5.7 |
| Ti | 11.8 | 12.7 | 22.6 | 22.9 | 19.4 | 20.3 | 28.7 | 20.4 | 18.1 | 22.3 |
| V | 8.3 | 20.1 | 19.7 | 21.6 | 12.9 | 11 | 18 | 18.2 | 18.8 | 20.2 |
| Cr | 1220 | 2573 | 3124 | 2856 | 3479 | 3162 | 1765 | 1944 | 2218 | 3029 |
| Co | 123.3 | 89 | 111.1 | 106.7 | 139.7 | 131.9 | 109.0 | 111.4 | 106.6 | 110.8 |
| Ni | 2994 | 1986 | 2513 | 2406 | 3075 | 2911 | 2496 | 2636 | 2508 | 2514 |
| Cu | 0.0 | 0.0 | 0.0 | 0.0 | 0.0 | 0.0 | 0.0 | 0.0 | 0.0 | 0.0 |
| Zn | 36.0 | 22.7 | 32.8 | 41.1 | 33.4 | 49.2 | 31.9 | 35.0 | 33.3 | 40.9 |
| Ga | | | | | | | | | | |
| Rb | | | | | 0.036 | | | | | |
| Sr | | | | | 6.964 | | 5.419 | 4.258 | | |
| Y | | | | | 0.018 | | | | | |
| Zr | | | | | 0.095 | | | | | |
| Nb | | | | | | | | | | |
| Cs | | | | | | | | | | |
| Ba | | | | | | | | | | |
| La | | | | | 0.0349 | | | | | |
| Ce | | | | | 0.0497 | | | | | |
| Nd | | | | | 0.0231 | | | | | |
| Sm | | | | | 0.0009 | | | | | |
| Eu | | | | | 0.0003 | | | | | |
| Gd | | | | | 0.0013 | | | | | |
| Dy | | | | | 0.0028 | | | | | |
| Er | | | | | 0.008 | | | | | |
| Yb | | | | | 0.0167 | | | | | |
| Lu | | | | | 0.0018 | | | | | |
| Th | | | | | 1.75 | | | | | |
| U | | | | | 0.47 | | | | | |

# Appendix D

| Sample | SA-132 | SA-276 | SA-278 | SA-79 | SA-408 | SA-20 | SA-405 | SA-284 | SA-216 | SA-201 |
|---|---|---|---|---|---|---|---|---|---|---|
| Rock | Gt Lherz | Gt Lherz | Gt Lherz | Sp Lherz | Sp Lherz | Sp Lherz | Tr Lherz | Tr Lherz | Pl Lherz | Pl Lherz |
| SiO2 | 44.50 | 43.81 | 45.52 | 42.40 | 43.74 | 44.22 | 44.23 | 45.06 | 43.98 | 44.97 |
| TiO2 | 0.129 | 0.116 | 0.186 | 0.049 | 0.075 | 0.106 | 0.123 | 0.147 | 0.135 | 0.122 |
| Al2O3 | 3.63 | 3.31 | 4.01 | 1.08 | 2.25 | 2.86 | 3.34 | 3.77 | 3.41 | 3.88 |
| Fe2O3 | 8.76 | 9.10 | 9.28 | 9.55 | 9.27 | 9.01 | 9.05 | 8.64 | 9.25 | 7.69 |
| MnO | 0.13 | 0.13 | 0.14 | 0.12 | 0.13 | 0.13 | 0.13 | 0.13 | 0.13 | 0.12 |
| MgO | 38.82 | 39.82 | 36.32 | 45.81 | 42.28 | 40.26 | 39.62 | 38.70 | 39.56 | 38.96 |
| CaO | 3.09 | 2.81 | 3.57 | 0.74 | 1.87 | 2.60 | 2.83 | 3.18 | 2.89 | 3.67 |
| Na2O | 0.188 | 0.272 | 0.309 | 0.044 | 0.128 | 0.206 | 0.135 | 0.116 | 0.211 | 0.218 |
| K2O | 0.055 | 0.013 | 0.016 | 0.013 | 0.011 | 0.015 | 0.011 | 0.020 | 0.022 | 0.054 |
| P2O5 | 0.016 | 0.009 | 0.008 | 0.011 | 0.020 | 0.016 | 0.013 | 0.015 | 0.008 | 0.009 |
| NiO | 0.27 | 0.28 | 0.25 | 0.32 | 0.28 | 0.27 | 0.27 | 0.25 | 0.27 | 0.26 |
| Cr2O3 | 0.38 | 0.37 | 0.35 | 0.23 | 0.30 | 0.36 | 0.37 | 0.37 | 0.36 | 0.39 |
| Total | 99.97 | 100.03 | 99.95 | 100.37 | 100.34 | 100.05 | 100.10 | 100.39 | 100.22 | 100.33 |
| LOI | 8.40 | 7.84 | 6.43 | 8.75 | 1.26 | 0.81 | 1.36 | 6.14 | 5.50 | 6.61 |
| Mg# | 90.23 | 90.12 | 89.09 | 90.91 | 90.48 | 90.31 | 90.13 | 90.33 | 89.92 | 91.35 |
| Sc | 15.41 | 13.2 | 16.42 | 6.48 | 9.80 | 14.02 | 15.21 | 16.39 | 15.00 | 17.88 |
| Ti | 705.6 | 633.9 | 1055.9 | 241.0 | 444.4 | 621.5 | 724.3 | 898.5 | 766.6 | 687.5 |
| V | 58.71 | 57.9 | 70.63 | 21.8 | 49.5 | 53.01 | 56.55 | 67.47 | 63.4 | 70.15 |
| Cr | 2592 | 2498 | 2393 | 1567 | 2027 | 2448 | 2510 | 2517 | 2486 | 2680 |
| Co | 96.55 | 102.9 | 96.24 | 113.24 | 112.4 | 106.5 | 103.4 | 97.8 | 103.9 | 94.65 |
| Ni | 2083 | 2234 | 1972 | 2536 | 2171 | 2157 | 2118 | 1992 | 2101 | 2075 |
| Cu | 20.41 | 17.70 | 27.22 | 7.95 | 5.2 | 30.1 | 32.4 | 20.9 | 20.6 | 25.96 |
| Zn | 45.43 | 41.60 | 42.96 | 40.86 | 50.4 | 44.9 | 39.8 | 38.3 | 48.2 | 46.01 |
| Ga | 2.45 | | 3.29 | 0.99 | | 2.1 | 2.4 | 2.5 | | 2.47 |
| Rb | 2.73 | | 0.7 | 0.06 | | 0.4 | 0.39 | 1.24 | | 1.76 |
| Sr | 9.99 | 9.9 | 22.21 | 6.76 | 5.7 | 9.64 | 11.66 | 10.51 | 10.2 | 13.29 |
| Y | 3.13 | 2.6 | 3.73 | 0.57 | 1.47 | 2.54 | 2.78 | 3.57 | 2.9 | 3.73 |
| Zr | 5.74 | 4.80 | 7.85 | 1.49 | 2.9 | 4.17 | 5.02 | 8.61 | 5.8 | 4.85 |
| Nb | 0.04 | | 0.08 | 0.03 | | 0.05 | 0.06 | 0.08 | | 0.04 |
| Cs | 0.28 | | 0.17 | 0.01 | | 0.07 | 0.09 | 0.06 | | 0.27 |
| Ba | 1.72 | | 13.59 | 0.34 | | 1.12 | 3.34 | 0.34 | | 7.02 |
| La | 0.13 | | 0.21 | 0.05 | | 0.1 | 0.13 | 0.21 | | 0.21 |
| Ce | 0.38 | | 0.65 | 0.11 | | 0.34 | 0.37 | 0.58 | | 0.55 |
| Nd | 0.47 | | 0.72 | 0.12 | | 0.34 | 0.44 | 0.56 | | 0.58 |
| Sm | | | | | | | | | | |
| Eu | | | | | | | | | | |
| Gd | | | | | | | | | | |
| Dy | | | | | | | | | | |
| Er | | | | | | | | | | |
| Yb | | | | | | | | | | |
| Lu | | | | | | | | | | |
| Th | | | | | | | | | | |
| U | | | | | | | | | | |

# Appendix D

| Sample | SA-93 | SA-245 | SA-54 | SA-32 | SA-246c | SA-331 | SA-47 | SA-285 | SA-436d | SA-270 |
|---|---|---|---|---|---|---|---|---|---|---|
| Rock | Pl Lherz | Pl Lherz | Pl Lherz | Sp Harz | Sp Harz | Sp Harz | Dun | Dun-Cpx | Cpx Web | Gt Lherz |
| SiO2 | 44.10 | 40.88 | 44.28 | 43.02 | 43.35 | 41.94 | 40.19 | 42.57 | 49.06 | 43.88 |
| TiO2 | 0.101 | 0.055 | 0.103 | 0.014 | 0.028 | 0.014 | 0.013 | 0.086 | 0.627 | 0.140 |
| Al2O3 | 2.86 | 5.88 | 3.24 | 0.73 | 1.02 | 0.92 | 0.17 | 0.96 | 4.51 | 3.54 |
| Fe2O3 | 9.03 | 9.29 | 8.79 | 8.40 | 8.89 | 8.50 | 9.58 | 10.47 | 6.99 | 9.23 |
| MnO | 0.13 | 0.13 | 0.13 | 0.11 | 0.12 | 0.12 | 0.12 | 0.13 | 0.11 | 0.13 |
| MgO | 40.92 | 38.34 | 39.84 | 46.77 | 45.15 | 46.77 | 49.20 | 42.82 | 21.75 | 39.26 |
| CaO | 2.51 | 4.15 | 2.99 | 0.52 | 0.90 | 1.08 | 0.08 | 2.38 | 15.40 | 3.01 |
| Na2O | 0.038 | 0.314 | 0.164 | 0.010 | 0.000 | 0.044 | 0.000 | 0.030 | 0.627 | 0.190 |
| K2O | 0.014 | 0.020 | 0.020 | 0.010 | 0.008 | 0.011 | 0.010 | 0.022 | 0.011 | 0.012 |
| P2O5 | 0.015 | 0.012 | 0.013 | 0.003 | 0.000 | 0.001 | 0.005 | 0.010 | 0.007 | 0.016 |
| NiO | 0.28 | 0.24 | 0.27 | 0.34 | 0.32 | 0.33 | 0.36 | 0.29 | 0.10 | 0.27 |
| Cr2O3 | 0.39 | 0.68 | 0.35 | 0.28 | 0.41 | 0.57 | 0.51 | 0.38 | 0.63 | 0.37 |
| Total | 100.38 | 99.98 | 100.19 | 100.21 | 100.19 | 100.28 | 100.24 | 100.13 | 99.82 | 100.05 |
| LOI | 9.60 | 6.42 | 5.88 | 9.33 | 7.09 | 12.05 | 13.38 | 10.48 | 3.48 | 6.90 |
| Mg# | 90.43 | 89.59 | 90.43 | 92.07 | 91.37 | 91.99 | 91.46 | 89.51 | 86.65 | 89.87 |
| Sc | 14.11 | 13.77 | 14.70 | 7.67 | 9.23 | 7.50 | 4.11 | 11.60 | 40.20 | 15.62 |
| Ti | 606.2 | 244.2 | 566.1 | 29.6 | 118.6 | 33.0 | 15.9 | 420.2 | 3448.1 | 794.1 |
| V | 60.3 | 51.13 | 66.1 | 19.61 | 30.61 | 21.5 | 8.63 | 52.3 | 175.8 | 60.08 |
| Cr | 2646 | 4628 | 2377 | 1947 | 2803 | 3868 | 3484 | 2612 | 4336 | 2535 |
| Co | 111.16 | 110.06 | 102.0 | 105.98 | 110.49 | 111.3 | 114.9 | 118.3 | 56.1 | 109.2 |
| Ni | 2210 | 1901 | 2113 | 2656 | 2481 | 2622 | 2831 | 2252 | 796 | 2119 |
| Cu | 22.62 | 47.73 | 23.2 | 1.75 | 9.63 | 9.2 | 0.62 | 48.6 | 86.4 | 25.40 |
| Zn | 42.54 | 57.39 | 44.3 | 33.30 | 40.81 | 39.8 | 39.08 | 46.6 | 39.6 | 48.25 |
| Ga | 2.07 | 3.36 | | 0.41 | 0.75 | | 0.33 | | | 2.67 |
| Rb | 0.3 | 0.77 | | 0.17 | 0.09 | | 0.05 | | | 0.28 |
| Sr | 38.13 | 102.12 | 2.1 | 0.98 | 15.07 | 1.6 | 38.8 | 6.3 | 44.8 | 15.11 |
| Y | 2.25 | 1.54 | 2.1 | 0.06 | 0.29 | | 0.07 | 0.4 | 4.3 | 3 |
| Zr | 3.08 | 0.67 | 1.9 | 0.19 | 0.50 | | 0.08 | 0.7 | 12.1 | 5.63 |
| Nb | 0.03 | 0.02 | | 0.03 | 0.03 | | 0.01 | | | 0.07 |
| Cs | 0.03 | 0.04 | | 0.01 | 0 | | 0.01 | | | 0.04 |
| Ba | 0.67 | 14.51 | | 0.74 | 0.33 | | 0.92 | | | 0.42 |
| La | 0.05 | 0.01 | | 0.01 | 0.02 | | 0.01 | | | 0.15 |
| Ce | 0.21 | 0.07 | | 0.04 | 0.07 | | 0.03 | | | 0.43 |
| Nd | 0.29 | 0.23 | | 0.04 | 0.08 | | 0.01 | | | 0.53 |
| Sm | | | | | | | | | | |
| Eu | | | | | | | | | | |
| Gd | | | | | | | | | | |
| Dy | | | | | | | | | | |
| Er | | | | | | | | | | |
| Yb | | | | | | | | | | |
| Lu | | | | | | | | | | |
| Th | | | | | | | | | | |
| U | | | | | | | | | | |

# Appendix D

| Sample | SA-302 | SA-224 | SA-121 | SA-453c | SA-55 | SA-61b | SA-449 | SA-121a | SA-246b | SA-55a |
|---|---|---|---|---|---|---|---|---|---|---|
| Rock | Sp Lherz | Tr Lherz | Pl Lherz | Pl Lherz | Pl Lherz | Pl Lherz | Pl Lherz | Amp Gab | Dun | Sp Harz |
| SiO2 | 44.10 | 45.26 | 45.67 | 45.48 | 44.18 | 43.67 | 43.78 | 47.65 | 39.31 | 44.00 |
| TiO2 | 0.059 | 0.227 | 0.393 | 0.196 | 0.094 | 0.241 | 0.054 | 0.276 | 0.027 | 0.017 |
| Al2O3 | 1.83 | 4.57 | 8.38 | 7.81 | 2.80 | 2.55 | 3.29 | 14.58 | 1.06 | 1.08 |
| Fe2O3 | 8.48 | 9.44 | 9.54 | 6.88 | 8.95 | 9.98 | 8.84 | 6.22 | 10.24 | 8.33 |
| MnO | 0.12 | 0.14 | 0.15 | 0.11 | 0.13 | 0.13 | 0.13 | 0.17 | 0.13 | 0.12 |
| MgO | 43.09 | 36.69 | 28.04 | 30.50 | 40.94 | 39.19 | 41.25 | 18.09 | 47.84 | 44.79 |
| CaO | 1.68 | 3.51 | 6.58 | 6.95 | 2.34 | 3.54 | 1.80 | 11.47 | 0.24 | 0.87 |
| Na2O | 0.082 | 0.163 | 0.843 | 0.828 | 0.114 | 0.055 | 0.130 | 1.119 | 0.000 | 0.027 |
| K2O | 0.011 | 0.010 | 0.027 | 0.036 | 0.021 | 0.010 | 0.016 | 0.038 | 0.009 | 0.011 |
| P2O5 | 0.009 | 0.016 | 0.016 | 0.008 | 0.009 | 0.009 | 0.004 | 0.022 | 0.011 | 0.010 |
| NiO | 0.30 | 0.25 | 0.17 | 0.20 | 0.28 | 0.25 | 0.27 | 0.06 | 0.33 | 0.31 |
| Cr2O3 | 0.37 | 0.36 | 0.28 | 1.16 | 0.37 | 0.32 | 0.39 | 0.16 | 0.98 | 0.39 |
| Total | 100.12 | 100.62 | 100.09 | 100.13 | 100.21 | 99.93 | 99.96 | 99.85 | 100.17 | 99.95 |
| LOI | 4.88 | 4.30 | 4.30 | 5.34 | 6.92 | 8.03 | 3.69 | 2.51 | 9.20 | 5.84 |
| Mg# | 91.38 | 89.02 | 85.97 | 90.24 | 90.51 | 89.12 | 90.68 | 85.84 | 90.69 | 91.81 |
| Sc | 10.16 | 17.67 | 23.48 | 6.77 | 13.55 | 13.20 | 7.93 | 50.10 | 5.7 | 8.03 |
| Ti | 287.5 | 1325.1 | 2177.7 | 1182.9 | 510.3 | 1317.6 | 33.1 | 1647.0 | 115.9 | 52.8 |
| V | 38.59 | 77.01 | 119.38 | 114.95 | 50.58 | 62.5 | 45.39 | 129.9 | 30.3 | 24.87 |
| Cr | 2547 | 2455 | 1921 | 7908 | 2519 | 2189 | 2636 | 1096 | 6704 | 2692 |
| Co | 111.7 | 107.9 | 94.4 | 92.76 | 113.2 | 111.0 | 108.5 | 55.3 | 110.9 | 111.8 |
| Ni | 2334 | 1973 | 1340 | 1539 | 2169 | 1944 | 2119 | 494 | 2612 | 2431 |
| Cu | 13.91 | 34.22 | 37.66 | 20.66 | 17.88 | 95.6 | 1.05 | 85.9 | 9.55 | 13.10 |
| Zn | 40.22 | 44.39 | 70.98 | 52.63 | 43.89 | 48.7 | 61.76 | 11.6 | 41.41 | 42.51 |
| Ga | 1.32 | 3.65 | 7.28 | 5.00 | 2.24 | | 0.54 | | 0.78 | 0.66 |
| Rb | 0.12 | 2.64 | 2.93 | 1.79 | 0.39 | | 0.19 | | 0.1 | 0.12 |
| Sr | 1.97 | 88.89 | 82.61 | 25.14 | 2.71 | 18.1 | 2.35 | 164.4 | 15.09 | 1.92 |
| Y | 0.99 | 4.94 | 8.24 | 7.11 | 2.23 | 1.7 | 0.21 | 7.2 | 0.28 | 0.06 |
| Zr | 1.09 | 11.17 | 15.95 | 10.65 | 1.63 | 5.9 | 0.20 | 7.7 | 0.43 | 0.57 |
| Nb | 0.04 | 0.14 | 0.07 | 0.12 | 0.01 | | 0.04 | | 0.03 | 0.01 |
| Cs | 0.01 | 0.57 | 1.16 | 0.08 | 0.02 | | 0.02 | | 0.01 | 0.01 |
| Ba | 0.69 | 12.96 | 5.00 | 1.48 | 0.58 | | 0.30 | | 0.33 | 2.07 |
| La | 0.04 | 0.17 | 0.52 | 0.25 | 0.01 | | 0.04 | | 0.02 | 0.03 |
| Ce | 0.11 | 0.66 | 1.79 | 0.76 | 0.07 | | 0.09 | | 0.06 | 0.15 |
| Nd | 0.13 | 0.86 | 2.07 | 0.91 | 0.19 | | 0.06 | | 0.06 | 0.16 |
| Sm | | | | | | | | | | |
| Eu | | | | | | | | | | |
| Gd | | | | | | | | | | |
| Dy | | | | | | | | | | |
| Er | | | | | | | | | | |
| Yb | | | | | | | | | | |
| Lu | | | | | | | | | | |
| Th | | | | | | | | | | |
| U | | | | | | | | | | |

| Sample | SA-170a |
|---|---|
| Rock | Cpxite |
| SiO2 | 49.31 |
| TiO2 | 0.418 |
| Al2O3 | 3.68 |
| Fe2O3 | 7.27 |
| MnO | 0.12 |
| MgO | 24.25 |
| CaO | 13.32 |
| Na2O | 0.582 |
| K2O | 0.011 |
| P2O5 | 0.011 |
| NiO | 0.18 |
| Cr2O3 | 0.64 |
| Total | 99.79 |
| LOI | 4.88 |
| Mg# | 87.43 |
| Sc | 33.00 |
| Ti | 2275.6 |
| V | 126.2 |
| Cr | 4359 |
| Co | 72.4 |
| Ni | 1381 |
| Cu | 226.9 |
| Zn | 39.5 |
| Ga | |
| Rb | |
| Sr | 22.2 |
| Y | 3.5 |
| Zr | 10.1 |
| Nb | |
| Cs | |
| Ba | |
| La | |
| Ce | |
| Nd | |
| Sm | |
| Eu | |
| Gd | |
| Dy | |
| Er | |
| Yb | |
| Lu | |
| Th | |
| U | |

# Appendix E
# Ion Microprobe Data

The following section gives trace element content of clinopyroxenes, orthopyroxenes and olivines from the Leg 125 peridotites. The analyses were by ion microprobe (see Appendix A). Calibration working curve accuracy and counting precision are given in the table.

# Appendix E

| Hole | 779A | | | | 779A | | | | 784A | |
|---|---|---|---|---|---|---|---|---|---|---|
| Core | 14R-2 | | | | 26R-2 | | | | 42R-1 | |
| Interval | 40-48 | | | | 18-25 | | | | 7-12 | |
| Mineral | Cpx 1 | Cpx 3 | Cpx 4 | Opx 1 | Cpx 1 | Cpx 3 | Opx 1 | Ol 1 | Cpx 1 | Cpx 2 |
| Ti | 133 | 147 | 156 | 59 | 86 | 121 | 43 | 6 | 111 | 105 |
| V | 148 | 179 | 162 | 111 | 143 | 149 | 109 | 6 | 107 | 105 |
| Cr | 3640 | 7408 | 4820 | 4310 | 3296 | 4163 | 3670 | 135 | 3767 | 3173 |
| Sr | 2.52 | 2.71 | 2.45 | 0.29 | 1.00 | 1.38 | 0.63 | 0.41 | 5.02 | 5.09 |
| Zr | 0.24 | 0.37 | 0.40 | 0.08 | 0.24 | 0.22 | - | 0.19 | 0.39 | 0.35 |
| Ce | 0.102 | 0.103 | 0.104 | - | 0.019 | 0.041 | - | - | 0.099 | 0.117 |
| Nd | 0.035 | 0.029 | 0.052 | - | 0.004 | 0.018 | - | - | 0.087 | 0.107 |
| Sm | 0.031 | 0.027 | 0.026 | - | 0.026 | 0.017 | - | - | 0.032 | 0.044 |
| Eu | 0.012 | 0.011 | 0.012 | - | 0.011 | 0.014 | - | - | 0.017 | 0.022 |
| Dy | 0.280 | 0.346 | 0.207 | - | 0.164 | 0.131 | - | - | 0.059 | 0.090 |
| Yb | 0.369 | 0.336 | 0.331 | - | 0.268 | 0.189 | - | - | 0.184 | 0.198 |
| Hf | 0.097 | 0.097 | 0.117 | - | 0.039 | 0.060 | - | - | 0.078 | 0.071 |

| Hole | 784A | | | 784A | | | 784A | | |
|---|---|---|---|---|---|---|---|---|---|
| Core | 42R-1 | | | 45R-1 | | | 45R-1 | | |
| Interval | 7-12 | | | 101-106 | | | 130-137 | | |
| Mineral | Cpx 3 | Opx 1 | Opx 2 | Cpx 1 | Cpx 2 | Opx 2 | Cpx 1 | Cpx 3 | Opx 1 |
| Ti | 111 | 48 | 47 | 131 | 118 | 59 | 132 | 127 | 61 |
| V | 107 | 62 | 64 | 125 | 114 | 71 | 122 | 131 | 76 |
| Cr | 4504 | 2808 | 3158 | 4594 | 3386 | 3233 | 4214 | 4692 | 3190 |
| Sr | 4.12 | 0.61 | 0.28 | 0.43 | 0.85 | 0.58 | 0.52 | 0.48 | 0.22 |
| Zr | 0.29 | 0.18 | 0.17 | 0.39 | 0.31 | 0.17 | 0.28 | 0.17 | 0.12 |
| Ce | 0.148 | - | - | 0.054 | 0.070 | - | 0.055 | 0.030 | - |
| Nd | 0.118 | - | - | 0.020 | 0.027 | - | 0.013 | 0.011 | - |
| Sm | 0.054 | - | - | 0.017 | 0.028 | - | 0.028 | 0.021 | - |
| Eu | 0.019 | - | - | 0.013 | 0.016 | - | 0.012 | 0.008 | - |
| Dy | 0.106 | - | - | 0.134 | 0.145 | - | 0.142 | 0.121 | - |
| Yb | 0.165 | - | - | 0.134 | 0.130 | - | 0.126 | 0.124 | - |
| Hf | 0.071 | - | - | 0.077 | 0.077 | - | 0.082 | 0.043 | - |

| | Calibr. working curve accuracy | Counting Precsion % |
|---|---|---|
| Ti | 2 | 3 |
| V | 3 | 2 |
| Cr | 4 | 3 |
| Sr | 2 | 14 |
| Zr | 6 | 33 |
| Ce | 9 | 40 |
| Nd | 15 | 50 |
| Sm | 10 | 50 |
| Eu | 10 | 50 |
| Dy | 20 | 30 |
| Yb | 15 | 25 |
| Hf | 35 | 50 |